

Dissertation zur Erlangung des Doktorgrades
der Fakultät für Chemie und Pharmazie
der Ludwig-Maximilians-Universität München

**Design and Synthesis of Clickable Nucleic Acid
Analogues for Cancer Therapy and Diagnosis**

Samuele Stazzoni

aus

Siena, Italy

2020

Erklärung

Diese Dissertation wurde im Sinne von §7 der Promotionsordnung von 28. November 2011 von Herrn Prof. Dr. Thomas Carell betreut.

Eidesstattliche Versicherung

Diese Dissertation wurde selbstständig, ohne unerlaubte Hilfe erarbeitet.

München, 21/06/2020

.....
Samuele Stazzoni

Dissertation eingereicht am:

26.05.2020

1. Gutachter:

Prof. Dr. T.Carell

2. Gutachterin:

Dr. Sabine Schneider

Mündliche Prüfung am:

19.06.2020

“Do. Or do not. There is no try!”

Yoda

“Siamo chimici, cioè cacciatori: nostre sono “le due esperienze della vita adulta” di cui parlava Pavese, il successo e l’insuccesso, uccidere la balena bianca o sfasciare la nave; non ci si deve arrendere alla materia incomprensibile, non ci si deve sedere. Siamo qui per questo, per sbagliare e correggerci, per incassare colpi e renderli. Non ci si deve mai sentire disarmati: la natura è immensa e complessa, ma non è impermeabile all’intelligenza; devi girarle intorno, pungere sondare, cercare il varco o fartelo.”

P. Levi, “Il sistema Periodico”

Summary

1	Abstract.....	1
2	Introduction.....	4
2.1	The immune system	4
2.2	Pattern recognition receptors (PRRs)	5
2.3	The cGAS-STING pathway	6
2.3.1	Structural features of STING-cGAMP binding.....	8
2.3.2	cGAMP transport/trafficking	10
2.3.3	cGAMP degradation.....	11
2.4	Innate immune system targeting in cancer immunotherapy	13
2.4.1	The tumour immune environment.....	13
2.4.2	Antibody immunotherapy	15
2.4.3	Cell immunotherapy	16
2.4.4	Small molecule based approaches	16
2.5	STING-targeting therapeutic agents.....	17
2.5.1	Small molecule STING agonists	17
2.6	Nucleoside analogues of cGAMP	19
2.6.1	Replacement of the phosphodiesteres	19
2.6.2	Modification of the nucleoside moieties.....	20
2.7	Drug delivery of negatively charged molecules: prodrugs	22
2.7.1	Chemical synthesis of cyclic dinucleotides and cGAMP.....	23
2.8	Aim of the project	26
3	Results and discussion	27
3.1	Synthesis of dideoxy-2',3'-cyclic -di-AMP	30

3.2	Synthesis of dideoxy-3',2'-cGAMP	33
3.3	Synthesis of the methylated 2',3'-cyclic-di-AMP	35
3.4	Biochemical and biological assays	38
3.4.1	Binding assays	38
3.4.2	Cellular assays	39
3.5	Conclusions and outlook	42
3.6	Design of prodrugs of cGAMP analogues.....	45
3.7	Synthesis of prodrugs of cyclic dinucleotides	47
3.7.1	Prodrugs of deoxy- and methoxy-2',3'-CDNs	48
3.8	Biochemical and biological assays	51
3.8.1	Enzymatic activation of cyclic dinucleotide prodrugs.....	51
3.8.2	Cellular tests with dd-2',3'-c-di-AMP prodrug	54
3.9	Click chemistry based modification of the CDN prodrugs	57
3.10	Towards the synthesis of hydroxyl-containing cGAMP prodrugs.....	59
3.11	Conclusions and outlook	62
4	Materials and methods.....	63
5	Published work	98
6	List of abbreviations	135
7	Literature.....	138

Acknowledgements

My first thank goes to my PhD supervisor *Prof. Thomas Carell*. It was a privilege to carry out my PhD work in your laboratory, working on challenging and intellectually stimulating topics with a great scientific freedom. This gave me the opportunity to become experienced in the field of chemical biology and to discover scientific interests that I am looking forward to face in my future.

I would like to thank *Dr. Sabine Schneider* for accepting to be my second evaluator, especially with a relatively short notice.

The other members of my PhD committee, *Prof. Veit Hornung*, *Prof. Konstantin Karaghiosoff*, *Prof. Lena Daumann* and *Dr. Stefanie Kellner* are also kindly acknowledged.

I would like to thank *Dr. Markus Müller* for the many scientific and non-scientific discussions, as well for your invaluable help in organizational issues, which made it possible for me to carry out my PhD work in the best possible conditions.

I thank *Frau Slava Gärtner* for the organization and management of every possible bureaucratic issue and *Kristof Hufnagel*, *Kerstin Kurz* and *Luis de La Osa de la Rosa* for their help in everyday laboratory needs.

For the comments and help with corrections to my PhD thesis, I would like to thank *Clemens Dialer*, *Simon Veth* and *Fabian Hernichel*.

I would like to thank all my students and interns, *Sonja Rieth*, *Johann de Graaf*, *Sebastian Hagenreiner*, *Jonas Grandke*, *Karina Betuker*, *Süleyman Cosgun* and *Tri Phi* for the enthusiasm, interest and commitment during their internships with me. Your work was a great help to reach many goals of my PhD projects.

I would like to thank my Master student and now co-worker *Fabian Hernichel* for his trust, his patience, and commitment to work during the preparation of his master thesis. It was a pleasure to work alongside you and assist you in your project and to see your progresses.

A special thank goes to my co-workers in the “cGAMP subgroup”: *Clemens Dialer* (the first member!), *Simon Veth*, *Fabian Hernichel*, *Katerina Pappa*, *Giacomo Ganazzoli* and *Johann de Graaf* in the chemical side and *Ewelina Kaminska* and *Dilara Özdemir* for the biological side. It was a real pleasure to work and discuss about progresses and ideas with you, and it was even more of a pleasure to enjoy some time together in the great cGAMP dinners!

I also thank my collaborators outside the Carell group, especially *Dr. David Drexler* in the Prof. Hopfner’s group and *Wilhelm Greulich* in the Prof. Hornung’s group. Part of this thesis would have been impossible without your cooperation.

In addition to the already mentioned people, I would like to give a big thank to all the people that I got to know during my time in the Carell group for creating a great working environment, for the coffees, for the many lunches, dinners and beers together and for many

other coffee kitchen celebrations and outside activities organized outside the laboratory. It was great to spend this time with you!

I also send a big thank to all the members of the great ClickGene Marie Curie network, *Nicolò Fantoni, Bastien Viverge, Alessandro Panattoni, Piotr Klimowski, Giorgia Giacometti, Gianluca Toniolo, Maria Louka, Georgia Menounou, Jan Matyasovski, Teresa Lauria, Giuseppe Avella, Stefano Ctoce* and *Sarah Walsh*. It was great to get to know all of you and to spend time together in all our meetings and training events!

The most important acknowledgements are coming at the end. First of all I would like to thanks my whole family for their infinite support, for the encouragement and for their trust in me which gave me the strength to reach the end of my PhD. I am in particular immensely grateful to my parents, *Rita Cellesi* and *Alfio Stazzoni*, for everything they did for me. You have been examples for me during my whole life and even more in the many difficult times that we, as a family, went through in the last few years, just after my move to Munich. Special thanks go also to my cousin and aunt *Chiara Barranchini* and *Roberta Cellesi*: since my childhood until now, you were for me like sisters and your nearness was very valuable to me to keep the motivation and the morale high enough during my PhD time.

Last but surely not least I would like to thank my beloved girlfriend *Jessica Fantacci*. I cannot find enough words to express my gratitude and appreciation for the support you gave me in this time where we have been mostly far away from each other. I am very much looking forward to being able to be together with you again and not worrying about catching planes, trains, buses or driving several hours to see each other!

Publications

- N. Raddaoui*, S. Croce*, F. Geiger, A. Borodavka, L. Möckl, **S. Stazzoni**, B. Viverge, C. Bräuchle, T. Frischmuth, H. Engelke, and T. Carell, *ChemBioChem* **2020**, accepted.
- C. R. Dialer, **S. Stazzoni**, D. J. Drexler, F. M. Müller, S. Veth, A. Pichler, H. Okamura, G. Witte, K.-P. Hopfner, T. Carell, *Chem. Eur. J.* **25**, 2089–2095 (2019).
- N. Raddaoui*, **S. Stazzoni***, L. Möckl, B. Viverge, F. Geiger, H. Engelke, C. Bräuchle, T. Carell, *ChemBioChem* **2017**, *18*, 1716–1720.

* = These authors contributed equally to this work

- M. Su, A. Kirchner, **S. Stazzoni**, M. Müller, M. Wagner, A. Schröder, T. Carell, *Angew. Chem.* **2016**, *55*, 11797–800.
- Pratesi, **S. Stazzoni**, M. Lumini, G. Sabatino, A. Carotenuto, D. Brancaccio, E. Novellino, M. Chinol, P. Rovero, M. Ginanneschi, et al., *Chem. Eng. Process. Process Intensif.* **2017**, *122*, 365–372.

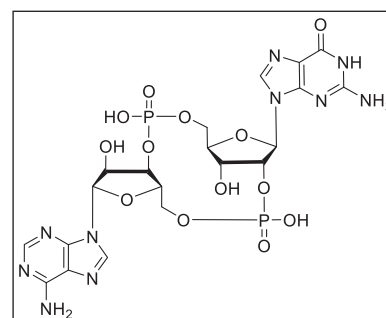
Conference and meeting attendance

- Oral presentation “*Novel methods for the detection and labeling of nucleic acids and nucleic acid sequences*”, **COST and ClickGene meeting**, 04/2016, Grenoble, France.
- Oral presentation “*Novel methods for the detection and labeling of nucleic acids and nucleic acid sequences*”, 12/2016: **ClickGene mid-term review meeting**, Bologna, Italy.
- Poster “*Quantification of 5-formylcytosine in specific genomic sites*”, 06/2017: **17th SCNAC conference**, Cesky Krumlov, Czech Republic.
- Oral presentation “*Designing synthetic dinucleotides for STING-targeted immunotherapies*”, 03/2018: **ClickGene symposium**, Oxford University, UK.
- Oral presentation “*Synthetic cyclic dinucleotides for STING-targeted immunotherapies*”, 6-7/12/2018: **ClickGene final meeting**, Dublin, Ireland.
- Oral presentation “*Clickable cGAMP analogues as immunomodulatory agents*”, SFB1032 meeting, Benediktbauern, Germany.
- Poster “*High yielding total synthesis of 2’3’-cGAMP*”, 09/2019: **Nucleic Acid Immunity in Health and Disease**, Ascona, Switzerland.

1 Abstract

The use of nucleic acid molecules in cancer therapy and diagnosis represents a field in continuous growth. During this thesis, bioconjugation and click chemistry techniques were applied to biological system in order to provide new tools for cancer therapy (chapters 1-4) or diagnosis (chapter 5).

In the first part the development of a series of STING agonists is described. STING is a key protein in the regulation of the innate immune system. The activation of the STING pathway begins when DNA is released in the cytosol. This DNA is seen by cells as a clear danger sign upon which the DNA sensor cGAS specifically recognizes and binds cytosolic DNA. Using ATP and GTP, cGAS can



synthesise the second messenger 2',3'-cGAMP (Figure 1). 2',3'-cGAMP is then recognized by STING and this leads to a conformational change of the protein structure which ultimately triggers interferon expression. Because of their ability to activate the immune system, the use of 2',3'-cGAMP analogues and STING agonists in medicine is gaining interest, with a constantly growing number of molecules currently in preclinical and clinical trials in the field of immunotherapy or vaccines. Because of the negative charge of 2',3'-cGAMP, which impairs its uptake by cells and because of its metabolic instability, there is high need for new 2',3'-cGAMP analogues that can cross the cell membrane or that are more stable towards the action of human or viral enzymes that are known to specifically degrade this cyclic dinucleotide. Therefore, we developed a series of cGAMP analogues that are based on a 2',3'-cyclic dinucleotide scaffold and that contain adenosine or guanosine nucleosides.

Figure 1: Structure of 2',3'-cGAMP

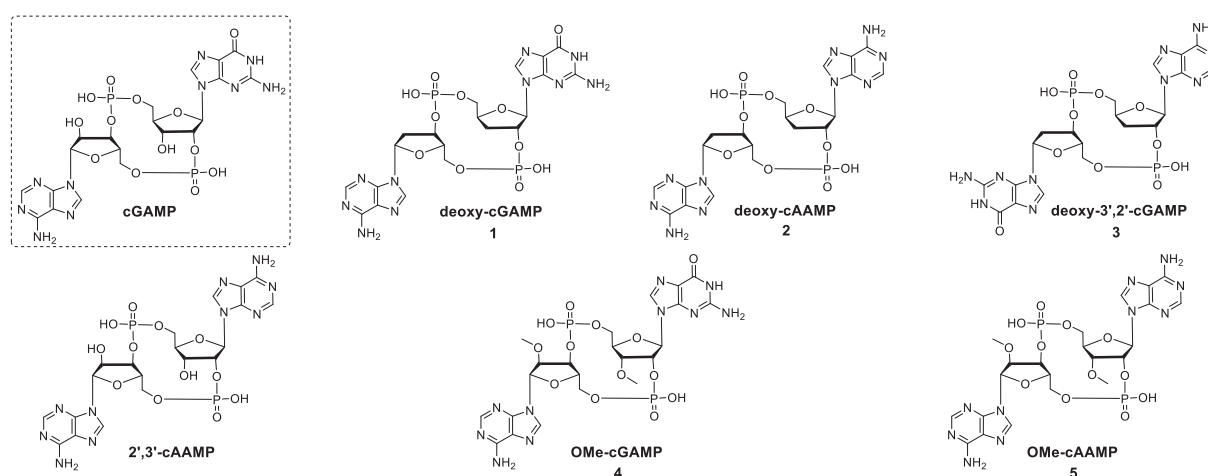


Figure 2: Structures of the designed and synthesised cGAMP analogues.

In addition to the natural cGAMP, we synthesised the 2',3'-cyclic adenosine monophosphate-adenosine monophosphate (cAAMP), the dehydroxylated analogues **1**, **2** and **3** and the methylated analogues **4** and **5** (Figure 2). In collaboration with *Dr. D. Drexler* (Hopfner group), the synthesised compounds were tested in thermal shift assays with the soluble portion of STING and then in isothermal titration calorimetry experiments in order to calculate the binding affinities of the synthesised analogues as well as the thermodynamic parameters of their interaction with the protein.

Compounds **1**, **2**, **3**, **4** and **5** were then further tested in cellular assays using THP-1 dual reporter cells, which allowed to measure the interferon expression triggered by these analogues and determine their EC_{50} value, reflecting the potency of the synthesised STING agonists. With these assays, the most potent STING agonist resulted to be compound **1** (EC_{50} = 8.5 μ M) while we calculated an EC_{50} value of 10.6 μ M for cGAMP and a value of 60.5 and 106.5 μ M for compounds **2** and **3**. The methylated analogues **4** and **5** did not induce STING activation in our assays, likely because of the conformation of their ribose moieties.

In the second part of this project we developed prodrug derivatives of compounds **2** and **5** described before in order to improve the cell permeability of these molecules and to achieve their efficient internalization. To do this, we modified the S-acylthioethyl (SATE) moiety, which is frequently used in prodrugs, to include a terminal alkyne which allows further late-stage functionalization by click chemistry to improve drug uptake (Figure 3).

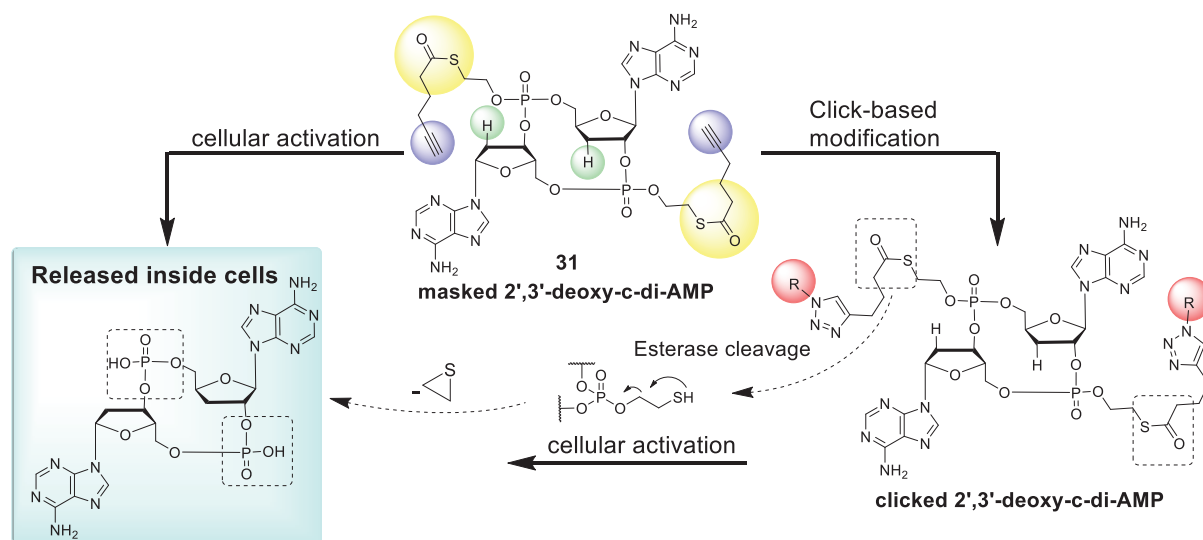


Figure 3: Design, structure and activation mechanism of the masked cGAMP analogues.

The synthesised analogue **31** was tested in THP-1 cells to determine its activity. With the introduction of the phosphate caging groups, we calculated an EC_{50} value of 47.6 nM indicating that **31** is approximately 200-fold more potent than cGAMP itself. In collaboration with *W. Greulich* (Hornung group) we studied the phosphorylation of the key proteins

involved in the STING and interferon pathways (STING, TBK1 and STAT1) by western blot and we detected a much higher phosphorylation level of these proteins using compound **31** compared to cGAMP. Furthermore, the masked derivatives containing an alkyne were further functionalized by click chemistry with an anandamide azide leading to compound **44** and **45**. Compound **44** was also tested in THP-1 cells, but, even if it proved to be more active than cGAMP, we measured a lower activity of derivative **44** compared to **31**.

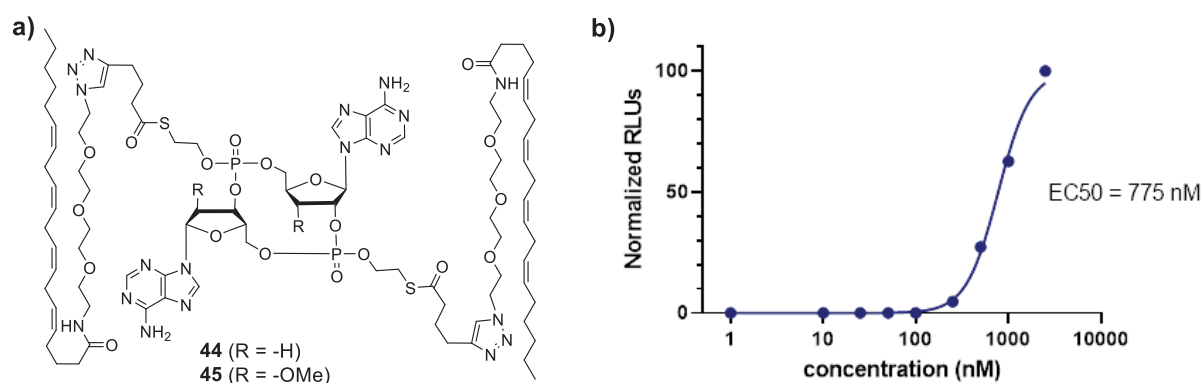


Figure 4: a) Chemical structure of the CDN-anandamide conjugates **44** and **45**. b) EC₅₀ curve of **44**.

In chapter 5 published work is presented, in which clickable dendrimers have been used in order to enhance the signal of a cell proliferation assay based on EdU incorporation. After cell feeding with EdU, a tetraazide dendrimer was employed to increase the number of reactive sites per each incorporated alkyne (Figure 5). In a second step, we reacted the multiple azides with a dye alkyne (double click procedure) or with another dendrimeric with four alkynes, exponentially increasing the number of reactive alkynes for each incorporated EdU (triple click procedure). In this last procedure, we finally performed a click reaction with a dye azide to allow detection of proliferating cells by fluorescence microscopy. By employing these clickable dendrimers it was finally possible to achieve a 6-fold enhancement in the fluorescent signal.

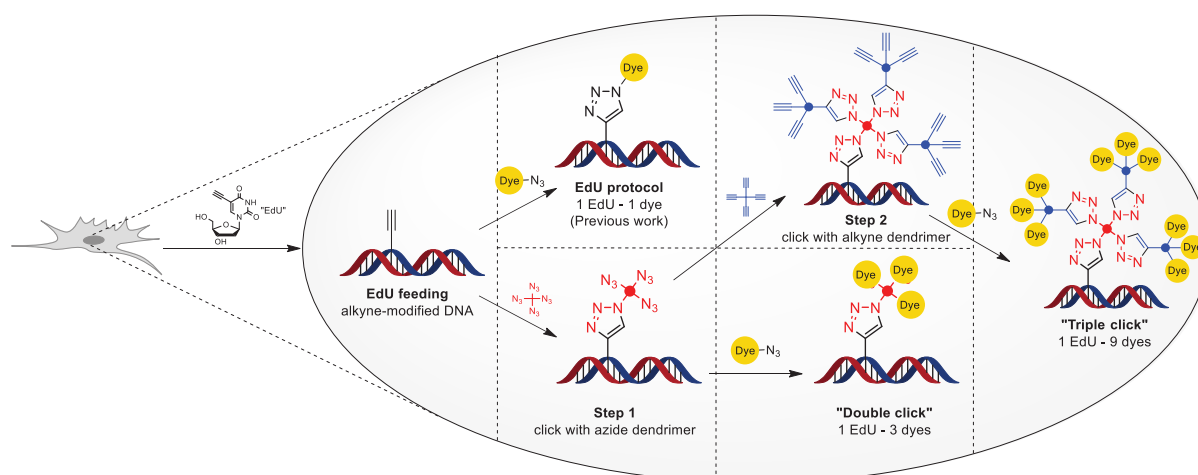


Figure 5: Illustration of the EdU assay and of the “double click” and “triple click” assays developed.

2 Introduction

2.1 The immune system

Human cells have evolved a defence system against external pathogens, which is composed of many levels. Physical or physiological barriers represent the first line of protection and have the function to not allow pathogens to enter the organism or to destroy them by exposing them to adverse conditions such as low pH in the stomach, or the presence of enzymes like lysozymes in the saliva.¹⁻³

The second key player in cell defence is the immune system, which can be divided into two independent, but interconnected compartments: the innate and the adaptive immune system. Evolutionally, the innate immune system was the first one to be developed and it is present in all multicellular organisms.^{4,5} It is the first defence mechanism to be activated when a pathogen enters the host and has many specific functions such as controlling the recruitment of immune cells to the infected area by releasing specific messenger molecules, the activation of the complement system to enhance the ability of cells of the innate immune system to clear cells from pathogens and the activation of cells of the innate immune system through the antigen presentation process.⁶⁻¹⁰

The activation of the innate immune system initially triggers an inflammation, in which immune cells, blood vessels and chemical factors contribute to avoid the spread of the infection and the clearance of damaged cells. This process is initiated by cells that are naturally present in all tissues, such as macrophages, dendritic cells, histiocytes, Kupffer cells and mast cells.^{11,12} They possess specific receptors on their surfaces called pattern recognition receptors (PRRs) that are able to recognize pathogen-associated molecular patterns (PAMPs) or damage-associated molecular patterns (DAMPs). PAMPs are molecules released by or associated with infecting non-self-pathogens, while DAMPs are originated from the host cell damage.^{7,13,14}

Upon recognition of these molecular patterns and activation of various immunological pathways, macrophages and mast cells release amines such as histamine or serotonin and prostaglandins that are able to induce vasodilation and make blood vessels more permeable.^{15,16} This leads to an increased concentration of blood into the infected tissue, which allows various components of the plasma, including lysozyme and antibodies, to quickly reach the site of infection and damage the pathogen reducing the likelihood of a serious infection.

2.2 Pattern recognition receptors (PRRs)

Pattern recognition receptors play a key role in the recognition of chemicals produced by pathogens or by damaged cells and in the activation of the innate immune system in response to these stimuli. The large number of different PRRs makes it possible for these receptors to specifically recognize a wide range of PAMPs, such as bacterial carbohydrates (lipopolysaccharides or mannose), viral or bacterial nucleic acids or peptides, peptidoglycans and many others. DAMPs are instead molecules such as uric acid, extracellular ATP or proteins such as BCL2 or heat-shock proteins, that are released by the host damaged cells.^{2,7,10} To date, many PRRs have been discovered and characterised, the most important of which are shown in Figure 6 and described more in detail below.

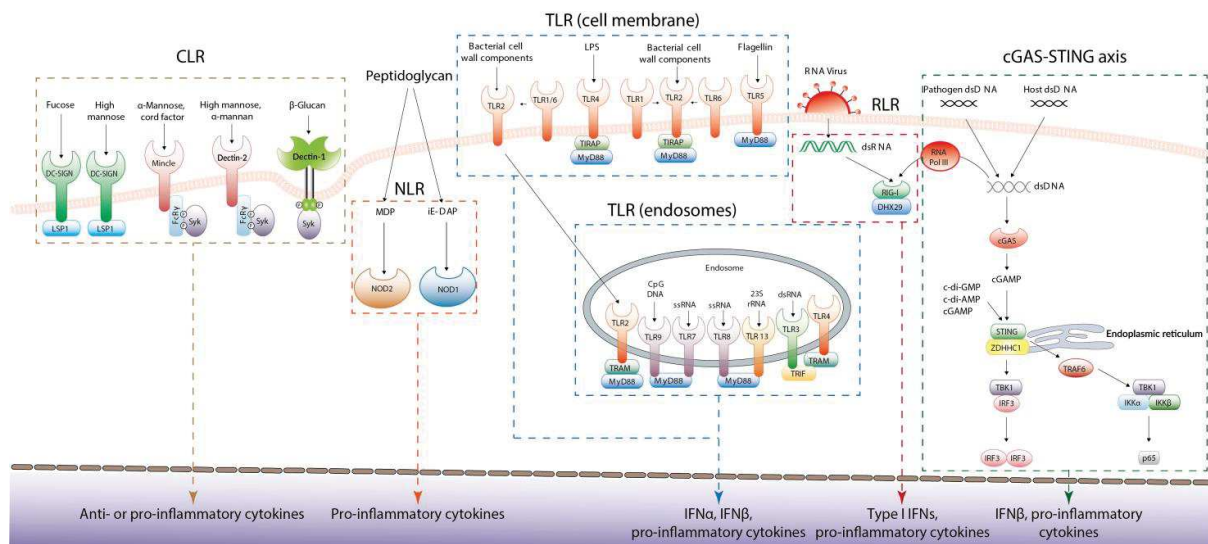


Figure 6: Illustration of the most important Pattern-recognition receptors and their ligands (adapted from Invivogen)

Toll-Like Receptors (TLRs): TLRs are considered among the most important PRRs. So far, 13 different TLRs have been discovered, 10 of which are present in humans. They are membrane receptors normally sitting on the cell membrane or in endosomes and they are able to bind a wide range of ligands and consequently initiate an innate immune response. Upon ligand binding, TLRs recruit adapter proteins that are able to activate transcription factors such as NF-κB, IRF3/7 and this activates various kinases that ultimately lead to the production of pro-inflammatory cytokines and interferons.^{8,17}

C-type lectin receptors (CLRs): CLRs are expressed by dendritic cells and constitute a crucial component in the immune response to pathogens. The main ligands of CLRs are carbohydrates such as mannose, fucose and glucans that are present in most bacteria, viruses

or fungi. After ligand binding, CLRs trigger complex signalling pathways that involve also other protein complexes and PRRs. This activates cytokine and interferon expression and leads to the pathogen internalization and degradation initiating the antigen presentation process necessary for the recruitment of native immune system components.¹⁸⁻²⁰

NOD-like receptors (NLRs): These cytoplasmic PRRs are highly conserved through evolution and are present both in immune cells such as lymphocytes, macrophages and dendritic cells, but also in non-immune cells, for example in the epithelium. They can recognize many PAMPs, the most important of which being peptidoglycan from bacterial cell membrane, meso-diaminopimelic acid and muramyl dipeptide, found in many Gram negative or positive bacteria. Together with other PRRs, NLRs are important elements in the formation of the inflammasome, which is a multiprotein complex responsible for the activation of the immune response through production of interleukins.^{14,21-23}

Cytosolic nucleic acid sensors: The presence of DNA or RNA inside the cytosol of a cell is a clear signal of an ongoing infection or of a cellular damage. For this reason, cells have evolved a series of mechanisms with the aim to detect nucleic acids and respond to them by activating the immune system. One example of this family of PRRs is retinoic acid inducible gene I (RIG-I), which is mainly responsible for the regulation of the antiviral immune response. RIG-I can in fact bind short single or double-stranded RNA which contain an uncapped 5'-triphosphate moiety and poly-uridine regions and this triggers a biochemical pathway to ultimately produce interferons via the expression of the transcription factor IRF3 or IRF7 and their translocation into the nucleus.²⁴⁻²⁶

Another important cytosolic nucleic acid sensor is the cyclic guanosine mono phosphate-adenosine monophosphate synthase (cGAS): a protein which recognises cytosolic DNA and initiates key biochemical pathways that also induce interferon and cytokine production.^{27,28} The biochemical pathways activated after cGAS-DNA interaction will be discussed in the following chapter.

2.3 The cGAS-STING pathway

The presence of DNA in the cytosol represents a danger signal for a cell. The enzyme cGAS is a cellular protein that can bind double-stranded cytosolic DNA and recruits ATP and GTP in its active site to synthesise the non-canonical dinucleotide 2',3'-cGAMP. cGAMP can then diffuse into the cytosol and come in contact with STING (stimulator of interferon genes), a protein which normally sits on the endoplasmic reticulum. After binding cGAMP, STING changes its conformation and translocates to the perinuclear region, becoming active and

inducing expression of immunostimulatory molecules via downstream signalling (Figure 7).^{28,29}

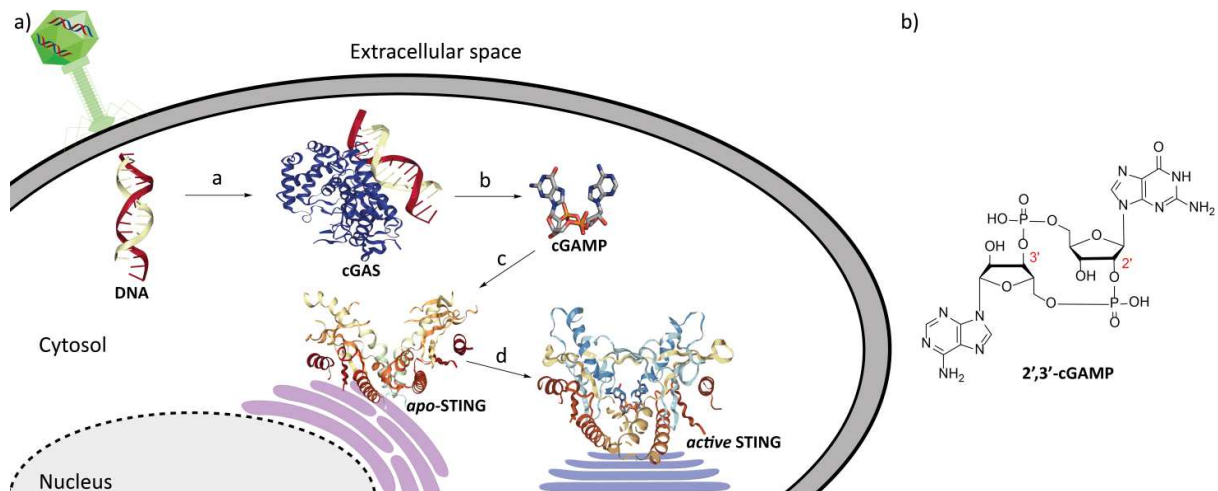


Figure 7: a) Illustration of the cGAS-STING pathway. Step a: DNA is released into the cytosol by pathogens (viruses, bacteria etc.) and is recognized by the enzyme cGAS. b: cGAS binds the DNA and uses ATP and GTP to synthesise cGAMP, which is released into the cytosol. c: cGAMP is recognized by the enzyme STING, which changes its conformation. d: STING is now activated and can trigger interferon expression. b) Structure of the second messenger 2',3'-cGAMP.

Structurally, cGAS is a small protein composed of 522 amino acids belonging to the nucleosyltransferase family. The N-terminal region is thought to be responsible for DNA binding, while the C-terminus contains the nucleosyltransferase motif. Both of these regions have been shown to be to create the catalytic pocket necessary for cGAS activity.^{30–32} After DNA binding, cGAS dimerizes and recruits ATP and GTP in its catalytic pocket to synthesise the second messenger 2',3'-cGAMP. Differently from other cyclic dinucleotides, such as the bacterial cyclic diadenosine monophosphate (c-di-AMP) or cyclic diguanosine monophosphate (c-di-GMP) 2',3'-cGAMP has a non-symmetrical structure, composed of a canonical 3',5'-phosphodiester between the 3'-OH of AMP and the 5'-OH of GMP and a non-canonical 2',5'-phosphodiester connecting the 2'-OH of GMP with the 5'-OH of AMP. The synthesis of cGAMP is a 2-step process carried out in the same active site of cGAS.^{28,29,31} ATP and GTP are first positioned respectively in the donor and acceptor sites, then the first linkage between the 2'-OH of GTP and the α -phosphate of ATP is formed with elimination of pyrophosphate. This pppG(2'-5')pA intermediate is then flipped by 180° in order to invert the donor and acceptor positions and the final cyclization step can take place with the formation of the canonical 3'-5' linkage (Figure 8). The produced 2',3'-cGAMP is then released into the cytosol and can induce interferon or cytokine expression in the cell. cGAMP can also be transferred to surrounding cells via gap junctions or in viruses and trigger immune response in a cooperative way.^{33,34}

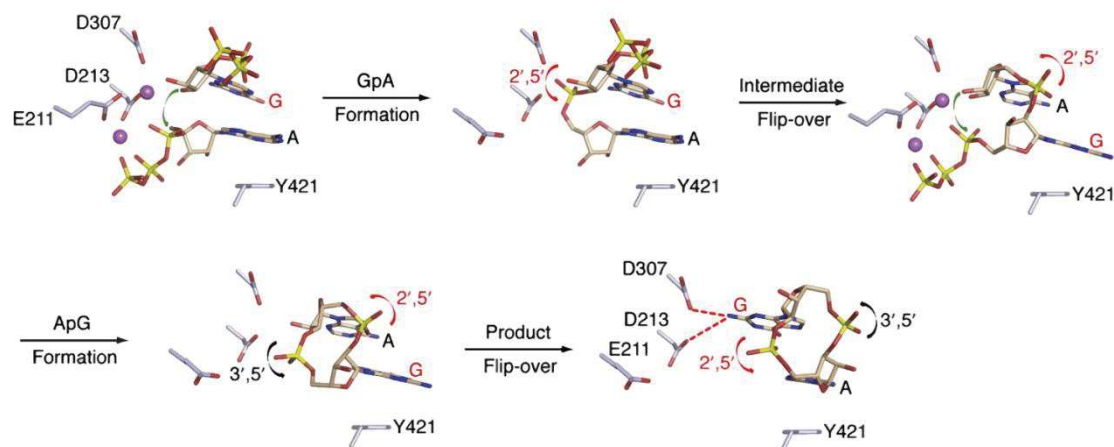


Figure 8: Synthesis of cGAMP in the cGAS catalytic pocket. Figure adapted from Gao *et al.*

As mentioned before, the cGAS product cGAMP can diffuse through the cytosol until it eventually reaches the endoplasmic reticulum where it binds and activates STING, a 378 amino acid protein.^{35–38} STING is a dimeric protein with a large binding pocket in the centre between the single monomers. Upon cGAMP binding STING changes its conformation assuming a closed structure and this induces translocation of the protein to the Golgi, where it can recruit the kinase TANK-binding kinase 1 (TBK1) that is able to phosphorylate its C-terminus.^{36,39,40} After phosphorylation, STING forms a complex with TBK1 and interferon regulatory factor 3 (IRF3) which is in turn phosphorylated, dimerizing and translocating to the nucleus.^{41–43} Here, expression of type I interferons is initiated. STING activation can also lead to cytokine expression, through NF- κ B signalling pathway.^{35,44,45} In addition to 2',3'-cGAMP recognition, STING is also thought to be involved in the detection of bacterial cyclic dinucleotides. STING-induced INFs expression was in fact observed in presence of c-di-AMP, c-di-GMP and canonical 3',3'-cGAMP, although the binding affinities of these dinucleotides are lower compared to 2',3'-cGAMP.^{46–49}

2.3.1 Structural features of STING-cGAMP binding

The apo-form of dimeric STING is characterized by an open conformation with a V-shaped large binding pocket that interacts with the cyclic dinucleotide ligands (Figure 9 c). After cGAMP (or other cyclic dinucleotides) binding, STING closes its binding pocket and forms a β -sheet structure that entraps the ligand and increases the surface of interaction between the two protein monomers.^{50–52} The interaction between STING and cGAMP is controlled by two main factors: pi-stacking between the purines and the aromatic side chains of Tyr167 and Tyr240 and ionic interactions between the negatively charged phosphates in the cGAMP scaffold and the Arginine side chains in position 238 and 232. Besides, hydrogen bonding

between the free 3'-OH in the GMP ribose and Ser162 as well as interactions between the guanine and Glu260 and Thr263 are further stabilizing the ligand-protein complex (Figure 9 a and b).

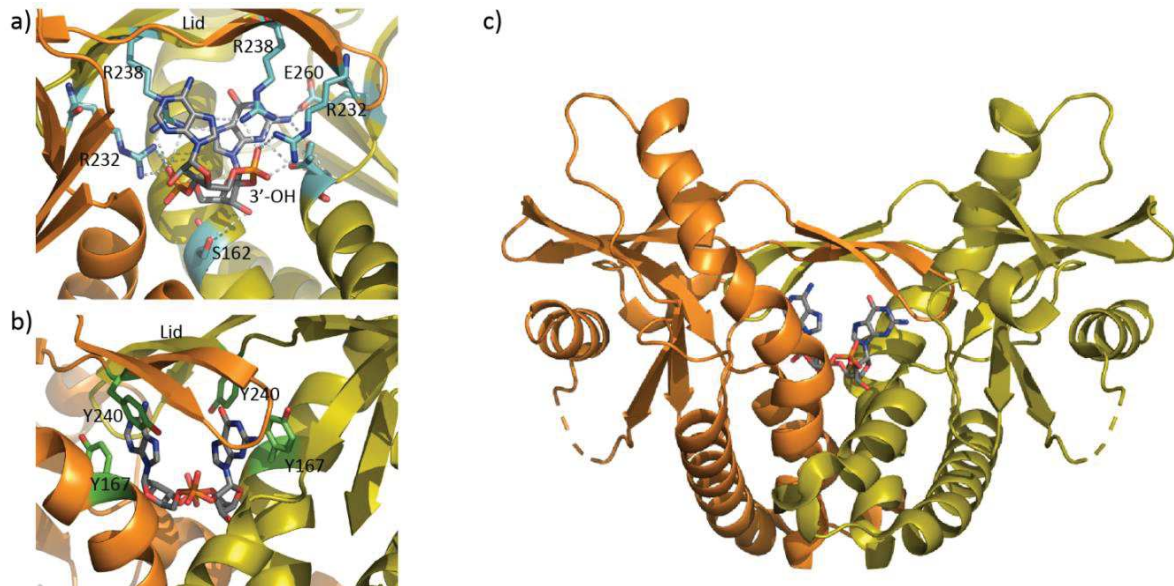


Figure 9: Interaction of STING with cGAMP. a) Polar interactions between Arginine side chains and phosphates or hydrogen bonds between -OH groups in the cGAMP and amino acid residues in the STING active site. b) pi-stacking interactions between purines and aromatic amino acids. c) Illustration of the STING protein conformation when bound to cGAMP.

While the STING-cGAMP interaction is well understood, a model explaining how STING activation leads to interferon production was proposed only very recently.^{29,47,53-55} A series of studies showed that the conformational change triggered by cGAMP is essential to allow STING oligomerization and that this oligomerization is required in order to initiate its phosphorylation by TBK1. According to the current model, after cGAMP binding, the cytosolic portion of STING undergoes a 180° rotation and the subsequent conformational change releases the C-terminal tail of the protein. This makes a polymerization surface accessible and exposes Cys148, initiating STING oligomerization through disulfide bond formation. The residues belonging to the C-terminal domain released after cGAMP binding can adopt a beta-strand structure, which allows this peptide to insert into a groove in the TBK1 kinase (Figure 10 a). After polymerization of STING and TBK1 recruitment each TBK1 can reach the Ser366 of the adjacent STING dimer and phosphorylate it. Phosphorylated STING contains a binding motif for the transcription factor IRF3 that can be recruited and again phosphorylated. IRF3 forms a homodimer and can then translocate to the nucleus to induce expression of immunomodulatory molecules (Figure 10 b).

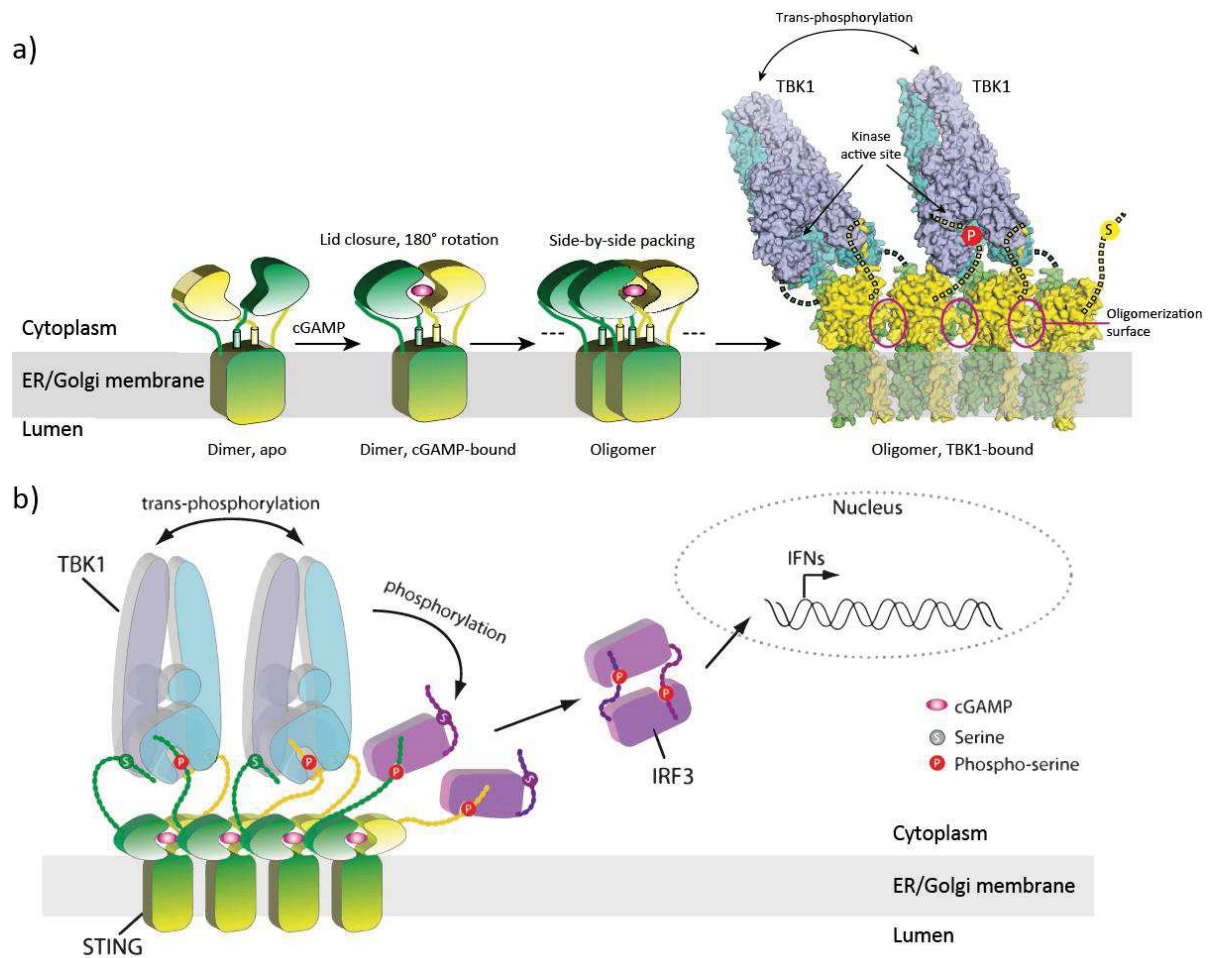


Figure 10: Illustration of the mechanism of STING-mediated interferon expression. a) cGAMP binding, oligomerization and TBK1-binding leading to STING phosphorylation. b) Recruitment of IRF3 and its translocation to the nucleus as a dimer, leading to interferon expression. Figure adapted from Zhang *et al.* and Shang *et al.*^{53,54}

2.3.2 cGAMP transport/trafficking

It is known that many immunostimulatory molecules such as cytokines and chemokines are secreted by immune cells in order to alert other cells that an infection has occurred.^{56,57} cGAMP itself, despite being produced inside the cytosol, can be transferred between cells and therefore prepares also other cells to counteract an ongoing infection by activating STING and subsequently interferon and cytokine expression.^{33,34} The main mechanism how cGAMP can be transferred is through gap junctions, intracellular connections between neighbouring cells.

Li *et al.* were able to prove that the solute carrier protein SLC19A1, a membrane protein expressed in many tissues and responsible for the uptake of reduced folate analogues such as folic acid or methotrexate, is able to efficiently import extracellular cGAMP and other cyclic dinucleotides into the cytosol.^{58,59} In agreement with this, it was also shown that cells

that express large amounts of SLC19A1 also produce more interferons when stimulated with extracellular cGAMP, confirming the active role of this protein in the uptake of cGAMP and cyclic dinucleotides.

2.3.3 cGAMP degradation

The non-canonical 2',3'-phosphodiester bond that characterizes cGAMP does not only allow higher binding affinity for STING, but is also important because it gives additional metabolic stability to the cyclic dinucleotide. While many bacterial and human enzymes can hydrolyse and degrade 3'-5' phosphodiester bonds of cyclic nucleotides and dinucleotides,⁶⁰⁻⁶⁶ only a few have been discovered that can hydrolyse the 2'-5' phosphate.⁶⁷⁻⁶⁹ In humans, the Ectonucleotide Pyrophosphatase/Phosphodiesterase 1 (ENPP1) is a transmembrane protein that has the primary function of hydrolysing ATP to form ADP and diphosphate. Mitchinson *et al.* showed that ENPP1 is also responsible for degrading 2',3'-cGAMP by specifically cleaving the 2'-5' phosphodiester, which suggests that this enzyme might contribute to the regulation of the innate immune system by controlling the amount of cGAMP present.⁶⁹ Nureki *et al.* discovered that the active site of the enzyme is located extracellularly and suggested therefore that cGAMP degradation does not occur in the cytosol.⁷⁰ In order to be a substrate for ENPP1, cGAMP adopts an open conformation different from the one adopted during STING binding. In this conformation, the two purines are far apart from each other and pointing in different directions (Figure 11 a). The adenine and guanine are then adapted into two different binding pockets and the phosphate coordinates two zinc ions that are also coordinated by the protein residues Asp358, His362, His517 and Asp200, Asp405 His406 (Figure 11 b). The recognition and preferential cleavage of the 2'-5' phosphodiester in respects to the 3'-5' phosphate can be attributed to the C2'-endo conformation of the guanosine ribose, which allows hydrogen bond formation with the Asn259. In this conformation, the 2'-5' phosphate has the correct orientation to be attacked by the nucleophile Thr238. The guanosine part of 3',3'-cGAMP, instead, assumes the C3'-endo conformation, which does not represent the ideal geometry for a nucleophilic attack from the threonine side chain.

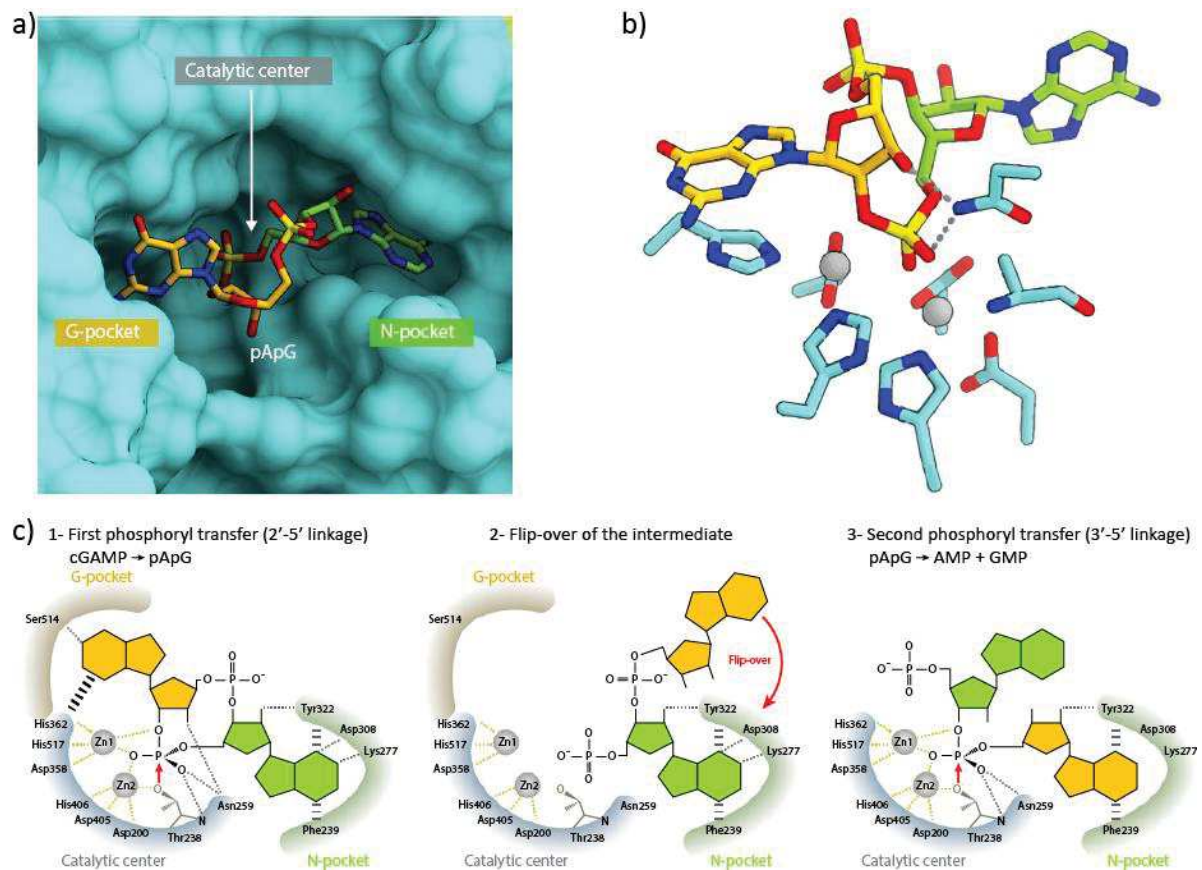


Figure 11: Structural basis for the binding and degradation of cGAMP by ENPP1. a) Representation of cGAMP in the ENPP1 catalytic centre. b) Residues participating to the hydrolysis of the phosphodiester bond and interaction with the 3'-OH of the guanosine. c) Mechanism of cGAMP degradation. Figures adapted from Mitchinson *et al.*⁶⁹

In addition to human enzymes, viral proteins are also able to hydrolyse cGAMP in order to escape the immune surveillance of their host.⁷¹ Many human poxviruses can in fact produce highly conserved proteins, called poxvirus immune nucleases or poxins, able to bind and degrade cGAMP, that would otherwise initiate a defence response against the virus itself. Contrarily to ENPP1, poxins can act intracellularly and act on the 3'-5' phosphodiester bond, leading to the formation of Gp[2'-5']Ap[3']. These protein were also shown to be specific for 2',3'-cGAMP, as no degradation was observed for any of the 3',3'-cyclic dinucleotides. Also different from ENPP1 is the mechanism of cGAMP binding and phosphodiester cleavage. In this case, the substrate is recognized specifically thanks to 6 amino acid residues present in the binding pocket. The guanine moiety is interacting with Ile105, Lys186 and Arg184, which also interacts with the 2'-5' phosphate, together with Arg182, and Gln169 and the adenine is recognized by Asn149, Arg60 and Ala145. His17, Lys142 and Tyr142 are located in the active site of the enzyme. After binding to poxin, the adenine part of a cGAMP molecule is rotated and the ribose conformation is switched to the 2'-OH-endo conformation. With the assistance of the His17 and Lys142 acting as an acid and base, this 2'-OH can act as a nucleophile and attack the phosphodiester. This results in the formation of a unstable cyclic

phosphate that can be further hydrolysed by H₂O to the final open 3'-phosphate molecule. The proposed mechanism enlightens the importance of the hydroxyl groups and especially of the adenosine 2'-OH which attacks the phosphate in the first step, leading to opening of the cycle.

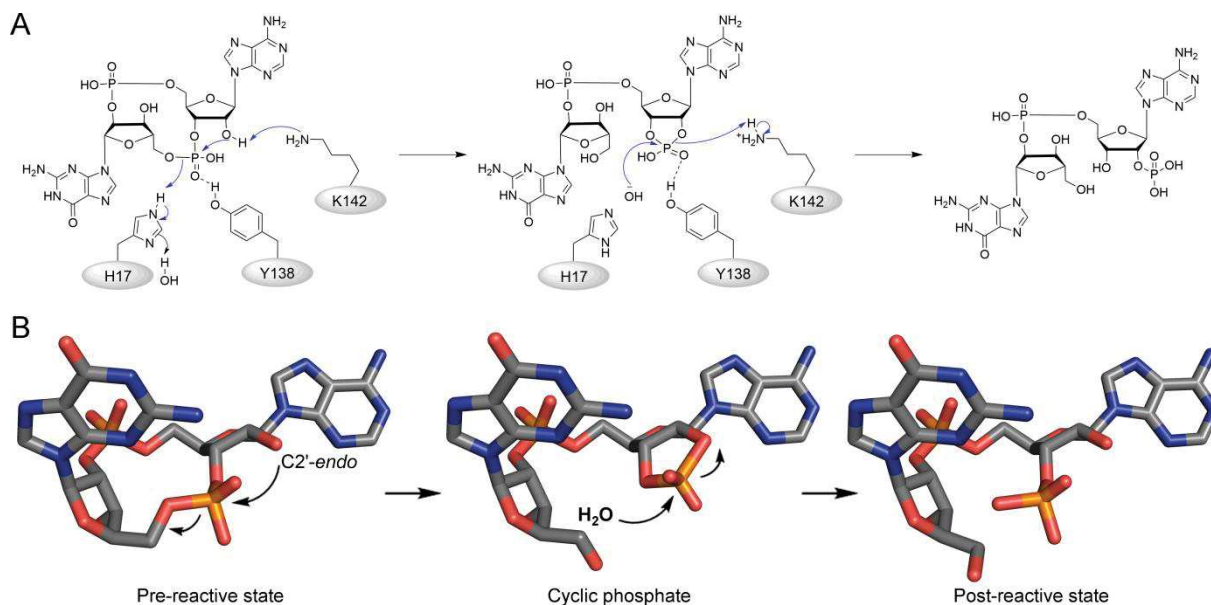


Figure 12: Hydrolysis of cGAMP by poxins. A) cGAMP degradation and interactions with the residues in the poxin catalytic site. B) 3D visualization of the intermediates formed during cGAMP degradation.⁷¹

2.4 Innate immune system targeting in cancer immunotherapy

2.4.1 The tumour immune environment

The relationship between immune system and cancer development has been examined since 150 years ago, when the physician Rudolf Virchow could detect leukocytes in a tumour tissue. Despite this early observation, only in the last 20-30 years significant steps forward were made in understanding the connection between immunity and cancer.⁷²⁻⁷⁶ Although carcinogenic cells have characteristics very similar to the healthy ones, they frequently present unique features that allows their recognition from the immune system. For example, they can express immunogenic mutated peptides or proteins, called neoantigens, as in the case of β -catenin, Caspase 8 or CDK4 in melanoma, overexpress cellular proteins, called tumour-associated antigens, like MUC1 or HER2/neu in various types of cancer cells, or express genes that would normally be silenced in normal cells.⁷⁷⁻⁸⁰ The discovery of the ability of these biomolecules to induce an immune response in the host paved the way to many studies with the purpose of understanding how this anti-tumoral immune defence works on a molecular level in order to use it to fight cancer.⁸⁰⁻⁸⁴

A series of antigen-presenting cells, such as immature dendritic cells, can phagocytize and recognize these tumour-associated antigens from dead cancer cells.⁸⁰ After this, they are

activated and start to develop into mature dendritic cells that present the antigens. Mature dendritic cells are then transported to the lymph nodes, while presenting the recognized antigen on their surface via the major histocompatibility complex (MHC) molecules. At the lymph node, the active dendritic cells come in contact with helper and killer-T cells and B-cells, which in turn get primed, activated and start to replicate and circulate in the body, in search for the tumour cells containing the original antigen (Figure 13). Despite the effectiveness of these mechanisms in normal conditions, cancer cells often evolve mechanisms to break this cycle and overcome immune surveillance. Tumour tissues contain a large number of different cells, which are normally cooperating to eradicate the tumour. However sometimes the same types of cells can instead promote immune suppression and therefore cancer progression and metastasis formation. Macrophages, which are components of the innate immune system and hence represent the first defence against host damage, can for example convert from M1 antitumorigenic macrophages in M2 pro-tumorigenic macrophages, which take part in tissue vascularization and therefore help tumour growth. Treg cells or myeloid-derived suppressor cells (MDSCs) can block autoimmunity and inflammation therefore downregulating the immune response against carcinogenic cells. Cancer-associated fibroblasts are also abundant in tumour tissues and they promote tumorigenesis, vascularization and immune escape.⁸⁴

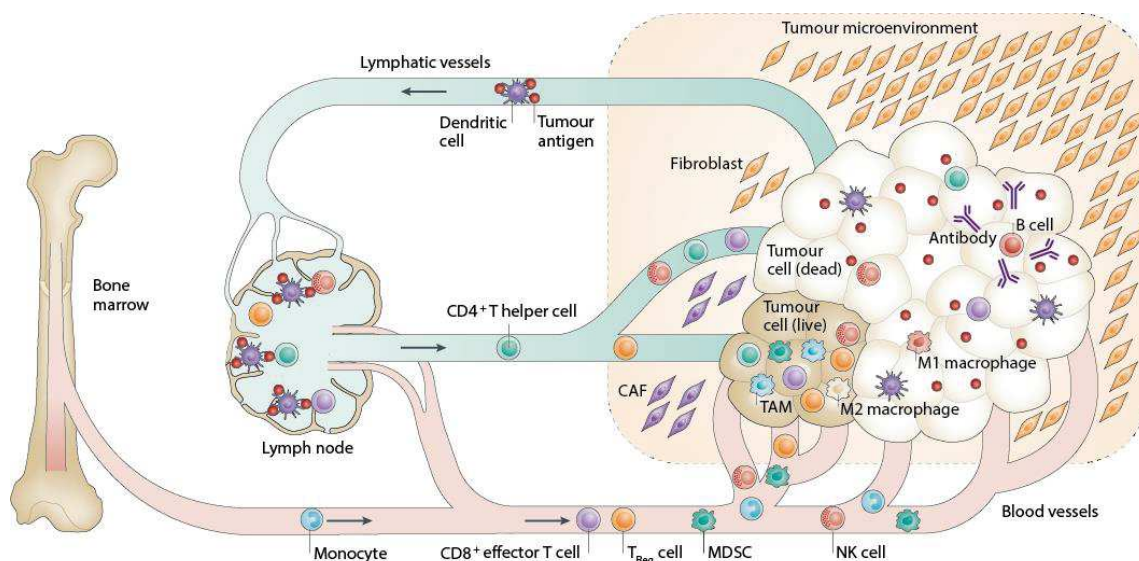


Figure 13: Illustration of the tumour microenvironment and the immune response to cancer. Figure adapted from Adams *et al.*⁸⁰

Given the extraordinary complexity and the immunosuppressive environment of tumours, targeting and silencing of these immune-blocking mechanisms is required in order to induce a positive immune response directed against cancer cells. Many strategies that are activating the immune system or removing the factors responsible for immune suppression have been

developed. These can be based on antibodies, engineered cells or even small molecules directed against specific PRRs and will be shortly discussed in the following paragraphs.⁸⁵

2.4.2 Antibody immunotherapy

Being key components of the adaptive immune system, antibodies have a very high specificity for their antigen targets and as such they can be used in cancer therapy to effectively discriminate carcinogenic from healthy cells. In the most common approach, monoclonal antibodies are used to recognize a specific antigen expressed by cancer cells.^{86–89} This recognition and binding to the cancer cell triggers in turn other pathways of the immune system that ultimately lead to cell death. Other approaches include the conjugation of antibody to cytotoxic chemotherapeutics or radionuclide, in order to combine the specificity of the antibody with the properties of the drug connected to it.^{90,91} Another application of antibodies in cancer treatment is checkpoint inhibitor therapy, whose discoverers were awarded with the Nobel Prize in Medicine and Physiology in 2018.^{92–95} In this approach, antibodies are directed against immune checkpoints, molecules that can act as controllers of the immune system. They are produced by T-cells and some cancer cells and they are able to downregulate the activity of the immune system itself, allowing these cells to escape its surveillance. When antibodies are directed against them, the immune checkpoints become inactive and the immune system activity against cancer cells is restored.

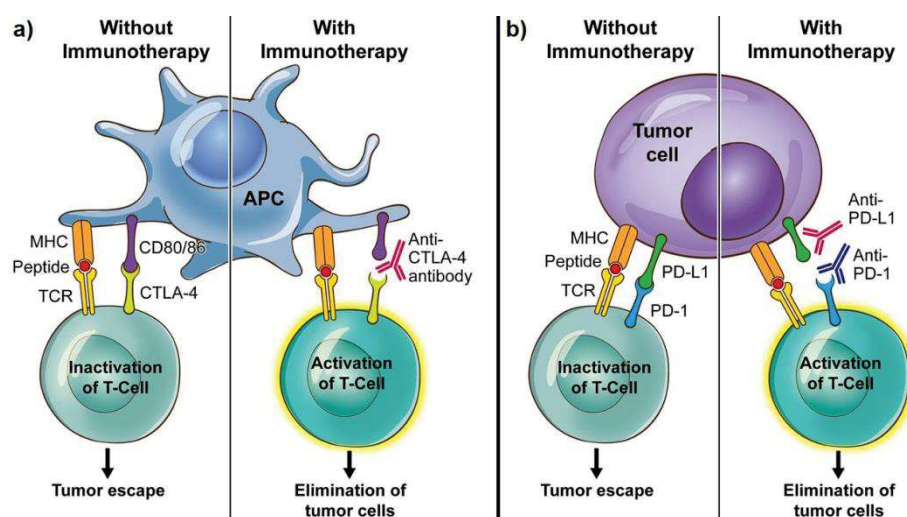


Figure 14: Immune checkpoint inhibitors. a) Anti-CTLA-4 antibody such as ipilimumab. In order to be activated, a T-cell needs to bind to the major histocompatibility complex (MHC) associated with an antigen on an antigen presenting cell (APC). At the same time, it needs to bind the CD80 or CD86 receptor with the CD28 costimulatory receptor on the T-cells. CTLA-4 competitively interacts with these receptors downregulating T-cell activation. Anti-CTLA-4 antibodies block the interaction of CTLA-4 with CD80 and CD86 favouring T-cell activation. b) Anti PD-1 or PD-L1 antibody such as Pembrolizumab or Avelumab. PD-1 is expressed by T-cells and regulates their activation while PD-L1 can be overexpressed in cancer cells. When they interact, expression of interferons and cytokines is downregulated. Anti-PD-1 or anti-PD-L1 antibodies inhibit this interaction and restore T-cell activity. Figure from Soularue *et al.*⁹⁶

The main targets of this kind of immunotherapy are the receptors CTLA-4 and PD-1, found mainly on T-cells and PD-L1 found in cancer cells. So far, a small number of antibodies targeting these receptors has been approved for cancer treatments. The first approved checkpoint inhibitor is Ipilimumab, a CTLA-4 used to treat melanoma, while inhibitors of PD-1 (such as Pembrolizumab or Nivolumab) or PD-L1 (such as Atezolizumab or Avelumab) have been approved later for the treatment of other tumours. Interestingly, the combination of two monoclonal antibodies directed against two different immune checkpoints or with PRR agonists gave better results than a monoclonal antibody alone and many clinical trials are currently undergoing further exploring this therapeutic possibility.⁹⁷

2.4.3 Cell immunotherapy

CAR-T immunotherapy represents one of the most recently developed and innovative cancer treatments currently on the market. In this approach, T-cells are harvested from a patient and genetically modified in the laboratory in order to make them produce artificial receptors that can be used against cancer cells.^{98,99} Differently from natural T-cells, these engineered cells combine the antigen recognition and the T-cell activating properties in one single receptor. The first CAR-T therapies developed and approved targeted CD19, a protein expressed in B-cells during their development, which is also overexpressed by many cancers originating from this type of cells.¹⁰⁰ Accordingly, the first two FDA-approved drugs of this class, tisagenlecleucel and axicabtagene ciloleucel were directed against acute lymphoblastic leukaemia and large B-cell lymphoma.¹⁰¹⁻¹⁰⁴ Despite being an innovative and promising new strategy to fight cancer and being a big leap towards the development of personalized medicine treatments, drawbacks of this therapy should also be considered. In addition to safety concerns because of potentially very serious side effects of these treatments, such as cytokine release syndrome which can be fatal, criticism aroused about the cost/benefit balance of CAR-T therapies, that can cost 500 thousand dollars or more for each therapy cycle.^{105,106}

2.4.4 Small molecule based approaches

In addition to the development of CAR-T or checkpoint inhibitors therapies, a large number of immunomodulatory molecules that are able to activate innate or adaptive immune system pathways have been developed, leading to the development of new strategies to fight cancer. Compared to the biological therapies described before, small molecules have the advantage of a better bioavailability, an easier access to the tumour sites and a higher capacity of crossing cell membranes, which opens to the possibility of targeting not only membrane receptors, but

also intracellular proteins and biochemical pathways.¹⁰⁷⁻¹⁰⁹ Small molecule structures can also be fine-tuned in order to control and modify their drug properties and even obtain specific cell targeting.

The use of small molecules in immunotherapy enables targeting of a wide range of biological structures, including many of the PRRs introduced before. Thanks to the ability of TLRs to trigger an immune response against tumours, their agonists are among the most intensively studied molecules to use in these treatments. Imiquimod, an imidazoquinoline derivative, is a TLR7/8 agonist that has been approved for basal cell carcinoma. Analogues of imiquimod, such as resiquimod, are currently in clinical trials for melanoma and T-cell lymphoma.^{110,111}

Small molecules allow to target many other receptors, which then directly or indirectly leads to T-cell priming and activation against tumor cells. Idelalisib, for example, was approved in 2014 for different types of leukemia. It acts by inhibiting the PI3K δ kinase, which is expressed by B-cells. The inhibition of this enzyme blocks cell proliferation of malignant B-cells by inducing apoptosis and therefore reduces tumour growth.^{112,113}

2.5 STING-targeting therapeutic agents

Because of the key role that STING plays in the regulation of the immune system, many efforts have been directed to the development of cGAMP analogues that can be used to modulate the immune system. Over-activation of cGAS or STING is for example linked to chronic inflammation and autoimmune diseases such as STING-associated vasculopathy with onset in infancy (SAVI), the Aicardi-Goutières syndrome (AGS) or systemic lupus erythematosus (SLE).¹¹⁴⁻¹¹⁹ To the contrary, the activation of STING constitutes a promising treatment option in cancer immunotherapy.^{46,120} Immunostimulatory molecules such as the type I IFNs expressed after STING activation are able to stimulate the presentation of tumour antigens therefore facilitating priming of tumour-associated T-cells. Interestingly, as observed for many other pathways associated with the activation of the immune system, the cGAS-STING pathway is also downregulated in various cancer types, which can facilitate tumour progression. The use of STING inhibitors could be beneficial to suppress an hyperactive STING protein, while STING agonists would in principle allow to unleash the immune system against cancer cells, but also in the case of a viral or bacterial infection.^{118,121}

2.5.1 Small molecule STING agonists

It was discovered long ago that a STING-dependent immune response can be triggered with cytosolic DNA after cGAS activation or directly with its natural cyclic dinucleotides ligands.

In this context, small molecule STING activators have been synthesised and studied, in order to solve the poor metabolic stability and membrane permeability of nucleic acid molecules.^{121,122}

One of the first molecules tested for this purpose is DMXAA, a xanthenone derivative that has been developed and studied as a chemotherapeutic agent.¹²³ Even if preclinical tests carried out to evaluate the anti-cancer properties of DMXAA showed promising results and revealed the ability of the molecule to produce immune responses by activation of the STING pathway and interferon expression, these effects showed to be mouse specific, while human trials showed no effect. In agreement with these observations, it was discovered in 2013 that DMXAA binds only mouse, and not human STING, despite the high similarity of the two proteins.^{52,124–127} A different xanthenone derivative, α -mangostin, was instead shown to be an agonist of human STING and induce IFN expression in human cells. However, the authors showed that the potency of this molecule is approximately 10-fold lower compared to cGAMP.¹²⁸

Other small molecule STING agonists were developed, that are able to activate STING and stimulate an interferon response in human cells. Recently Ramanjulu *et al.* developed a series of amidobenzimidazole STING agonists that were able to bind to STING with a remarkable k_D of 1.6 nM. Co-crystallization of these molecules with STING showed that they are binding to STING in its open conformation, which suggests that the mechanism by which they activate the protein might be different from the physiological mechanism described before.¹²⁹ Further optimization of the amidobenzimidazole precursors, carried out independently by Xi *et al.* led to the discovery of other STING agonists with the same scaffold but with varied substituents.¹³⁰ Also using HTS methods, Zhang *et al.* discovered other small molecule agonists of STING, but their potency showed to be lower than cGAMP.¹³¹

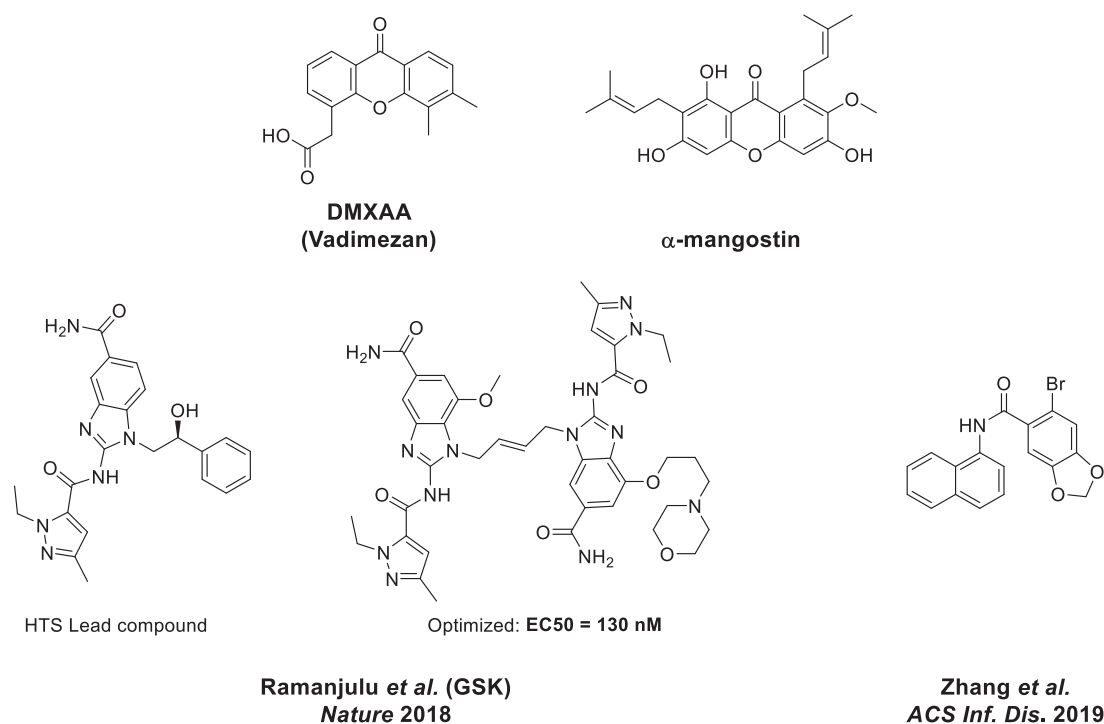


Figure 15: Chemical structures of selected small molecule STING agonists

2.6 Nucleoside analogues of cGAMP

Nucleoside analogues of cGAMP have the advantage of keeping the main features of the natural bioactive molecule, combined with a higher metabolic stability or better drug delivery properties. Many strategies have been explored so far by companies or university research groups in order to create CDN STING agonists that are more stable in physiological conditions or that can be delivered to cells more easily.

2.6.1 Replacement of the phosphodiester

The first efforts towards the development of cyclic dinucleotides STING agonists involved the replacement of the phosphodiester with biologically more robust moieties. Phosphorothioates, in which the negatively charged oxygen atom of a phosphate is replaced with a negatively charged sulfur can be excellent options, as they are very resistant to the action of phosphodiesterases and have been already studied in the framework of siRNA and antisense therapy.^{132,133} A series of phosphorothioate cGAMP analogues have been synthesised and tested in biochemical and biological assays.^{134–137} In particular, the 2',3'-cG^SA^SMP showed similar binding affinity to STING compared to cGAMP and produced 10 times more interferon in THP-1 monocytes compared to the natural STING ligand, mainly because of its higher metabolic stability.

Another phosphate analogue, which has been used in prodrugs or RNAi drug development is the boranophosphate. This chemical group also retains the negative charge, but possesses better membrane crossing properties, compared to phosphates and phosphorothioates.^{138,139} cGAMP analogues in which the phosphates have been replaced by the boranophosphate group have been reported recently.¹⁴⁰ They showed to be good agonists, able to activate STING with a potency similar to cGAMP and at the same time they also showed higher stability when exposed to ENPP1. With the goal to increase the cell permeability of cGAMP analogues by reducing the negative charges of the molecule, recently the first neutral nucleoside analogues of cGAMP containing urea, thiourea, amide and triazole linkages have been reported.^{141,142} While urea and thiourea analogues induced interferon expression in THP-1 cells, the neutral molecule containing a triazole and an amide bond replacing the phosphates did not show any binding to STING in ITC experiments despite its high similarity to cGAMP, which confirms the hypothesis that the phosphates play a key role in the protein-ligand recognition.¹⁴²

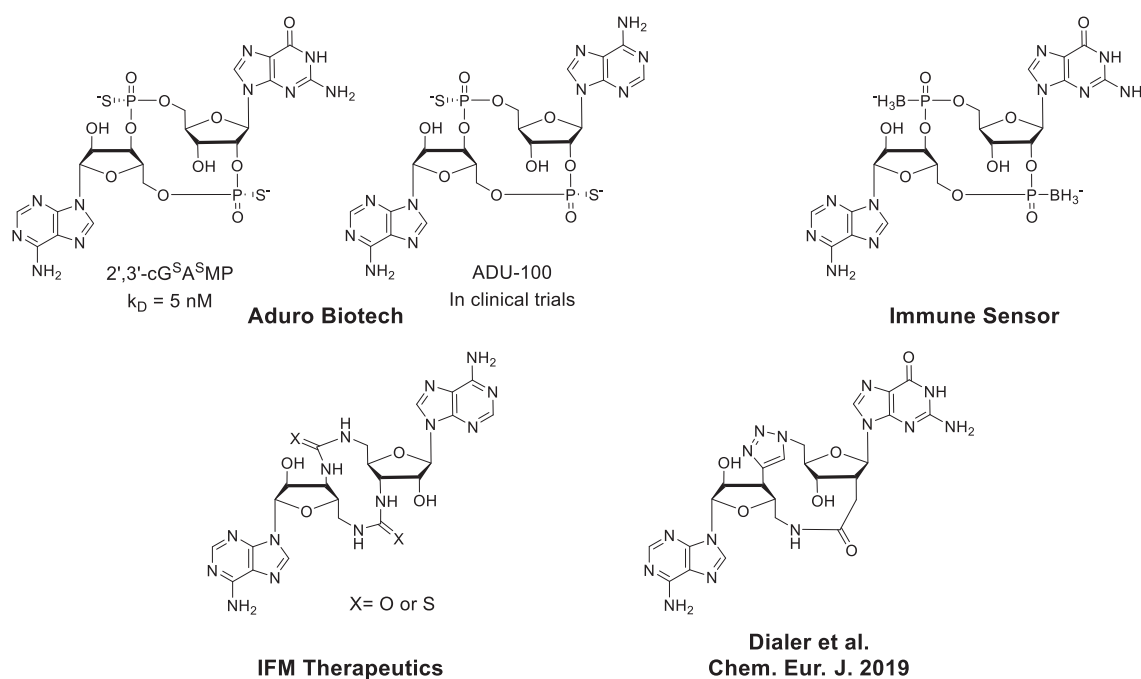


Figure 16: Examples of phosphorothioate and neutral cGAMP analogues.

2.6.2 Modification of the nucleoside moieties

Modifications of the ribose or of the base moieties of the nucleosides forming a CDN can increase the size and diversity of nucleoside-base STING agonists libraries. One of the first modifications to be applied in the synthesis of CDNs was the introduction of fluorine atoms replacing the free $-\text{OH}$ groups. This modification is frequently applied in nucleic acid therapy especially in the siRNA or mRNA-based techniques in order to increase the half-life of the

molecules or to favour a specific conformation of the ribose ring. When applied to CDNs, fluorination proved to be a viable method to increase cell uptake and STING binding of the cGAMP analogues. A c-di-AMP analogue developed and patented by Novartis which combines the substitution of the ribose –OH with fluorine atoms and the substitution of the phosphates with phosphorothioates for example showed a higher activity compared to 2',3'-cGAMP and its phosphorothioates shown in figure 16. Other modifications of the ribose rings of cGAMP included for example introduction of an azido group replacing the free 3'-OH, de-hydroxylation or various alkylations. All these modifications retained or slightly improved the potency of the cGAMP analogues increasing their resistance towards phosphate hydrolysis by phosphodiesterases or nucleases.

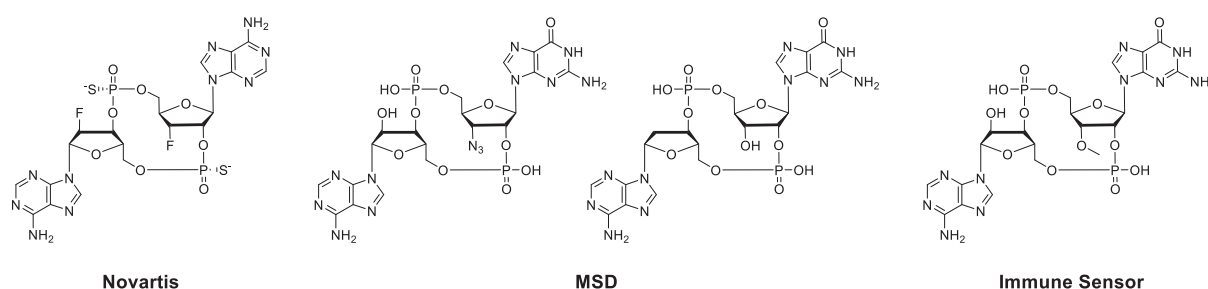


Figure 17: Chemical structures of ribose-modified cGAMP analogues.

Many efforts were also directed to the development of cGAMP analogues with modifications on the nucleobases composing the CDN. In this regard, a study from Lioux *et al.*¹⁴³ reported a series of CDNs in which the guanosine part was substituted with inosine, forming cyclic adenosine-inosine monophosphate (cAIMP) structures. In their study, they observed the highest activity for the 3',3'-cAIMP isomer, in contrast to the trend observed in the cGAMP analogues.⁵¹ In agreement with the other approaches showed before, they were able to increase the potency of their CDN by substituting the phosphate with phosphorothioates and by introducing two fluorine atoms in place of the 2' and 3' free –OH groups, obtaining an EC₅₀ value of 0.4 μM.

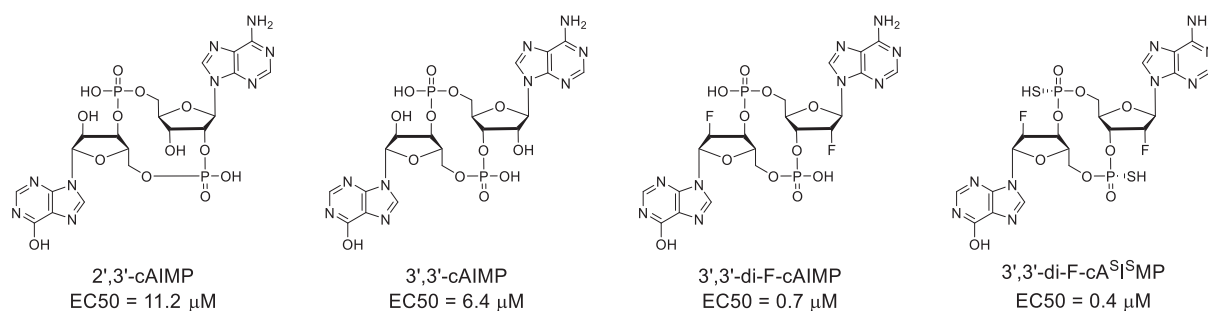
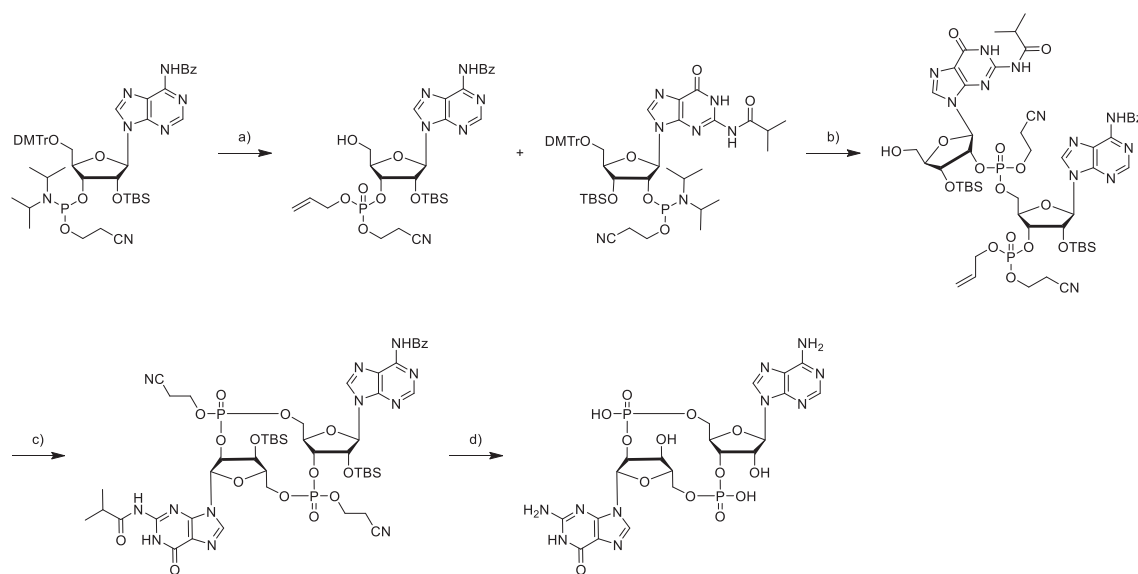


Figure 18: Chemical structures of cGAMP analogues containing inosine (cAIMP derivatives).

2.7 Drug delivery of negatively charged molecules: prodrugs

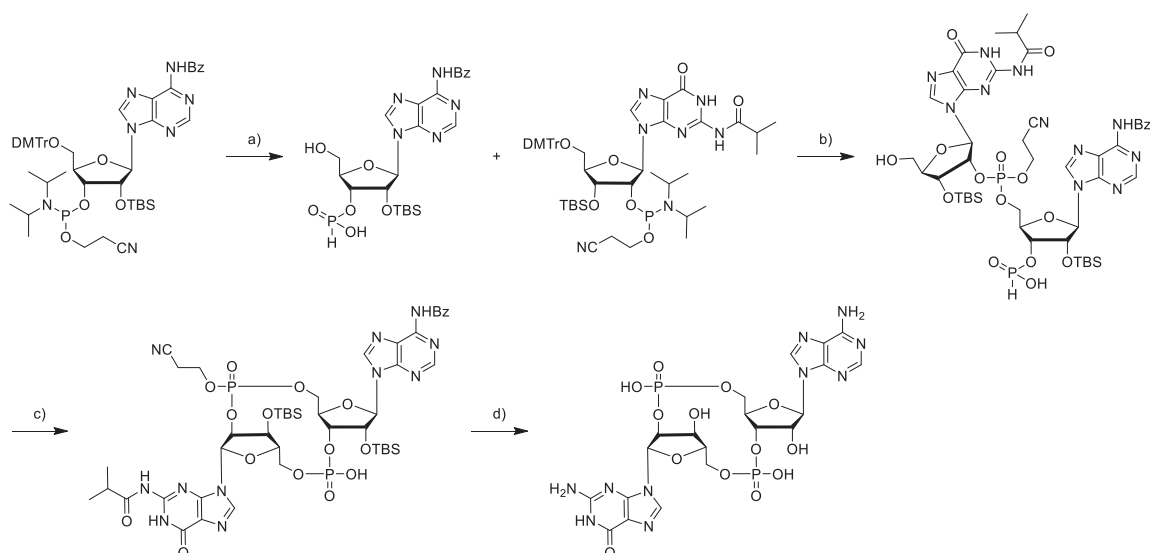
Despite the high potential of negatively charged molecules such as nucleic acid-based ones, these molecules often have the drawback of not being directly usable as drugs because of their unsuitable physicochemical properties. Among the many techniques that have been developed over time in order to solve the problems of membrane permeability and metabolic stability is the prodrug technology. It proved to be a valuable tool to achieve efficient drug uptake of negatively charged molecules.¹⁴⁴⁻¹⁴⁶ A prodrug contains chemical groups that are designed to mask moieties that could give problems during circulation in body fluids and uptake by target cells. An example of the prodrug working principle is the antiviral drug sofosbuvir as shown in figure 19 and explained below.¹⁴⁷⁻¹⁴⁹ The active form of sofosbuvir is its triphosphate, that can inhibit replication of the Hepatitis C virus. Being negatively charged, as mentioned before, free phosphoesters cannot be used directly because they are not able to enter cells easily. A first route to overcome this challenge can be the use of the free modified nucleoside that can be mono- and then tri-phosphorylated inside the cell thanks to the action of kinases. This strategy is however often not applicable because of the slow rate of the first phosphorylation step, which can sometimes completely fail, especially in the case of heavily modified nucleosides.¹⁵⁰ The second and more widely used possibility is the prodrug technique, where a chemically modified monophosphate is used in place of the free nucleoside. The chemical groups on the phosphate can be cleaved typically very fast by a series of enzymatic or chemical reactions that ultimately lead to release of the free monophosphate into the cytosol. This monophosphate can then be easily recognized by other kinases that add two more phosphates leading to the active form of sofosbuvir, that can now exert its biological action.

to P(V) using *t*BuOOH and then 5'-DMTr deprotection. The second phosphoramidite can now react with this building block and then the P(III) is also oxidised to P(V), yielding the linear dinucleotide. After deprotection of the 5'-DMTr group and removal of the allyl protecting group on the terminal phosphate, a final cyclization step can be carried out that proceeds via phosphate activation. The exocyclic amines of the nucleobases and the -OH groups on the ribose moieties can be finally deprotected with triethylamine/HF to yield the free cGAMP (Scheme 1).



Scheme 1: cGAMP synthesis based on phosphoramidite and phosphate chemistry. a) 1: BTT, AlIOH, 2: *t*BuOOH, 3: 3 % DCA/DCM; b) 1: BTT, 2: *t*BuOOH, 3: 3% DCA/DCM; c) 1: NaI/acetone, 2: TPSCl, N-methylimidazole, 3 Å MS; d) 33 % MeNH₂ in EtOH.

In the second approach, the starting materials are the same two phosphoramidites seen before. One of the two is in this case hydrolysed to an H-phosphonate and deprotected from both the 5'-DMTr and the cyanoethyl group. The second phosphoramidite can now be coupled with the deprotected H-phosphonate and after DMTr removal from the linear dimer, a final cyclization can be performed using H-phosphonate chemistry. Final deprotection can be finally carried out as described above to afford cGAMP (Scheme 2).



Scheme 2: cGAMP synthesis based on phosphoramidite and H-phosphonate chemistry. a) pyridine trifluoroacetate, H_2O , 2: $t\text{BuNH}_2$, 3: 3 % DCA/DCM; b) 1: MeCN, 2: 3 % DCA/DCM, 3: $t\text{BuOOH}$; c) 1: DMOCP, 2: $\text{I}_2/\text{H}_2\text{O}$; d) 1: $t\text{BuNH}_2$, 2: MeNH₂, 3: HF/triethylamine.

The advantage of the second methods is that all reactions can be performed sequentially in one pot, with no need to purify the intermediates by column chromatography. In the first method, at least 3 column chromatography purification steps are required, which prolongs the time needed to obtain the final product, but also makes possible to obtain a cleaner final product.

2.8 Aim of the project

Because of their ability to activate the innate immune system, analogues of cGAMP hold a great promise in medicinal chemistry and could be excellent drug candidates to be used in cancer immunotherapy or as vaccine adjuvants. However, the natural STING ligand itself does not possess the required properties that would allow it to be used as a drug. Being negatively charged, in fact, the molecule is not able to easily cross the cell membrane, which contains an also negatively charged phospholipid bilayer. In addition to this, as described in the introduction, the natural phosphate bonds can be easily hydrolysed by human or viral enzymes, leading to the cycle opening and ultimately to the release of AMP and GMP. For this reason, molecules that can still activate STING, but that feature more desirable chemical and biochemical properties are sought-after.

The goal of the first part of this chapter was to design and synthesise a series of cGAMP analogues based on the general 2',3'-cyclic dinucleotide scaffold that characterizes 2',3'-cGAMP. These molecules retain the main structure of the STING substrate, but contain small structural variation on the ribose or on the nucleobase moieties. We also performed biochemical and cellular test of the synthesised analogues in THP-1 monocytes in order to evaluate the potency of the synthesised analogues.

In the second part of this chapter we aimed to perform a chemical derivatization of cGAMP analogues in order to mask the negative charges on the phosphate moieties with biologically cleavable chemical groups. This allows to make the molecule more lipophilic and can increase the membrane crossing abilities of cGAMP analogues. By connecting clickable linkers to the phosphates we aimed to further functionalize the analogues and achieve receptor-mediated uptake of the drug, as well as specific cell type targeting. The final goal of the project is to create an efficient delivery platform for cGAMP based on the prodrug approach, where a cGAMP molecule or one of its active analogues is taken up by target cells thanks to receptor-mediated uptake and then, when the drug has entered the cell, the natural cGAMP is released into the cytosol in order to activate STING.

3 Results and discussion

Part I- Synthesis and biological evaluation of modified cGAMP analogues

Many of the known cyclic dinucleotides (CDNs), of human or bacterial origin, have been studied in relations to their STING binding properties and ability to trigger interferon expression and many analogues containing one or more modifications of the CDN structure were synthesized.¹²¹ However, a reliable synthetic pathway leading to cGAMP analogues containing modification on the two ribose halves, as well as a study describing how these modifications influence STING binding or metabolic stability of the analogues is currently lacking. Therefore, a first goal of this PhD work was to design and synthesise a series of 2',3'-cyclic dinucleotides in order to perform a structure-activity relationship study to evaluate how each modification can affect STING-ligand interaction.

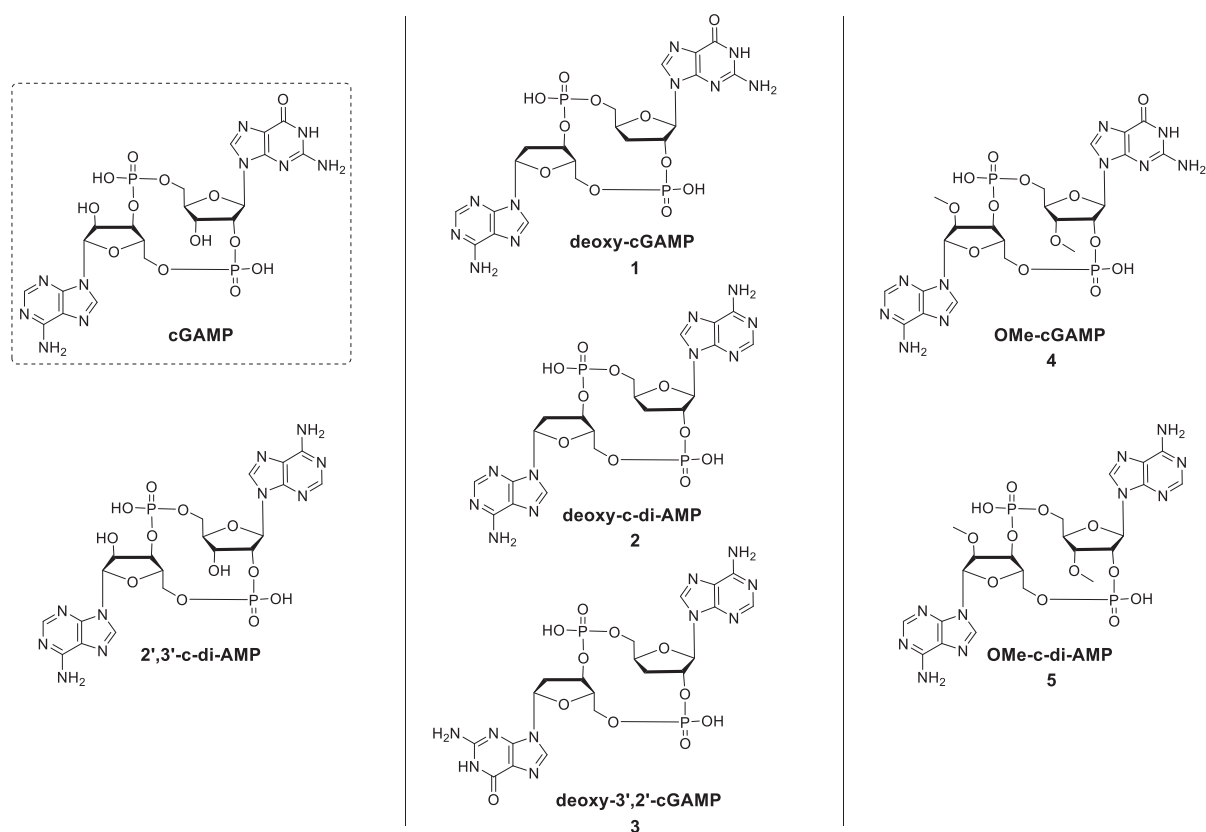


Figure 20: Chemical structure of cGAMP and the designed analogues.

The library of compounds designed is composed of cGAMP and 6 other cyclic dinucleotides containing two adenosines or one adenosine and one guanosine. Furthermore, we decided to modify symmetrically the two halves of the CDN with methylation or complete removal of the 2' and 3' -OH groups which leads to simplified cGAMP analogues. The first column in figure 20 shows the two CDNs that can be made using natural RNA nucleosides. The first is

the natural STING ligand 2',3'-cGAMP while the second is the corresponding 2',3'-cyclic diadenosine monophosphate, (2',3'-c-di-AMP). In the second column three dehydroxylated analogues are represented. All of them contain a DNA nucleoside half connected to a 3'-deoxynucleoside, maintaining therefore the 2',3'-linkage but lacking the -OH groups on the ribose ring. In this family of compounds, we synthesized 2',3'-dideoxy cGAMP (dd-cGAMP, **1**), 2',3'-dideoxy-c-di-AMP (dd-cAAMP, **2**) and 3',2'-dideoxy-cGAMP (dd-cAGMP, **3**). The last column shows instead two analogues that can be made using *O*-methylated RNA nucleosides. Compound **4** contains one guanosine and one adenosine while compound **5** contains two adenosines. Studying the STING binding properties of these compounds and their ability to induce interferon response allows to evaluate the contribution that each modification has on the protein-ligand interaction in order to find new cyclic dinucleotides cGAMP analogues. In addition to this, the synthesised molecules will also be useful for assessing which positions in the cyclic dinucleotide could be further modified in the future, maintaining at the same time a good binding affinity for the target protein. It is also noteworthy that the three cyclic dinucleotide classes (RNA, deoxy- and methylated nucleosides) are characterised by different preferential conformations of the ribose moieties,

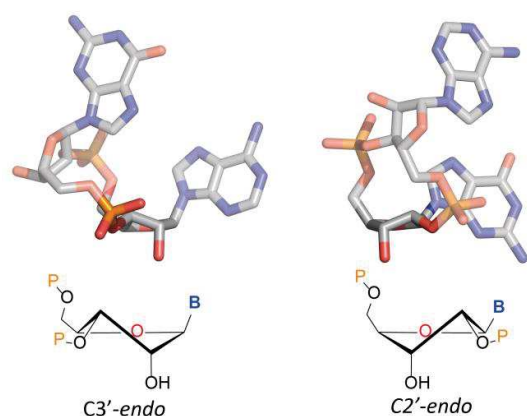


Figure 21: Conformations of the ribose moieties of cGAMP when bound to STING.

which can affect binding to STING. As it is clear from the STING-cGAMP crystal structure, in fact, the two CDN halves assume an opposite conformation. The guanosine nucleoside, containing a 2'-phosphate and a free 3'-OH assumes the *C2'-endo* conformation, while the adenosine part assumes a more canonical *C3'-endo* conformation.¹⁶¹ The introduction of deoxynucleotides and methylated nucleosides respectively confers more conformational flexibility and in principle allows to assume

slightly different conformations, that could be crucial for binding of the cyclic dinucleotides to their protein interactors.

In order to design a general strategy that could be applied for the synthesis of all the analogues, we took advantage of reactions often used in nucleoside and nucleotide chemistry and adapted them to our purpose. Because most methods in nucleoside chemistry have been developed and optimised to obtain 5'-(poly)phosphates or 3',5'-internucleosidic linkages, the most challenging step consisted in obtaining the 2',5'-phosphodiester bond which represents the key feature of cGAMP and is essential for strong STING binding. After a series of test reactions in which we compared and optimised different synthetic approaches to obtain cyclic

dinucleotides, we decided to adopt a strategy based on phosphoramidite and phosphate chemistry, which in our hands gave cleaner intermediates and an easier to purify final product. The orthogonal reactivity of the two phosphorous-containing nucleosides allows to perform chemoselective reactions, limiting by-products formation. For our synthesis, two suitably protected nucleoside precursors were chosen and one of them was turned into a 2'-protected phosphate while the other one into a 3'-phosphoramidite. We then coupled the two precursors to obtain a protected linear dimer that could be cyclized using P(V) chemistry after selective removal of one of the protecting groups on the phosphate. After macrocyclization, we performed the last deprotection step and purified the final products by HPLC to obtain the desired cGAMP analogues in high purity.

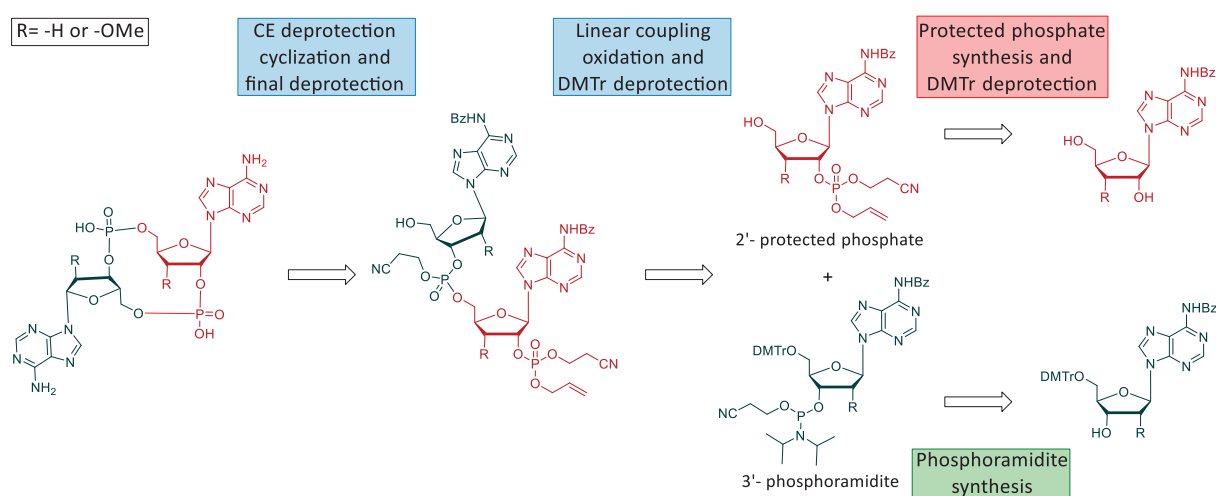


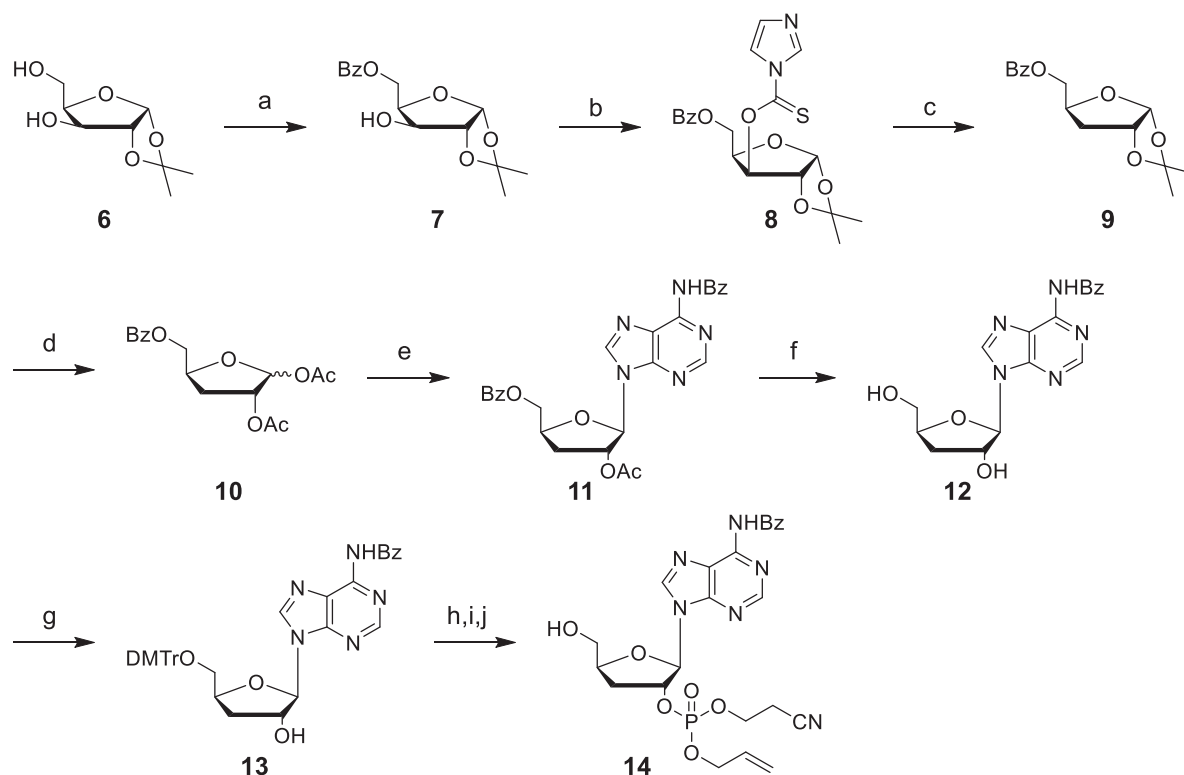
Figure 22: Retrosynthetic approach to obtain cGAMP analogues.

After purification, all the synthesised analogues were tested in biochemical assays to evaluate their STING binding parameters using isothermal titration calorimetry (ITC) or thermal shift assays (nano-differential scanning calorimetry - DSC). Cellular assays using THP-1-Dual cells in order to measure interferon expression after feeding with the analogues was also performed to confirm the bioactivity of the synthesised molecules.

In this thesis, the syntheses of the analogues **1** and **5** containing two adenosines and the synthesis of the dehydroxylated 3',2'-cGAMP **3** are described in detail, while the other compounds shown in Figure 20 have been synthesised using the same chemistry on adenosine or guanosine precursors.

3.1 Synthesis of dideoxy-2',3'-cyclic -di-AMP

The first steps towards synthesis of dideoxy-2',3'-cyclic-di-AMP **2** requires the preparation of the 3'-deoxyadenosine **12**, which can then be protected on the 5'-OH and converted in the phosphate **14** as shown in scheme 3.



Scheme 3: Synthesis of the 3'-deoxyadenosine-2'-phosphate **14**. a) BzCl , pyridine, DCM, 18h, 0 \rightarrow rt, quant. yield; b) thiocarbonyldiimidazol, imidazole, DMF, 18h, rt, 77 %; c) TMS_3SiH , AIBN, toluene, 2h30, 90 $^\circ\text{C}$, 82 %; d) AcOH, Ac_2O , cat. H_2SO_4 , 18h, rt, 61 %; e) N^6 -benzoyladenine, BSA, TMSOTf , 18h, 80 $^\circ\text{C}$, 79 %; f) 2 M NaOH, pyr/MeOH, 20 min, 0 $^\circ\text{C}$, 89 %; g) DMTrCl, pyridine, 12h, 0 $^\circ\text{C}$ \rightarrow rt, 94 %; h) 2-Cyanoethyl N,N,N',N' -tetraisopropylphosphorodiamidite, pyridine trifluoroacetate, DCM, 3h, then BTT, allyl alcohol, 1 h; i) $t\text{BuOOH}$, 40 min; j) 3 % DCA/DCM, 15 min, 61 % over 4 steps.

The first step consisted in a selective benzoyl protection of the 5-OH of the 1,2-isopropylidene xylofuranose **6**. After preparation of the thiocarbonylimidazole derivative **8** we performed a Barton-McCombie deoxygenation reaction. This deoxygenation was carried out using tris(trimethylsilyl)silane and AIBN as radical initiator, which gave the deoxyribose derivative **9** in a 82 % yield. Simultaneous deprotection of the isopropylidene and acetylation of the 1- and 2- OH provided the starting material for the base coupling step, which we carried out using a classical Vorbrüggen glycosylation procedure with silylated N -benzoyladenine and trimethylsilyl trifluoromethanesulfonate to obtain the deoxyadenosine derivative **11** in good yields. The acyl groups on the ribose were selectively deprotected using NaOH in

pyridine/methanol 4:1, which gave **12** in 89 % yield, keeping the benzoyl protection on the adenine untouched. DMTr protection of the 5'-OH gave the nucleoside **13** that was used to obtain the 2'-protected phosphate **14**. First of all, using 2-Cyanoethyl *N,N,N',N'*-tetraisopropylphosphorodiamidite and pyridine trifluoroacetate as activator, the 2'-cyanoethyl phosphoramidite could be synthesised. Isolation of this 2'-phosphoramidite resulted in poor yields and hydrolysis, therefore, we decided to directly couple the phosphoramidite intermediate with allyl alcohol using BTT to further activate the P(III) species. Oxidation of the trialkylphosphite intermediate with *t*BuOOH, followed by DMTr deprotection with 3 % DCA in DCM afforded the desired phosphate **14** in a 76.5 % yield over four steps. Overall, we were able to synthesise the adenosine phosphate building block in a 15 % yield over 11 steps. Because of the chirality of the trisubstituted phosphate, **14** was obtained as a mixture of 2 diastereomers, which was not further purified (Figure 23).

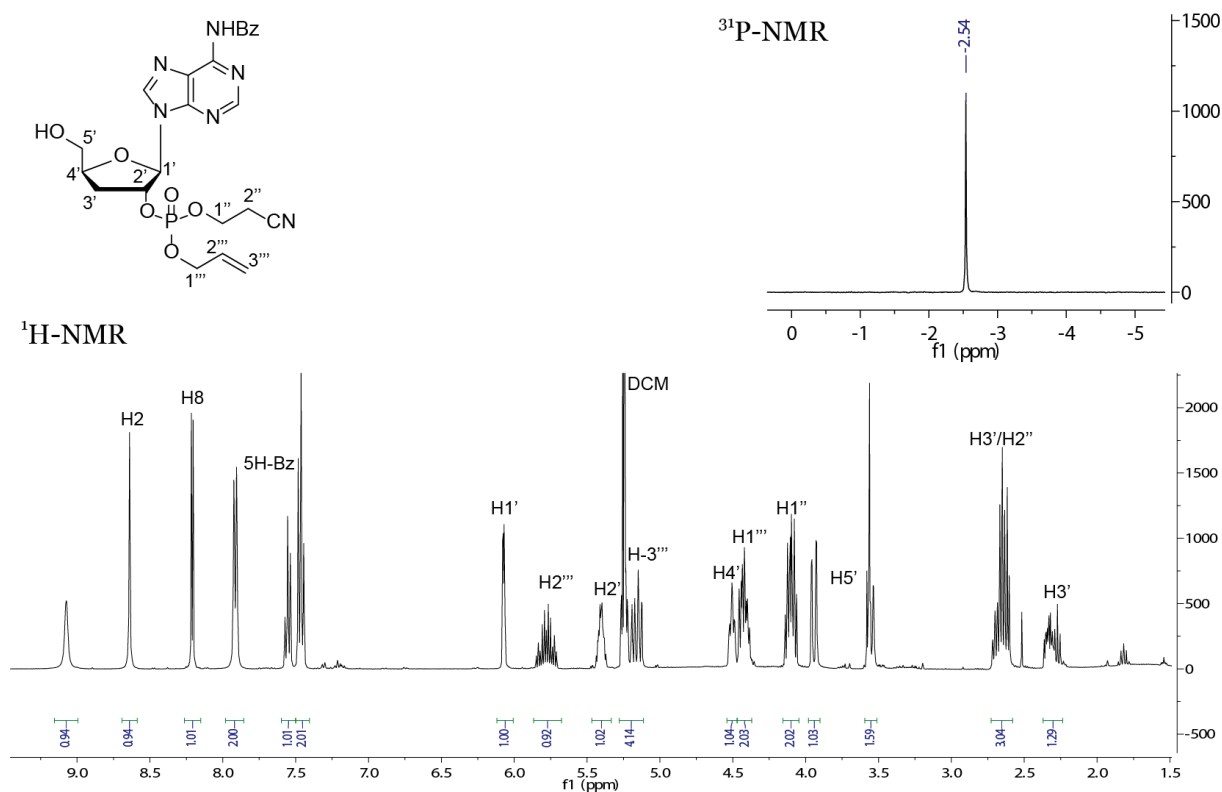
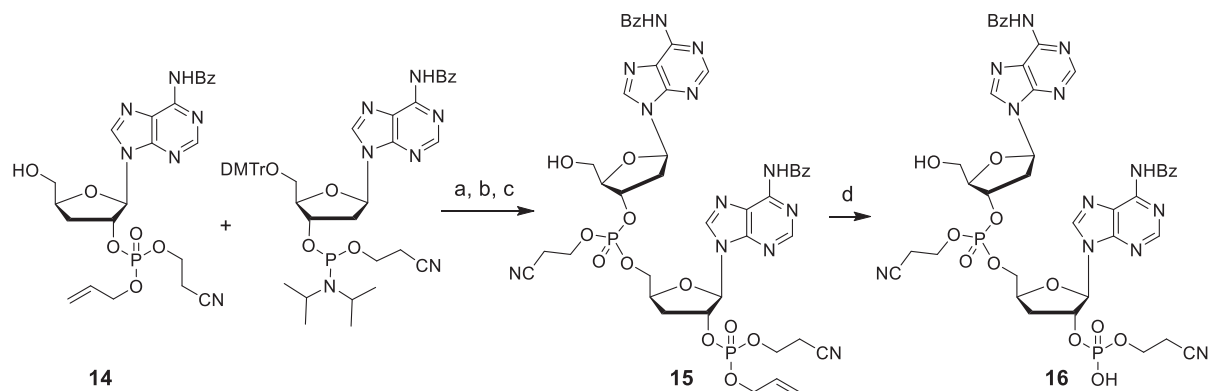


Figure 23: Structure, 400 MHz ¹H-NMR and 162 MHz ³¹P-NMR spectra of **14** (mixture of 2 diastereomers).

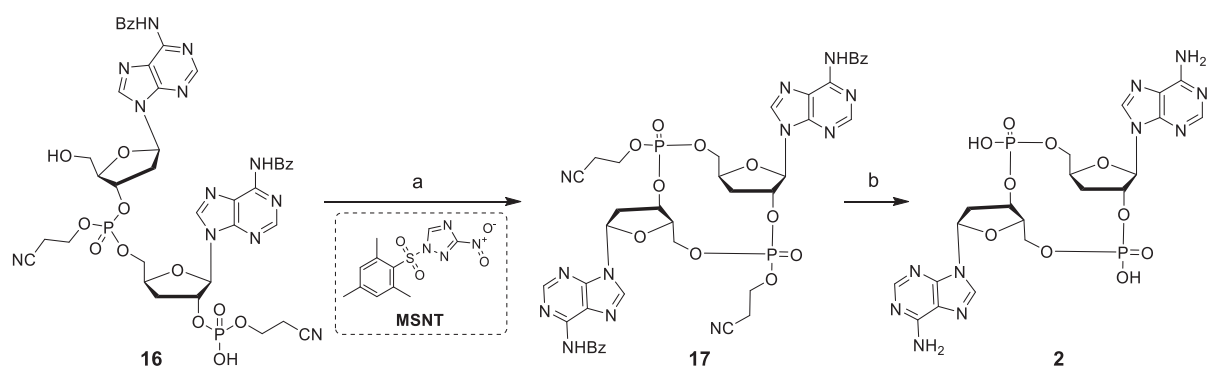
Because the second half of the designed analogue **2** consists in a DNA nucleoside monophosphate, the commercially available adenosine 3'-phosphoramidite can be coupled with the 2'-phosphate **14** in the presence of BTT. The intermediate trialkylphosphite was oxidised as shown before with *t*BuOOH and then the DMTr group was again removed in 3 % DCA to afford **15** with a 47 % yield over 3 steps after column chromatography. Because of the presence of 2 chiral phosphotriester moieties, which gives rise to a mixture of 4

diastereomers, characterisation of this intermediate by NMR was not possible at this stage. Deprotection of the allyl protective group on the phosphate was performed with sodium iodide in refluxing acetone. After precipitation of this linear intermediate, characterization of the crude product, containing 2 diastereomers, became possible (Scheme 4).



Scheme 4: Synthesis of the linear dimer. a) BTT, MeCN, 1h, rt; b) *t*BuOOH, 40 min, rt; c) 3 % DCA in DCM, 10 min, rt, yield: 60.5 % over 3 steps; d) NaI in acetone, 2h, reflux, quant. yield.

The final cyclization was performed using 1-(Mesitylene-2-sulfonyl)-3-nitro-1*H*-1,2,4-triazole (MSNT) to activate the phosphate. The reaction was followed by LC-MS and the product was not isolated, but used directly in the final step which consisted in methylamine deprotection of the nucleobases and phosphates to obtain the final dd-cAAMP **2**, which was precipitated from cold acetone and then further purified by RP-HPLC using a gradient of H₂O and MeCN with 0.1 % TFA (Scheme 5).



Scheme 5: Cyclization and final deprotection step to obtain compound 2. a) MSNT, pyridine, 18h, rt; b) 33 % MeNH₂ in EtOH, 4h, rt, yield: 28.6 % over 2 steps after HPLC.

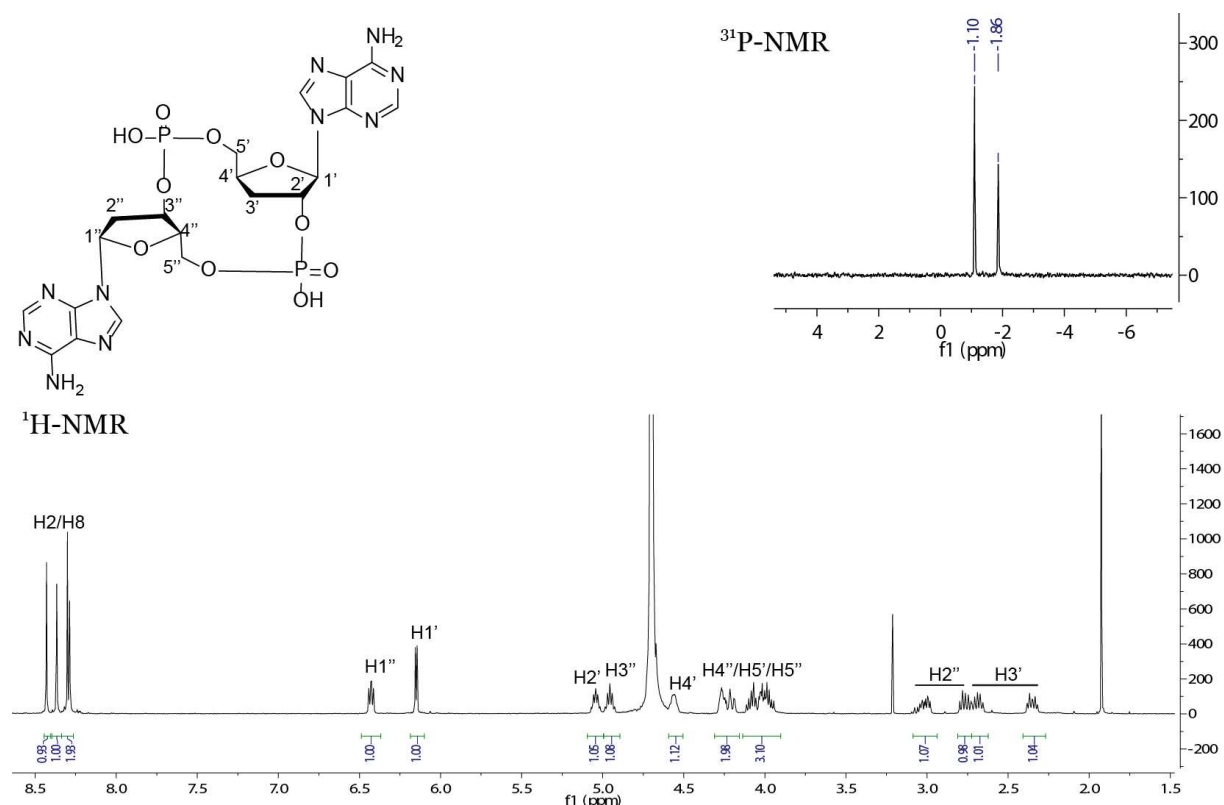
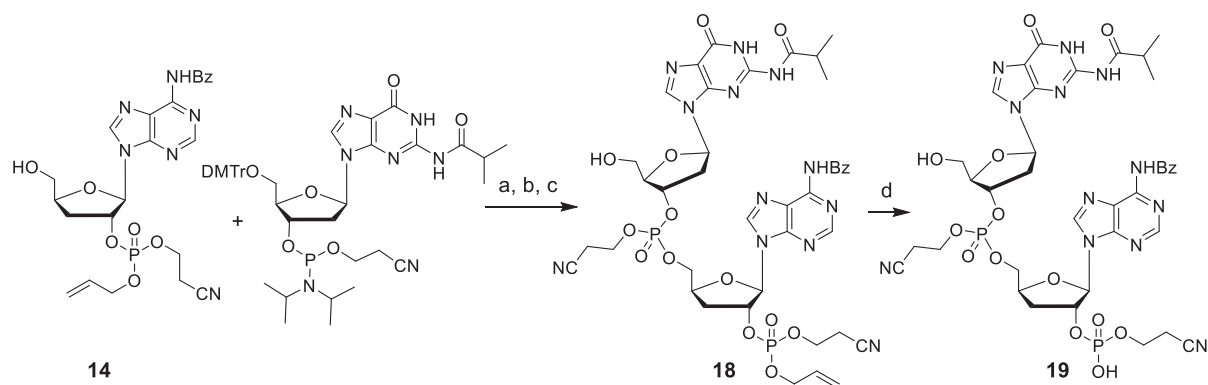


Figure 24: Structure, 400 MHz $^1\text{H-NMR}$ and 162 MHz $^{31}\text{P-NMR}$ spectra of compound 2.

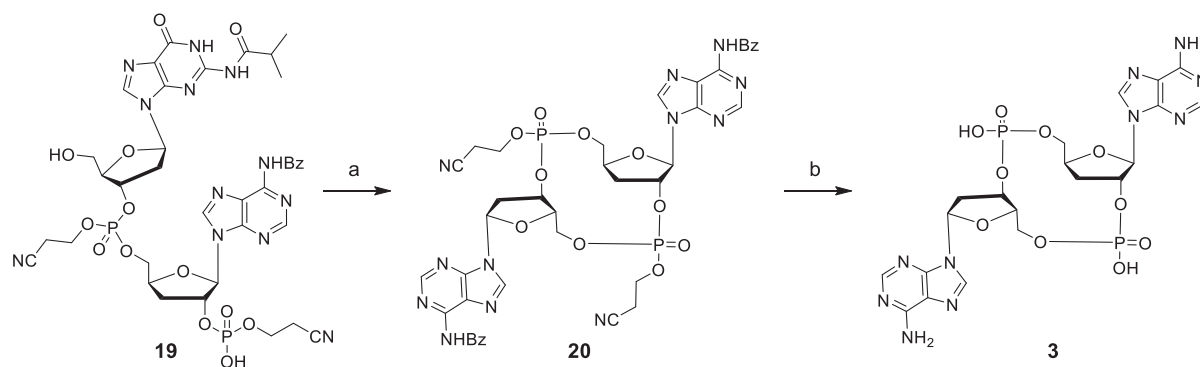
3.2 Synthesis of dideoxy-3',2'-cGAMP

Because of the higher flexibility of deoxyribonucleosides that allows this class of CDNs to assume conformations that are not favoured in natural CDNs, we decided to synthesise a “reversed” cGAMP analogue (dideoxy-3',2'-cGAMP or dd-cAGMP, **3**) to evaluate its binding to STING and cellular activity. For this purpose, we used the phosphate **14** shown before and coupled it with guanosine 3'-phosphoramidite to obtain the linear intermediate **18** that could then be deprotected on the phosphate to afford **19** (Scheme 6).



Scheme 6: Synthesis of the linear dimer. a) BTT, MeCN, 1h, rt; b) *t*BuOOH, 40 min, rt; c) 3 % DCA in DCM, 10 min, rt, yield: 39.3 % over 3 steps; d) NaI in acetone, 2h, reflux, quant. yield.

This intermediate was cyclized using the same reactions described before, deprotected and purified by HPLC, obtaining the desired analogue **3** (Scheme 7).



Scheme 7: Cyclization and final deprotection step to obtain compound **3**. a) MSNT, pyridine, 18h, rt; b) 33 % MeNH₂ in EtOH, 4h, rt, yield: 40.1 % over 2 steps after HPLC.

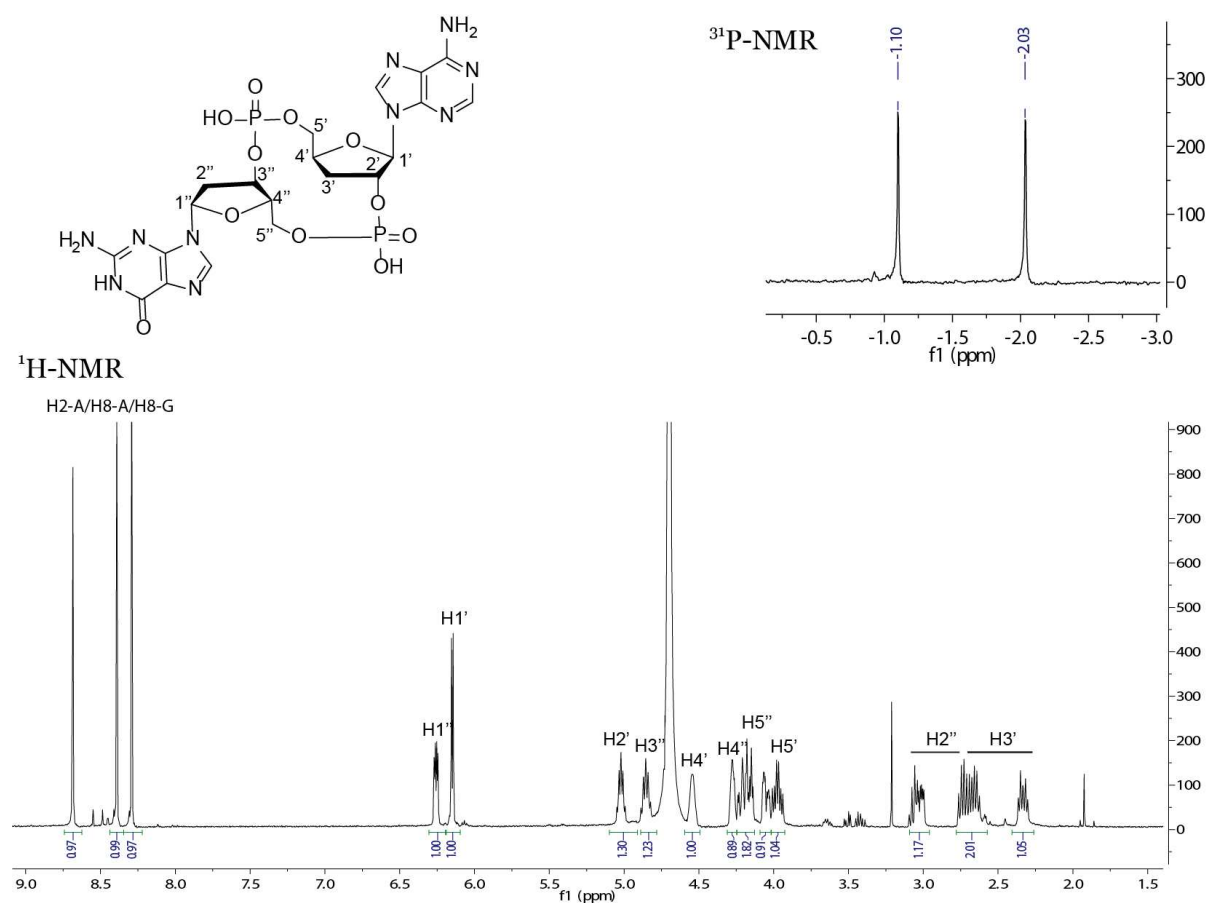
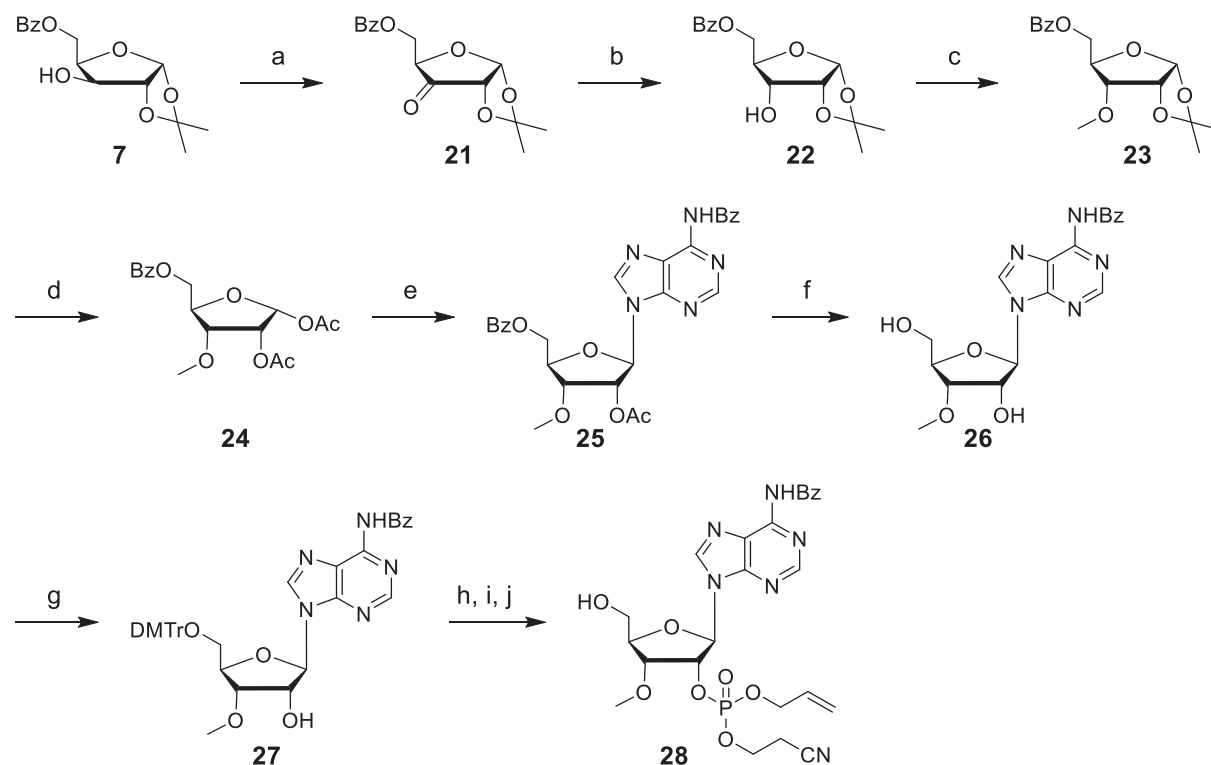


Figure 25: Structure, 400 MHz ¹H-NMR and 162 MHz ³¹P-NMR spectra of compound **3**.

3.3 Synthesis of the methylated 2',3'-cyclic-di-AMP

Similarly to the synthesis shown before, also in this case the crucial part of the synthesis consisted in obtaining the 3'-methoxynucleoside precursor, which was synthesised again starting from the 5-benzoyl-1,2-isopropylidene xylose derivative **7** as shown in Scheme 8.



Scheme 8: Synthesis of the 3'-methyladenosine 2'-phosphate. a) Dess-Martin periodinane, DCM, rt, 18h, 97 %; b) NaBH₄, THF/H₂O, 45 min, 0°C, 69 %; c) NaH, MeI, DMF, 0 °C, 3h; AcOH, Ac₂O, cat. H₂SO₄; N⁶-benzoyladenine, BSA, TMSOTf, 18h, 80 °C, 41.5 % over 2 steps; f) 2 M NaOH, pyr/MeOH, 20 min, 0 °C, 78.7 %; g) DMTrCl, pyridine, 12h, 0 °C to rt, 85.3 %; h) 1: 2-Cyanoethyl N,N,N',N'-tetraisopropylphosphorodiamidite, pyridine trifluoroacetate, DCM, 3h, then BTT, allyl alcohol, 1h; i) tBuOOH, 40 min; j) 3 % DCA/DCM, 15 min, 62.7 % over 4 steps.

Here the first step consisted in an oxidation of the 3'-OH to a carbonyl group using Dess-Martin periodinane, which allows to obtain the ketone **21**. Afterwards, **21** was reduced stereoselectively with NaBH₄, which provided us with the protected ribose **22** in a 69 % yield. **22** was methylated on the 3-OH group with an S_N2 reaction using sodium hydride and methyl iodide obtaining **23**, which was then acetylated to create a Vorbruggen structural motif and allow base coupling. Nucleoside synthesis with N⁶-benzoyladenine with the same procedure used before afforded the completely protected nucleoside **25**. We then deprotected the ribose moiety and protected again the 5'-OH with the DMTr group with good yields to obtain **27**.

Finally, with the same reaction sequence described above, the phosphate **28** could be successfully synthesised as a mixture of two diastereomers in a 40 % yield over 4 steps.

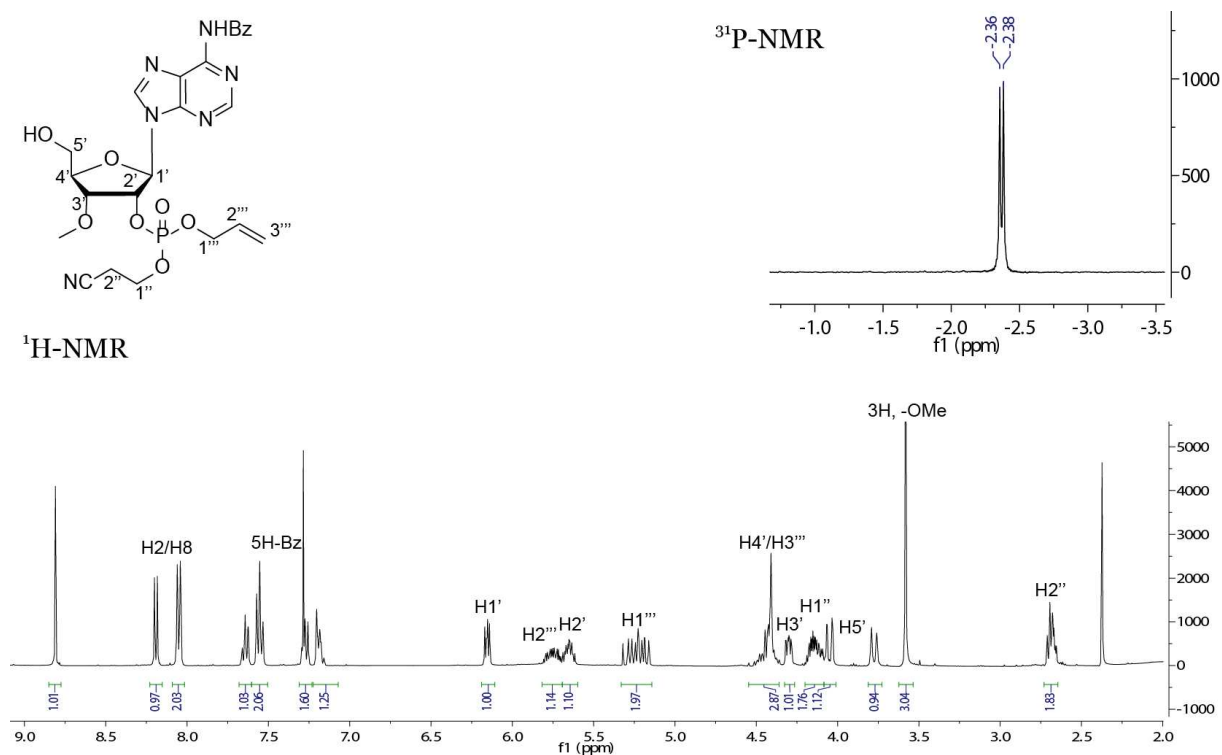
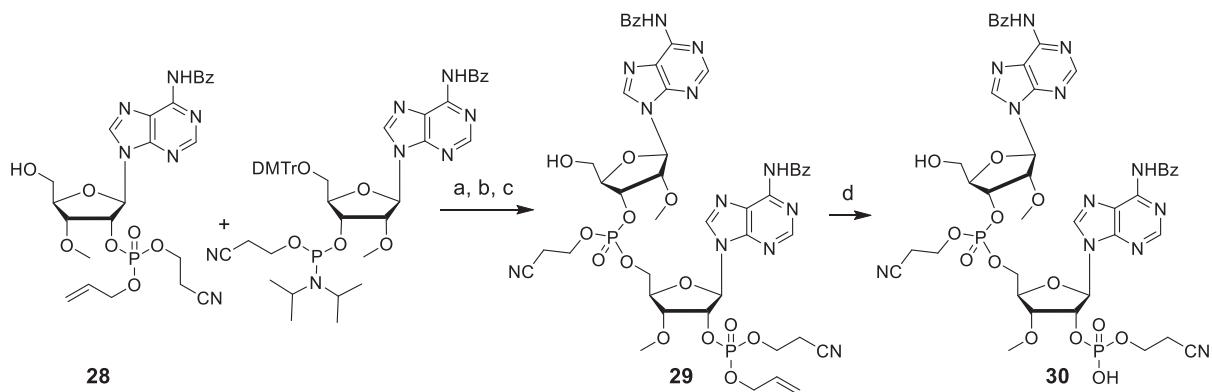


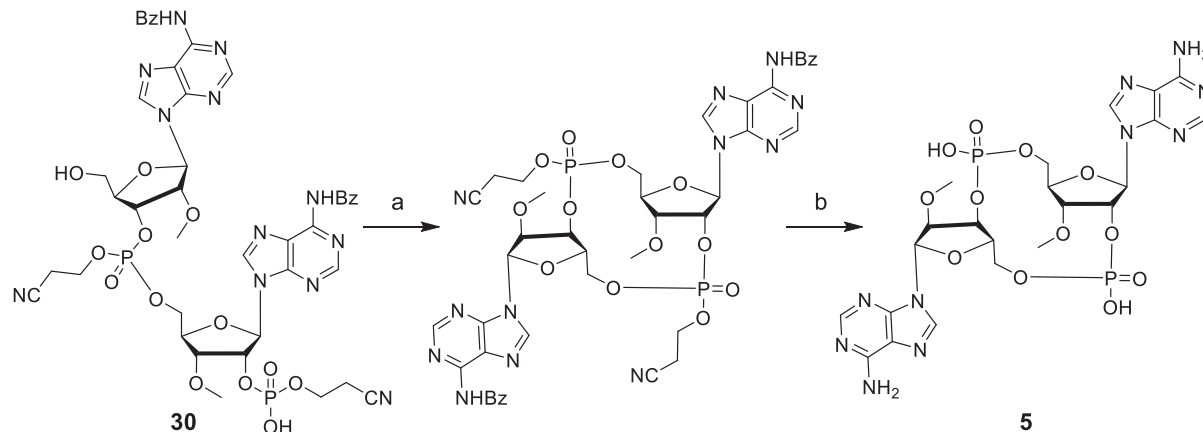
Figure 26: Structure, 400 MHz $^1\text{H-NMR}$ and 162 MHz $^{31}\text{P-NMR}$ spectra of compound **28**.

The coupling of phosphate **28** with 2'-OMe-adenosine 3'-phosphoramidite was performed using BTT as activator. Oxidation and subsequent oxidation with *t*BuOOH led to the linear dimer **29**, which was isolated by column chromatography. As mentioned before, also in this case full characterization of this product, consisting of a mixture of 4 different diastereomers, was not possible. Deprotection of the allyl group of the terminal phosphate with sodium iodide in acetone reduced the number of chiral centres to only one. It was now possible to analyse the intermediate **30** (mixture of 2 diastereomers) by mass spectrometry and NMR in order to confirm the structure of the linear dimer (Scheme 9).



Scheme 9: Synthesis of the linear dimer **29**. a) BTT, MeCN, 1h, rt; b) *t*BuOOH, 40 min, rt; c) 3 % DCA in DCM, 10 min, rt, 69.1 % over 3 steps; d) NaI in acetone, 2h, reflux, 71 %.

The final cyclization step was again carried out using MSNT in pyridine. When HPLC-MS analysis confirmed product formation the crude mixture was dried and directly dissolved in 30 % MeNH₂ in absolute ethanol leading to the final product **5**, which was precipitated from acetone and then purified by RP-HPLC.



Scheme 10: Cyclization and final deprotection step to obtain compound **5**. a) MSNT, pyridine, 18h, rt; b) 33 % MeNH₂ in EtOH, 4h, rt, 11 % over 2 steps after HPLC.

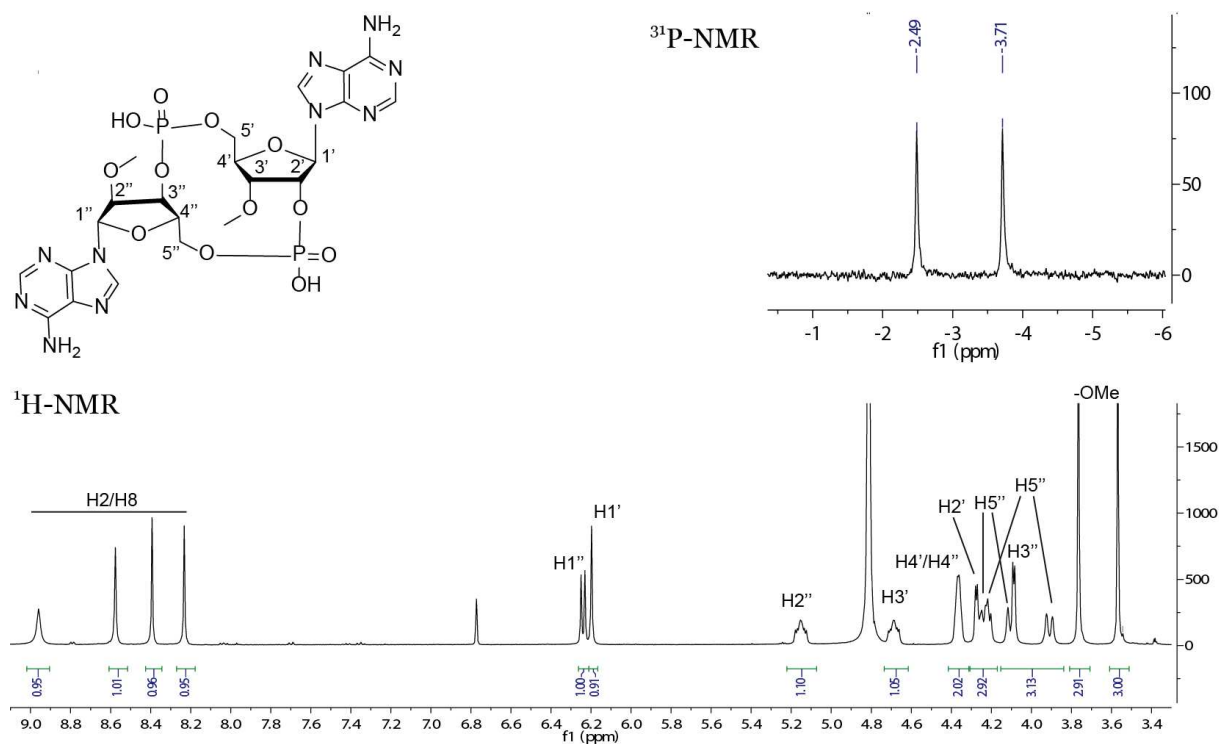


Figure 27: Structure, 400 MHz ¹H-NMR and 162 MHz ³¹P-NMR spectra of compound **5**.

In addition to the molecules described in detail here, the deoxy-2',3'-cGAMP **1** and the methyl-2',3'-cGAMP **4** as well as 2',3'-c-di-AMP were also synthesised using similar strategies, in collaboration with *F. Hernichel*, *A. Pappa* and *S. Veth*.

3.4 Biochemical and biological assays

3.4.1 Binding assays

In order to evaluate the binding properties of the synthesised analogues, in collaboration with *Dr. D. Drexler* (Prof. Hopfner group) we performed thermal shift assays. With this technique we measured the shift in the STING C-terminal domain melting temperature, which indicates that an interaction between the protein and the analogue is occurring (Figure 28).

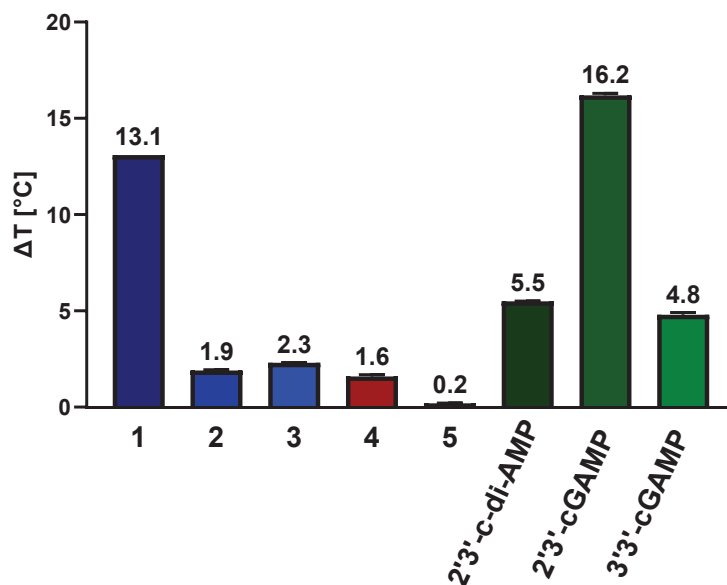


Figure 28: Results of the thermal shift assays using the C-terminal domain of human STING. Values above the bars represent the shift in the melting temperature of STING, following incubation with each analogue. The data was acquired in collaboration with *Dr. D. Drexler* (Hopfner group).

These studies showed that the synthesised analogues **1**, **2**, **3** and 2',3'-c-di-AMP interact with STING, generating a shift in the melting temperature of the protein. Analogue **1** proved to be the best binder with an induced thermal shift of 13.1 °C. Compounds **2** and **3** provoked a smaller shift in the melting temperature of STING, respectively of 1.9 and 2.3 °C, and we measured a shift of 5.5 °C for 2',3'-c-di-AMP. The methylated cGAMP analogue **4** induced a small shift in the melting temperature (1.6 °C) while **5** did not show any interaction with the protein (0.2 °C) likely because of a higher sterical hindrance that does not allow the molecule to fit into the protein binding pocket with the correct conformation. For this reason, the weakest binders **4** and **5** were not further studied in biochemical assays.

Successively we performed isothermal titration calorimetry (ITC) experiments with the dehydroxylated compounds **1**, **2**, **3** and with 2',3'-c-di-AMP in which we titrated a solution of each CDN analogue into the instrument cell containing the STING C-terminal domain. With this method we could obtain the k_D values for these four analogues (Figure 29).

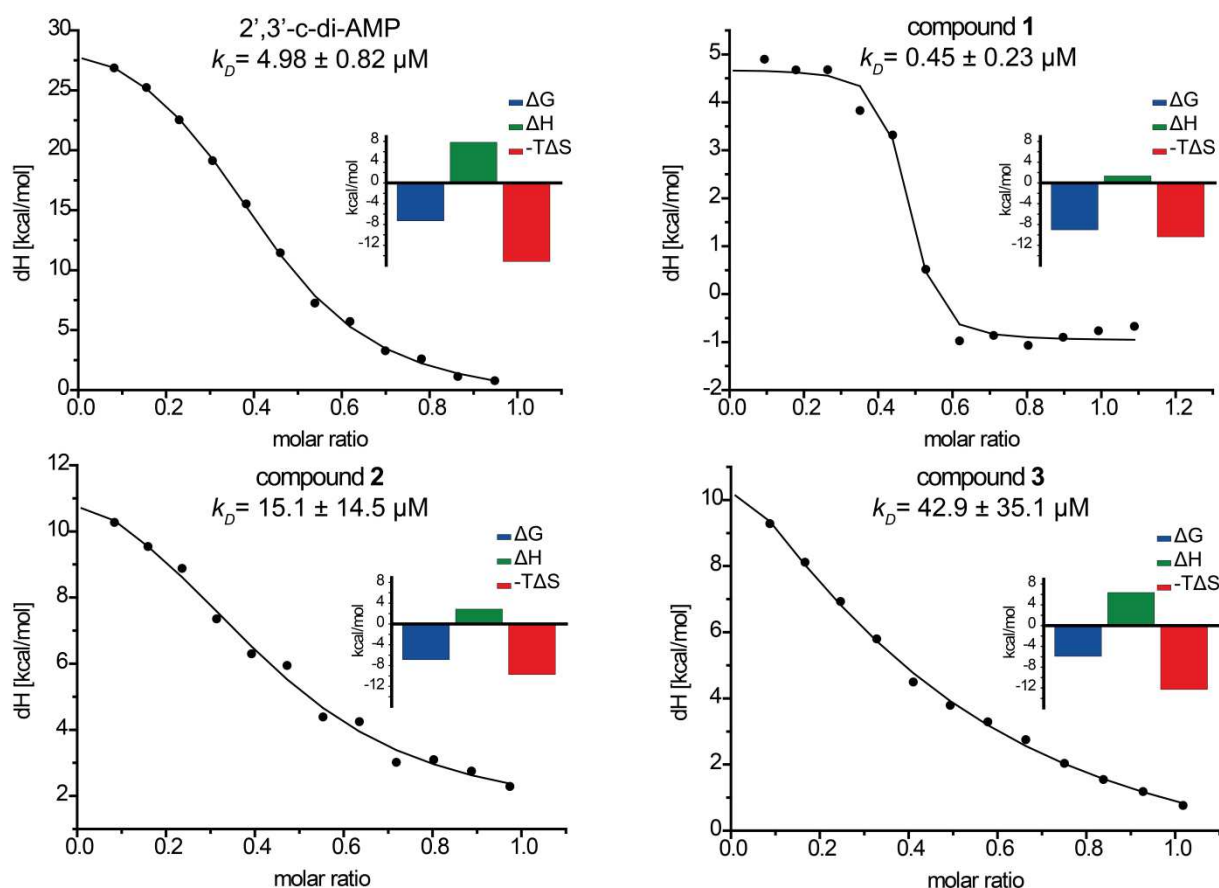


Figure 29: ITC curves and thermodynamic parameters for compound 1, 2, 3 and 2',3'-c-di-AMP. The data was acquired in collaboration with Dr. D. Drexler (Hopfner group).

According to the results of these studies, the deoxy-2',3'-cGAMP analogue **1** proved to be the strongest binder, with a k_D of $0.45 \mu\text{M}$. The other analogues showed k_D values in the μM range ($15.1 \mu\text{M}$ for **2**, $42.9 \mu\text{M}$ for **3** and $4.98 \mu\text{M}$ for 2',3'-c-di-AMP), which indicates a weaker interaction compared to both cGAMP and to compound **1**. However, previous studies showed that in the case of c-di-AMP the k_D values obtained with ITC experiments can also not be in total agreement with the activity measured in biochemical and cellular assays. In particular, Li *et al.* reported in a paper in 2019 that even if they could not measure STING binding to c-di-AMP, they could crystallize the protein-ligand complex and prove that STING itself assumes the same conformation observed when it binds cGAMP. They also show, in agreement with previous studies, that c-di-AMP triggers IFN expression in human lymphocytes.^{46,47}

3.4.2 Cellular assays

In addition to the biochemical assays described above, we tested the synthesised compounds in *in vitro* assays to evaluate their ability to induce an interferon response in immune cells. For this purpose, we used a commercially available reporter cell line derived from THP-1

monocytes. These cells contain a Lucia Luciferase gene under the control of a promoter in conjunction with 5 IFN-stimulated response elements. This allows to study the activation of the IRF pathway by simply measuring luminescence after stimulating cells with cGAMP or one of its analogues.

Initially we aimed to study the cellular activity of the synthesised analogues **2** and **5**. Therefore, we fed cells with cGAMP or with the analogues **2** and **5** at the same concentration of 100 μ M to compare the induced cellular response. After incubation at 37 $^{\circ}$ C for 24 hours, we could quantify the intensity of interferon expression for each compound (Figure 30).

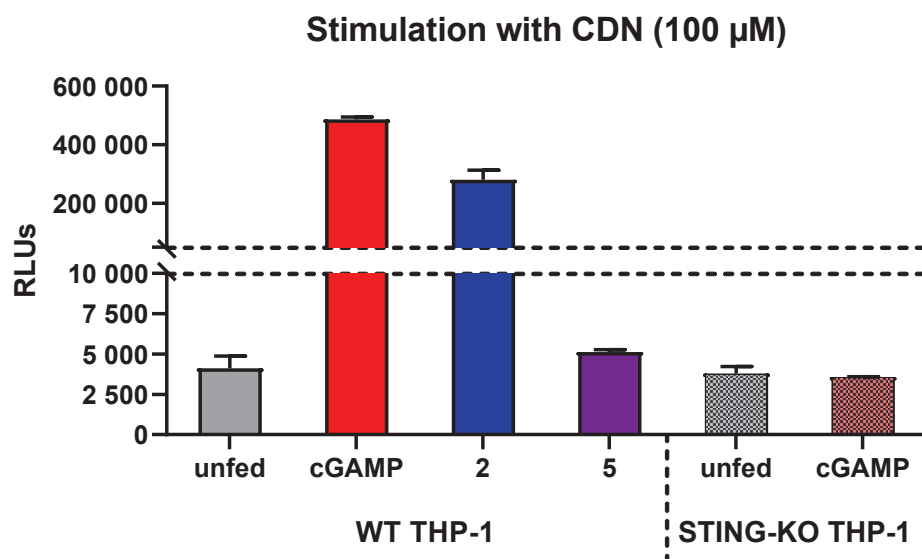


Figure 30: Measured luminescence signals after incubation of THP-1-Dual cells with 100 μ M of each CDN. RLU = Relative Light units. Data acquired in collaboration with *E. Kaminska* (Carell group)

From these data, we could successfully prove that, in addition to the natural cGAMP, also deoxy-c-di-AMP **2** stimulates IFN expression at 100 μ M concentration. Moreover, we showed that the interferon expression that we measured is STING-specific because no IFN expression was observed using THP-1 reporter cells where STING is knocked-out. However, we could not measure any luciferase activity when we incubated cells with the methylated c-di-AMP analogue **5** indicating that methylated CDNs are not able to efficiently bind to and activate STING, in agreement with the observations made in the biochemical assays described before.

We then stimulated cells with CDN concentrations ranging from 10 nM to 300 μ M in order to calculate the EC_{50} , a parameter that indicates the concentration of agonist necessary to obtain 50 % of the maximal response. The EC_{50} is an excellent estimation of the activity of an agonist, but in our case its value depends not only on the enzyme-agonist interaction, but also

on the compound stability in the cell culture medium and on the cell membrane permeability of each compound, which can be impaired by the negative charge of the CDN used for this assay.

After incubating THP-1 cells with each analogue for 24 hours, we transferred them in 96 wells plates and proceeded to measure the luminescence following the same protocol used before. We plotted the obtained values against the concentration, and normalized the luminescence values on a scale from 0 to 100 to allow direct comparison of the results. We could then fit the data to the Hill's equation using the formula:

$$Y = 100 \frac{x^{n_H}}{EC_{50}^{n_H} + x^{n_H}}$$

In this equation, n_H represents the Hill coefficient, connected to the slope of the curve. The results of this study are shown in Figure 31.

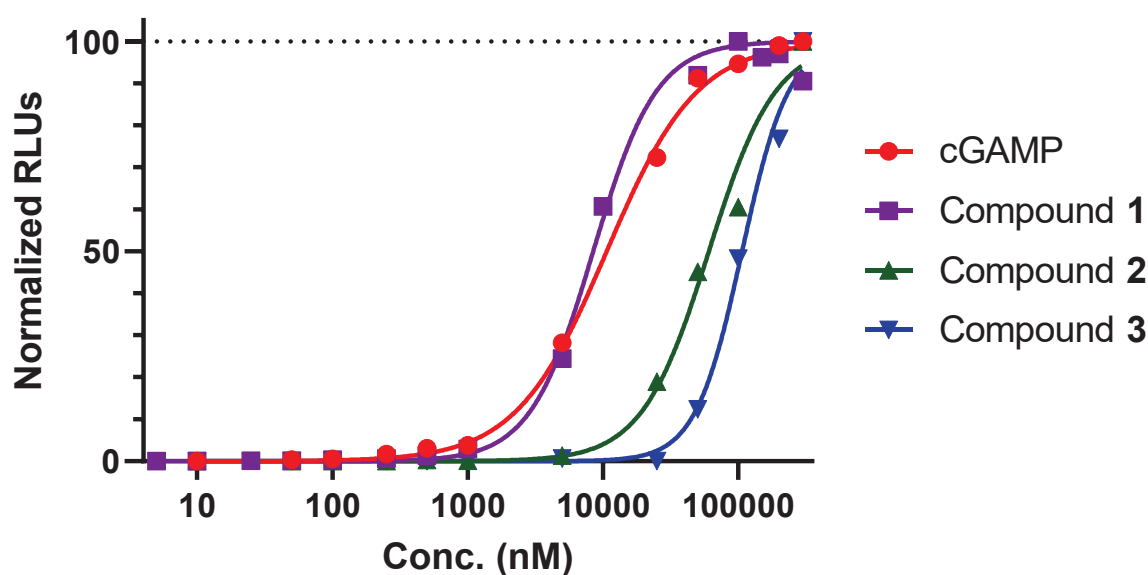


Figure 31: EC_{50} curves of compound 1, 2, 3 and cGAMP. Data acquired in collaboration with *E. Kaminska* (Carell group). EC_{50} values: cGAMP = 10.6 μ M, 1 = 8.5 μ M, 2 = 60.5 μ M, 3 = 106.5 μ M.

With this assay, the EC_{50} value for cGAMP resulted to be 10.6 μ M, which is consistent with the value reported before for an enzyme-synthesized cGAMP.¹⁶² Compounds 2 and 3 showed an EC_{50} of 60.5 μ M and 106.5 μ M respectively. Interestingly, the deoxy-cGAMP 1 unexpectedly showed higher activity (EC_{50} = 8.5 μ M) in our cellular assays compared to cGAMP. In agreement with the results of the binding assays described before, the methylated

cGAMP **4** or the methylated 2',3'-c-di-AMP **5** did not show any effect in this assay, which confirmed the very weak interaction of STING with these CDNs.

3.5 Conclusions and outlook

In this first part of the project we could successfully establish a reliable and reproducible route to obtain dehydroxylated or methylated cGAMP analogues in high purity. By adapting and optimizing reported syntheses we were able to obtain the required 3'-deoxy and 3'-*O*-methylated nucleoside precursors which were used to synthesise the 2'-phosphates. These phosphates were then connected to a 3'-phosphoramidite and then cyclized to obtain the cGAMP analogues. We were able to characterize the key intermediates and the final products by NMR and MS in order to confirm the structure of the synthesised analogues. Biochemical assays using ITC or thermal shift experiments confirmed binding of the dehydroxylated analogues **1**, **2** and **3** (k_D order: cGAMP > **1** > 2',3'-c-di-AMP > **2** > **3**). The methylated analogues **4** and **5** showed instead very weak or no interaction with STING. Cellular assays confirmed these biochemical data: in particular the dehydroxylated analogues **1**, **2** and **3** showed a good activity in THP-1 cells, with EC₅₀ values of 8.5, 60.5 and 106.5 μM, compared to an EC₅₀ value of 10.6 μM for cGAMP.

Following a similar trend to that reported for natural CDNs, analogues containing one guanosine 2'-phosphate and one adenosine 3'-phosphate bind better than analogues containing two adenosines and are more potent when used in THP-1 cell lines. For the dd-cGAMP **1** we measured an activity even higher than the activity measured for cGAMP. However, for further development the better drug properties (solubility, distribution, transport etc.) of adenosine compared to guanosine as well as higher reaction yields usually obtained using adenosine, especially in the phosphoramidite coupling steps, should also be considered.^{121,163} The 3'-2'-cGAMP analogue **3** containing a 2'-adenosine phosphate and a 3'-guanosine phosphate can still bind to and activate STING, but with a lower potency than **2** as shown by its EC₅₀. Even if methylated and alkylated analogues were shown before to bind to STING and trigger IFN expression, double methylation of the two nucleoside halves of our CDNs in compounds **4** and **5** resulted in a complete loss of activity, as we could not observe any binding to STING in ITC assays and no effect in cellular assays in THP-1 cells.

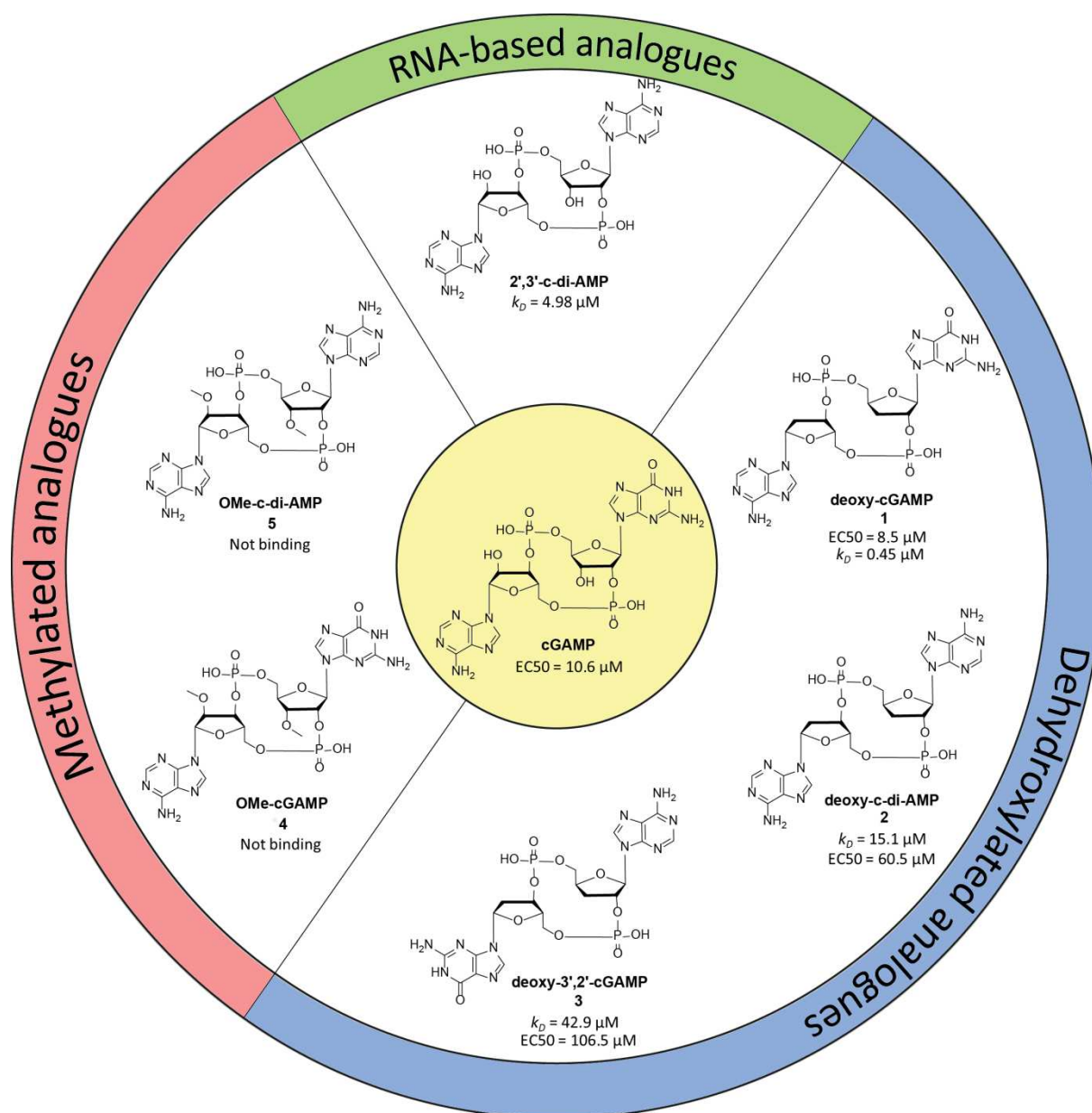


Figure 32: Summary figure showing the structures of the cGAMP analogues synthesised in the first part of this project and principal biochemical data.

Because the lack of hydroxyl groups on the 2'- and 3'-positions of the ribofuranose moiety should confer higher metabolic stability to CDNs against ENPP1 and poxins, HPLC and mass spectrometry experiments to study the degradation of the synthesised CDNs **1**, **2**, **3**, **4** and **5** are currently ongoing in collaboration with *Dr. M. Wagner*, *E. Kaminska* and *D. Özdemir* (Carell group).

Part II- Design and synthesis of cell permeable prodrugs of cGAMP analogues

In the second part of this project, we focused on cell delivery of cGAMP analogues and therefore tried to modify them in order to make them able to easily cross the cell membrane. In a first attempt, in order to neutralize the negative charge of the molecule, a macrocycle containing one adenosine and one guanosine analogues connected with triazole or amide bonds was developed.¹⁴² Despite the similarity of this analogue to cGAMP, binding studies with the soluble part of STING, as well as preliminary cellular assays in BLaER1 macrophages showed that this neutral molecule is not recognized by STING and does not induce interferon expression, confirming the importance of the phosphate-arginine interactions in the binding pocket of the protein. It was also shown that the main conformation of the synthesised neutrally charged analogue in solution, determined by NMR spectroscopy, is very different from the conformation required for STING binding (Figure 33).

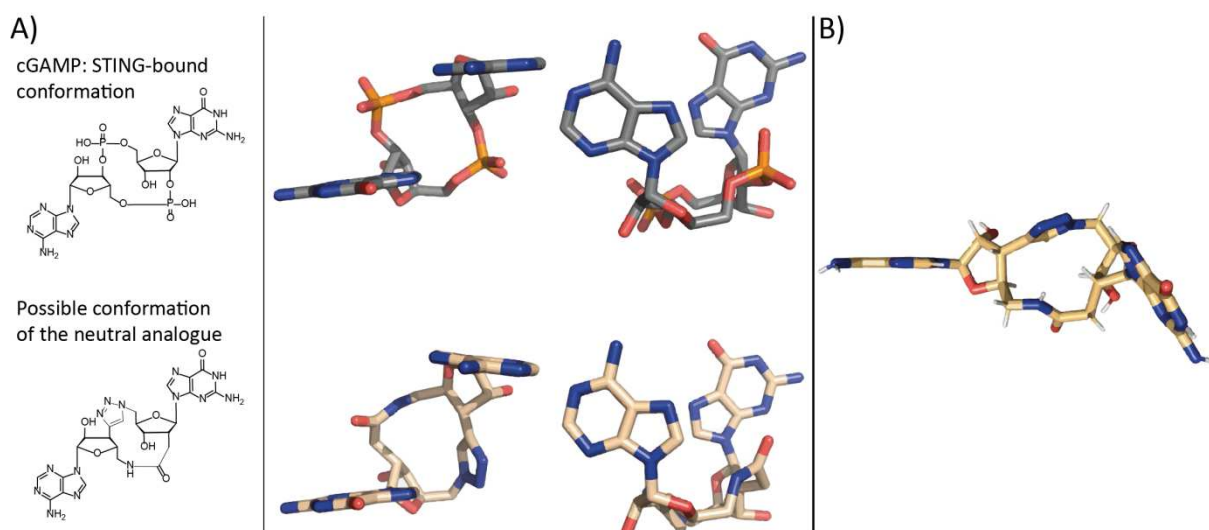


Figure 33: Comparison between cGAMP and its neutral analogue. A) 3D illustration showing the potential conformational similarity between cGAMP and the neutral analogue. B) Preferential conformation in DMSO of the neutral analogue determined by NOE-NMR studies.

In order to solve this problem and create a cell-permeable cGAMP analogue that is able to bind to STING and induce interferon expression, we decided to take advantage of the prodrug technology to make masked cGAMP analogues. For this purpose, we designed cyclic dinucleotides in which the two phosphodiester groups are substituted by phosphotriester moieties with linkers that can facilitate drug uptake and that will be cleaved inside the cell to release the free cyclic dinucleotide and activate STING as shown in Figure 34.

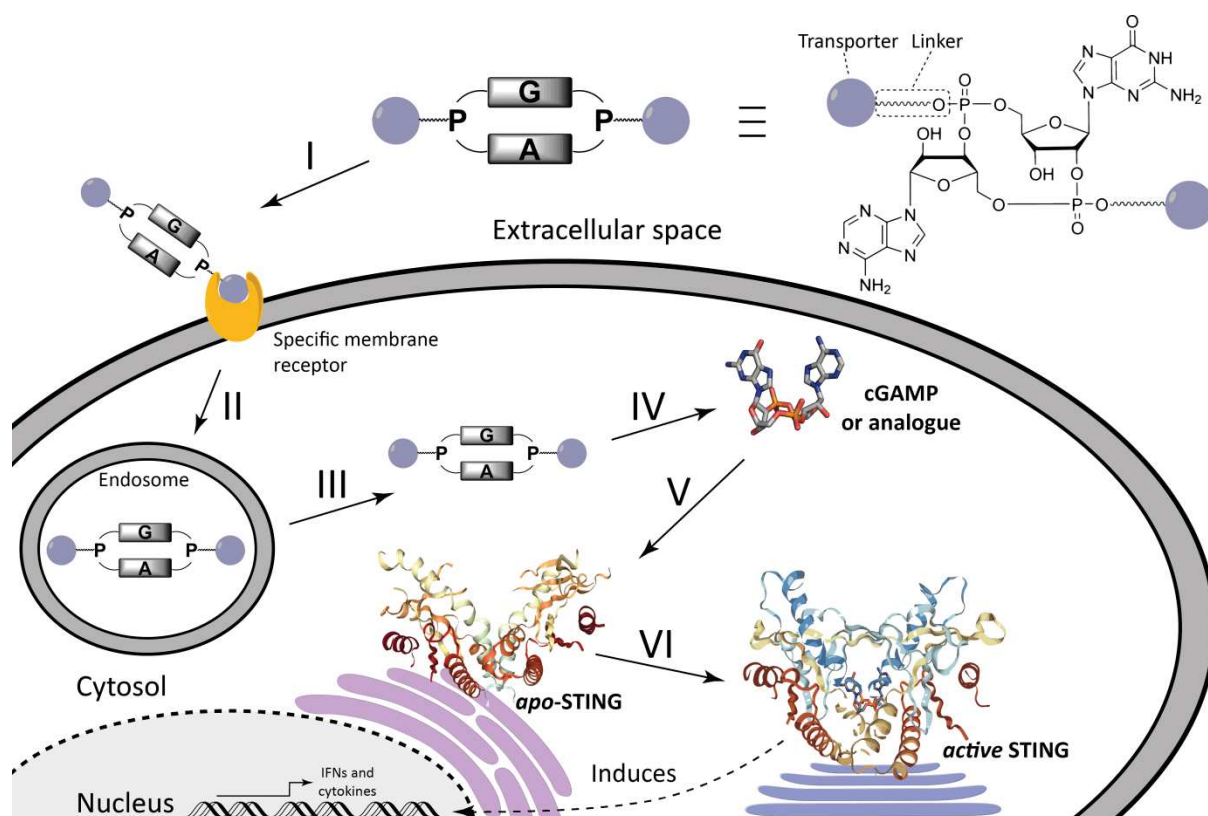


Figure 34: Illustration of the proposed CDN prodrug working principle. I) a cGAMP prodrug can interact with receptors expressed in the target cells, II) the prodrug is internalized by receptor-mediated uptake, III) After endosomal escape, the cGAMP prodrug is released into the cytosol, IV) with the action of hydrolytic enzymes such as esterases, the prodrug linker is cleaved, releasing natural cGAMP, V) in the cytosol, cGAMP can interact with STING, f) upon cGAMP binding, STING gets activated and induces IFN and cytokine expression through downstream signalling pathways.

3.6 Design of prodrugs of cGAMP analogues

To obtain release of the free cyclic dinucleotides, the caging moiety has to be carefully chosen in a way that it can be cleaved selectively, leaving the other phosphoester bonds untouched. An uncontrolled hydrolysis of the two phosphotriesters would in fact lead to the opening of the cycle and give rise to a complicated mixture of linear products which are not anymore active towards STING. For this reason, we decided to select prodrug moieties which are cleaved in the cells thanks to reactions not taking place directly on the phosphorous atom as explained in Figure 35.

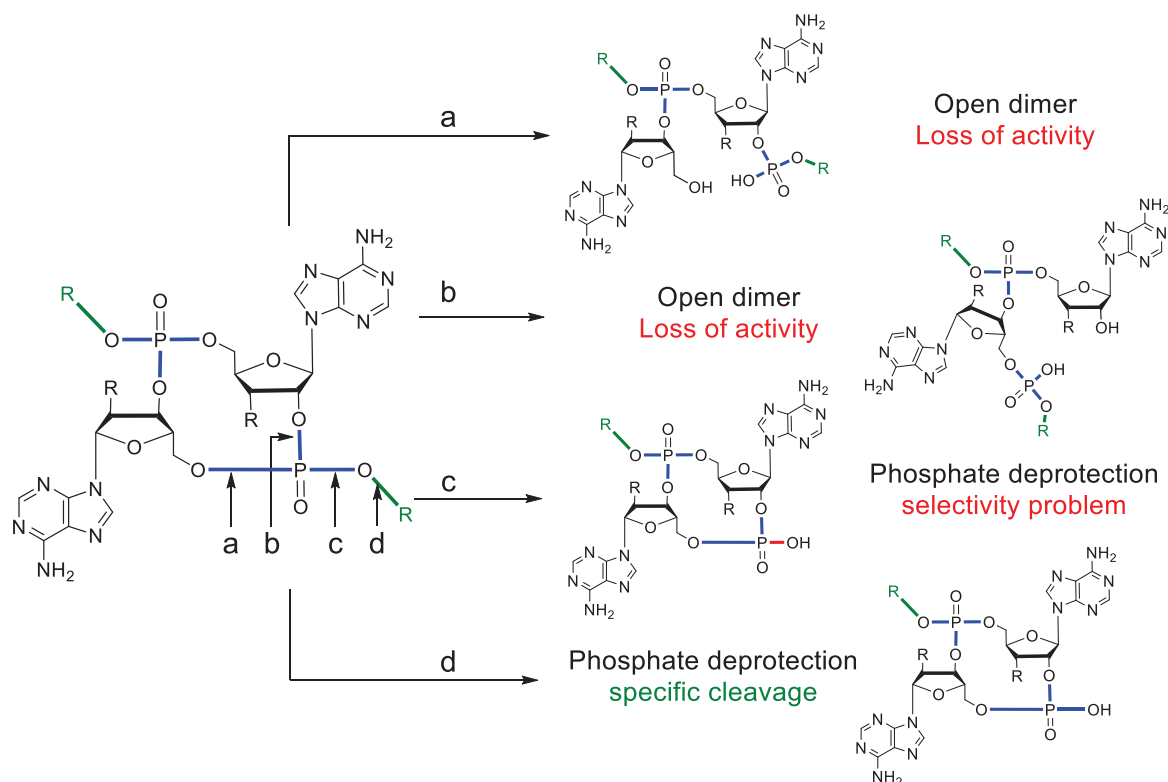


Figure 35: Possible phosphotriester cleavage pathways. a), b) cleavage of the “in-ring” phosphoesters leading to an open inactive cyclic dinucleotide; c) cleavage of the ex-ring phosphoester releasing the free phosphate. Problem: selectivity of the cleavage following attack on the phosphate; d) cleavage position of the designed CDN prodrugs. The cleavage reaction does not require nucleophilic attack on the phosphate itself.

The designed cleavage mechanism allowed us to construct a molecule that can easily enter the cell thanks to the caging groups on the phosphates and release the active cyclic dinucleotide only into the cytosol to activate STING. With this in mind, we based the structure of the caging groups on the *S*-Acyl-2-thioethyl (SATE) moiety, which contains a biocleavable thioester. The activation of these molecules proceeds *via* a first step in which the thioester is hydrolysed enzymatically by cytosolic esterase enzymes. The resulting thiol then spontaneously attacks the first carbon next to the phosphate releasing the free phosphate and a thiirane as by-product as shown in Figure 36. Furthermore, we modified the SATE linker to enable late-stage functionalization that can be achieved using click chemistry (Figure 36) to increase the membrane permeability of the synthesised masked cGAMP analogues even further.

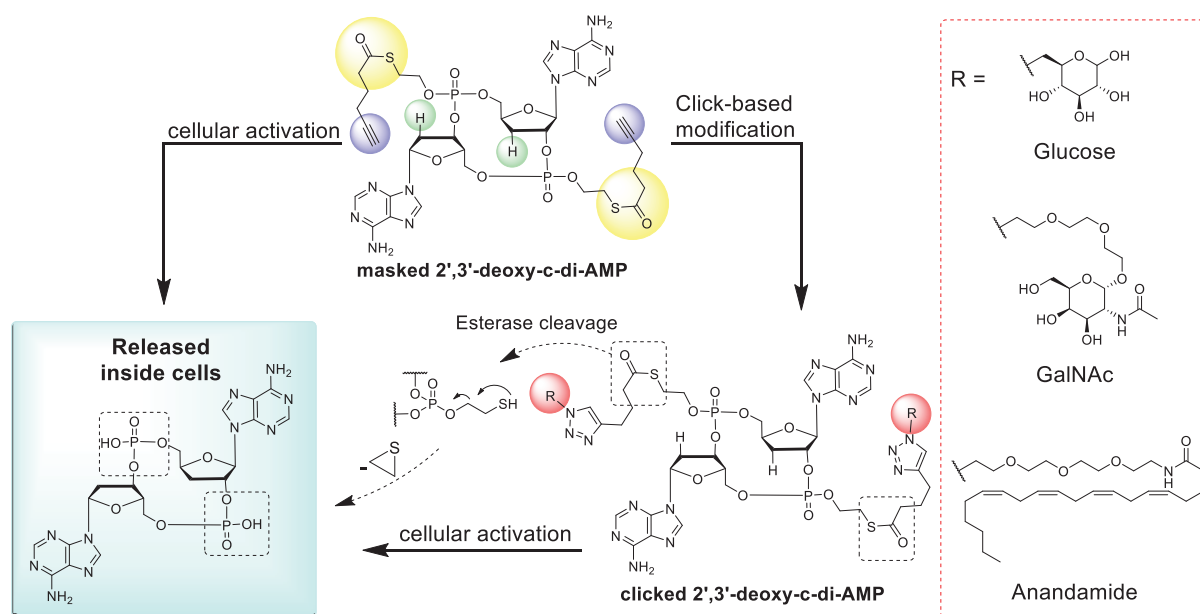


Figure 36: Design of the synthesized dd-cAAMP prodrug derivatives and pathway of activation. The key features are highlighted with coloured circles. Green: Substitution of the –OH groups with hydrogens. Yellow: biocleavable thioester. Blue: alkyne to enable functionalization via Cu(I)-catalyzed azide-alkyne cycloaddition reaction (click chemistry). Red: examples of ligands to enhance uptake of the analogues.

3.7 Synthesis of prodrugs of cyclic dinucleotides

In order to synthesise the designed prodrugs of cGAMP analogues we designed and optimized a strategy similar to the one shown in the first part for the synthesis of cGAMP analogues. We decided to use again P(V) chemistry to perform a final cyclization step from a linear dimer which can be obtained using P(III) chemistry to link a modified phosphoramidite with a protected phosphate. Suitably protected nucleosides can be used as starting materials (Figure 37).

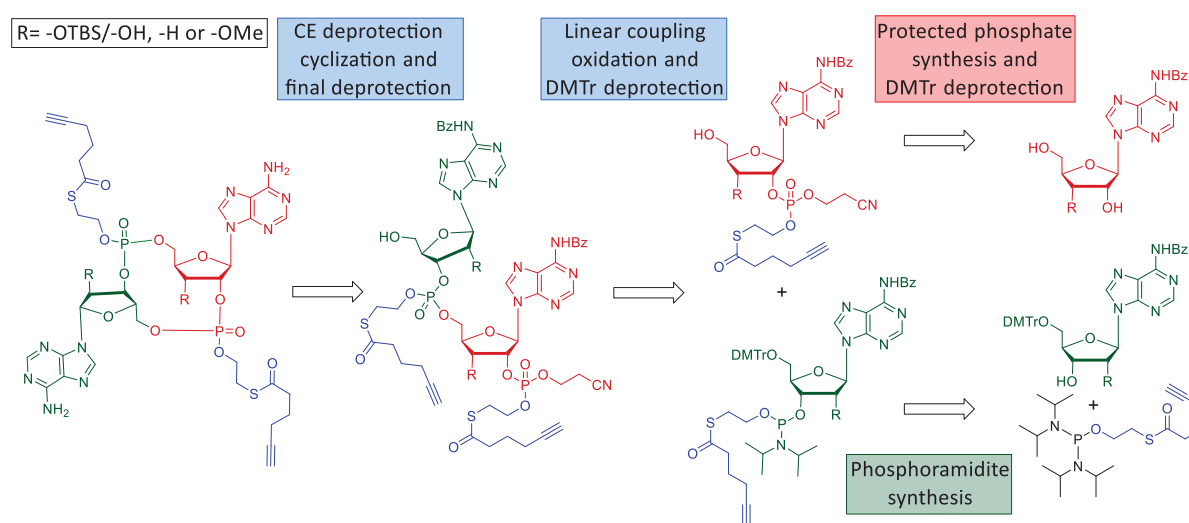


Figure 37: Retrosynthetic analysis for the synthesis of cGAMP analogues prodrugs.

3.7.1 Prodrugs of deoxy- and methoxy-2',3'-CDNs

After synthesising and testing the cyclic dinucleotides shown in part I, we started by designing and preparing prodrug derivatives of the dehydroxylated and methylated cyclic dinucleotides **2** and **5** (Figure 38).

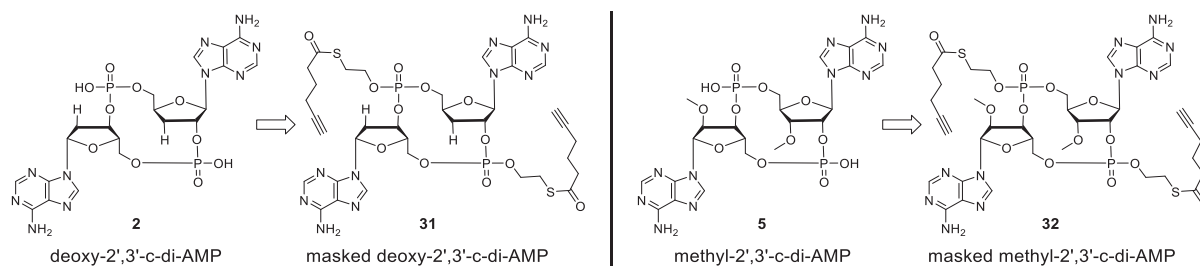
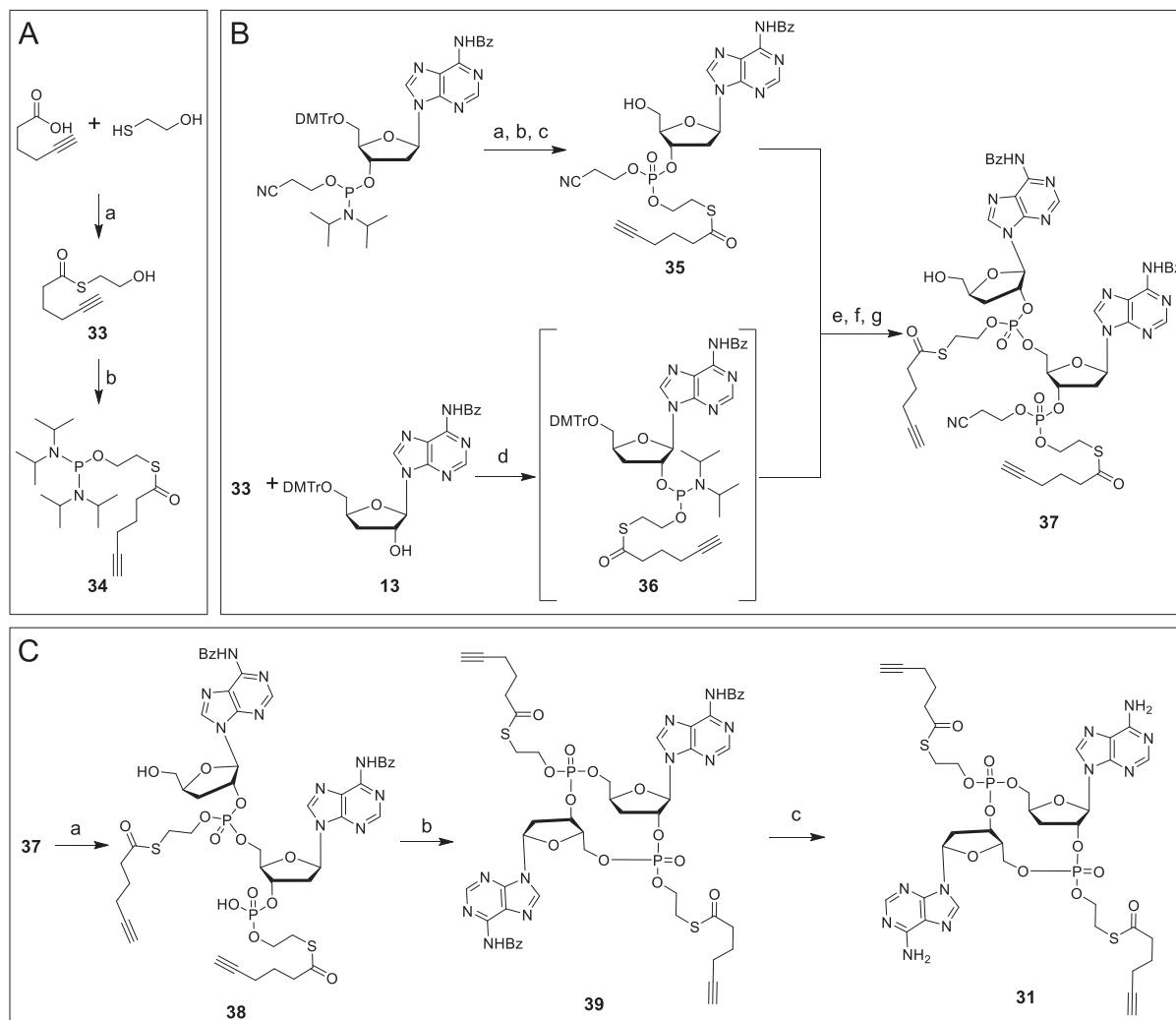


Figure 38: Structures of compounds **2 and **5** and their masked prodrug derivatives**

For the synthesis of the dehydroxylated prodrug **31** we started on one side from a commercially available adenosine phosphoramidite, which was coupled with the thioester-containing linker **33** that can be synthesised in two steps from β -mercaptoethanol and hexynoic acid. Oxidation and deprotection of the 5'-DMTr group yielded the phosphate half **35**. The synthesis of the other half of the cyclic dinucleotide started from the 3'-deoxyadenosine **13** whose synthesis is described in details in the first part. **13** was converted into the modified phosphoramidite **36** and directly coupled with **35** in one pot using BTT. After oxidation and DMTr deprotection with 3 % DCA, we obtained the linear dimer **37**. Phosphate deprotection with $t\text{BuNH}_2$ and cyclization using MSNT led to the base-protected macrocycle **39**. Deprotection of the adenines with reagents normally used in oligonucleotide synthesis such as ammonia or methylamine was not possible in our case because we observed rapid decomposition of the thioesters leading to formation of the free cyclic dinucleotide. We finally managed to cleave the benzoyl groups and obtain the final product **31** using a solution of zinc bromide in chloroform/methanol 4:1 over 48-72 hours (Scheme 11).



Scheme 11: Synthesis of the thioester and alkyne-containing phosphotriester dd-cAAMP derivative. **A)** Synthesis of the thioester-containing phosphoramidite reagent. Conditions: a) DCC, DMF, overnight, 0°C to rt; b) bis-diisopropylamino chlorophosphine, NEt_3 , Et_2O , 3h, 0°C. **B)** Assembly of the linear dinucleotide using P(III) chemistry. Conditions: a) BTT, MeCN, 1h, rt; b) $t\text{BuOOH}$, 40 min, rt; c) 3 % DCA in DCM, 10 min, rt, 75.5 % over 3 steps; d) pyridine trifluoroacetate, DCM, 1h, rt; e) BTT, MeCN, 1h, rt; f) $t\text{BuOOH}$, 40 min, rt; g) 3 % DCA in DCM, 10 min, 48.4 % over 4 steps. **C)** Deprotection and macrocyclization of the linear precursor to give the target compound ready for click chemistry based further modification. Conditions: a) $t\text{BuNH}_2$, MeCN, 20 min, rt, ; b) TPSCI, N-methylimidazol, THF, 30h, rt, 46 % over 2 steps; c) ZnBr_2 , $\text{CHCl}_3/\text{MeOH}$ 4:1, 4 days, 28 % after HPLC.

Because of the presence of the two phosphotriester moieties, **31** was obtained as a mixture of diastereomers which was hard to characterize. In order to confirm the structure of the cyclic molecule, we performed a further HPLC purification of the diastereomeric mixture and we were able to separate one of the four diastereomers which we then characterized by high resolution mass spectrometry and NMR (Figure 39).

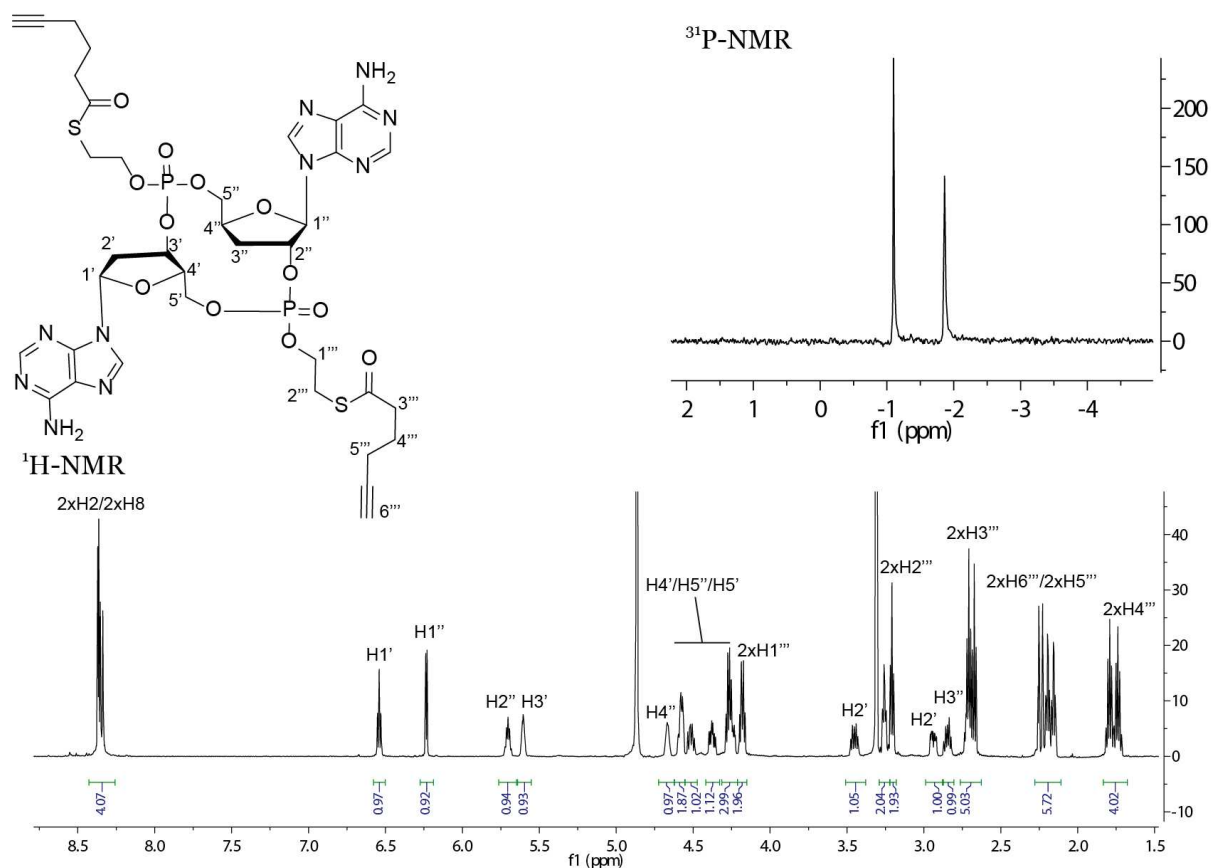
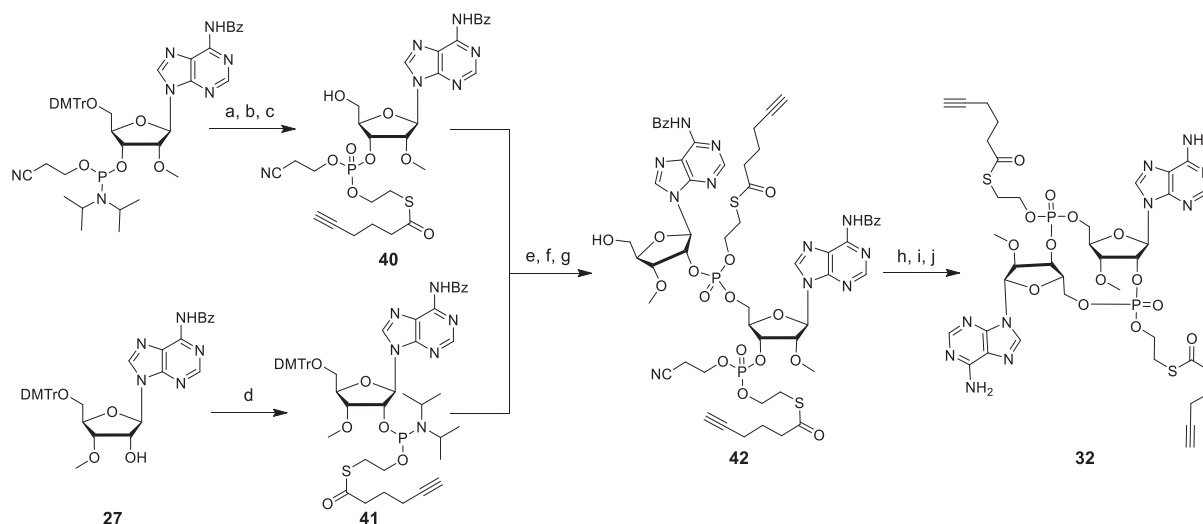


Figure 39: Structure, 600 MHz $^1\text{H-NMR}$ and 162 MHz $^{31}\text{P-NMR}$ spectra of compound 31 (single isomer).

The methylated prodrug **32** was also synthesised following the same strategy. A commercially available 2'-*O*-methyladenosine-3'-phosphoramidite was used to obtain the protected phosphate **40** via phosphoramidite coupling with the thioester-containing linker **33**, oxidation with *t*BuOOH and DMTr deprotection. The 3'-*O*-methylated adenosine precursor **27** described before was instead reacted with the phosphordiamidite **34** to synthesize the thioester-containing adenosine phosphoramidite **41**. This building block was coupled with the phosphate **40** to obtain the linear precursor **42** that was cyclized using TPSCl and *N*-methylimidazole to activate the phosphate. Final deprotection using zinc bromide as described before yielded the methylated CDN prodrug **32** as a mixture of four diastereomers (Scheme 12).



Scheme 12: Synthesis of the methylated 2',3'-c-di-AMP prodrug 32. Conditions: a) 33, BTT, MeCN, 1h, rt; b) *t*BuOOH, 40 min, rt; c) 3 % DCA in DCM, 10 min, rt; d) 34, pyridine trifluoroacetate, DCM, 1h, rt; e) BTT, MeCN, 1h, rt; f) *t*BuOOH, 40 min, rt; g) 3 % DCA in DCM, 10 min; h) *t*BuNH₂, MeCN, 20 min, rt; i) MSNT, pyridine, overnight, rt; j) ZnBr₂, CHCl₃/MeOH 4:1, 4 days.

3.8 Biochemical and biological assays

3.8.1 Enzymatic activation of cyclic dinucleotide prodrugs

In order to evaluate the decaging properties of our CDN prodrugs we designed a biochemical assay in which we incubated the prodrug 31 with carboxylesterase 1 in order to see prodrug cleavage occurring. Enzymes belonging to the carboxylesterase (CES) family are in fact hydrolytic enzymes involved in the cleavage and activation of many ester-based prodrugs and in drug metabolism.¹⁶⁴ Two main isoforms (CES1 and CES2) are known, the main difference being their distribution in various tissues. In humans CES1 is highly expressed in the liver, lung and immune cells such as monocytes and macrophages, while CES2 is mostly expressed in the intestine and kidneys. The mechanism by which CESs are able to hydrolyse esters or other carboxylic acid derivatives is the same for both isoforms and is also similar to other related proteins of the esterase or lipase families.¹⁶⁴ The active site of the enzyme contains the catalytic triad Ser-His-Glu and each one of these amino acids plays an important role in ester hydrolysis (Figure 40). In the first step, the -OH on the Ser side chain attacks on the carbonyl carbon atom of the ester bond, thanks to the neighbouring assistance of the imidazole ring of His which acts as a base. In the next step, the His side chain now acts as an acid catalyst and promotes ester hydrolysis and elimination of the alcohol. The acyl part of the original ester is now bound to the Ser side chain and can be hydrolysed following the same mechanism described before, with water acting now as a nucleophile (Figure 40).

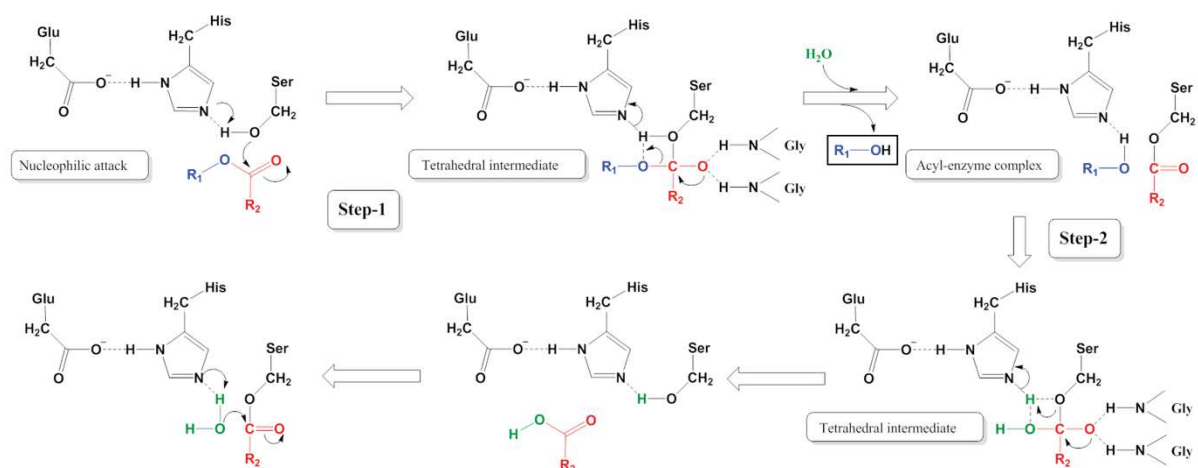


Figure 40: Mechanism of action of human carboxylesterase enzymes.¹⁶⁴

In our prodrug cleavage assay, 10 nmols of the analogue **31** were incubated with 5 units of carboxylesterase 1c (CES1c) and the advancement of the reaction was controlled by analytical HPLC, using the free phosphate cyclic dinucleotide dd-cAAMP **2** as a reference for the completely deprotected CDN. The results of this experiment clearly show that CES1c is able to hydrolyse the thioester, releasing the free phosphate according to the mechanism described above in Figure 40. At the same time, we could also prove that the decomposition and activation of the prodrug proceeds in a very specific way, as we did not observe uncontrolled decomposition of the phosphotriester to form open dimers but only formation of the desired dd-cAAMP. We were also able to show that the protected dinucleotides are stable in aqueous buffers, as we could not detect decaying or decomposition of **31** when the esterase was absent.

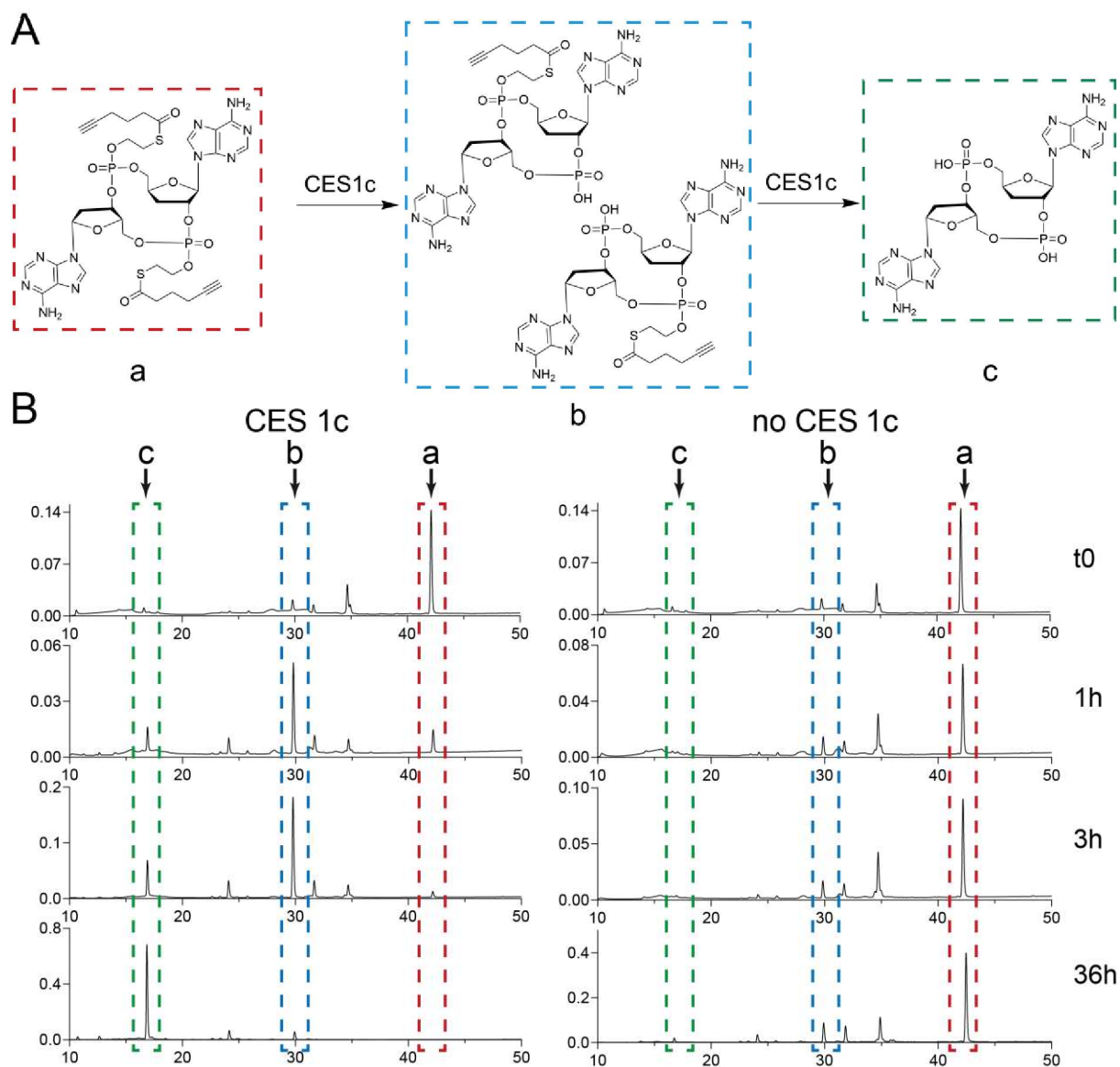


Figure 41: Enzymatic assays showing cleavage of the phosphate protective groups in the presence of CES1c. Experimental conditions: 10 nmol of prodrug analogues **31** with 5 units of carboxylesterase 1c in 0.1 M HEPES buffer at 37 °C. HPLC conditions: 0-50 % buffer B in 45 min. Buffer A: 0.1 M TEAA buffer pH 7.0 in H₂O. Buffer B: 0.1 M TEAA buffer, pH 7.0 in MeCN/H₂O 80:20. Flow: 0.5 mL/min.

This assay gave us the required validation that SATE prodrugs can be successfully cleaved by carboxylesterase enzymes leading to the formation of the free CDN. In order to confirm prodrug cleavage in a more complex and biologically relevant system, we decided to perform a cell feeding experiment in which we incubated THP-1 cells with the synthesized prodrug compound **31** in a 50 μ M concentration for 24 hours. We then extracted the soluble pool and analysed it by UHPLC-HRMS to detect the three species shown before. As shown in Figure 42, the most abundant molecule that we could detect was the completely deprotected CDN **2** (metabolite **c**). We could however still detect, even if in lower amounts, the protected

molecule **31** (indicated with the letter **a**) and the half-cleaved intermediate **b**, likely because of the very high concentration of compound **31** used in the cell feeding step.

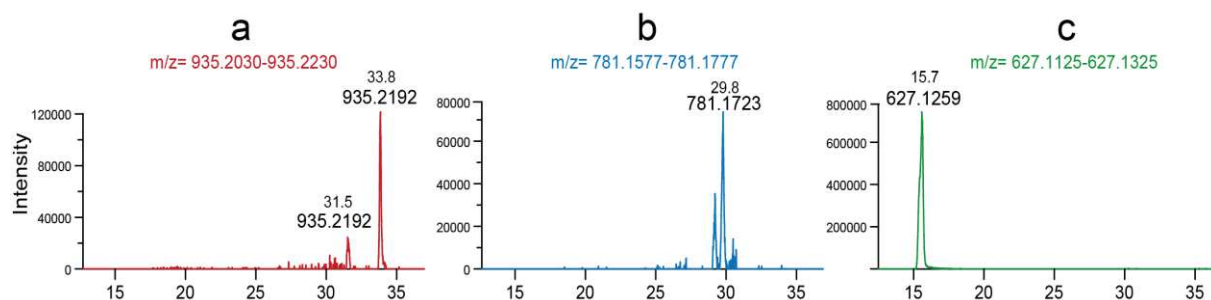


Figure 42: LC-MS analysis of the cell lysate after incubation with 50 μM of **31** for 24 h. MS measurements performed in collaboration with Dr. *M. Wagner* (Carell group).

Altogether, these preliminary assays showed us that thioester-containing linkers can be successfully cleaved in THP-1 cells, likely thanks to the action of esterase-type enzymes such as CES1. In the absence of these enzymes, we did not see any relevant decomposition in aqueous buffer, confirming the stability of our prodrug analogue in biologically-compatible conditions.

3.8.2 Cellular tests with dd-2',3'-c-di-AMP prodrug

Because the methylated cGAMP analogue **5** showed to be inactive in the biochemical and cellular assays shown before in part I, we decided to further study only the prodrug of the dd-cAAMP **2** which we proved to be a good STING agonist able to stimulate interferon expression. In order to find the concentration range to be used in further assays with the purpose of measuring the EC_{50} value, we started by testing the interferon expression induced by the CDN prodrug **31** and compared it with the free CDN **2** (Figure 43 a). As shown before, when we fed cells with the free CDN **2** we did not observe any interferon expression at a concentration of 5 μM , while concentrations of 50 μM or higher triggered an interferon response that we could quantify using the luciferase-based assay described before. When we used the prodrug **31** we could already see strong interferon expression at a concentration of 5 μM . The same response was also measured at 50 μM , while higher concentrations (100 μM) gave a slightly lower signal, which might suggest that the amount of compound internalized is toxic for the cells. In order to prove that the observed effect is STING-dependent, we tested the highest concentration of the prodrug (100 μM) in STING-KO THP-1 cells and we could not observe any interferon expression (figure 43 b).

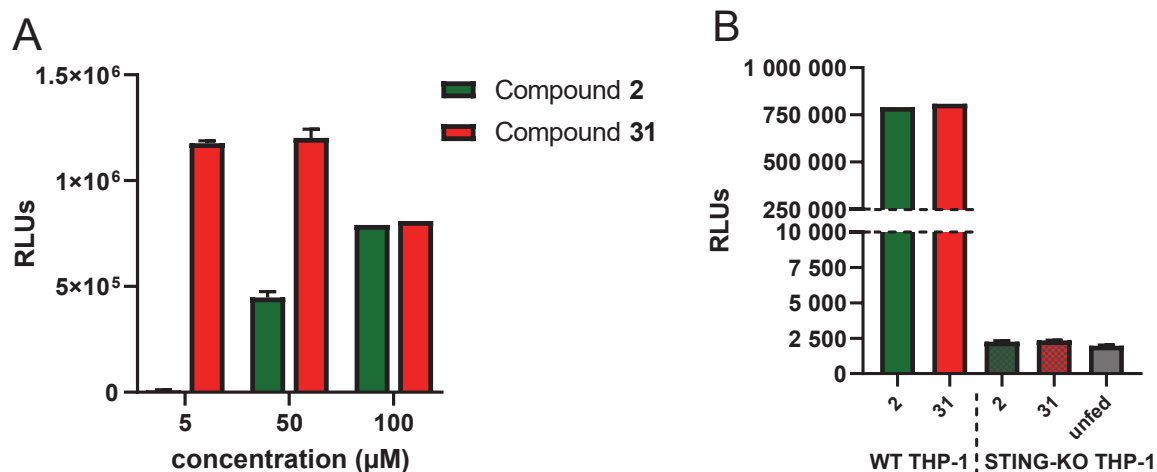


Figure 43: Cellular tests with the cyclic dinucleotide prodrug 31. A) Comparison of the free phosphate molecule 2 and its prodrug derivative 31. B) Test of wild type (WT) and STING-KO THP-1 cells to prove the STING-specificity of the measured activity. Data acquired in collaboration with *E. Kaminska* (Carell group)

These experiments already proved that by using a CDN prodrug we were able to increase interferon expression through STING activation thanks to a better drug uptake. In order to better evaluate the improvement in interferon expression, we decided to repeat the same assay described before in a wider concentration range, with the purpose to measure the EC_{50} value and compare it to the EC_{50} of cGAMP and the free CDN 2. In this assay we incubated cells with different concentrations of compound 31 for 24 hours. After this time, we measured IFN expression with a luciferase assay and calculated the EC_{50} as described in part I (Figure 44).

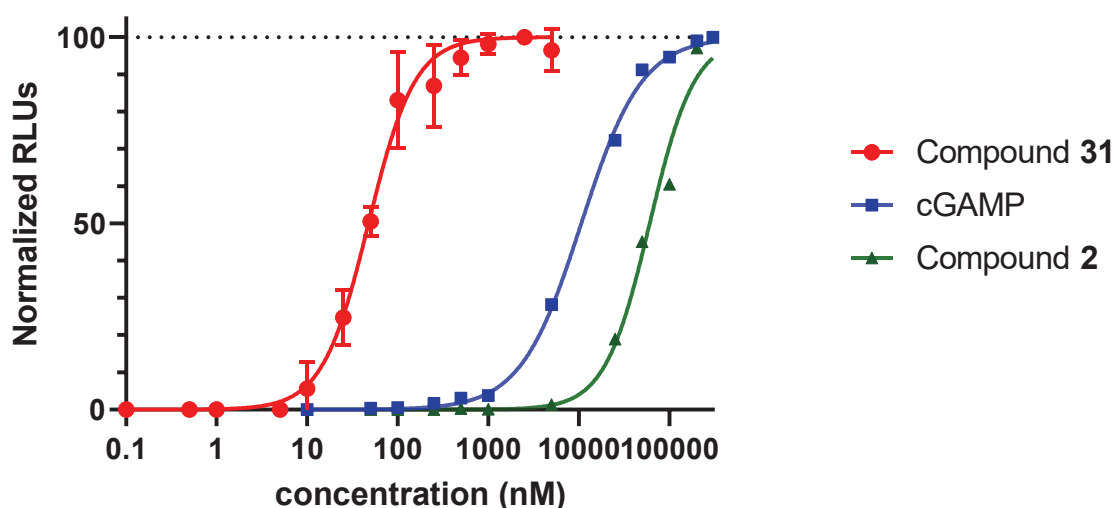


Figure 44: EC_{50} curves for cGAMP (blue), compound 2 (green) and the prodrug compound 31 (red). Calculated values: cGAMP: 10.6 µM; compound 2: 60.5 µM; compound 31: 47.6 nM. Data for compound 31 were obtained from 3 biological replicates.

The introduction of the SATE prodrug moiety clearly resulted in an increase in the cellular response to our cGAMP analogue prodrug. After 3 biological replicates, we calculated in fact an EC₅₀ value of 47.6 nM for the prodrug compound **31** which represent a more than 1000-fold improvement if compared to the free dd-cAAMP analogue **2** and a 200-fold improvement against the natural STING ligand cGAMP. Therefore, we next decided to test the activity of the compounds in primary immune cells, in collaboration with *W. Greulich* (Prof. Hornung's group).

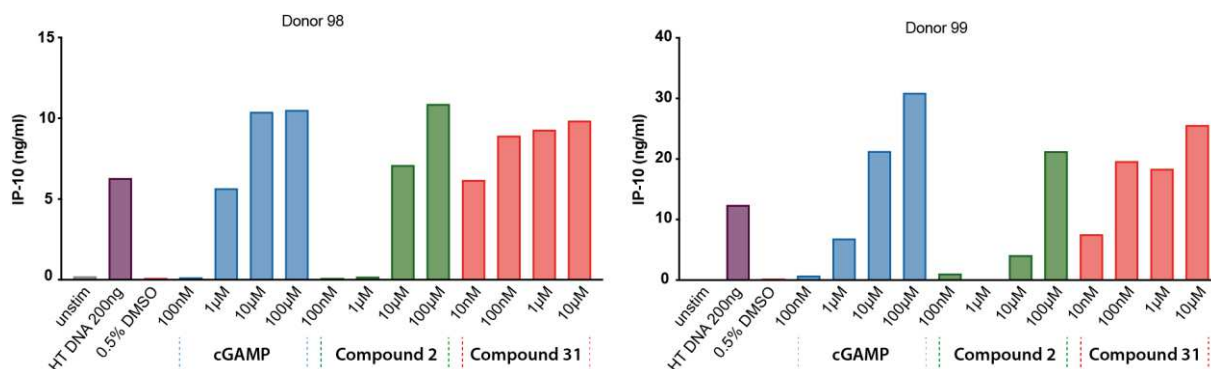


Figure 45: Activity of cGAMP, compound 2 and prodrug compound 31 in primary cells. The amount of secreted IP-10 was measured using an ELISA assay on a BLaER1 cell line. Data acquired in collaboration with *W. Greulich* (Hornung group).

The tests in primary cells confirmed what we observed in THP-1 monocytes. When we used cGAMP, we could measure STING activation at concentrations above 1 µM. The deoxy-2',3'-c-di-AMP **2** was able to activate STING only at concentrations above 10 µM, while the cyclic dinucleotide prodrug **31** was much more potent and led to high STING activation and interferon expression already in a concentration of 10 nM, which represents a high increase in the potency of the prodrug derivative when compared to the free cyclic dinucleotides. Because STING activation results in its phosphorylation and then leads to phosphorylation of IRF3, we decided to perform a series of western blot assays in order to detect these phosphorylated proteins in collaboration with the Hornung group. We also detected STAT1, whose phosphorylation is triggered by interferons themselves (Figure 46).

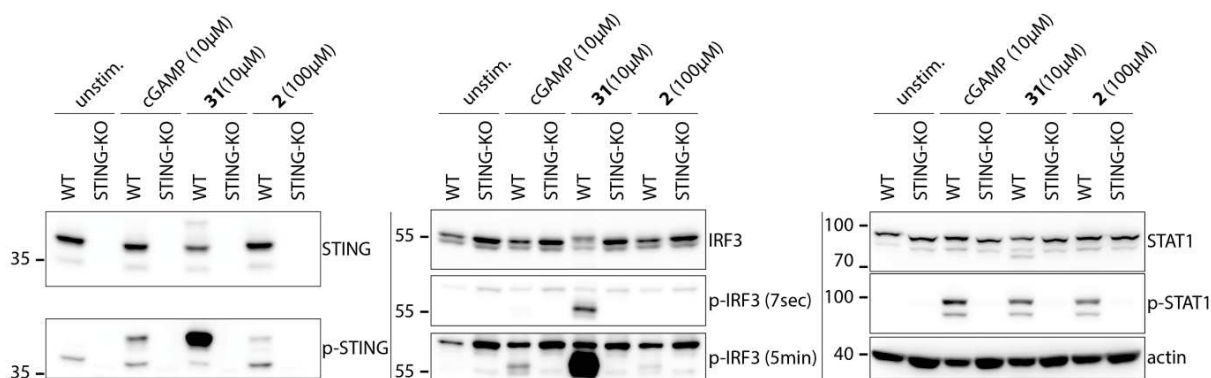


Figure 46: Western blot analysis to detect phosphorylated STING, IRF3 and STAT1. Data acquired in collaboration with *W. Greulich* (Hornung group).

This study validated once more the results described before. We were able to detect phosphorylation of STING, IRF3 and STAT1 in WT BLaER1 immune cells after incubation with cGAMP, compound **2** or compound **31**. We could not detect STING, IRF3 or STAT1 phosphorylation when STING-KO cells were used, which again indicates a STING-dependent signalling cascade. When we used our prodrug derivative **31** at the same concentration as cGAMP in WT cells, we detected a much higher phosphorylation level in all three proteins, meaning that the activation of the STING pathway and consequent interferon expression is stronger compared to the free cyclic dinucleotides.

3.9 Click chemistry based modification of the CDN prodrugs

Although reducing the polarity of the molecule already improves the potential field of application of cGAMP analogues by eliminating the electrostatic repulsion between negatively charged cGAMP and phospholipids on the cell membrane, we decided to go one step further and test if click chemistry could be a viable option to achieve post-synthetic modification of these prodrugs. This would allow to conjugate the prodrug-alkynes with ligand-azides that can interact with membrane receptors expressed in particular cell types, resulting in enhanced uptake and specific targeting. A similar strategy was previously developed in the Carell group to achieve cell delivery of siRNA or siRNA dendrimers to immune cells or neurons.^{165,166} Therefore, we aimed to develop CDN-ligand conjugates that can be internalized by receptor-mediated uptake and that can be cleaved and activated into the cytosol to execute their biological effect. In order to achieve efficient delivery in immune cells, we initially selected anandamide as ligand, because it can be internalized after being recognized by cannabinoid receptors that are highly expressed in immune cells. For this reason, we used the anandamide-PEG₃-azide **43**, which was synthesised from arachidonic acid following a previously reported procedure.^{165,166}

The click reaction to connect the alkyne prodrug to the anandamide azide ligand was performed in a DMSO/H₂O mixture using CuSO₄ as Cu (I) source and sodium ascorbate as reducing agent. Due to the low polarity of **31** and **32** and of the anandamide derivative **43** in fact, H₂O alone was not suitable to achieve complete dissolution of the reagents. After the click reaction, which was completed in 2 hours according to LC-MS analysis, we extracted the product in dichloromethane and washed with H₂O to remove most of the copper salts and sodium ascorbate. The two clicked products could finally be purified by RP-HPLC, yielding **44** and **45**. The structure and purity of the two products could be confirmed by LC-MS analysis (Figure 47).

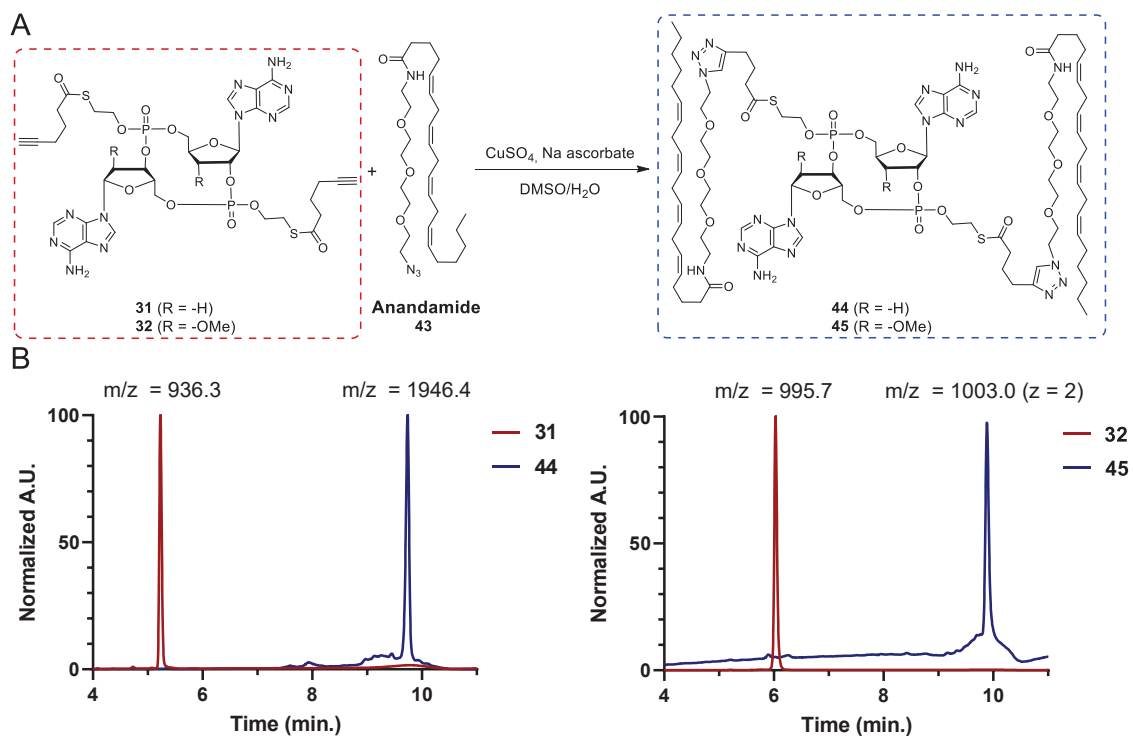


Figure 47: Click chemistry based functionalization of the cyclic dinucleotide prodrugs 31 and 32. A) Click reaction conditions; B) LC-MS analysis of the starting materials 31 and 32 (in red) and of the clicked products 44 and 45 (in blue).

As before, we again decided to test only the activity of the most potent dehydroxylated analogue **44**, because we showed that the methylated analogue does not induce interferon expression in THP-1 cells. For this purpose, we again incubated THP-1 reporter cells with different concentrations of the clicked molecule **44** in order to calculate the EC_{50} value (figure 48).

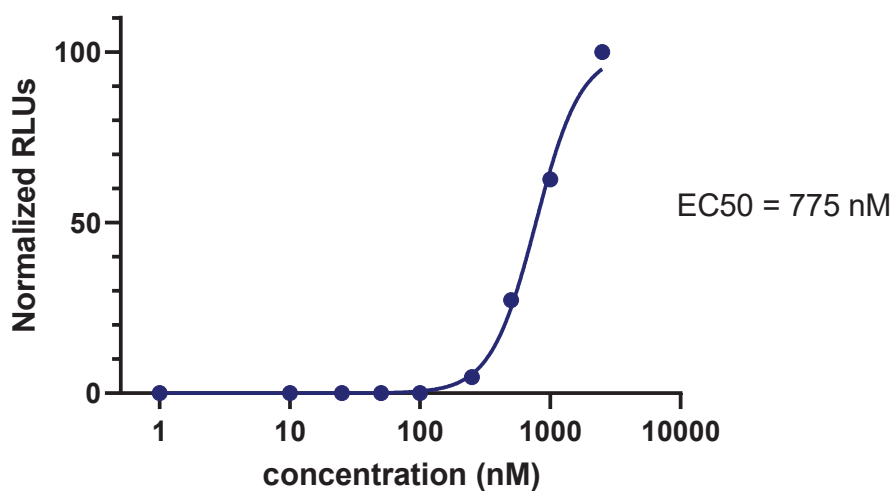
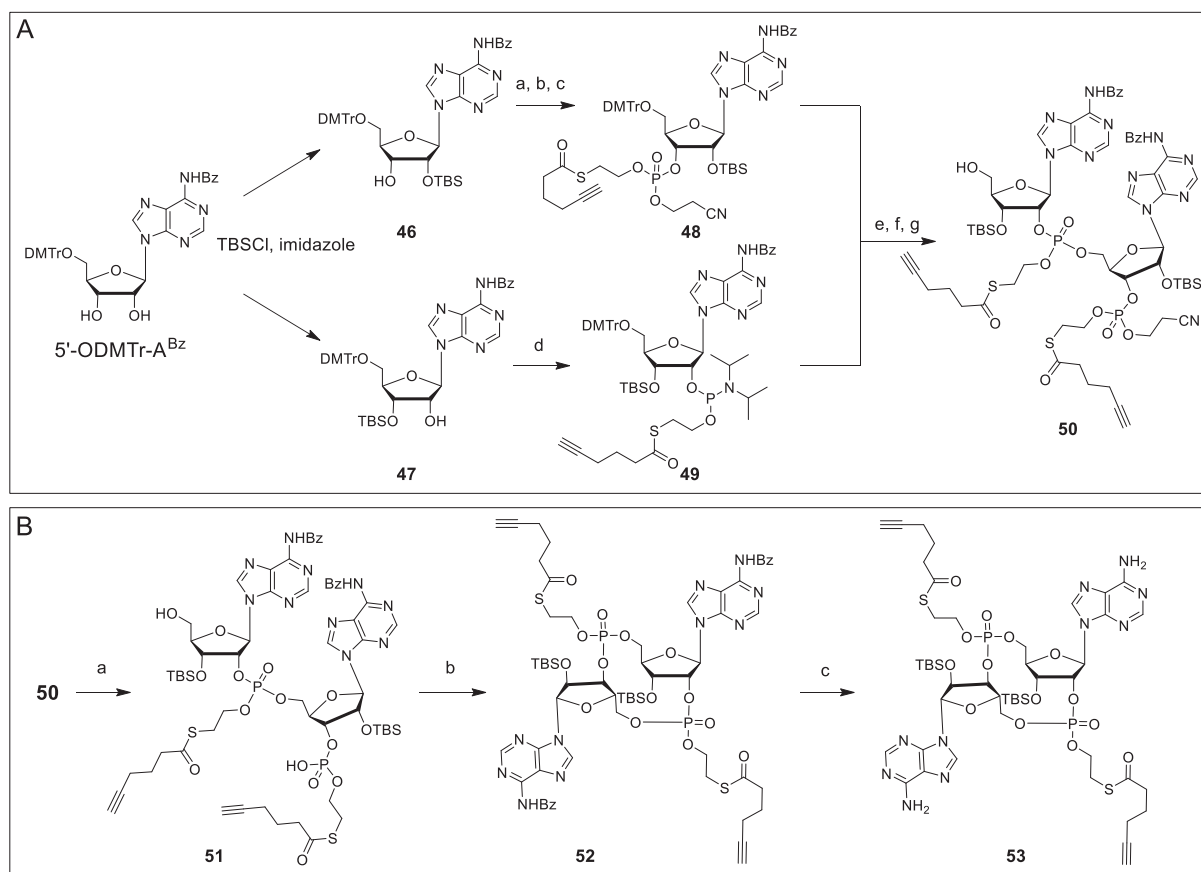


Figure 48: EC_{50} curve of the anandamide conjugated compound **44**.

This experiment showed that even if we could measure a higher activity for the clicked prodrug **44** compared to both cGAMP and the dd-cAAMP, the interferon expression that we measured was much lower compared to the activity of the unclicked prodrug **31**. Furthermore, when we used concentrations higher than 2.5 μM we observed a fast decrease in the luciferase signal, likely indicating a cellular toxicity of the compound at such concentrations. One possible explanation for the decrease in the cellular activity of **44** can be the lower water solubility of this compound compared to the unclicked analogue **31** which might lead to precipitation of the compound in the cell medium. Another possibility is the slower deprotection of the prodrug linker containing arachidonic acid. This ligand alone is in fact known to be an inhibitor of human carboxylesterases that are responsible for thioester hydrolysis and prodrug activation.¹⁶⁴

3.10 Towards the synthesis of hydroxyl-containing cGAMP prodrugs.

In parallel to the synthesis of the molecules **31**, **32**, **44** and **45** described before, a similar synthetic approach to obtain a prodrug derivative of cGAMP itself was tested. This would in fact in principle allow to obtain specific cytosolic release of the natural STING ligand obtaining an even higher activity. For this purpose we prepared the suitably protected adenosines **46** and **47** containing a DMTr protective group on the 5'-OH and a TBS on the 2'- or 3'-OH. The 3'-OH, 2'-O-TBS adenosine **46** was now used to prepare the protected phosphate **48**, while the other isomer **47** was coupled with the thioester-containing phosphoramidite reagent **34** to obtain the thioester-containing phosphoramidite **49**. These two intermediates were connected to yield the linear dimer **50** which was deprotected and then cyclized with TPSCl and N-methylimidazol. Deprotection of the nucleobases of **52** with methylamine failed also in this case because we observed complete decomposition of the molecule, giving rise to a series of unwanted products that we believe followed decomposition of the phosphotriester moieties. Using zinc dibromide as shown before we were able to finally deprotect the adenines and obtain the TBS-protected cyclic dinucleotide **53** (Scheme 13).

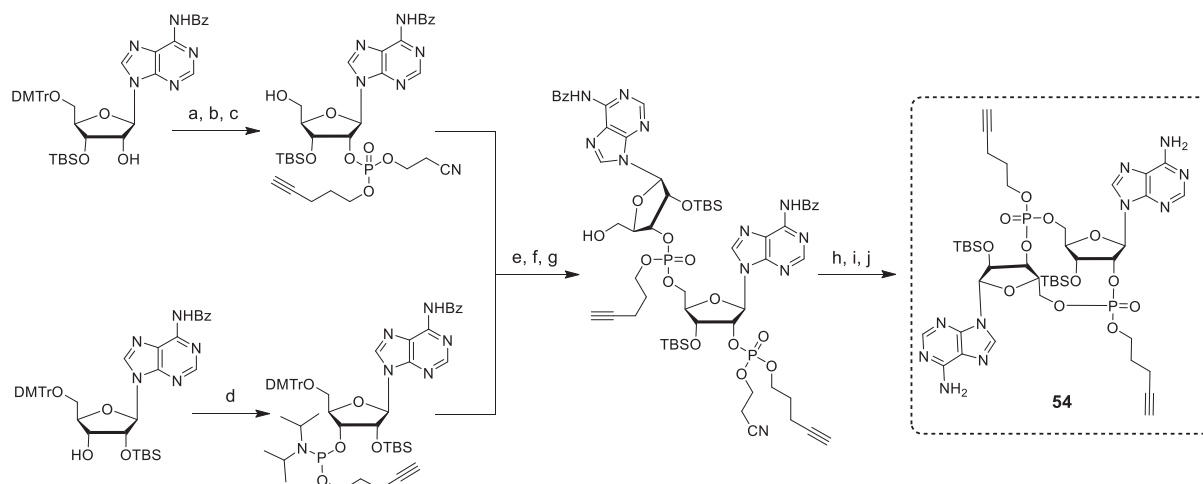


Scheme 13: Synthetic strategy to obtain TBS-protected CDN prodrugs. A) Assembly of the linear dinucleotide using P(III) chemistry. Conditions: a) 2-Cyanoethyl *N,N,N',N'*-tetraisopropylphosphorodiamidite, pyridine trifluoroacetate, DCM, then 33, BTT, MeCN, 1h, rt; b) *t*BuOOH, 40 min, rt; c) 3 % DCA in DCM, 10 min, rt; d) 34, pyridine trifluoroacetate, DCM, 1h, rt; e) BTT, MeCN, 1h, rt; f) *t*BuOOH, 40 min, rt; g) 3 % DCA in DCM, 10 min. B) Deprotection and macrocyclization of the linear precursor to give the target compound 53 ready for click chemistry based further modification. Conditions: a) *t*BuNH₂, MeCN, 20 min, rt; b) MSNT, pyridine, overnight, rt; c) ZnBr₂, CHCl₃/MeOH 4:1, 4 days.

Deprotection of the TBS groups on the ribose moiety of 53 with the classical procedure (triethylamine/HF) was unfortunately impossible to perform in our hands because of very fast decomposition of the starting material. We then tested a wide variety of methods reported in literature based on fluorides (pyr/HF, pyr/HF + AcOH, fluoride on polymer support, TBAF on silica gel, NH₄F, KF) obtaining decomposition in any case. Acidic reagents such as HCl, toluenesulfonic acid, camphorsulfonic acid which are known to deprotect secondary TBS-protected hydroxyl groups did not give any reaction even if used in high excess, perhaps because of the highly hindered situation of these chemical groups.

We therefore hypothesised that the reason for the fast decomposition of the molecule could be the presence of an activated thioester in the prodrug linker. In order to prove that, in collaboration with *F. Hernichel* during his Master thesis in the Carell group, compound 54 was synthesised following the same synthetic route shown before, but using pentynol as a

linker. In contrast with the SATE group that contains an activated thioester, this linker cannot be easily activated or hydrolysed, making it possible to understand if the decomposition is due to the hydrolysis of the thioester or if instead the opening of the cycle is a consequence of phosphoester decomposition. The higher stability of this caging group was confirmed during the synthesis, as we were able to remove the protective groups on the nucleobases by simply using methylamine, which was not possible with the SATE prodrug moieties.



Scheme 14: Synthesis of the 2',3'-c-di-AMP prodrug **54** (performed by *F. HERNICHEL* during his Master thesis project). Conditions: a) 2-Cyanoethyl *N,N,N',N'*-tetraisopropylphosphorodiamidite, pyridine trifluoroacetate, DCM, then 5-pentynol, BTT, MeCN, 1h, rt; b) *t*BuOOH, 40 min, rt; c) 3 % DCA in DCM, 10 min, rt; d) pyridine trifluoroacetate, DCM, 1h, rt; e) BTT, MeCN, 1h, rt; f) *t*BuOOH, 40 min, rt; g) 3 % DCA in DCM, 10 min; h) *t*BuNH₂, MeCN, 20 min, rt; i) MSNT, pyridine, overnight, rt; j) 33 % MeNH₂ in EtOH, 4h, rt.

Unfortunately, when we tried to remove the silyl groups we again obtained a complex mixture of products probably originated from the decomposition of the trisubstituted phosphates themselves (Figure 49).

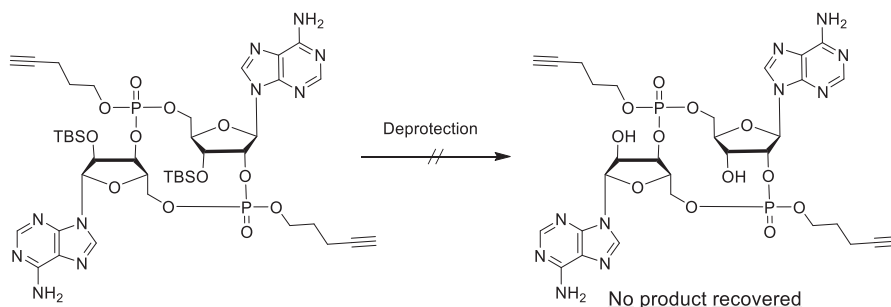


Figure 49: Final TBS deprotection reaction was not possible.

Further investigations of the possible decomposition routes are currently ongoing but lay outside of the purpose of this project. At the same time, further deprotection tests, as well as alternative synthetic approaches not requiring TBS as protective group are also being pursued.

3.11 Conclusions and outlook

In this part of the thesis, a reliable synthesis leading to prodrugs of cGAMP analogues was developed. These molecules contain a thioester linker which can be cleaved inside the cells thanks to the action of esterases and a terminal alkyne which can be employed for further functionalization of these CDN analogues to enhance cellular uptake of the synthesised molecules. One of the synthesised prodrug compounds (the dd-cAAMP prodrug **31**) was incubated with carboxylesterase 1 in order to prove efficient and specific cleavage of the phosphate protecting groups and release of the free CDN **2**. We showed that compound **31** is significantly more active than cGAMP itself in THP-1 monocytes ($EC_{50} = 47.6$ nM), likely thanks to better transport across the cell membrane. Biological tests in primary immune cells showed equally excellent results. Western blot assays to detect phosphorylation of the most important proteins in the STING and interferon pathways proved that these phosphorylation steps are taking place as expected in immune cells following feeding with compound **31**. The terminal alkyne that we inserted in our prodrug linker was used to further modify the cyclic dinucleotides by connecting an anandamide derivative *via* click chemistry to obtain compounds **44** and **45**. However, even if the CDN-anandamide conjugate **44** was still more potent than cGAMP, we did not see any improvement compared to the unclicked molecule **31**. We instead observed a decrease in the interferon expression at higher concentrations of compound **44**, which might indicate inhibition of the prodrug activation pathway or cell toxicity of the synthesised conjugates. Different clickable ligands based on carbohydrate structures such as glucose, N-acetylgalactosamine or mannose are currently being synthesised and will be tested in the near future to evaluate their ability to improve the potency of CDN prodrugs.

The synthesis of prodrug derivatives of natural 2',3'-cGAMP or of 2',3'-c-di-AMP was not yet achieved. We developed a synthetic strategy which allowed us to obtain the protected CDN prodrug **53**, but we were unable to achieve final deprotection without decomposition of the phosphotriester moieties. Further investigations in order to find a suitable synthetic approach to obtain prodrugs of cGAMP are currently ongoing.

4 Materials and methods

General methods

Chemicals and dry solvents for organic synthesis were purchased from commercial suppliers such as *Sigma-Aldrich*, *Carbosynth*, *TCI*, *ABCR*, *Alfa Aesar* or *Acros Organics* and used without further purification. Water was purified by a Milli-Q Plus system from *Merck Millipore*. All chemical reactions were carried out with magnetic stirring, and, when necessary, in oven-dried glassware (>12 h, 110 °C) under dry argon or nitrogen atmosphere. The temperature of reactions (except rt) was adjusted with a solvent/dry ice-, solvent/ice-mixture or an oil bath and the temperature monitored with a thermometer outside the flask. The literature references indicated for known compounds regard the available analytical data. Synthetic procedures were optimized and adapted for each compound as described.

Chromatographic purification of products was accomplished using flash column chromatography on *Merck Geduran* Si 60 (40 – 63 µm) silica gel (normal phase) or by reversed-phase high-performance liquid chromatography (RP-HPLC) with conditions described below. Thin layer chromatography (TLC) was performed on *Merck* 60 (silica gel F254) plates and visualized under UV light ($\lambda = 254$ and 366 nm) and staining with potassium permanganate (1.5 g KMnO₄, 10.0 g K₂CO₃, 125 mg NaOH in 200 mL water) or ceric ammonium molybdate (10.0 g ammonium molybdate tetrahydrate, 2 g Ce(SO₄)₂·4H₂O, 180 mL ddH₂O, 20 mL conc. H₂SO₄).

¹H, ¹³C and ³¹P NMR spectra were recorded in deuterated solvents on *Varian Oxford 200*, *Bruker ARX 300*, *Varian VXR400S*, *Varian INOVA 400*, *Bruker Avance III 400*, *Bruker AMX 600* and *Bruker Avance III HD 800* spectrometers and calibrated to the residual solvent peak using reported values. The chemical shifts are given in ppm, the coupling constants (J) in Hz. Multiplicities are abbreviated as follows: s = singlet, d = doublet, t = triplet, q = quartet, m = multiplet, br = broad and combinations of these. For assignment of the structures, additional 2D-NMR spectra (such as COSY, HSQC, HMBC) were measured. When the amount of compound obtained was not sufficient for a ¹³C-NMR with a high signal-to-noise ratio, 2D-NMR spectra were used to detect ¹³C peaks when possible.

High resolution electrospray ionization mass spectra (HRMS-ESI) were recorded on a *Thermo Finnigan LTQ-FT* (ESI-FTICR), and high-resolution electron impact ionization mass spectra (HRMS-EI) were recorded on a *Thermo Finnigan MAT 95*. LC-MS and ESI-MS were

measured on a *Dionex* micro UHPLC-System coupled to a MSQ-single quadrupole. As mobile phases water and acetonitrile with 0.01 % formic acid were used.

IR measurements were performed on a *Perkin Elmer BX FT-IR* spectrometer with a diamond ATR unit. Band frequencies in the region between 4400 and 1400 cm⁻¹ are reported to the nearest cm⁻¹. Signal intensities are reported as very strong (vs), strong (s), medium (m), weak (w), broad (br).

For the reverse-phase HPLC analysis and purification the following instruments were used:

Analytical HPLC: *Waters 2695 Separation Module, 2996 Photodiode Array Detector* equipped with a *Macherey-Nagel EC 250/4 NUCLEOSIL 120-3 C18* or *Macherey-Nagel EC 250/4 NUCLEODUR 120-3 C18ec* column with a flow rate of 0.5 mL/min.

Preparative HPLC: *Waters 1525 Binary HPLC Pump, 2487 Dual λ Absorbance Detector* equipped with a *Macherey-Nagel VP 250/10 NUCLEOSIL 100-7 C18* or *Macherey-Nagel VP 250/10 NUCLEODUR 100-7 C18* column with a flow rate of 5 mL/min.

Gradients of buffered solutions of H₂O and MeCN were used as mobile phases. Buffer compositions and elution methods were optimized for each product with analytical HPLCs and then the same methods were used for purification.

For the luminescence measurements we used a *Genios Pro TECAN* Microplate reader with an injector.

Biochemical and biological methods

THP1-DualTM cells and STING-KO THP1-DualTM were purchased from Invivogen and stored frozen in liquid nitrogen (freezing medium : 90 % FBS, 10 % DMSO).

Thawing procedure: the vials were first thawed in a water bath at 37°C, then transferred in a 50 mL falcon and growth medium was added dropwise (RPMI 1640 + 2 mM glutamine, 25 mM HEPES pH 7.0, 10 % heat-inactivated FBS, 100 µg/mL Pen-Strep, 100 µg/mL normocyn). Cells were spun down at 300 rcf for 5 minutes, resuspended in the appropriate amount of growth medium (6 mL for T25 or 12 mL for T75) and transferred in the culture flasks. Selective antibiotics were then added directly in the flask (10 µg/mL Blasticidin and 100 µg/mL Zeocin).

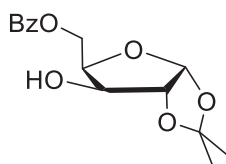
For the measurement of the activity of each STING agonist, 0.125×10^6 cells and the appropriate amount of each compound were transferred in a well in 200 μL of total volume of growth medium. After 24 hours, 20 μL of medium was transferred in a well of a 96-wells plate (in technical duplicates or triplicates) and the luminescence signal was measured in a TECAN reader using luminescence measurement parameters according to Invivogen recommended protocols.

Data from these measurements were analysed using GraphPad Prism 8 software. The absolute RLU values obtained were normalized on a 0-100 % scale to allow better comparison of the results. Then the data were fitted using the function [Agonist] vs. normalized response – variable slope. The data points and the fitted curve were then plotted in a logarithmic scale. When biological replicates were measured, the technical replicates were first averaged, then the values of the biological replicates were analysed as described before (normalization – analysis and plotted against the logarithm of the concentrations).

Procedures for organic synthesis

Dehydroxylated cGAMP analogues (compounds 2 and 3)

5-*O*-Benzoyl-1,2-*O*-isopropylidene- α -D-xylofuranose (**7**)¹⁶⁷



1,2-*O*-Isopropylidene- α -D-xylofuranose (10.0 g, 52.6 mmol) was dissolved in 210 mL of dry DCM. Pyridine (16 mL) was added and the solution was cooled down at 0°C. Benzoyl chloride (6.72 mL, 57.8 mmol) was added dropwise over 45 minutes and the reaction mixture was stirred overnight allowing it to warm up to room temperature. The reaction was then quenched with 20 mL of MeOH and the solvents evaporated *in vacuo*. The residue was redissolved in DCM, washed with sat. NaHCO_3 , brine, dried over Na_2SO_4 , filtered and the solvent was evaporated to yield **7** as a colourless syrup that was used as a crude in the next reactions (15.5 g, quant. yield).

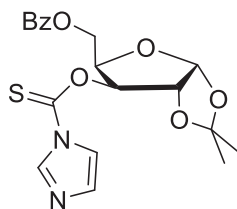
ESI-MS: calculated for $\text{C}_{15}\text{H}_{19}\text{O}_6^+$ $[\text{M}+\text{H}]^+$: 295,11761; found: 295.2.

¹H NMR (400 MHz, CDCl_3) δ 8.11 – 7.97 (m, 2H, Bz), 7.60 (m, 1H, Bz), 7.53 – 7.38 (m, 2H, Bz), 5.99 (d, $J = 3.6$ Hz, 1H, H-1), 4.89 – 4.75 (m, 1H, H_a -5), 4.62 (d, $J = 3.6$ Hz, 1H, H-2),

4.49 – 4.35 (m, 2H, H-4 and H_b-5), 4.22 (d, $J = 2.2$ Hz, 1H, H-3), 1.53 (s, 3H, isopropylidene), 1.34 (s, 3H, isopropylidene).

¹³C NMR (101 MHz, CDCl₃) δ 167.35 (CO - Bz), 133.56, 129.90, 128.50 (6C, aryl), 111.85 (C quat. Isopropylidene), 104.77 (C₁), 85.06 (C₂), 78.56 (C₄), 74.37 (C₃), 61.43 (C₅), 26.82, 26.16 (2C, isopropylidene).

3-*O*-(1*H*-imidazolethiocarbonyl)-5-*O*-Benzoyl-1,2-*O*-isopropylideneoxyfuranose (**8**)¹⁶⁷

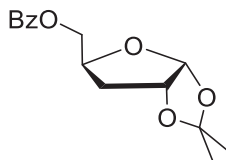


7 (10.0 g, 34.0 mmol) was dissolved in 150 mL of DMF. Thiocarbonyldiimidazole (6.1 g, 34.0 mmol) was added, followed by imidazole (462.7 mg, 6.8 mmol) and the dark red solution was stirred overnight at room temperature. After 18 hours, the solvent was removed *in vacuo* and the residue redissolved in 200 mL of EtOAc and washed with sat. NaHCO₃ and brine. The organic phase was dried over Na₂SO₄, filtered and the solvent evaporated. The product was purified by column chromatography (EtOAc/*iso*-hexane 1:9 to 1:1) to afford **8** as a very viscous slightly yellow oil (10.61 g, 26.3 mmol, 77.2 %).

ESI-HRMS: calculated for C₁₉H₂₁N₂O₆S⁺ [M+H]⁺: 405.11148; found: 405.11105.

¹H NMR (400 MHz, CDCl₃) δ 8.30 (s, 1H), 7.96 (dt, $J = 7.1, 1.4$ Hz, 2H), 7.64 – 7.50 (m, 1H), 7.44 (t, $J = 7.8$ Hz, 2H), 7.04 (t, $J = 1.2$ Hz, 1H), 6.02 (d, $J = 3.8$ Hz, 1H, C₁H), 5.97 (d, $J = 2.9$ Hz, 1H), 4.74 (m, 2H), 4.58 (d, $J = 6.1$ Hz, 2H), 1.55 (s, 3H, isopropylidene), 1.33 (s, 3H, isopropylidene).

5-*O*-Benzoyl-1,2-*O*-isopropylidene-3-deoxyribofuranose (**9**)¹⁶⁷



8 (3.90g, 9.6 mmol) was dissolved in 60 mL of dry toluene. Nitrogen was bubbled through the solution for 20 min, then tris(trimethylsilyl)silane (3.57 mL, 11.6 mmol) was added dropwise, followed by AIBN (316.7 mg, 1.9 mmol). The solution was heated at 90°C and stirred at this temperature for 2 hours and 30 min, until TLC (*iso*-hexane/EtOAc 9:1) showed

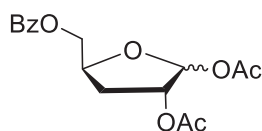
full conversion of the starting material. The solution was then evaporated to approximately half of the initial volume, and then loaded directly into a column packed with *iso*-hexane/EtOAc 95:5 and eluted with *iso*-hexane/EtOAc 9:1. The product was obtained as a colourless oil (2.20 g, 7.9 mmol, 82.1 %)

ESI-MS: calculated for $[C_{15}H_{19}O_5]^+ [M+H]^+$: 279,12270 ; found: 279.2.

1H NMR (400 MHz, $CDCl_3$) δ 8.14 – 8.00 (m, 2H, Bz), 7.63 – 7.50 (m, 1H, Bz), 7.50 – 7.36 (m, 2H, Bz), 5.88 (d, $J = 3.7$ Hz, 1H, H-1), 4.79 (dd, $J = 4.7, 3.8$ Hz, 1H, H-2), 4.61 – 4.45 (m, 2H, H-4 and Ha-5), 4.42 – 4.29 (m, 1H, Hb-5), 2.18 (dd, $J = 13.3, 4.2$ Hz, 1H, Ha-3), 1.85 – 1.69 (m, 1H, Hb-3), 1.54 (s, 3H, isopropylidene), 1.33 (s, 3H, isopropylidene).

^{13}C NMR (101 MHz, $CDCl_3$) δ 166.36 (CO - Bz), 133.15, 129.77, 128.37 (6C, aryl), 111.35 (C quat. isopropylidene), 105.73 (C-1), 80.27 (C-2), 75.81 (C-4), 65.27 (C-5), 35.42 (C-3), 26.76, 26.16 (2C, isopropylidene).

1,2-*O*-di-acetyl-5-*O*-benzoyl-3-deoxyribofuranose (**10**)¹⁶⁷

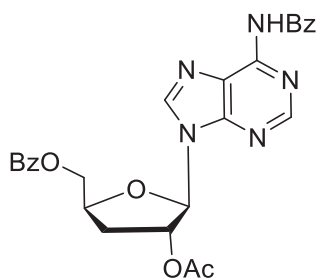


9 (2.20 g, 7.9 mmol) was dissolved in 40 mL of AcOH. Acetic anhydride (4.48 mL, 47.4 mmol) was added, followed by 6 drops of H_2SO_4 . The solution was stirred overnight at room temperature and then carefully quenched initially with solid $NaHCO_3$ and then with sat. $NaHCO_3$. The product was extracted 3 times with DCM and the combined organic phases were washed with brine and dried over Na_2SO_4 . The solvent was removed *in vacuo* to afford **10** as a colourless oil (1.55 g, 4.8 mmol, 60.8 %).

ESI-HRMS: calculated for $C_{16}H_{18}O_7Na^+ [M+Na]^+$: 345,09447; found: 345.09466.

1H NMR (400 MHz, $CDCl_3$) δ 8.06 (m, 2H, Bz), 7.62 – 7.50 (m, 1H, Bz), 7.44 (m, 2H, Bz), 6.19 (s, 1H, H-1), 5.23 (dd, $J = 4.8, 1.0$ Hz, 1H, H-2), 4.79 – 4.64 (m, 1H, H-4), 4.58 – 4.25 (m, 2H, H-5), 2.23 (m, 2H, H-3) 2.09 (s, 3H, Ac), 1.96 (s, 3H, Ac).

^{13}C NMR (101 MHz, $CDCl_3$) δ 170.12 (CO), 169.46 (CO), 166.38 (CO), 133.42 (Bz), 129.91 (Bz), 129.88 (Bz), 128.57 (Bz), 99.61 (C-1), 78.89 (C-4), 66.15 (C-5), 31.71 (C-3), 21.25 (Ac), 21.07 (Ac).

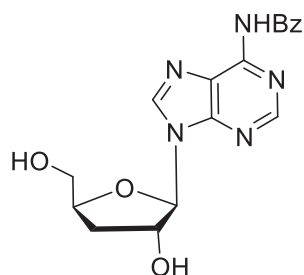
2'-*O*-Ac-5'-*O*-benzoyl-*N*⁶-benzoyl-3'-deoxyadenosine (**11**)¹⁶⁸

*N*⁶-benzoyladenine (1.73 g, 7.2 mmol) and **10** (1.55 g, 4.8 mmol) were dissolved in 60 mL of dichloroethane. Bis(trimethylsilyl)acetamide (4.70 mL, 19.2 mmol) was added, and the mixture heated at 80°C for 1 hour. After cooling down to room temperature, TMSOTf (1.74 mL, 9.6 mmol) was added and the solution heated again at 80°C overnight. The solution was cooled to room temperature and then quenched with 50 mL of sat. NaHCO₃. The product was extracted 3 times with DCM and the combined organic layers were washed with brine, dried over Na₂SO₄, filtered and the solvent evaporated. The product was purified by column chromatography (*iso*-hexane/EtOAc 1:5 to 1:5 to 100 % EtOAc) to yield **11** as a white foam (1.91 g, 3.8 mmol, 79.1 %).

ESI-HRMS: calculated for C₂₆H₂₄N₅O₆⁺ [M+H]⁺: 502.17211; found: 502.17179.

¹H NMR (400 MHz, CDCl₃) δ 8.76 (s, 1H, H-2), 8.15 (s, 1H, H-8), 8.13 – 7.89 (m, 4H, Bz), 7.68 – 7.47 (m, 4H, Bz), 7.44 (dd, *J* = 8.4, 7.0 Hz, 2H, Bz), 6.13 (d, *J* = 1.4 Hz, 1H, H-1'), 5.90 (dt, *J* = 6.2, 1.5 Hz, 1H, H-2'), 4.80 (dq, *J* = 7.7, 2.8 Hz, 1H, H-4'), 4.75 – 4.49 (m, 2H, H-5'), 2.91 (m, 1H, Ha-3'), 2.36 (m, 1H, Hb-3'), 2.18 (s, 3H, Ac).

¹³C NMR (101 MHz, CDCl₃) δ 170.22 (CO), 166.26 (CO), 164.57 (CO), 152.69 (C-2), 151.04 (C-4), 149.60 (C-6), 141.97 (C-8), 133.60 (Bz), 133.38 (Bz), 132.83 (Bz), 129.62 (Bz), 129.38 (Bz), 128.89 (Bz), 128.49 (Bz), 127.86 (Bz), 123.55 (C-5), 90.44 (C-1'), 78.98 (C-4'), 77.85 (C-2'), 64.81 (C-5'), 33.06 (C-3'), 20.94.

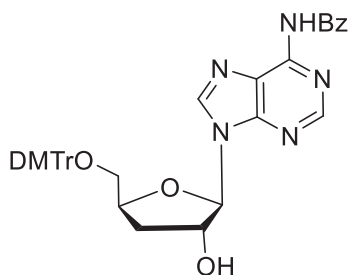
N^6 -benzoyl-3'-deoxyadenosine (**12**)¹⁶⁹

11 was dissolved in a 4:1 mixture of pyridine/methanol (30mL). The resulting solution was cooled down to 0°C and 5.8 mL of 2 M NaOH were added, and the mixture stirred for 20 min. and then quenched with 5 mL of 2 M HCl. 25 mL of pyridine were added and the solvent were removed *in vacuo*. The residue was coevaporated once more with pyridine and then purified by column chromatography (7 % methanol in DCM) to yield **12** as a white solid (1.20 g, 3.4 mmol, 88.9 %).

ESI-HRMS: calculated for $C_{17}H_{18}N_5O_4^+$ $[M+H]^+$: 356.1352 ; found: 356.1356.

¹H NMR (400 MHz, DMSO-*d*₆) δ 11.21 (s, 1H), 8.75 (2 s, $J = 10.4$ Hz, 2H, H-2 and H-8), 8.12 – 7.98 (m, 2H, Bz), 7.71 – 7.61 (m, 1H, Bz), 7.56 (dd, $J = 8.3, 6.9$ Hz, 2H, Bz), 6.05 (d, $J = 1.9$ Hz, 1H, H-1'), 5.87 – 5.68 (m, 1H, 2'-OH), 5.10 (s, 1H, 5'-OH), 4.78 – 4.55 (m, 1H, H-2'), 4.42 (td, $J = 5.9, 2.9$ Hz, 1H, H-4'), 3.66 (ddd, $J = 73.3, 12.1, 3.6$ Hz, 2H, H-5'), 2.30 (ddd, $J = 13.2, 9.2, 5.5$ Hz, 1H, Ha-3'), 2.04 – 1.85 (m, 1H, Hb-3').

¹³C NMR (151 MHz, DMSO) δ 166.04 (CO), 152.20 (C-4), 151.95 (C-2), 150.64 (C-6), 143.00 (C-8), 133.79, 132.86, 128.88 (C-Bz), 126.17 (C-5), 91.34 (C-1'), 81.59 (C-4'), 75.30 (C-2'), 62.66 (C-5'), 34.24 (C-3').

5'-O-DMTr- N^6 -benzoyl-3'-deoxyadenosine (**13**)¹⁶⁹

12 (1.0 g, 2.8 mmol) was dissolved in 220 mL of dry pyridine. The solution was cooled down to 0°C, DMTrCl (1.0 g, 3.0 mmol) was added and the mixture stirred overnight allowing to warm up to room temperature. The solvents were evaporated and the residue redissolved in

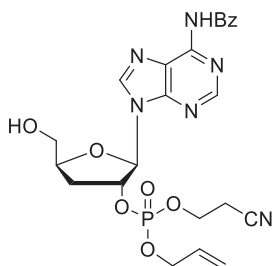
DCM, washed with NaHCO₃ and brine, dried over Na₂SO₄, filtered and the solvent removed *in vacuo*. The crude was purified by column chromatography (3 % methanol in DCM + 0.1 % NEt₃). The product **13** was obtained as a white foam (1.73 g, 2.6 mmol, 93.5 %).

ESI-MS: calculated for C₃₈H₃₆N₅O₆⁺ [M+H]⁺: 658,26601; found: 658.26616.

¹H NMR (400 MHz, CD₂Cl₂) δ 8.70 (s, 1H, H-2), 8.31 (s, 1H, H-8), 8.11 – 7.95 (m, 2H), 7.70 – 7.15 (m, 13H), 6.90 – 6.74 (m, 4H), 6.08 (d, *J* = 2.2 Hz, 1H, H-1'), 4.90 (ddd, *J* = 6.1, 3.7, 2.3 Hz, 1H, H-2'), 4.72 (tdd, *J* = 8.1, 4.5, 3.0 Hz, 1H, H-4'), 3.79 (s, 6H, DMTr), 3.50 – 3.28 (m, 2H, H-5'), 2.43 – 2.11 (m, 2H, H-3').

¹³C NMR (101 MHz, CD₂Cl₂) δ 164.62 (CO), 158.63 (DMTr), 152.04 (C-4), 150.77 (C-2), 149.55 (C-6), 144.72 (DMTr quat. C), 141.25 (C-8), 135.73, 135.63, 133.89, 132.69, 130.00, 129.96, 129.05, 128.78, 128.01, 127.85, 126.83, 123.38, 113.08 (Bz and DMTr Cs), 92.89 (C-1'), 86.38 (DMTr), 80.48 (C-4'), 76.04 (C-2'), 64.81 (C-5'), 55.20 (CH₃ DMTr), 34.01 (C-3').

*N*⁶-benzoyl-3'-deoxyadenosine-2'-(cyanoethyl, allyl protected) phosphate **14**



13 (0.3 g, 0.456 mmol) was dissolved in 5 mL of DCM under an argon atmosphere. 2-Cyanoethyl *N,N,N',N'*-Tetraisopropylphosphordiamidite (0.188 mL, 0.593 mmol) was added, followed by pyridine trifluoroacetate (105.7 mg, 0.547 mmol). The mixture was stirred at room temperature for 3 hours until TLC (*iso*-hexane/EtOAc 1:5) showed disappearance of the starting material. Allyl alcohol (0.155 mL, 2.28 mmol) was added, followed by BTT (0.3 M solution in acetonitrile, 3.0 mL, 0.912 mmol) and the reaction was stirred for 1h at room temperature. *t*-butyl hydroperoxide (5 M in decane, 0.274 mL, 1.37 mmol) was added and the solution stirred for 40 minutes and then quenched with a solution of NaHSO₃ (1 mL, 0.5 g/mL). The mixture was diluted with 50 mL of EtOAc, washed with brine and the organic phase was collected and directly evaporated *in vacuo*. The residue was redissolved in 20 mL of DCM and DCA (0.65 mL, final concentration of DCA = 3 %) was added. The deep red solution was stirred for 15 minutes and then carefully quenched with NaHCO₃ (30 mL). The product was extracted 3 times with 40 mL of EtOAc and the combined organic layers were washed with brine, dried over Na₂SO₄ filtered and evaporated *in vacuo*. The crude was

purified by column chromatography (5 % to 10 % MeOH in DCM) to yield **14** as a white foam (0.147 g, 61 %).

ESI-HRMS: calculated for $C_{23}H_{26}N_6O_7P^+$ $[M+H]^+$: 529.1595; found: 529.1592.

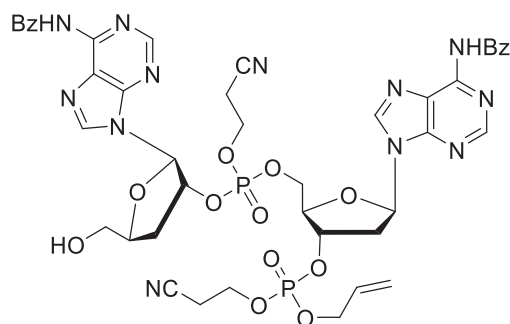
IR (ATR): $\tilde{\nu}$ (cm^{-1}) 3268 (br), 3058 (m), 2928 (m), 2256 (w), 1697 (m), 1582 (m), 1453 (m).

^{31}P NMR (162 MHz, CD_2Cl_2) δ -2.54.

1H NMR (400 MHz, CD_2Cl_2) δ 8.64 (s, 1H, H-2), 8.21 (2 s, 1H, H-8), 7.97 – 7.84 (m, 2H, Bz), 7.60 – 7.39 (m, 3H, Bz), 6.07 (dd, $J = 3.9, 1.8$ Hz, 1H, H-1'), 5.78 (tdt, $J = 16.4, 10.4, 5.7$ Hz, 1H, $-OCH_2CH=CH_2$), 5.48 – 5.32 (m, 1H, H-2'), 5.28 – 5.11 (m, 2H, $-OCH_2CH=CH_2$), 4.51 (td, $J = 6.9, 6.5, 1.9$ Hz, 1H, H-4'), 4.42 (dddt, $J = 14.2, 7.1, 4.4, 1.4$ Hz, 2H, $-OCH_2CH=CH_2$), 4.10 (ddt, $J = 10.8, 8.1, 6.1$ Hz, 2H, $-CH_2CH_2CN$), 3.94 (m, 1H, Ha-5'), 3.63 – 3.49 (m, 1H, Hb-5'), 2.75 – 2.56 (m, 3H, Ha-3' and CH_2CN), 2.39 – 2.22 (m, 1H, Hb-3').

^{13}C NMR (101 MHz, CD_2Cl_2) δ 164.52 (CO), 152.14 (C-2), 150.82 (C-4), 150.02 (C-6), 142.64 and 142.57 (C-8), 133.76 and 132.77 (C-Bz), 131.84 ($OCH_2CH=CH_2$), 128.83 (C-Bz), 127.84 (C-Bz), 124.11 (C-5), 118.94 ($-OCH_2CH=CH_2$), 116.60 and 116.52 (CN), 91.06 and 90.99 (C-1'), 81.21 and 81.18 (C-4'), 79.94 and 79.89 (C-2'), 69.11 and 69.03 ($-OCH_2CH=CH_2$), 63.33 and 63.31 (C-5'), 62.39 ($-CH_2CH_2CN$), 32.38 and 32.34 (C-3'), 19.68 and 19.64 (CH_2CN).

Protected diadenosine phosphate **15**

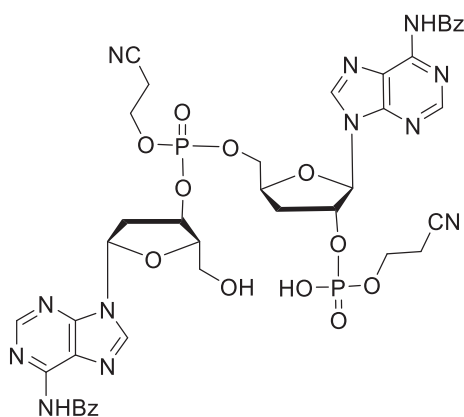


14 (70.0 mg, 132.5 μ mol) was dissolved in 3 mL of dry acetonitrile. 2'-deoxyadenosine phosphoramidite (125.0 mg, 146 μ mol) and BTT (0.3 M solution in acetonitrile, 0.88 mL, 265 μ mol) were added and the solution stirred at room temperature for 1 h. *t*BuOOH (5 M solution in decane, 79.5 μ L, 397 μ mol) was added and the mixture stirred for 40 min and then quenched with $NaHSO_3$ (1 mL, 0.5 g/mL). The solution was diluted with 50 mL of EtOAc,

washed with brine and the organic phase was directly evaporated *in vacuo*. The residue was dissolved in 6.2 mL of 3 % DCA in DCM, stirred at room temperature for 15 min and quenched with sat. NaHCO₃ and the product extracted with EtOAc 3 times (30 mL each). The combined organic layers were washed with brine and dried over Na₂SO₄, filtered and dried *in vacuo*. The crude was purified by column chromatography (2 % to 7.5 % MeOH in DCM) to yield **15** as a white solid (80.0 mg, 80.1 μmol, 60.5 %). The product **15** was obtained as a mixture of 4 diastereomers and therefore not further characterized at this stage.

ESI-HRMS: calculated for C₄₃H₄₃O₁₃N₁₂P₂⁻ [M-H]⁻: 997.25533; found: 997.25543.

Deprotected di-deoxy-adenosine phosphate **16**



15 (80.0 mg, 80.1 μmol) was suspended in 10 mL of acetone. NaI (180.1 mg, 1.2 mmol) was added and the mixture vigorously stirred under reflux for 3 hours. The cloudy mixture was cooled down to room temperature and filtered. The solid was collected, coevaporated 3 times with pyridine and dried overnight under high vacuum to afford **16** (78 mg, 80.1 μmol, quant. yield) as a white foam. The analytical data below are relative to a mixture of two diastereomers.

ESI-HRMS: calculated for C₄₀H₃₉O₁₃N₁₂P₂⁻ [M-H]⁻: 957.22403; found: 957.22365.

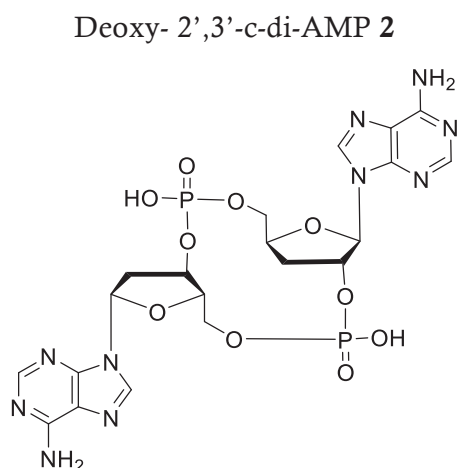
IR (ATR): $\tilde{\nu}$ (cm⁻¹) 3347 (br), 2656 (s), 2923 (vs), 2853 (s), 2360 (w), 1728 (w), 1614 (w), 1455 (m).

³¹P NMR (162 MHz, MeOD) δ -1.30, -1.35, -3.03, -3.08.

¹H NMR (800 MHz, MeOD) δ 8.72 (s, 1H), 8.68 (2 s, 1H), 8.58 (4 s, 2H), 8.12 – 8.07 (m, 2H), 8.02 (ddd, J = 40.2, 8.3, 1.4 Hz, 2H), 7.68 (dddq, J = 8.9, 5.8, 3.1, 1.5 Hz, 1H), 7.59 (tdd, J = 8.4, 4.5, 2.2 Hz, 2H), 7.56 – 7.48 (m, 2H), 6.55 – 6.32 (m, 2H, H-1' and H-1''), 5.49 (dddd, J = 15.2, 13.3, 6.7, 1.4 Hz, 1H, H-2'), 5.23 (tt, J = 6.1, 1.8 Hz, 1H, H-3''), 4.81 (s, 1H,

H-4'), 4.53 (ddd, $J = 11.5, 6.3, 2.4$ Hz, 1H, Ha-5'), 4.44 (dddd, $J = 25.9, 11.4, 6.4, 5.1$ Hz, 1H, Hb-5'), 4.35 – 4.23 (m, 3H, and Ha-4''), 4.09 (p, $J = 6.2$ Hz, 3H, and Hb-4''), 3.78 – 3.69 (m, 2H, H-5''), 2.99 – 2.88 (m, 3H, Ha-2''), 2.87 – 2.66 (m, 4H, Ha-3', Hb-2''), 2.53 (dddd, $J = 13.6, 6.0, 4.5, 1.6$ Hz, 1H, Hb-3').

^{13}C NMR (101 MHz, MeOD) δ 166.70, 151.99, 151.50, 149.71, 143.31, 133.37, 132.65, 128.38, 128.31, 128.08, 127.93, 123.57, 118.06, 117.23, 91.22, 86.48, 85.33, 85.07, 79.67, 79.27, 78.77, 68.68, 63.08, 61.52, 60.48, 18.97, 18.79.



The crude product **16** (75.0 mg, 78.2 μmol) was redissolved in 15 mL of dry pyridine and MSNT (231.8 mg, 782.3 μmol) was added. The mixture was stirred overnight at room temperature and then solvents were removed *in vacuo*. This intermediate was directly used without further purification. The solid residue was dissolved in 8 mL of 33 % MeNH₂ in absolute ethanol. The solution was stirred for 3 hours at room temperature, after which time LC-MS showed no more starting material present. The solvent was evaporated, the residue coevaporated twice with pyridine and dried under high vacuum. When dried, the solid was redissolved in a minimal amount of methanol, transferred in a falcon tube and precipitated with cold acetone. The precipitate was collected after centrifugation and purified by RP-HPLC (0->10 % B in 45 minutes. Buffer A = 0.1 % TFA in H₂O, buffer B = 0.1 % TFA in MeCN). Compound **2** was obtained as a white solid (14.0 mg, 28.6 % after HPLC purification).

ESI-HRMS: calculated for C₂₀H₂₅N₁₀O₁₀P₂⁺ [M+H]⁺: 627.1225; found: 627.1240.

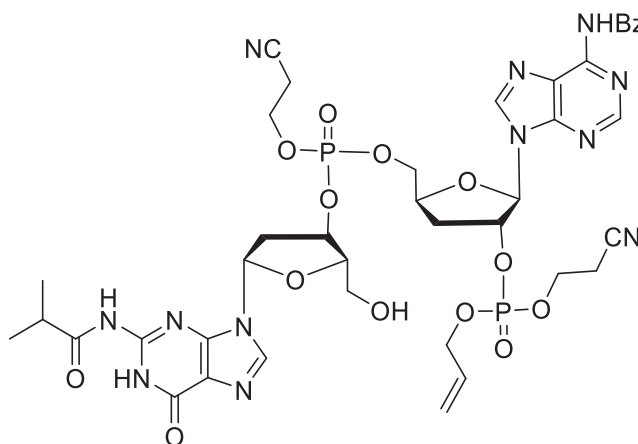
IR (ATR): $\tilde{\nu}$ (cm⁻¹) 3074 (br), 2362 (w), 1692 (s), 1606 (w), 1418 (w).

^{31}P NMR (162 MHz, D₂O) δ -1.10, -1.86.

¹H NMR (400 MHz, D₂O) δ 8.43 (s, 1H), 8.37 (s, 1H), 8.30 (s, 1H), 8.29 (s, 2H), 6.43 (dd, *J* = 6.9, 4.7 Hz, 1H, H-1''), 6.15 (d, *J* = 4.3 Hz, 1H, H-1'), 5.08 – 5.00 (m, 1H, H-2'), 4.96 (p, *J* = 5.9 Hz, 1H, H-3''), 4.56 (d, *J* = 6.3 Hz, 1H, H-4'), 4.32 – 4.16 (m, 2H, H-4'' and Ha-5'), 4.08 (dt, *J* = 11.2, 5.5 Hz, 1H, Ha-5''), 4.05 – 3.92 (m, 2H, Hb-5' and Hb-5''), 3.09 – 2.95 (m, 1H, Ha-2''), 2.76 (dt, *J* = 13.8, 6.7 Hz, 1H, Hb-2''), 2.69 (dt, *J* = 13.5, 6.8 Hz, 1H, Ha-3'), 2.41 – 2.27 (m, 1H, Hb-3').

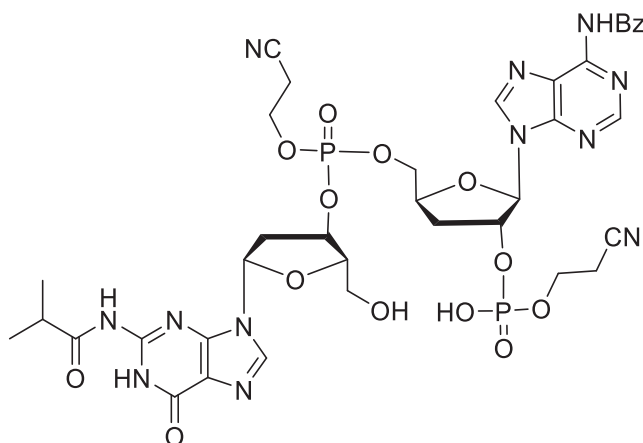
¹³C NMR (201 MHz, D₂O) δ 150.33, 150.30, 148.38, 147.88, 145.05, 144.97, 143.47, 141.79, 118.51, 115.51, 88.43 (C-1'), 84.51 (C-1''), 83.26 (C-4''), 78.28 (C-2'), 77.89 (C-4'), 72.91 (C-3''), 68.33 (C-5'), 62.88 (C-5''), 38.22 (C-2''), 34.26 (C-3').

Protected guanosine-adenosine dimer phosphate **18**



14 (70.0 mg, 132 μmol) was dissolved in 3 mL of dry acetonitrile. 2'-deoxyguanosine phosphoramidite (122.3 mg, 146 μmol) and BTT (0.3 M solution in acetonitrile, 0.88 mL, 265 μmol) were added and the solution stirred at room temperature for 1h. *t*-butyl hydroperoxide (5 M solution in decane, 79.5 μL, 397 μmol) was added and the mixture stirred for 40 min and then quenched with NaHSO₃ (1 mL, 0.5 g/mL). The solution was diluted with 50 mL of EtOAc, washed with brine and the organic phase was directly evaporated *in vacuo*. The residue was redissolved in 6.2 mL of 3 % DCA in DCM and stirred at room temperature for 15 min. The reaction was quenched with sat. NaHCO₃ and the product extracted with EtOAc 3 times (30 mL each). The combined organic layers were washed with brine and dried over Na₂SO₄, filtered and dried *in vacuo*. The crude was purified by column chromatography (2 % to 7.5 % MeOH in DCM) to yield **18** as a white solid (51 mg, 52.0 μmol, 39.3 %). The product was obtained as a mixture of 4 diastereomers and therefore not further characterized at this stage.

ESI-HRMS: calculated for C₄₀H₄₇N₁₂O₁₄P₂⁺ [M+H]⁺: 981.2804; found: 981.2824.

Deprotected guanosine-adenosine dimer phosphate **19**

18 (50.0 mg, 51.0 μmol) was suspended in 10 mL of acetone. NaI (114.6 mg, 0.76 mmol) was added and the mixture vigorously stirred under reflux for 3h. The cloudy mixture was cooled down to room temperature and filtered. The solid was collected, coevaporated 3 times with pyridine and dried overnight under high vacuum to afford **19** (48.2 mg, 51 μmol , quant. yield) as a white solid. The analytical data below are relative to a mixture of two diastereomers.

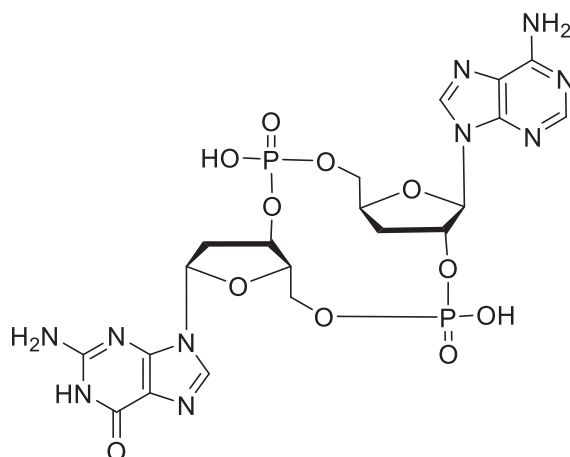
ESI-HRMS: calculated for $\text{C}_{37}\text{H}_{43}\text{N}_{12}\text{O}_{14}\text{P}_2^+$ $[\text{M}+\text{H}]^+$: 941.2491; found: 941.2502.

IR (ATR): $\tilde{\nu}$ (cm^{-1}) 3349 (br), 2956 (s), 2923 (vs), 2854 (s), 2358 (w), 1676 (m), 1603 (m), 1456 (m).

^{31}P NMR (162 MHz, MeOD) δ -1.31, -1.41, -2.70, -3.01.

^1H NMR (800 MHz, MeOD) δ 8.77 (2 s, 1H), 8.59 (2 s, 1H), 8.20 (2s, 1H), 8.05 – 8.00 (m, 1H), 8.00 – 7.91 (m, 1H), 7.69 – 7.59 (m, 1H), 7.59 – 7.51 (m, 1H), 6.46 – 6.37 (m, 1H, H-1'), 6.32 – 6.16 (m, 1H, H-1''), 5.51 (dt, $J = 28.6, 6.6$ Hz, 1H, H-2'), 5.10 (tdt, $J = 6.4, 4.5, 1.8$ Hz, 1H, H-3''), 4.80 (s, 1H, H-4'), 4.54 – 4.36 (m, 2H, H-5'), 4.33 – 4.20 (m, 2H, -OCH₂CH₂CN), 4.16 – 3.89 (m, 3H, -OCH₂CH₂CN and H-4''), 3.73 – 3.56 (m, 2H, H-5''), 2.98 – 2.84 (m, 2H, Ha-3' isomer A and -OCH₂CH₂CN), 2.79 (tdd, $J = 10.5, 7.3, 5.0$ Hz, 4H, Ha-3' isomer B, -NHCOCHMe₂, -OCH₂CH₂CN), 2.65 – 2.56 (m, 1H, Hb-2''), 2.53 (dtd, $J = 13.7, 5.9, 1.6$ Hz, 1H, Hb-3') 1.36 – 1.18 (m, 6H, NHCOCHMe₂).

^{13}C NMR (201 MHz, D₂O) δ 180.41, 166.57, 155.86, 152.01, 151.46, 149.70, 148.76, 148.21, 143.30, 138.20, 133.18, 132.59, 128.20, 127.97, 127.83, 123.65, 119.92, 117.98, 117.24, 91.21, 86.07, 83.75, 79.56, 78.75, 68.61, 63.04, 61.08, 60.49, 38.72, 38.17, 35.58, 33.27, 18.99, 18.05.

Deoxy-3',2'-cGAMP **3**

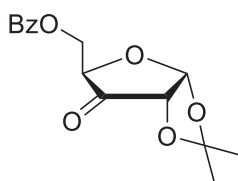
The crude product **19** (47.0 mg, 50.0 μmol) was redissolved in 10 mL of dry pyridine and MSNT (148.0 mg, 499.6 μmol) was added. The mixture was stirred overnight at room temperature and the solvents were removed *in vacuo*. The product was directly used in the next step as a crude without further purification. It was dissolved in 5 mL of 33 % MeNH₂ in absolute ethanol. The solution was stirred for 3 h at room temperature, after which time LC-MS showed no more starting material present. The solvent was evaporated, the residue coevaporated twice with pyridine and dried under high vacuum. When dried, the solid was redissolved in a minimal amount of methanol, transferred in a falcon tube and precipitated with cold acetone. The precipitate was collected after centrifugation and purified by RP-HPLC (0-10 % B in 45 minutes. Buffer A = 0.1 % TFA in H₂O, buffer B = 0.1 % TFA in MeCN) and freeze-dried to obtain **3** (13.1 mg, 20 μmol , 40.1 %) as a white solid.

ESI-HRMS: calculated for C₂₀H₂₃N₁₀O₁₁P₂⁻ [M-H]⁻: 641,10285; found: 641.10241.

³¹P NMR (162 MHz, D₂O) δ -1.10, -2.04.

¹H NMR (400 MHz, D₂O) δ 8.68 (s, 1H, H-8-A), 8.39 (s, 1H, H-8-G), 8.29 (s, 1H, H-2-A), 6.26 (dd, J = 6.8, 3.1 Hz, 1H, H-1''), 6.15 (d, J = 4.2 Hz, 1H, H-1'), 5.02 (m, J = 5.8 Hz, 1H, H-2'), 4.85 (p, J = 6.6 Hz, 1H, H-3''), 4.59 – 4.50 (m, 1H, H-4'), 4.31 – 4.25 (m, 1H, H-4''), 4.24 – 4.02 (m, 3H, H-5'' and Ha-5'), 3.97 (td, J = 11.3, 5.5 Hz, 1H, Hb-5'), 3.11 – 2.97 (m, 1H, Ha-2'), 2.69 (m, 2H, Hb-2' and Ha-3''), 2.33 (dt, J = 12.8, 5.8 Hz, 1H, Hb-3'').

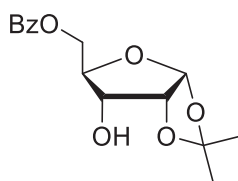
¹³C NMR (201 MHz, D₂O) δ 155.20, 149.78, 149.12, 148.20, 144.51, 142.04, 137.11, 135.56, 118.55, 109.21, 88.53, 85.82, 83.61, 78.58, 77.90, 71.67, 68.29, 62.74, 38.23, 34.31.

Methylated cGAMP analogue (Compound 5)5-*O*-benzoyl-1,2-*O*-isopropylideneribofuranos-3-ulose (**21**)¹⁷⁰

7 (2.0 g, 6.8 mmol) was dissolved in 150 mL of DCM. Dess-Martin periodinane (4.32 g, 10.2 mmol) was added and the mixture stirred at room temperature for 18 hours. The reaction was then quenched by adding 50 mL of sat. NaHCO₃ and 50 mL of sat. Na₂S₂O₃ and the product was extracted twice with DCM. The combined organic layers were washed with brine and dried over Na₂SO₄ and the solvent removed *in vacuo* to yield **21** as a colourless oil (1.92 g, 6.6 mmol, 96.5 %). NMR spectra were in agreement with those reported in the literature. This product was directly used as a crude in the following step.

¹H NMR (400 MHz, CDCl₃) δ 8.02 – 7.90 (m, 2H, Bz), 7.67 – 7.53 (m, 1H, Bz), 7.53 – 7.38 (m, 2H, Bz), 6.17 (d, *J* = 4.4 Hz, 1H, H-1), 4.77 – 4.70 (m, 2H, Ha-5 and H-4), 4.56 – 4.42 (m, 2H, H-2 and Hb-5), 1.54 (s, 3H), 1.46 (s, 3H).

¹³C NMR (101 MHz, CDCl₃) δ 207.76 (CO), 133.44, 129.56, 128.54, 114.45 (Bz), 103.09 (C-1), 77.13 (C-4), 76.17 (C-2), 63.45 (C-5), 27.47 (CH₃), 27.08 (CH₃).

5-*O*-benzoyl-1,2-*O*-isopropylideneribofuranose (**22**)¹⁷⁰

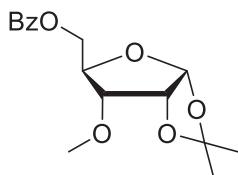
21 (1.92 g, 6.6 mmol) was dissolved in 12 mL of THF and 9.5 mL of H₂O were added. The mixture was cooled down to 0°C, NaBH₄ (257.6 mg, 6.8 mmol) was added and the mixture stirred at 0°C for 45 min. The reaction was then diluted with H₂O and DCM (70 mL each) and the product extracted twice with DCM. The organic layers were dried over Na₂SO₄, filtered and the solvent evaporated. The crude was purified by column chromatography (DCM/acetone 10:1) to afford **22** as a white solid (1.37 g, 4.7 mmol, 68.5 %).

EI-HRMS: calculated for C₁₄H₁₅O₆⁺ [M-CH₃]⁺: 279,0863; found: 279.0863.

$^1\text{H NMR}$ (400 MHz, CDCl_3) δ 8.25 – 7.33 (m, 5H), 5.87 (d, $J = 3.8$ Hz, 1H, H-1), 4.90 – 4.30 (m, 3H, H-5 and H-2), 4.11 (ddd, $J = 9.0, 5.3, 2.5$ Hz, 1H, H-4), 3.96 (dd, $J = 9.0, 5.1$ Hz, 1H, H-3), 1.61 (s, 3H, CH_3), 1.40 (s, 3H, CH_3).

$^{13}\text{C NMR}$ (101 MHz, CDCl_3) δ 166.53, 133.20, 129.79, 128.38 (Bz), 112.83, 104.04 (C-1), 78.43 (C-4), 78.25 (C-2), 72.07 (C-3), 63.33 (C-5), 26.51 (CH_3), 26.48 (CH_3).

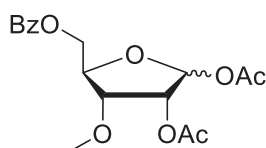
5-*O*-benzoyl-3-*OMe*-1,2-*O*-isopropylideneribofuranose (**23**)¹⁷⁰



22 (1.37 g, 4.7 mmol) was dissolved in 30 mL of DMF and cooled down to 0°C. NaH (194 mg of a 60 % suspension, 4.9 mmol) was added and the mixture stirred at 0°C for 30 min. MeI (550 μL , 8.83 mmol) was added and the solution was stirred at 0°C for 2 hours allowing it to warm up to room temperature and then quenched with a saturated solution of NH_4Cl . The product was extracted 3 times with DCM, washed with NaHCO_3 and brine, dried over Na_2SO_4 and dried under vacuum to obtain **23** as a colourless viscous oil which was used as a crude in the next step (measured mass 1.41 g, assumed quant. yield).

$^1\text{H NMR}$ (400 MHz, CDCl_3) δ 8.05 – 7.96 (m, 2H, Bz), 7.55 – 7.32 (m, 3H, Bz), 5.75 (d, $J = 3.6$ Hz, 1H), 4.72 (t, $J = 4.0$ Hz, 1H), 4.65 (dd, $J = 12.3, 2.6$ Hz, 1H), 4.63 – 4.30 (m, 2H), 4.24 (m, 1H), 3.57 (dd, $J = 9.1, 4.3$ Hz, 1H), 3.44 (s, 3H), 1.55 (s, 3H), 1.32 (s, 3H).

5-*O*-benzoyl-3-*OMe*-1,2-*O*-acetylribofuranose (**24**)¹⁷⁰

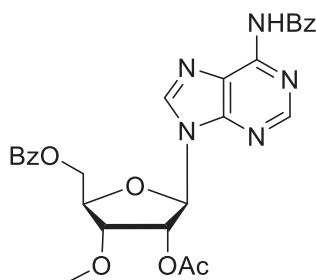


23 (5.90 g, 19.2 mmol) was dissolved in 96 mL of glacial acetic acid. Acetic anhydride (10.9 mL, 114.9 mmol) was added, followed by 4 drops of concentrated sulfuric acid. The solution was stirred at room temperature for 20 hours, then ice was added and the product extracted three times with DCM. The combined organic phases were washed with sat. NaHCO_3 , brine and dried over Na_2SO_4 . The solid was filtered off and the solvent removed *in vacuo* and the product purified by column chromatography (iso-hexane/ethyl acetate 85:15) to obtain a colourless oil (6.03 g, 17.1 mmol, 89.4 %).

¹H NMR (400 MHz, CDCl₃) δ 8.12 – 8.05 (m, 2H, Bz), 7.64 – 7.53 (m, 1H, Bz), 7.45 (dd, *J* = 8.4, 7.1 Hz, 2H, Bz), 6.15 (s, 1H, H-1), 5.34 (d, *J* = 4.3 Hz, 1H, H-2), 4.70 – 4.36 (m, 2H, H-5), 4.32 (ddd, *J* = 7.9, 4.4, 3.2 Hz, 1H, H-4), 4.08 (dd, *J* = 8.2, 4.3 Hz, 1H, H-3), 3.41 (s, 3H), 2.17 (s, 3H), 1.93 (s, 3H).

¹³C NMR (101 MHz, CDCl₃) δ 169.80, 168.99, 166.16, 133.30, 129.73, 128.49, 128.24, 98.42, 79.76, 78.93, 73.03, 63.63, 59.39, 20.93, 20.75.

*N*⁶-benzoyl-5'-*O*-benzoyl-3'-*OMe*-2'-*O*-acetyl adenosine (**25**)

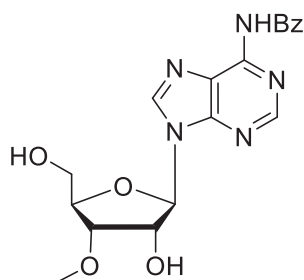


24 (0.426 g, 1.21 mmol) and benzoyladenine (570 mg, 2.38 mmol) were dissolved in 20 mL of dry dichloroethane. BSA (1.55 mL, 6.35 mmol) was added, and the resulting solution was heated at 80 °C for 1 h and then cooled down to room temperature. TMSOTf (0.57 mL, 3.18 mmol) was added and the clear solution was stirred at 80 °C for 2 h. After cooling down to room temperature, the reaction was quenched with sat. NaHCO₃ and extracted 3 times with 50 mL of DCM. The combined organic layers were washed with brine, dried over Na₂SO₄, filtered and evaporated *in vacuo*. The crude mixture was purified by column chromatography (iso-hexane/EtOAc 1:2) to yield **25** as a white solid (301 mg, 0.564 mmol, 46.7 %)

ESI-HRMS: calculated for C₂₇H₂₆N₅O₇⁺ [M+H]⁺: 532,18267; found: 532.18237.

¹H NMR (400 MHz, CDCl₃) δ 9.08 (brs, 1H), 8.60 (s, 1H), 8.02 (s, 1H), 7.99 – 7.86 (m, 4H, Bz), 7.57 – 7.30 (m, 6H, Bz), 6.14 – 6.04 (m, 1H, H-1'), 5.98 (dd, *J* = 5.3, 3.8 Hz, 1H, H-2'), 4.68 (dd, *J* = 12.4, 3.2 Hz, 1H, Ha-5'), 4.54 – 4.44 (m, 2H, H-3' and Hb-5'), 4.38 (ddd, *J* = 6.3, 4.4, 3.1 Hz, 1H, H-4'), 3.42 (s, 3H, OMe), 2.11 (s, 3H, Ac).

¹³C NMR (101 MHz, CDCl₃) δ 169.87, 166.16, 164.4, 152.73, 151.28, 149.72, 142.10, 133.50, 133.41, 132.86, 129.60, 129.33, 128.87, 128.54, 127.91, 123.68, 87.78 (C-1'), 80.41 (C-4'), 78.32 (C-3'), 73.44 (C-2'), 63.36 (C-5'), 59.32 (CH₃-Ac), 20.71 (CH₃).

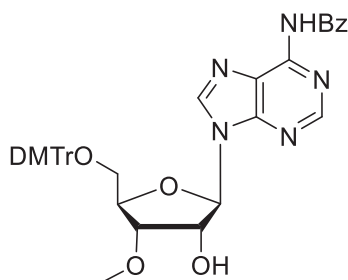
N^6 -benzoyl-3'-OMe adenosine (**26**)¹⁷¹

25 (270 mg, 0.5 mmol) was dissolved in 5 mL of a pyridine/methanol 4:1 solution and the mixture cooled down to 0 °C. 0.86 mL of 2 M NaOH were added and the solution stirred at 0 °C for 20 minutes and then quenched with 0.75 mL of 2 M HCl. The crude mixture was coevaporated with pyridine (2 x 10 mL) and toluene (2 x 10 mL) and purified by column chromatography (DCM/MeOH 93:7) to yield **26** as a white foam (154 mg, 400 μ mol, 79 %).

ESI-MS: calculated for $C_{18}H_{20}N_5O_5^+$ $[M+H]^+$: 386,14590; found: 386.3.

¹H NMR (400 MHz, CD_2Cl_2) δ 9.25 (s, 1H), 8.71 (s, 1H), 8.11 (s, 1H), 8.06 – 7.97 (m, 2H), 7.71 – 7.51 (m, 3H), 5.85 (d, $J = 7.3$ Hz, 1H, H-1'), 5.00 (dd, $J = 7.3, 5.5$ Hz, 1H, H-2'), 4.40 (q, $J = 1.7$ Hz, 1H, H-4'), 4.12 (dd, $J = 5.4, 1.3$ Hz, 1H, H-3'), 4.07 – 3.68 (m, 2H, Ha/b-5'), 3.57 (s, 3H, OMe).

¹³C NMR (101 MHz, CD_2Cl_2) δ 164.45 (CO), 151.82, 150.48, 150.20, 143.08, 133.72, 132.79, 128.82, 127.84, 124.44, 92.16 (C-1'), 84.73 (C-4'), 80.87 (C-3'), 73.58 (C-2'), 63.44 (C-5'), 57.93 (CH_3).

 N^6 -benzoyl-5'-O-DMTr-3'-OMe adenosine (**27**)¹⁷¹

26 (140 mg, 0.36 mmol) was dissolved in 17 mL of pyridine and cooled down to 0 °C. DMAP (4.4 mg, 36 μ mol) and DMTrCl (148 mg, 0.44 mmol) were added and the resulting solution was stirred at room temperature for 4 hours, until TLC showed no more starting material. Methanol was added and the solvents removed *in vacuo*. The product was purified

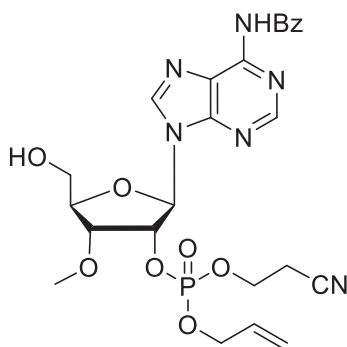
by column chromatography (DCM/MeOH 95:5) to yield **27** as a white foam (213 mg, 309 μmol , 85 %).

ESI-HRMS: calculated for $\text{C}_{39}\text{H}_{38}\text{N}_5\text{O}_7^+$ $[\text{M}+\text{H}]^+$: 688,27658; found: 688.27648.

^1H NMR (400 MHz, CD_2Cl_2) δ 9.06 (s, 1H), 8.58 (s, 1H), 8.49 (dt, $J = 4.4, 1.7$ Hz, 3H), 8.11 (s, 1H), 7.93 – 7.86 (m, 2H), 7.64 – 7.49 (m, 2H), 7.48 – 7.40 (m, 2H), 7.35 – 7.28 (m, 2H), 7.25 – 7.10 (m, 10H), 6.79 – 6.66 (m, 4H), 5.96 (d, $J = 5.0$ Hz, 1H, H-1'), 4.85 (q, $J = 5.0$ Hz, 1H, H-2'), 4.22 (q, $J = 4.2$ Hz, 1H, H-4'), 4.06 (dd, $J = 5.3, 4.1$ Hz, 1H, H-3'), 3.68 (s, 6H, DMTr), 3.39 (s, 3H, OMe), 3.38 – 3.24 (m, 2H, Ha/b-5').

^{13}C NMR (101 MHz, CD_2Cl_2) δ 164.49 (CO), 158.66, 152.34 (C-2), 151.44 (C-4), 149.59, 144.68, 141.81 (C-8), 135.58, 133.94, 132.65, 129.96, 128.79, 127.98, 127.87, 127.79, 126.88, 123.48 (C-5), 113.10, 89.63 (C-1), 86.52, 81.90 (C-4'), 79.97 (C-3'), 73.53 (C-2'), 63.24 (C-5'), 58.23 (CH_3), 55.22 (CH_3 -DMTr).

*N*⁶-benzoyl-3'-OMe adenosine-2'-(cyanoethyl, allyl protected) phosphate **28**



27 (570 mg, 829 μmol) was dissolved in 10 mL of dry DCM. 2-Cyanoethyl *N,N,N,N'*-Tetraisopropylphosphordiamidite (394 μL , 1.24 mmol) was added, followed by pyridine trifluoroacetate (192 mg, 995 μmol) and the mixture was stirred overnight at room temperature. Allyl alcohol (564 μL , 8.3 mmol) and then BTT (5.5 mL of a 0.3M solution in MeCN, 1.66 mmol) were added and the solution was stirred for 1 h at room temperature. *t*BuOOH (497 μL of a 5 M solution in decane, 2.49 mmol) was added and the reaction was stirred at room temperature for 30 min before quenching with NaHSO_3 (1.5 mL of a 0.5 g/mL solution). The product was extracted in EtOAc and the organic phase was washed with brine and dried under vacuum. This intermediate was dissolved in 30 mL of 3 % DCA in DCM and the red solution was stirred for 10 minutes and then quenched with sat. NaHCO_3 . The product was extracted with EtOAc and the organic layer was washed with brine, dried

over Na₂SO₄ and concentrated under vacuum. The crude mixture was purified by column chromatography (DCM/MeOH 95:5) to afford **28** as a white foam (290 mg, 519 μmol, 63 %).

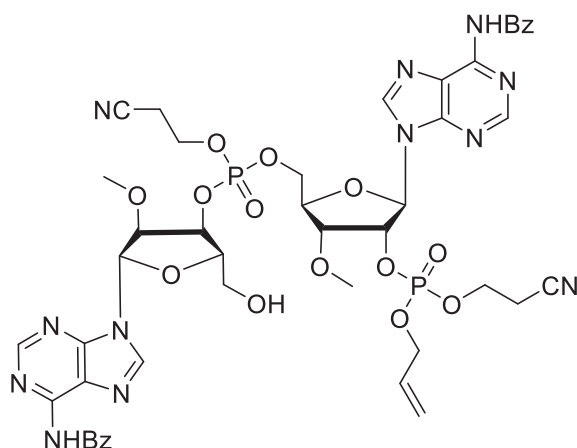
ESI-MS: calculated for C₂₄H₂₈N₆O₈P⁺ [M+H]⁺: 559,17007; found: 559.3.

³¹P NMR (162 MHz, CD₂Cl₂) δ -2.37.

¹H NMR (400 MHz, CD₂Cl₂) δ 9.19 (s, 1H), 8.63 (2s, 1H), 8.13 (2 s, 1H), 7.99 – 7.81 (m, 2H), 7.61 – 7.39 (m, 3H), 6.07 (dd, *J* = 6.7, 5.0 Hz, 1H, H-1'), 5.78 – 5.58 (m, 1H, All-CH₂=CHCH₂), 5.58 – 5.43 (m, 1H, H-2'), 5.21 – 4.99 (m, 2H, All-CH₂=CHCH₂), 4.45 – 4.23 (m, 3H, H-4' and All-CH₂=CHCH₂), 4.17 (ddd, *J* = 7.3, 5.0, 2.2 Hz, 1H, H-3'), 4.10 – 3.93 (m, 2H, CH₂CH₂CN), 3.77 (ddd, *J* = 103.2, 13.0, 1.9 Hz, 2H, Ha/b-5'), 3.44 (2 s, 3H, CH₃), 2.67 – 2.50 (m, 2H, CH₂CN).

¹³C NMR (101 MHz, CD₂Cl₂) δ 164.77 (CO), 152.06 (C-2), 150.78 (C-4), 150.26 (C-6), 143.10 (C-8), 133.64 (quat. Bz), 132.86 (Bz), 131.69 (All-CH₂=CHCH₂), 128.59 (Bz), 127.70 (Bz), 124.37 (C-5), 118.76 (All-CH₂=CHCH₂), 116.53 (CN), 88.71 (C-1'), 85.20 (C-4'), 79.52 (C-3'), 77.08 (All-CH₂=CHCH₂), 69.01 (All-CH₂=CHCH₂), 62.59 (C-5'), 62.42 (CH₂CH₂CN), 58.47(CH₃), 19.58 (CH₂CN).

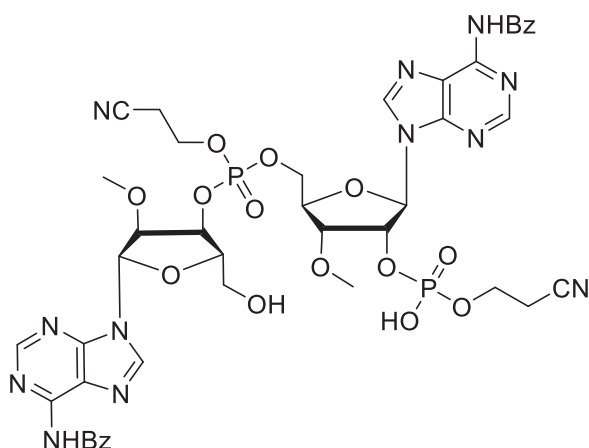
Protected di-OMe-adenosine phosphate **29**



28 (0.29 g, 0.519 mmol) and 2'-OMe-adenosine 3'-phosphoramidite (0.507 g, 0.571 mmol) were dissolved in 3.46 mL of BTT solution (3.46 mL of a 0.3 M solution in MeCN, 1.04 mmol of BTT) and the mixture was stirred at room temperature for 1h. *t*BuOOH (312 μL of a 5 M solution in decane, 312 μmol) was added and the resulting solution was stirred at room temperature for 30 minutes before quenching with NaHSO₃ (1 mL of a 0.5 g/mL solution). The product was extracted with EtOAc, washed with brine and dried *in vacuo*. The residue was redissolved in 20 mL of 3 % DCA in DCM and the red solution was stirred for 10

minutes before quenching with sat. NaHCO₃. The product was extracted with EtOAc, washed with brine dried over Na₂SO₄ and concentrated under vacuum. The crude was purified by column chromatography (DCM/MeOH 96:4) to afford **29** as a mixture of 4 diastereomers (0.38 g, 0.359 mmol, 69 %) that was directly used for the next step.

Deprotected di-OMe-adenosine phosphate **30**



29 (0.38 g, 0.359 mmol) was dissolved in 20 mL of acetone and NaI (0.538 g, 3.59 mmol) was added. The mixture was refluxed for 150 min and then cooled down to room temperature and then to 0 °C to allow precipitation of the product **30**. The mixture was filtered and the white precipitate collected and coevaporated with pyridine (2 x 20 mL) and toluene (20 mL) to obtain **30** as a white solid (0.26 g, 254 μmol, 71 %) that was used without further purification in the next step.

ESI-HRMS: calculated for C₄₂H₄₅N₁₂O₁₅P₂⁺ [M+H]⁺: 1019,25971; found: 1019.26484.

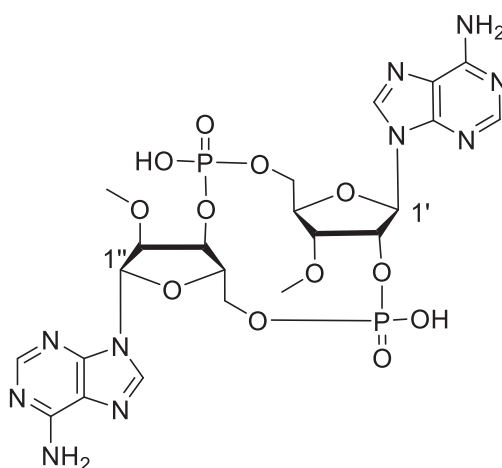
IR (ATR): $\tilde{\nu}$ (cm⁻¹) 3392 (br), 2924 (m), 1695 (m), 1613 (s), 1582 (m), 1451 (s).

³¹P NMR (162 MHz, MeOD) δ -0.73, -0.84, -2.80, -2.98.

¹H NMR (800 MHz, MeOD) δ 8.80 (2 s, 1H), 8.72 (2 s, 1H), 8.67 (2 s, 1H), 8.63 (2 s, 1H), 8.12 – 7.94 (m, 5H), 7.70 – 7.47 (m, 8H), 6.41 (dd, J = 4.1, 2.6 Hz, 1H, H-1'), 6.22 and 6.04 (d, J = 6.8 Hz, 1H, H-1''), 5.58 (dt, J = 9.0, 4.6 Hz, 1H, H-2'), 5.21 (dddd, J = 30.8, 6.8, 4.6, 2.0 Hz, 1H, H-3''), 4.75 and 4.71 (m, 1H, H-2''), 4.68 – 4.50 (m, 3H, H-3' and H-5'), 4.49 – 4.42 (m, 1H, H-4'), 4.39 – 4.26 (m, 3H, H-4''-isomer A and -OCH₂CH₂CN), 4.13 (td, J = 2.9, 1.8 Hz, H-4'' isomer B), 4.05 – 3.87 (m, 2H, -OCH₂CH₂CN), 3.79 (qd, J = 12.5, 2.9 Hz, 2H, H-5'' isomer A) and 3.71 (d, J = 3.0 Hz, 2H, H-5'' isomer B), 3.66 and 3.65 (s, 3H, 3'-OMe),

3.44 and 3.41 (s, 3H, 2''-OMe), 3.01 – 2.88 (m, 2H, -OCH₂CH₂CN), 2.73 (dt, *J* = 19.2, 6.2 Hz, 2H, -OCH₂CH₂CN).

¹³C NMR (201 MHz, MeOD) δ 166.78 (CO), 166.70 (CO), 152.07, 152.01, 151.83, 151.78, 151.69, 151.56, 151.41, 150.02, 149.85, 143.75, 143.41, 133.51, 132.57, 132.45, 132.41, 117.82, 117.13, 88.81 and 88.52 (C-1'), 86.89 (C-1''), 85.17 (C-4''), 81.80 (C-2''), 81.01 (C-4'), 78.46 and 78.27 (C-3'), 76.52 and 76.35 (C-3''), 75.22 and 75.13 (C-2''), 67.73 and 67.43 (C-5'), 63.22 and 63.09 (-OCH₂CH₂CN), 61.11 and 60.34 (C-5''), 57.88, 57.78 (2x CH₃), 18.82, 18.78, 18.72 and 18.68 (-OCH₂CH₂CN).

Methylated c-di-AMP **5**

The crude product **30** (240.0 mg, 235.6 μmol) was redissolved in 30 mL of dry pyridine and MSNT (349 mg, 1.18 mmol) was added. The mixture was stirred overnight at room temperature and then the solvents were removed *in vacuo*. This product was directly used in the next step as a crude without further purification. The resulting solid was dissolved in 20 mL of 33 % MeNH₂ in absolute ethanol. The solution was stirred for 3h at room temperature, after which time LC-MS showed no more starting material present. The solvent was evaporated, the residue coevaporated twice with pyridine and dried under high vacuum. When dried, the solid was redissolved in a minimal amount of methanol, transferred in a falcon tube and precipitated from cold acetone. The precipitate was collected after centrifugation and part of the solid was purified by RP-HPLC (0->10 % B in 45 minutes. Buffer A = 0.1 % TFA in H₂O, buffer B = 0.1 % TFA in MeCN) and freeze-dried to obtain **5** (18 mg, 25.9 μmol, 11 % after HPLC purification) as a white solid.

ESI-HRMS: calculated for C₂₂H₂₇N₁₀O₁₂P₂⁻ [M-H]⁻: 685,12906; found: 685.12851.

IR (ATR): $\tilde{\nu}$ (cm⁻¹) 3301 (w), 2924 (s), 2854 (m), 1647 (m), 1559 (w), 1457 (w).

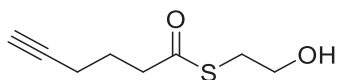
³¹P NMR (162 MHz, MeOD) δ -2.49, -3.71.

¹H NMR (800 MHz, MeOD) δ 9.12 (s, 1H), 8.82 (s, 1H), 8.53 (s, 1H), 8.41 (s, 1H), 6.39 (d, *J* = 7.8 Hz, 1H, H-1'), 6.34 (s, 1H, H-1''), 5.30 (s, 1H, H-2'), 4.87 (d, *J* = 4.2 Hz, 1H, H-3''), 4.55 – 4.42 (m, 4H, H-4', H-4'', Ha-5'', H-2''), 4.36 (dd, *J* = 11.3, 5.5 Hz, 1H, Ha-5'), 4.22 (d, *J* = 4.5 Hz, 2H, H-3' and Hb-5'), 4.08 (d, *J* = 11.1 Hz, 1H, Hb-5''), 3.89 (s, 3H, CH₃), 3.70 (s, 3H, CH₃).

¹³C NMR (201 MHz, MeOD) δ 150.15, 149.83, 149.44, 147.25, 145.19, 144.95, 142.28 (C4), 141.45 (C4), 118.16 (C5), 117.31 (C5), 87.22 (C-1''), 84.39 (C-1'), 83.48 (C-2''), 82.75 (C-4'), 82.32 (C-3'), 80.78 (C-2'), 79.37 (C-4''), 70.70 (C-3''), 67.17 (C-5'), 61.66 (C-5''), 58.35 (CH₃), 57.96 (CH₃).

cGAMP analogue prodrugs

S-(2-hydroxyethyl)hex-5-ynethioate (SATE-alkyne-alcohol **33**)

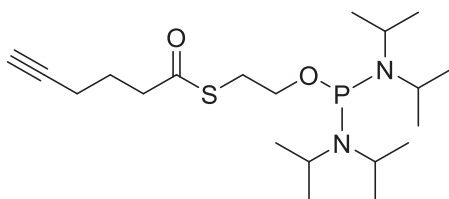


Hexynoic acid (3.0 g, 2.94 mL, 26.8 mmol) and β-mercaptoethanol (3.14 g, 2.82 mL, 40.1 mmol) were dissolved in 250 mL of MeCN. The mixture was cooled at 0°C and DCC was added (5.52 g, 26.8 mmol). The solution was stirred for 20 hours allowing it to reach room temperature, then the solid formed is filtered off and the solution dried under vacuum. The residue was redissolved in Et₂O cooled down and the solid filtered off. The filtrate was dried under vacuum to afford **33** as a viscous oil that was used as a crude in the next step (quant. yield, 4.6 g, 26.8 mmol).

IR (ATR): $\tilde{\nu}$ (cm⁻¹) 3360 (br), 3291 (m), 2936 (w), 1682 (s), 1433 (w).

¹H NMR (400 MHz, CDCl₃) δ 3.75 (t, *J* = 6.0 Hz, 2H), 3.08 (t, *J* = 6.0 Hz, 2H), 2.76 – 2.69 (m, 2H), 2.25 (td, *J* = 6.9, 2.7 Hz, 2H), 1.93 – 1.83 (m, 2H).

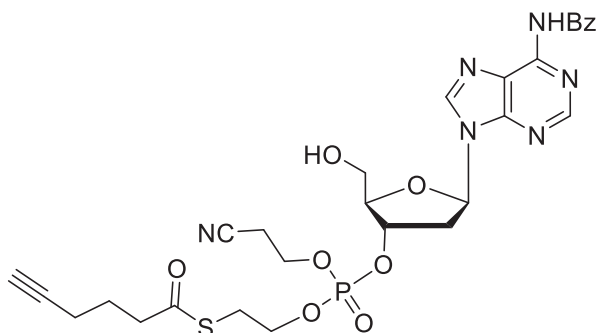
¹³C NMR (101 MHz, CDCl₃) δ 199.26, 82.96, 69.47, 61.80, 42.58, 31.83, 24.07, 17.74.

SATE-alkyne bis-phosphoramidite **34**

33 (2.3 g, 13.5 mmol) and triethylamine (3.13 mL, 22.5 mmol) were dissolved in 50 mL of ether under an argon atmosphere. The clear solution was cooled at 0°C and bis-diisopropylamino chlorophosphine (3.0 g, 11.2 mmol) was added. The mixture was stirred at room temperature for 2 hours, then a 9:1 ether/ NEt_3 solution (80 mL) was added and the solvent evaporated under vacuum until half of the initial volume. 50 mL of cyclohexane were added and the mixture evaporated again until approximately 30 mL of solution were left. This solution was loaded directly into a column packed with cyclohexane + 6 % triethylamine and eluted with the same solvent. The fractions containing the product were evaporated to afford **34** as a colourless oil (3.5 g, 8.7 mmol, 77.3 %).

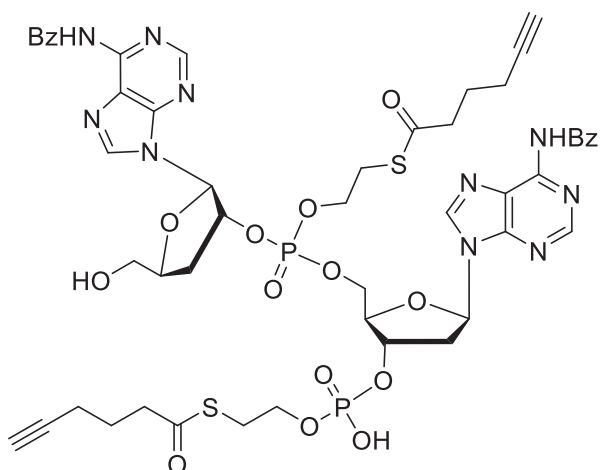
^{31}P NMR (162 MHz, CDCl_3) δ 124.3.

^1H NMR (400 MHz, CDCl_3) δ 3.60 (dt, $J = 7.4, 6.3$ Hz, 2H), 3.44 (dhept, $J = 10.8, 6.7$ Hz, 4H), 3.07 (t, $J = 6.3$ Hz, 2H), 2.67 – 2.59 (m, 2H), 2.19 (td, $J = 6.9, 2.7$ Hz, 2H), 1.91 (t, $J = 2.6$ Hz, 1H), 1.80 (q, $J = 7.2$ Hz, 2H), 1.09 (dd, $J = 6.8, 4.9$ Hz, 24H).

*N*⁶-benzoyl-2'-deoxyadenosine-3'-(cyanoethyl, SATE) phosphate **35**

2'-deoxyadenosine phosphoramidite (1.85 g, 2.2 mmol) and SATE-alkyne-alcohol **33** (742.8 mg, 4.3 mmol) were dissolved in 15 mL of MeCN. BTT (14.4 mL of a 0.3 M sol. in MeCN, 4.3 mmol) was added, and the solution was stirred at room temperature for 1 hour. *t*BuOOH (1.26 mL of 5-6 M solution in decane, approx. 7.6 mmol) was added, and the resulting mixture was stirred at room temperature for 30 min. The reaction was quenched with NaHSO_3 (0.5 g/mL in H_2O , 1.5 mL) and extracted with EtOAc. The organic phase was

trifluoroacetate (176.2 mg, 912.2 μmol) and the solution was stirred overnight at room temperature. After 16 hours, **35** (732.7 mg, 1.14 mmol) and BTT (5.1 mL of a 0.3 M sol. In MeCN, 1.5 mmol) were added and the mixture was stirred at room temperature for 1 hour. *t*BuOOH (0.46 mL of a 5 M sol. In decane, 2.3 mmol) was added and the reaction stirred for 40 min. and then quenched with NaHSO₃. After diluting with EtOAc, the organic layer was washed with NaHCO₃ and brine, dried over Na₂SO₄, filtered and dried *in vacuo*. The residue was redissolved in 35 mL of 3 % DCA in DCM, stirred for 15 min. and then quenched with sat. NaHCO₃. The product was extracted with EtOAc and the organic layer washed with brine, dried over Na₂SO₄, filtered and the solvent evaporated. The product was purified by column chromatography (DCM/acetone/methanol 80:15:5) to obtain **37** as a white solid (447.0 mg, 368.2 μmol , 48.4 %). **37** was composed of a mixture of 4 diastereomers and therefore not characterized at this stage and directly used for the next step.

Deprotected di-deoxyadenosine phosphate **38**

37 (220 mg, 0.181 mmol) was dissolved in 7 mL of MeCN. 2.5 mL of *t*BuNH₂ were added and the mixture stirred for 20 minutes at room temperature. The solvents were removed *in vacuo* and the residue coevaporated twice with pyridine and twice with toluene to obtain **38** as a white foam. (210 mg, quant. yield).

ESI-HRMS: calculated for C₅₀H₅₃N₁₀O₁₅P₂S₂⁻ [M-H]: 1159,26140; found: 1159.26312.

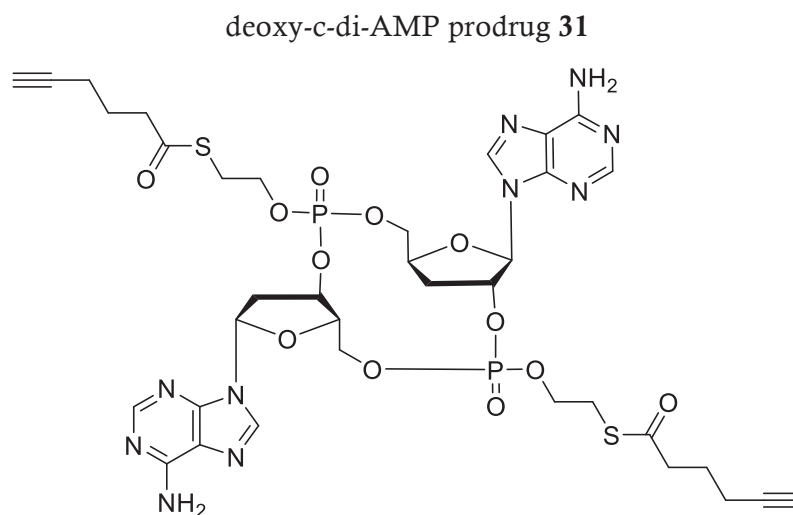
IR (ATR): 3292 (br), 2922 (br), 1688 (m), 1612 (m), 1455 (m).

³¹P NMR (162 MHz, CD₂Cl₂) δ -2.33, -2.63, -2.88, -3.38.

¹H NMR (400 MHz, DMSO-*d*₆) δ 11.25 (4 s, 2H), 8.81 – 8.70 (m, 3H), 7.95 (s, 3H), 7.70 – 7.59 (m, 2H), 7.55 (t, *J* = 7.6 Hz, 4H), 6.46 (dt, *J* = 13.6, 6.9 Hz, 1H, H-1''), 6.32 (dd, *J* =

7.7, 2.1 Hz, 1H, H-1'), 5.52 – 5.29 (m, 2H, H-2' and), 4.85 (tt, $J = 6.4, 3.1$ Hz, 1H), 4.39 (dq, $J = 13.9, 5.3$ Hz, 2H, H-4' and), 4.31 – 4.16 (m, 2H), 4.02 (dq, $J = 13.9, 6.8$ Hz, 2H), 3.82 – 3.74 (m, 2H, H-5'), 3.73 – 3.45 (m, 2H, H-5'), 3.06 (tq, $J = 10.3, 6.2, 4.7$ Hz, 5H), 2.95 (dt, $J = 13.9, 6.9$ Hz, 1H), 2.80 (dt, $J = 4.0, 2.2$ Hz, 2H), 2.71 – 2.57 (m, 5H, H-3' ,), 2.26 (tdd, $J = 13.4, 6.0, 2.7$ Hz, 1H, H-3'), 2.21 – 2.08 (m, 5H), 1.76 – 1.60 (m, 4H).

¹³C NMR (101 MHz, DMSO) δ 198.48, 198.03, 198.01, 166.03, 152.35, 152.16, 150.77, 143.51, 143.26, 133.79, 132.90, 128.97, 128.91, 126.31, 126.14, 89.21, 84.31, 83.89, 81.60, 72.40, 63.38, 62.36, 51.24, 45.87, 42.58, 42.50, 40.63, 40.58, 40.42, 40.37, 40.21, 40.16, 40.00, 39.95, 39.74, 39.53, 39.32, 29.86, 29.78, 28.81, 28.73, 27.59, 24.37, 24.27, 17.42, 17.38, 8.97.



38 (150 mg, 129.2 μ mol) was dissolved in 40 mL of THF and 3 Å molecular sieves were added, followed by TPSCl (1.96 g, 6.46 mmol) and N-methylimidazole (0.515 mL, 6.46 mmol). The mixture was stirred for 30 hours at room temperature and then quenched with water. The product was extracted with EtOAc 3 times and the combined organic phases were evaporated. The product was purified by column chromatography (5 % MeOH in DCM) to afford the cyclized product as a mixture of 4 P-diastereomers as a white solid (68 mg, 59.5 μ mol, 46 %). This product was directly dissolved in a solution of zinc dibromide (5.95 mL of a 1M solution in $\text{CHCl}_3/\text{MeOH}$ 4:1, 5.95 mmol of ZnBr_2) and stirred at room temperature for 72 hours. The reaction was diluted with sat. NaHCO_3 and the product was extracted 5 times with DCM, washed with brine, dried over Na_2SO_4 , filtered and dried *in vacuo*. The residue was redissolved in $\text{H}_2\text{O}/\text{MeCN}$ 80:20 and purified by RP-HPLC (Buffer A: 0.1 % TFA in H_2O , buffer B: 0.1 % TFA in MeCN, gradient: 20-50 % buffer B in 45 minutes, flow: 5 mL/min) to obtain **31** as a mixture of 4 diastereomers (16.1 mg, 28 % after HPLC). Part of

the product was further purified by HPLC to isolate one single isomer which was further characterized by MS and NMR.

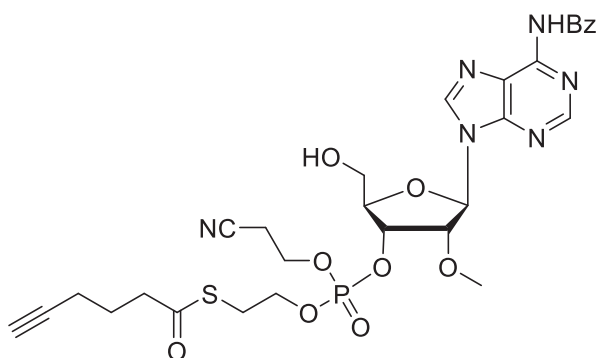
ESI-HRMS: calculated $C_{36}H_{45}N_{10}O_{12}P_2S_2^+$ $[M+H]^+$: 935,21296; found: 935.21480.

^{31}P NMR (162 MHz, MeOD) δ -4.01, -4.37.

1H NMR (599 MHz, MeOD) δ 8.41 – 8.28 (4 s, 4H, H2/H8), 6.55 (t, J = 6.8 Hz, 1H, H-1'), 6.24 (d, J = 5.1 Hz, 1H, H-1''), 5.71 (p, J = 6.1 Hz, 1H, H-2''), 5.61 (tt, J = 5.8, 3.0 Hz, 1H, H-3'), 4.67 (dtt, J = 7.4, 4.8, 2.5 Hz, 1H, H-4''), 4.63 – 4.55 (m, 2H, H-4' and Ha-5''), 4.52 (ddd, J = 10.5, 8.8, 6.5 Hz, 1H, Ha-5'), 4.42 – 4.33 (m, 1H, Hb-5''), 4.32 – 4.22 (m, 3H, Hb-5', -SCH₂CH₂O-), 4.18 (dt, J = 8.0, 6.4 Hz, 2H, -SCH₂CH₂O-), 3.46 (dt, J = 13.9, 6.6 Hz, 1H, Ha-2'), 3.26 (td, J = 6.4, 2.6 Hz, 2H, -COSCH₂CH₂-), 3.21 (t, J = 6.4 Hz, 2H, -COSCH₂CH₂-), 2.94 (ddd, J = 14.5, 6.6, 3.3 Hz, 1H, Hb-2'), 2.85 (dt, J = 14.2, 7.4 Hz, 1H, Ha-3''), 2.70 (dt, J = 21.0, 7.3 Hz, 5H, Hb-3'' and -COCH₂CH₂CH₂CCH), 2.32 – 2.10 (m, 6H, 2x -CH₂CCH and 2x -CH₂CH₂CCH), 1.77 (dp, J = 31.6, 7.1 Hz, 4H, 2x CH₂CH₂CCH).

^{13}C NMR (151 MHz, MeOD) δ 199.34 (CO), 199.31 (CO), 154.81, 154.31, 150.42, 149.93, 149.08, 143.60, 142.51, 121.11 and 120.92 (C-5), 89.02 (C-1''), 86.74 (C-1'), 84.34 (C-4'), 83.76 and 83.73 (C quat. Alkyne), 80.33 (C-3''), 79.65 (C-3'), 77.66 (C-4''), 71.88 (C-5''), 70.59 (2x CH alkyne), 68.49 and 68.05 (-SCH₂CH₂O-), 67.07 (C-5''), 43.37 (COCH₂CH₂CH₂CCH), 37.75 (C-2'), 34.89 (C-3''), 29.75 and 29.59 (-COSCH₂CH₂-), 25.40 (CH₂CH₂CCH), 18.27 (CH₂CH₂CCH).

*N*⁶-benzoyl-2'-OMe-adenosine-3'-(cyanoethyl, SATE) phosphate **40**



2'-OMe adenosine 3'-phosphoramidite (1.0 g, 1.13 mmol) was dissolved in 5 mL of dry DCM and SATE-alkyne alcohol **33** (0.39 g, 2.25 mmol) was added, followed by BTT (7.51 mL of a 0.3 M solution in MeCN, 2.25 mmol of BTT). The mixture was stirred at room temperature for 90 min and *t*BuOOH (0.68 mL of a 5 M solution in decane, 3.38 mmol of *t*BuOOH) was

added. The solution was stirred for 40 min and quenched with a NaHSO₃ solution (0.5 g/mL). The product was extracted with EtOAc, washed with brine and dried *in vacuo* to afford a white foam. This residue was redissolved in 3 % DCA in DCM (42 mL) and the red solution stirred for 15 minutes. The reaction was quenched with sat. NaHCO₃ and the product extracted with EtOAc, washed with brine, dried over Na₂SO₄ and dried *in vacuo*. The crude product was purified by column chromatography (DCM/MeOH 90:10) to afford **40** as a white solid (mixture of two isomers, 0.42 mg, 0.63 mmol, 55.8 %).

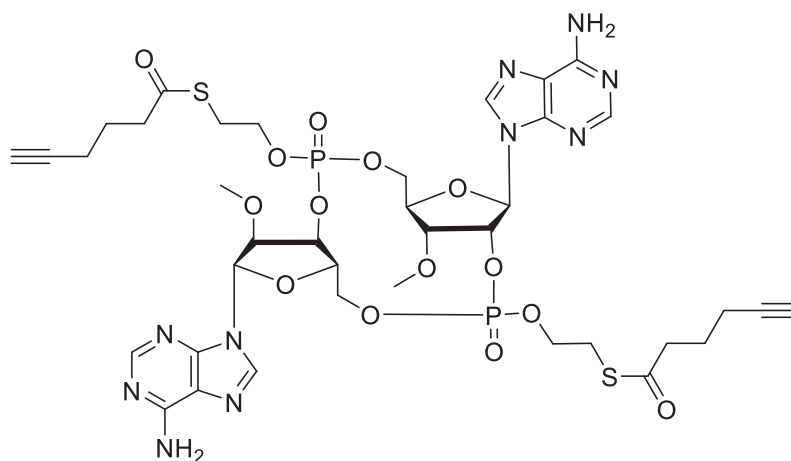
ESI-HRMS: calculated for C₂₉H₃₄N₆O₉PS⁺ [M+H]⁺: 673,18401; found: 673.18408.

³¹P NMR (162 MHz, CD₂Cl₂) δ -2.50, -2.61.

¹H NMR (400 MHz, CD₂Cl₂) δ 9.59 – 9.43 (m, 1H), 8.75 (s, 1H), 8.22 (d, *J* = 8.9 Hz, 1H), 8.03 (dd, *J* = 8.3, 1.3 Hz, 2H), 7.70 – 7.59 (m, 1H), 7.59 – 7.49 (m, 2H), 6.12 – 5.96 (m, 2H, H-1' and 5'-OH), 5.31 (ddd, *J* = 7.1, 4.6, 1.8 Hz, 1H, H-3'), 4.83 (ddt, *J* = 7.1, 4.5, 2.3 Hz, 1H, H-2'), 4.55 (s, 1H, H-4'), 4.42 – 4.20 (m, 4H, -OCH₂CH₂CN and -OCH₂CH₂S-), 4.03 – 3.81 (m, 2H, H-5'), 3.41 (d, *J* = 1.5 Hz, 3H, OCH₃), 3.28 (dt, *J* = 10.4, 6.5 Hz, 2H, -OCH₂CH₂S-), 2.87 (tdd, *J* = 6.0, 4.5, 1.0 Hz, 2H, -OCH₂CH₂CN), 2.78 (td, *J* = 7.4, 0.9 Hz, 2H, -COCH₂CH₂CH₂CCH), 2.36 – 2.20 (m, 2H, CH₂CH₂CCH), 2.08 (dt, *J* = 7.0, 2.7 Hz, 1H, -CH₂CCH), 1.98 – 1.80 (m, 2H, CH₂CH₂CCH).

¹³C NMR (101 MHz, CD₂Cl₂) δ 198.80, 197.87, 197.75, 164.75, 151.96, 150.62, 150.51, 143.36, 133.73, 132.81, 128.80, 127.97, 124.69, 116.76, 88.89, 86.91, 83.00, 81.18, 76.86, 76.79, 69.29, 69.11, 66.56, 62.50, 61.41, 58.83, 58.76, 42.55, 31.72, 28.77, 24.18, 24.07, 19.74, 17.59.

Methyl-c-di-AMP prodrug **32**



27 (390 mg, 0.57 mmol) was dissolved in 5 mL of DCM and **34** (273.9 mg, 0.68 mmol) was added, followed by pyridine trifluoroacetate (125.9 mg, 0.65 mmol). The mixture was stirred under argon overnight, then **40** (418 mg, 0.62 mmol) and BTT (3.77 mL of a 0.3 M solution in MeCN, 1.13 mmol) were added and the solution was stirred at room temperature for 90min. *t*BuOOH (0.34 mL of a 5 M solution in decane, 1.69 mmol) was added and the solution was stirred for 40 minutes and then quenched with NaHSO₃ (0.5 mL of a 0.5 g/mL solution). The product was extracted with EtOAc, washed with brine and dried *in vacuo*. The residue was redissolved in 3 % DCA in DCM (27 mL) and the red solution was stirred for 30 minutes and then quenched with saturated NaHCO₃. The product was extracted with EtOAc, washed with brine and dried over Na₂SO₄. The crude was purified by column chromatography to afford the protected linear dimer as a mixture of 4 diastereomers (144 mg, 113 μmol, 20 %). This intermediate was dissolved in 4 mL of MeCN and 1 mL of *t*BuNH₂ was added. The mixture was stirred at room temperature for 20 minutes and then dried *in vacuo*. The foam obtained was coevaporated twice with pyridine and twice with toluene. The dry residue was dissolved in 40 mL of MeCN and 3 Å molecular sieves were added to this solution. TPSCl (1.79 g, 5.9 mmol) and N-methylimidazole (0.47 mL, 5.9 mmol) were added and the solution was stirred at room temperature for 48 hours. 20 mL of H₂O were added and the mixture was stirred for 45 minutes and then extracted 3 times with EtOAc. The combined organic phases were washed with brine dried over Na₂SO₄, filtered and dried *in vacuo*. The crude was purified by column chromatography (DCM/MeOH 95:5) to afford the protected cyclic dinucleotide as a mixture of 4 diastereomers (43 mg, 35.7 μmol, 30.3 %). This intermediate was deprotected by dissolving it into a 1 M solution of ZnBr₂ in CHCl₃/MeOH 4:1 (3.57 mL, 805 mg of ZnBr₂, 3.57 mmol). The mixture was stirred for 48 hours until when LC-MS analysis showed complete reaction. The product was extracted 5 times with DCM, washed with brine and the solvent was evaporated. The crude mixture was purified by RP-HPLC obtaining **32** as a mixture of 4 diastereomers (25.2 mg, 25.3 μmol, 70.9 %). One of the isomers was isolated by RP-HPLC and further characterized by MS and ¹H-NMR.

ESI-HRMS: calculated for C₃₈H₄₉N₁₀O₁₄P₂S₂⁺ [M+H]⁺: 995,23409; found: 995.23690.

³¹P NMR (162 MHz, MeOD) δ -2.55, -3.91.

¹H NMR (400 MHz, MeOD) δ 8.76 (s, 1H), 8.41 (s, 1H), 8.28 (2s, 2H), 6.37 (d, *J* = 8.5 Hz, 1H, H-1'), 6.25 (d, *J* = 4.8 Hz, 1H, H-1''), 5.52 (ddt, *J* = 11.2, 8.7, 4.3 Hz, 2H, H-2' and H-3''), 5.01 (t, *J* = 4.9 Hz, 1H, H-2''), 4.65 – 4.30 (m, 11H, H-3', H-5', H-5'', H-4', H-4''), 2x -SCH₂CH₂O-, 3.64 (2 s, 6H, 2x CH₃), 3.34 (m, 4H, 2x COSC_HCH₂-) 2.84 – 2.63 (m, 4H, 2x

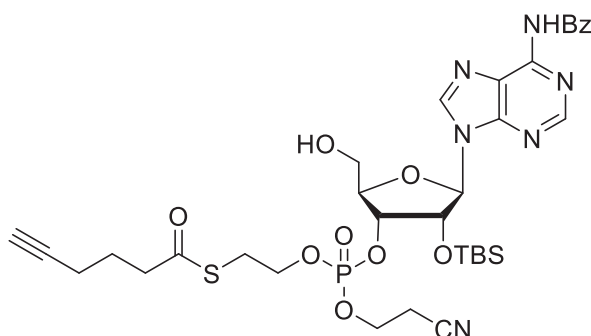
COCH₂CH₂CH₂CCH), 2.33 – 2.17 (m, 6H, 2x -CH₂CCH and 2x -CH₂CH₂CCH), 1.87 (p, *J* = 7.1 Hz, 2H, CH₂CH₂CCH), 1.79 (p, *J* = 7.1 Hz, 2H, CH₂CH₂CCH).

The amount of the single isomer obtained was not sufficient to obtain a ¹³C-NMR spectrum of this product with a sufficiently high signal-to-noise ratio. 2D-NMR spectra such as HSQC and HMBC were recorded and used to assign ¹H-NMR peaks.

Towards the synthesis of hydroxyl-containing cGAMP prodrugs

The syntheses described below did not lead to the desired final products. Therefore, full analytical data for these intermediates were not collected. LC-MS retention times and measured *m/z* are reported for the products for completeness.

*N*⁶-benzoyl-2'-*O*-TBS-adenosine-3'-(cyanoethyl, SATE) phosphate **48**



2'-*O*-TBS-5'-*O*-DMTr *N*⁶-benzoyl-adenosine (3.00 g, 3.81 mmol) was dissolved in 20 mL of dry DCM under N₂. bis(diisopropylamino) chlorophosphine (1.72 g, 1.81 mL, 5.71 mmol) and pyridine trifluoroacetate (1.10 g, 5.71 mmol) were added and the mixture stirred overnight at room temperature. After 18 hours, TLC (*iso*-hexane/ethyl acetate 1:1) confirmed disappearance of the starting material and the mixture was directly loaded into a short column (*iso*-hexane/ethyl acetate 2:1). The fractions containing the product were evaporated resulting in 3.47 g of adenosine phosphoramidite as a white foam (3.52 mmol, 92.3 %).

³¹P-NMR: δ(ppm)= 149.19, 150.67.

The *N*⁶-benzoyl-adenosine phosphoramidite obtained above (3.47 g, 3.52 mmol) was dissolved in 20 mL of dry MeCN. **33** (1.81 g, 10.53 mmol) was added, followed by BTT (1.35 g, 23.41 mL of a 0.3 M solution in MeCN, 7.02 mmol) and the mixture was stirred for 90 min at room temperature. *t*BuOOH (5 M in decane, 2.11 mL, 10.53 mmol) and the solution stirred at room temperature for 45 min, then quenched with a NaHSO₃ solution (0.5 g/mL, 2.0 mL). The product was extracted with 150 mL of ethyl acetate, washed with brine and the organic

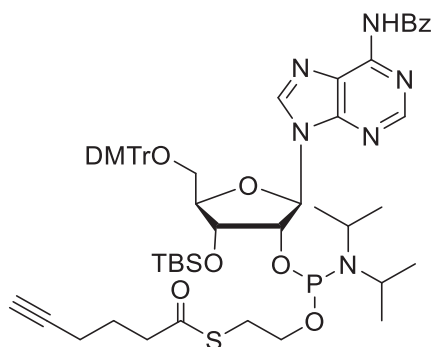
phase was dried over Na_2SO_4 , filtered and the filtrate was evaporated. The solid residue was dissolved in 100 mL of 3 % DCA in DCM and the deep red solution was stirred for 10 min at room temperature and quenched with sat. NaHCO_3 . The product was extracted twice with 500 mL of ethyl acetate, washed with brine and the organic phase was dried over Na_2SO_4 , filtered and the filtrate evaporated. The crude mixture was purified by flash column chromatography eluting with DCM/acetone/methanol 77:20:3. The product **48** consisting of a mixture of two diastereomers was obtained as a white foam (1.70 g, 2.20 mmol, 62.7 %)

LC-MS: (Buffer A = 0.01 % formic acid in H_2O , buffer B = 0.01 % formic acid in MeCN, method: 5-80 % buffer B in 7 minutes, then 95 % B for 1 minute): t_R : 7.2 min, m/z = 773.5 $[\text{M}+\text{H}]^+$.

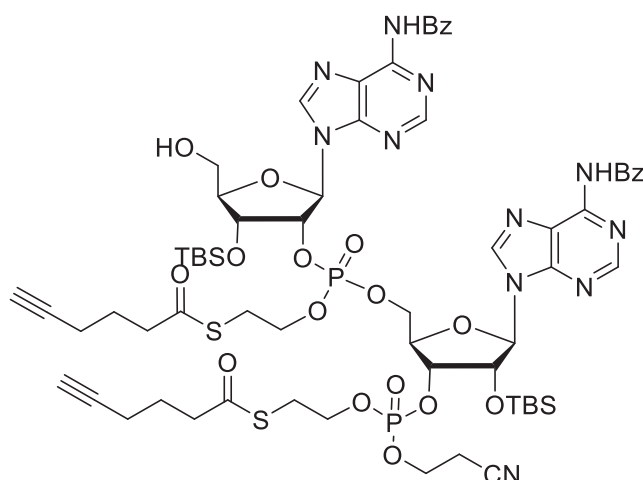
^{31}P NMR (162 MHz, CD_2Cl_2) δ -2.30, -2.38.

^1H NMR (400 MHz, CD_2Cl_2) δ 9.23 (s, 1H), 8.88 (s, 1H), 8.25 (d, J = 9.3 Hz, 1H), 8.15 – 8.08 (m, 2H), 7.82 – 7.57 (m, 3H), 6.08 (dd, J = 7.7, 5.4 Hz, 1H), 6.02 (dd, J = 12.0, 2.4 Hz, 1H), 5.35 (ddd, J = 7.5, 4.7, 2.6 Hz, 1H), 5.13 (dt, J = 8.2, 4.3 Hz, 1H), 4.66 (s, 1H), 4.50 – 4.38 (m, 2H), 4.38 – 4.28 (m, 2H), 4.14 – 3.85 (m, 2H), 3.41 – 3.30 (m, 2H), 2.94 (tdd, J = 6.2, 1.9, 0.9 Hz, 2H), 2.87 (td, J = 7.4, 1.8 Hz, 2H), 2.39 (tt, J = 6.8, 2.6 Hz, 2H), 2.17 (td, J = 2.6, 1.5 Hz, 1H), 2.06 – 1.94 (m, 2H), 0.86 (d, J = 3.0 Hz, 9H), -0.21 (d, J = 1.6 Hz, 3H).

Adenosine 3'-*O*-TBS-2'-SATE-alkyne phosphoramidite **49**

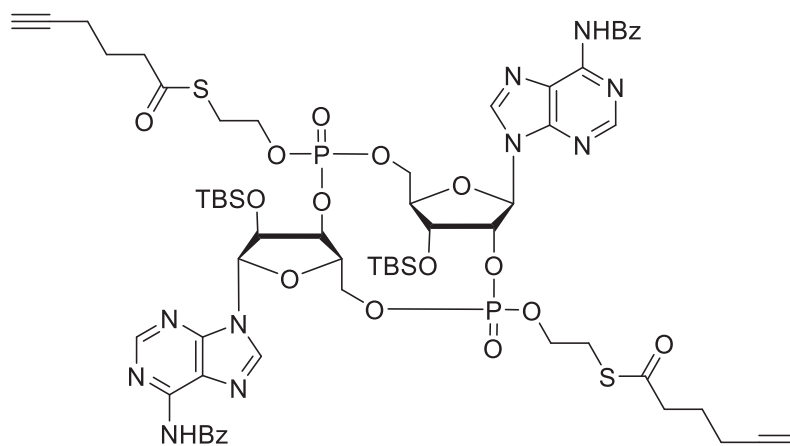


*N*⁶-benzoyl-3'-*O*-TBS-5'-*O*-DMTr adenosine (2.20g, 2.79 mmol) was dissolved in 15 mL of dry DCM. **34** (1.91 g, 4.75 mmol) was added followed by pyridine trifluoroacetate and the mixture was stirred at room temperature for 18h. The mixture was directly loaded into a column and the product was eluted with ihexane/EtOAc 3:2 to afford **49** as a white foam (2.29 g, 2.10 mmol, 75.3 %) which was directly used in the next step.

Protected diadenosine bis-SATE-alkyne phosphate **50**

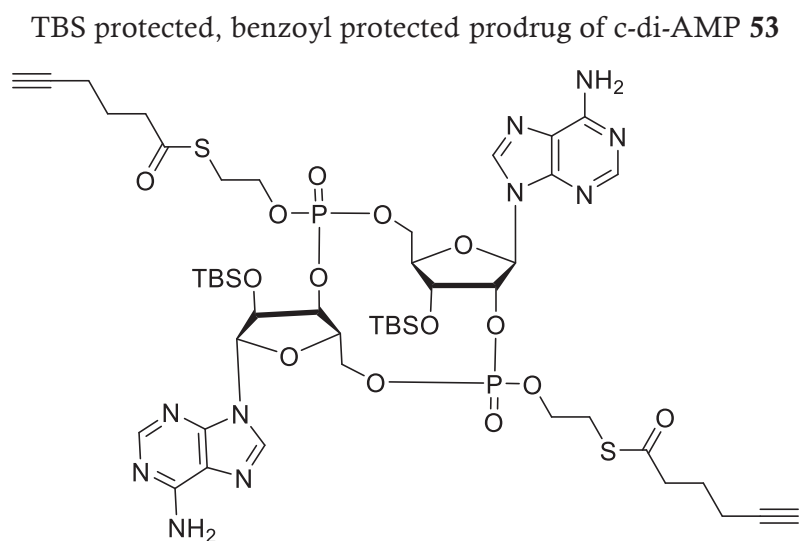
49 (1.50 g, 1.38 mmol) and **48** (1.06 g, 1.38 mmol) were dissolved in 10mL of dry MeCN under N₂. BTT (9.18 mL of a 0.3 M solution in MeCN, 2.75 mmol) was added and the solution stirred at room temperature for 90 minutes. *t*BuOOH (826μL of a 5 M solution in decane, 4.13 mmol) was added and the mixture stirred for 45 minutes, then quenched with a NaHSO₃ solution (0.5 g/mL, 0.6 mL). The product was extracted with ethyl acetate and washed with brine. The organic phase was dried over Na₂SO₄, filtered and the solvent evaporated to afford a crude mixture that was purified by flash column chromatography (eluent: DCM/acetone/methanol 80:19:1 to 80:16:4) to afford 1.22 g of **50** as a white solid (0.83mmol, 60.1 %).

LC-MS (Buffer A = 0.01 % formic acid in H₂O, buffer B = 0.01 % formic acid in MeCN, method: 5-80 % buffer B in 7 minutes, then 95 % B for 1 minute): *t*_R: 8.80 min, *m/z*= 1474.9 [M+H]⁺.

TBS protected, benzoyl protected prodrug of c-di-AMP **52**

50 (1 g, 0,678 mmol) was dissolved in 25 mL of a 4:1 mixture of acetonitrile and *t*BuNH₂ to remove the cyanoethyl group. The mixture was stirred at room temperature for 15 minutes and the solvent removed. The solid residue was co-evaporated with pyridine and then 3 times with acetonitrile to obtain the free phosphate intermediate **51** and redissolved in 180 mL of dry THF. Molecular sieves were added, followed by TPSCl (5.13 g, 16.95 mmol) and N-methylimidazole (1.39 g, 1.35 mL, 16.95 mmol). The mixture was stirred at room temperature for 36 hours, then molecular sieves were filtered off and the reaction was quenched with 100 mL of H₂O and stirred for one more hour. THF was evaporated and the product was extracted with 250 mL of ethyl acetate. The organic phase was washed with brine, dried over Na₂SO₄, filtered and the filtrate was evaporated to afford a white-yellow solid that was purified by flash column chromatography (eluent: DCM/methanol 98:2 to 93:7). 700 mg of product **52** were obtained as a white solid (498.7 μmol, 73.5 %).

LC-MS (Buffer A = 0.01 % formic acid in H₂O, buffer B = 0.01 % formic acid in MeCN, method: 5-80 % buffer B in 7 minutes, then 95 % B for 1 minute): *t*_R: 8.98-9.32 min (4 diastereomers), *m/z*= 1403.9 [M+H]⁺.



LC-MS (Buffer A = 0.01 % formic acid in H₂O, buffer B = 0.01 % formic acid in MeCN, method: 5-80 % buffer B in 7 minutes, then 95 % B for 1 minute): t_R : 8.2-8.6 min (4 diastereomers), m/z = 1196.8 [M+H]⁺.

5 Published work

“Dendrimer-Based Signal Amplification of Click-Labelled DNA in Situ”

Nada Raddaoui[#], Samuele Stazzoni[#], Leonhard Möckl, Bastien Viverge, Florian Geiger, Hanna Engelke, Christoph Bräuchle, and Thomas Carell, *ChemBioChem* **2017**, *18* 1716-1720.

[#]: These authors contributed equally to this work.

Introduction and summary

Cell proliferation is defined as the increase of the number of cells in a sample. Measuring cell proliferation rate is highly important from basic to clinical research, because it allows to study cell health and behaviour.^{172,173} In drug discovery, for example, measuring cell proliferation can be an excellent method of quantifying the toxic effects of a drug candidate. In cancer research and diagnosis, instead, the fast proliferation rate of tumour cells can be used as tool to recognize them from healthy cells, allowing rapid and reliable detection of carcinogenic cells in a sample. Many methods are used to measure and quantify cell proliferation rate, depending of which cell cycle phase is used for the measurement itself.¹⁷³

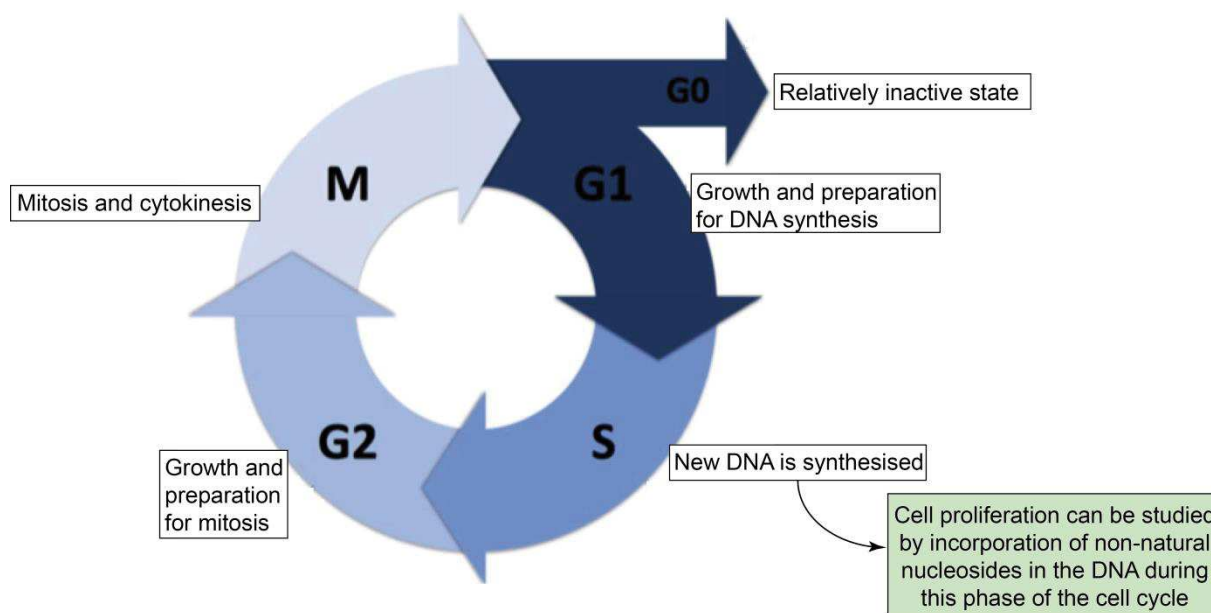


Figure 50: Illustration of the cell cycle. Figure adapted from Romar *et al.*¹⁷³

Of all these methods, the ones taking advantage of the DNA synthesis process occurring during the cell S-phase are among the most used ones especially in live cell samples because of their accuracy and reliability. In order to measure cell proliferation with these methods, nucleoside analogues that can be incorporated into the newly synthesised DNA are added to

the cell culture medium for a fixed amount of time. The amount of incorporated modified nucleoside can then be detected using specific reporters and quantified.

One of the first examples of this technique relies on the incorporation of a radioactive thymidine analogue ($[^3\text{H}]\text{TdR}$) which is added to cell culture and incubated for several days. After washing steps to remove the excess $[^3\text{H}]\text{TdR}$, the incorporated radioactive nucleoside analogue can be detected and quantified using a scintillation counter, allowing to accurately measure the cell proliferation rate of a sample compared to a control. The use of radioactive material represents a drawback of this method, which requires careful handling of the samples and expensive procedure for the measurements and for waste disposal.^{174,175}

A similar cell proliferation assay is the BrdU assay, in which the thymidine analogue 5-bromo-deoxyuridine (BrdU) is used. Incorporated BrdU can finally be detected by a specific monoclonal antibody which can be directly connected to a fluorescent dye or quantified in a following step with a secondary antibody. Quantification of the incorporated analogue can be achieved using fluorescence microscopy or flow cytometry.^{176–179}

More recently, a novel cell proliferation technique has been developed, relying on the use of 5-ethynyl-deoxyuridine (EdU) as nucleoside analogue. Quantification of incorporated EdU can be achieved by employing click-chemistry with a reporter fluorescent azide that can be covalently linked to EdU after cell fixation and permeabilization, allowing precise quantification by fluorescence microscopy or flow cytometry.^{180–182}

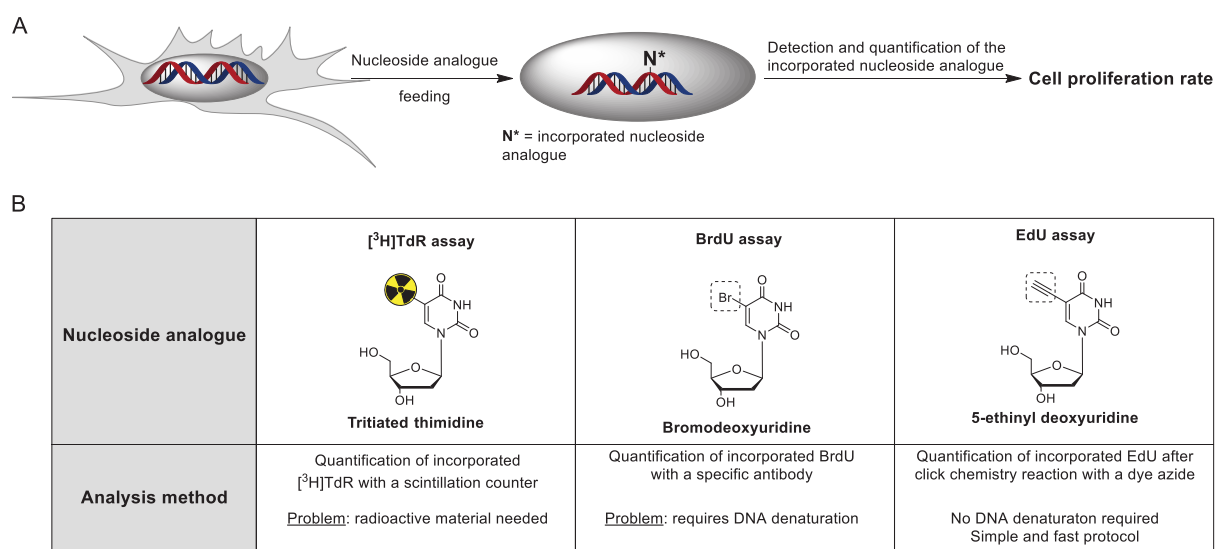


Figure 51: Comparison of the most used methods to study cell proliferation by DNA synthesis. A) General procedure of a cell proliferation assay based on the incorporation of nucleoside analogues. B) Comparison between the three most used methods based on the incorporation of thymidine analogues.

The sensitivity of the described methods is limited by the number of nucleoside analogues that can be incorporated in the newly synthesised DNA during cell division. This can lead to the problem that carcinogenic cells that are proliferating with a faster, but similar rate to healthy cells, can escape detection.

In this work we aimed to develop a method that could be used to increase the detection signal obtained in the EdU cell proliferation assay by using a sandwich-type assay. We designed and synthesised dendrimeric molecules with multiple azides and alkynes that allow further functionalization with multiple dyes. By using the synthesised molecules in two different protocols, we were able to improve the signal intensity and the signal-to-noise ratio to allow better detection of fast proliferating cell using fluorescence microscopy or high-throughput content assays.

Declaration of contribution

In this work, I was responsible for the design, synthesis and purification of the tetraazide dendrimers while the synthesis and purification of the alkyne-containing dendrimer was performed by *B. Viverge*. Furthermore, I performed and optimised the labelling experiments on alkyne-containing oligonucleotides and analysed the products by MALDI-TOF mass spectrometry and HPLC analysis. I also performed initial cellular assays with the azide dendrimers and alkyne-containing dyes to provide the first results showing the feasibility of the designed assay. The optimization of the experimental condition for cellular assays and the high throughput assays were performed by *N. Raddaoui*. The final fluorescence microscopy measurements were performed by *L. Möckl*. All the described experiments and obtained data were planned and analysed together by all the authors of this manuscript.

Authorization

Copy of the final published version of the paper reproduced with the authorization of the publisher. Copyright Wiley-VCH Verlag GmbH & Co. KGaA.

Dendrimer-Based Signal Amplification of Click-Labelled DNA in Situ

Nada Raddaoui⁺, Samuele Stazzoni⁺, Leonhard Möckl, Bastien Viverge, Florian Geiger, Hanna Engelke, Christoph Bräuchle, and Thomas Carell^{*[a]}

The in vivo incorporation of alkyne-modified bases into the genome of cells is today the basis for the efficient detection of cell proliferation. Cells are grown in the presence of ethynyl-dU (EdU), fixed and permeabilised. The incorporated alkynes are then efficiently detected by using azide-containing fluorophores and the Cu^I-catalysed alkyne–azide click reaction. For a world in which constant improvement in the sensitivity of a given method is driving diagnostic advancement, we developed azide- and alkyne-modified dendrimers that allow the establishment of sandwich-type detection assays that show significantly improved signal intensities and signal-to-noise ratios far beyond that which is currently possible.

The proliferation rate of cells is a key parameter that in many contexts requires precise determination.^[1] Cell-proliferation assays routinely help, for example, to evaluate the toxicity of compounds in the framework of the development of new pharmaceuticals.^[2] Also, in cancer diagnostics, it is required to measure the proliferation of cells with high precision.^[3] In this field in particular, the highest sensitivity possible is desired to detect, at best, even single cancer cells in a patient sample. Today, the most precise way to measure cell proliferation is to culture the cells in the presence of C5-ethynyl-dU (EdU), which is incorporated into the genome of proliferating cells as a typical antimetabolite.^[4] The amount of incorporated EdU is subsequently measured by treating the alkynes within the DNA with azido-modified fluorescent dyes by using the Cu^I-catalysed alkyne–azide click reaction^[5] and by detecting with fluorescent microscopy.^[6] These reactions proceed on DNA with extreme efficiency, likely because Cu^I is loosely pre-coordinated to the electron-rich centres at the nucleobases.^[6] This technology is used in established commercially available kits (e.g., EdU-Click kit from baseclick and Click-iT from Thermo Fisher). However, in all of the available methods, the sensitivity is limited by the number of alkynes that is incorporated during the culturing phase of the experiment in the presence of EdU (one alkyne). This creates the problem that slowly proliferating, but still

carcinogenic, cells often escape detection.^[7] We report herein a sandwich-type approach with alkyne- and azide-containing dendrimers **1** and **2** (Scheme 1) that allows significant chemical-signal amplification. The method was shown to provide unprecedented detection sensitivities for proliferating cells. The synthesis of needed amplifying tetraazide/alkyne molecules **1** and **2** is depicted in Scheme 1 (see also Schemes S1 and S2 in the Supporting Information). In both cases, the principle design idea was to stay as close as possible to poly(ethylene glycol)-based structures, because of the needed high solubility in water. The starting point towards **1** was ethylene glycol derivative **3**, which we first converted into azide **4**. The hydroxy group was subsequently tosylated by using 4-toluenesulfonyl chloride (TsCl) to give **5** to enable the fourfold substitution reaction with ethylenediamine ultimately to give desired tetraazide compound **1**.

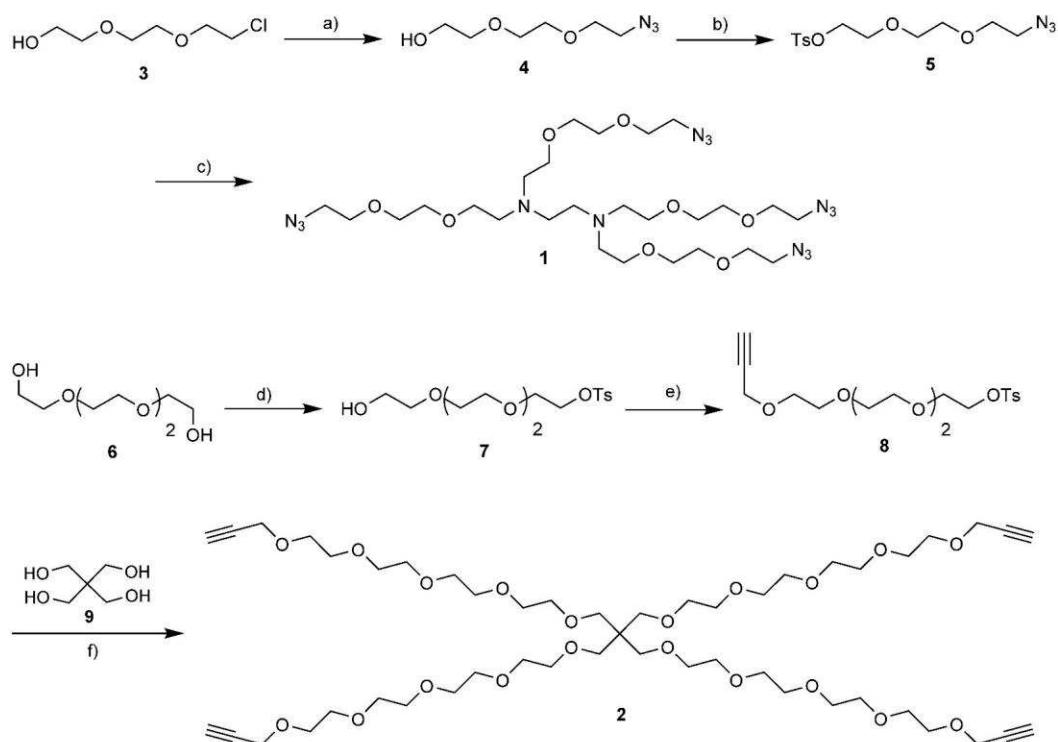
The synthesis of tetraalkyne **2** started with ethylene glycol derivative **6**, which was monotosylated in excellent yield to provide **7**. Reaction with propargyl bromide furnished compound **8**, which was used for a fourfold substitution reaction with pentaerythritol (**9**) to give dendrimer **2**. Both compounds **1** and **2** were subsequently purified by flash column chromatography.

In a first approach to amplify the cell-proliferation signal, we used poly(ethylene glycol)-based tetraazide molecule **1** (Figures 1A and S3). For the experiments, we grew HeLa cells in μ -slides in the presence of 10 μ M EdU for 2 h. The medium was removed and 3.7% formaldehyde in phosphate-buffered saline supplemented with 0.02% Tween (1 \times PBS-T) buffer was added to fix the cells. After being washed twice with 1 \times PBS-T, the cells were permeabilised with 0.5% Triton X-100 in 1 \times PBS-T for 20 min at room temperature (RT). We then added the click cocktails successively. In one experiment, we just added TAMRA–azide **10** (20 μ M) as a positive control. In the other experiment, we performed a first reaction with dendrimer **1** (20 μ M) for 1 h followed by a second click reaction with TAMRA–alkyne **11** (5 μ M) for 30 min. (For more detailed characterisation of the reaction products, determined with a simplified model by using synthetic oligonucleotides, see the Supporting Information.) In both experiments, we washed the fixed cells twice with 3% bovine serum albumin (BSA) in PBS buffer. In the dendrimer-amplified experiment with TAMRA–alkyne **11**, we noted an unusually high background, even after the intensive washing steps. Screening for appropriate washing conditions showed that best results were obtained if we washed with a solution of guanidinium isocyanate (Figure S4). We then determined the TAMRA fluorescence by using a fluorescence

[a] N. Raddaoui,⁺ S. Stazzoni,⁺ Dr. L. Möckl, B. Viverge, F. Geiger, Dr. H. Engelke, Prof. Dr. C. Bräuchle, Prof. Dr. T. Carell
Center for Integrated Protein Science (CiPSM)
Department of Chemistry, LMU München
Butenandtstrasse 5–13, 81377 München (Germany)
E-mail: thomas.carell@lmu.de

[⁺] These authors contributed equally to this work.

Supporting Information and the ORCID identification numbers for the authors of this article can be found under <https://doi.org/10.1002/cbic.201700209>.



Scheme 1. Synthesis of ethylene glycol based tetraazide **1** and tetraalkyne **2** needed for the study. Reagents and conditions: a) NaN_3 , DMF, 90°C , overnight, 96%; b) TsCl , Et_3N , CH_2Cl_2 , overnight, 90%; c) ethylenediamine **5**, KOH , LiBr , DMF, 60°C , overnight, 63%; d) TsCl , Et_3N , THF, RT, overnight, 92%; e) propargyl bromide, NaH , THF, 0°C to RT, 82%; f) **8**, K_2CO_3 , acetone, 80°C , overnight, 31%.

microscope. The data are depicted in Figure 1B. Clearly visible is that the first click reaction with dendrimer-azide **1** furnished a sixfold increase in the fluorescence signal. This is particularly visible in the fluorescence microscopic evaluation of the click-modified cells (Figure 1C).

We noted that after extensive washing with guanidinium isocyanate, the background was reduced but was steadily higher than that in the non-dendrimer experiments. We speculated that this background problem may have been caused by dye-alkyne **11**, possibly because alkynes are known to react to some extent with nucleophiles. Thiol-containing nucleophiles are abundantly present in cells. Control experiments performed without the addition of tetraazide **1** confirmed this hypothesis and showed a still-high background signal even without the use of our dendrimers (Figure S4).

In order to solve the background problem and to increase the sensitivity (signal-to-noise ratio) of detection further, we next experimented with a double-dendrimer approach (Figure 2), by which we first treated the fixed DNA with tetraazide **1**, and this was followed by an additional click reaction with tetraalkyne-dendrimer **2**. Then, we performed a final click reaction with TAMRA-azide **10** (Figure S5). In this way, we planned to circumvent the use of the problematic dye-alkynes.

For this experiment, we again cultured HeLa cells in μ -slides in the presence of $10\ \mu\text{M}$ EdU for 2 h. The medium was removed, and 3.7% formaldehyde in $1\times$ PBS-T was again added to fix the cells. We washed the cells two times with $1\times$ PBS-T and permeabilised the cells with 0.5% Triton in $1\times$ PBS-T for

20 min at RT. We then added the click cocktails successively: First, we added Cu^I and tetraazide **1**. We washed the cells twice with a $0.2\ \text{M}$ acetate buffer pH 4.7, which was followed by two washing steps with $1\times$ PBS-T, and we subsequently performed the second click reaction with tetraalkyne **2** and Cu^I for 1 h. The cells were again washed twice with $1\times$ PBS-T. Finally, we added Cu^I and TAMRA-azide **10** to the cells and allowed the final click cocktail to penetrate the cells for 30 min. After the cells had again been washed twice with guanidinium isocyanate, we studied them by fluorescence microscopy. This time the experiment was a full success. We detected a strongly reduced background, not higher than that in the control experiment with just EdU (Figure 2B, C). The obtained fluorescence signal was highly improved by a factor of 2.5. Most importantly, direct inspection of the cells by fluorescence microscopy showed a strongly improved signal-to-noise ratio (Figures 2C and S5).

Next, the new single- and double-dendrimer-based methods were applied for high-throughput screening (HTS). This method is the most widely used tool not only for the development of new pharmaceutical compounds but also for the measurement of the response of cells to different nutrients, mitogens, cytokines, growth factors and toxic agents.^[8] With the signal amplification provided by our dendrimers, we were able to detect a strong, specific signal even if only a very small number of cells, such as just 100 cells, was present per well (Figure 3). This is a significant improvement over contemporary methods that need 500 to 1000 cells per well, and thus, we

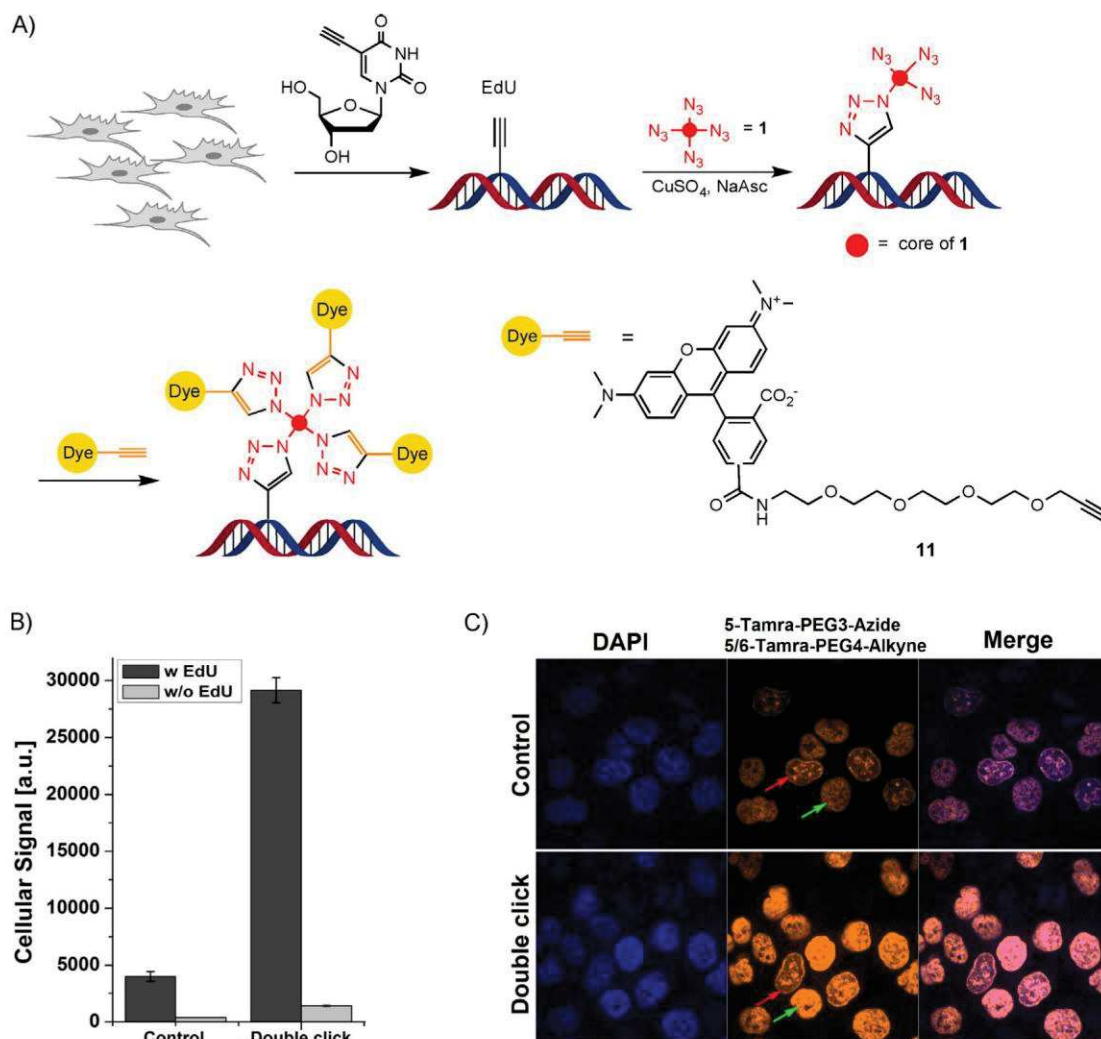


Figure 1. A) Depiction of the single dendrimer (double click) amplified cell-proliferation assay. Cells were grown in the presence of 5-ethynyl-dU. The cells were fixed, and the present alkynes were treated with tetraazide-dendrimer **1** in the presence of Cu^{I} (double click). The multiple-azide-containing DNA was then detected in situ with alkyne-modified dye **11** by again using the Cu^{I} -catalysed click reaction. B) The control experiment was performed by using the dendrimer-free standard proliferation assay with **10**. Double click shows data after dendrimer amplification. C) Fluorescence microscopy pictures of cells detected with the standard assay as control (top) and after dendrimer amplification (bottom). Red arrays show cells in the early S-phase with partial EdU incorporation. Green arrows show cells in late S-phase, for which the DNA synthesis is almost finished and EdU is incorporated into the whole genome. Scale bars: 20 μm .

can now reliably detect a small number of proliferating cells that would otherwise escape staining and detection. What we noted, however, was a reduction in the signal intensity in the double-dendrimer approach, which was likely due to self-quenching of the then densely packed fluorophores. To solve this, optimisation of the dendrimers is now required.

In summary, click-based detection of cell proliferation is today state-of-art technology. We showed herein that by using a dendrimer-type tetraazide (i.e., compound **1**) and a dendrimer-type tetraalkyne (i.e., compound **2**), sandwich-type detection assays could be established that yielded strongly improved signal intensities with low background and that gave higher signal-to-noise ratios for imaging and high-throughput-content assays. We expect that the so-improved cell-proliferation assay will be able to detect either slowly or even single proliferating cancer cells with unprecedented sensitivity.

Acknowledgements

We thank the Deutsche Forschungsgemeinschaft for financial support through SFB1032 (TP-A5), GRK2062 and CA275 and the Excellence Cluster CiPS^M. Further support from the European Union through the Marie Curie International Training and Mobility Network "Clickgene" (grant No. 642023) is acknowledged.

Conflict of Interest

The authors declare no conflict of interest.

Keywords: cell proliferation · click chemistry · dendrimers · fluorescence microscopy · high-throughput screening

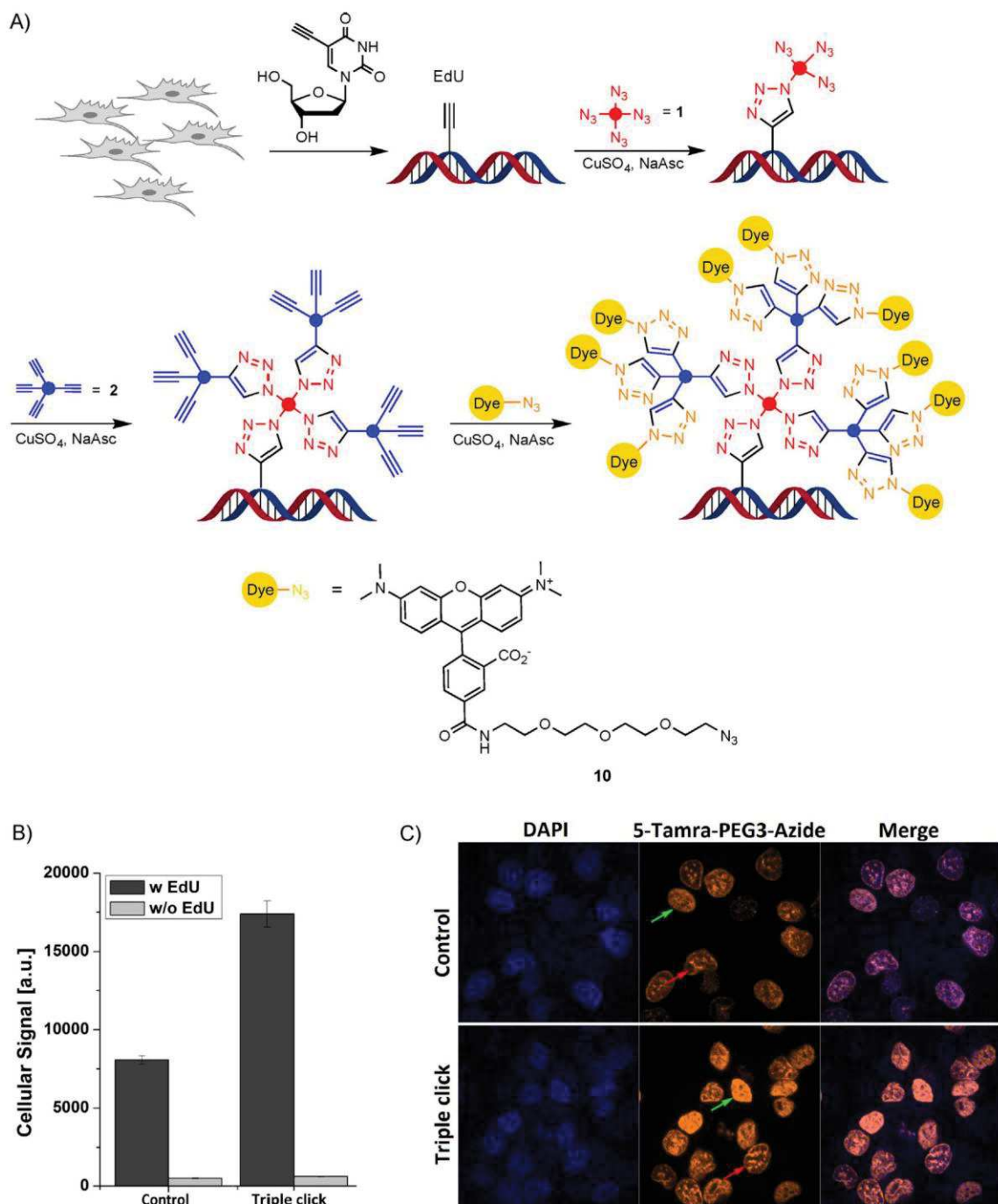


Figure 2. A) Depiction of the double dendrimer (triple click) amplified cell-proliferation assay. Cells were grown in the presence of 5-ethynyl-dU. After fixation and permeabilisation, the present alkyne is first treated with tetraazide-dendrimer **1** in the presence Cu^{I} . The multiple-azide-containing DNA was then treated with tetraalkyne **2**. The so-double-modified DNA (triple click) was finally detected with azide-modified dye **10** again by using the Cu^{I} -catalysed click reaction. B) The control experiment was performed by using the dendrimer-free standard proliferation assay. Triple click shows data after double dendrimer amplification. C) Fluorescence microscopy pictures of cells detected with the standard EdU assay as control (top) and after double dendrimer amplification with triple click (bottom). Red arrows show cells in the early S-phase. Green arrows show cells in late S-phase. Scale bars: 20 μm .

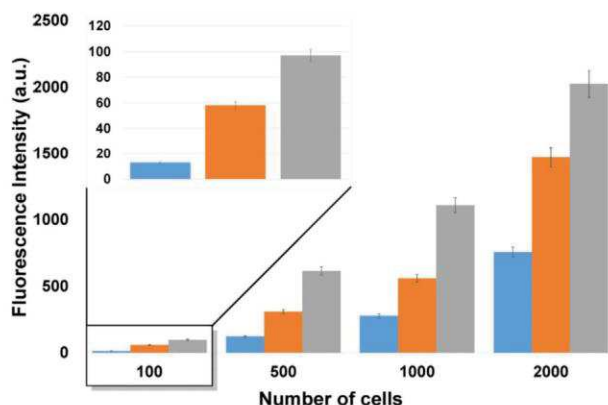


Figure 3. Application of the single and double dendrimer amplified assay in high-throughput screening. Cells were grown on a microplate with different densities (100, 500, 1000 and 2000 cells per well) and were incubated for 2 h with 5-ethynyl-dU at 37 °C. Negative control cells were grown without EdU labelling. The cells were fixed and permeabilised, and the present alkynes were treated with tetraazide dendrimer **1** and TAMRA-alkyne (double click, grey bars) or with tetraazide **1**, tetraalkyne **2** and TAMRA-azide (triple click, orange bars) in the presence of Cu^I in situ. Positive control cells were treated with TAMRA-azide in the presence of Cu^I (control, blue bars). The cellular signal of duplicate samples was measured with a Tecan microplate reader. After subtraction of the background fluorescence, it was possible to detect a stronger signal even with only 100 cells. Blue: standard click protocol; grey: single-dendrimer approach with dendrimer **1**; orange: double-dendrimer approach with dendrimers **1** and **2**.

[1] a) M. G. Daidone, R. Silvestrini, *J. Natl. Cancer Inst. Monogr.* **2001**, 27–35; b) S. H. Torp, C. F. Lindboe, U. S. Granli, T. M. Moen, T. Nordtømme, *Clin. Neuropathol.* **2001**, 20, 190–195; c) M. A. Aleskandarany, A. R. Green, A. A. Benhasouna, F. F. Barros, K. Neal, J. S. Reis-Filho, I. O. Ellis, E. A. Rakha, *Breast Cancer Res.* **2012**, 14, R3; d) M. Wang, J. Wu, Y. Guo, X. Chang, T. Cheng, *Mol. Med. Rep.* **2017**, 15, 1607–1612; e) T. Wieder, E. Brenner, H. Braumuller, O. Bischof, M. Rocken, *Cancer Metastasis Rev.* **2017**, DOI: 10.1007/s10555-017-9667-z; f) A. S. Thorat, N. A. Sonone, V. V. Choudhari, R. M. Devarumath, K. H. Babu, *3 Biotech* **2017**, 7, 16; g) H. Chen, X. Gu, Y. Liu, J. Wang, S. E. Wirt, R. Bottino, H. Schorle, J. Sage, S. K.

Kim, *Nature* **2011**, 478, 349–355; h) K. D. Poss, L. G. Wilson, M. T. Keating, *Science* **2002**, 298, 2188–2190.

- [2] a) X. Lu, J. W. Horner, E. Paul, X. Shang, P. Troncoso, P. Deng, S. Jiang, Q. Chang, D. J. Spring, P. Sharma, J. A. Zebala, D. Y. Maeda, Y. A. Wang, R. A. DePinho, *Nature* **2017**, 543, 728–732; b) N. V. Jordan, A. Bardia, B. S. Wittner, C. Benes, M. Ligorio, Y. Zheng, M. Yu, T. K. Sundaresan, J. A. Licausi, R. Desai, R. M. O’Keefe, R. Y. Ebricht, M. Boukhali, S. Sil, M. L. Onozato, A. J. lafrate, R. Kapur, D. Sgroi, D. T. Ting, M. Toner, S. Ramaswamy, W. Haas, S. Maheswaran, D. A. Haber, *Nature* **2016**, 537, 102–106; c) M. A. Erb, T. G. Scott, B. E. Li, H. Xie, J. Paulk, H. S. Seo, A. Souza, J. M. Roberts, S. Dastjerdi, D. L. Buckley, N. E. Sanjana, O. Shalem, B. Nabet, R. Zeid, N. K. Offei-Addo, S. Dhe-Paganon, F. Zhang, S. H. Orkin, G. E. Winter, J. E. Bradner, *Nature* **2017**, 543, 270–274.
- [3] a) G. I. Evan, K. H. Vousden, *Nature* **2001**, 411, 342–348; b) G. Evan, T. Littlewood, *Science* **1998**, 281, 1317–1322.
- [4] a) A. Salic, T. J. Mitchison, *Proc. Natl. Acad. Sci. USA* **2008**, 105, 2415–2420; b) M. Ababou, V. Dumaire, Y. Lecluse, M. Amor-Gueret, *Oncogene* **2002**, 21, 2079–2088; c) B. L. Cavanagh, T. Walker, A. Norazit, A. C. Mee-deniyi, *Molecules* **2011**, 16, 7980–7993.
- [5] a) H. C. Kolb, M. G. Finn, K. B. Sharpless, *Angew. Chem. Int. Ed.* **2001**, 40, 2004–2021; *Angew. Chem.* **2001**, 113, 2056–2075; b) P. M. Gramlich, C. T. Wirges, A. Manetto, T. Carell, *Angew. Chem. Int. Ed.* **2008**, 47, 8350–8358; *Angew. Chem.* **2008**, 120, 8478–8487.
- [6] J. Gierlich, G. A. Burley, P. M. Gramlich, D. M. Hammond, T. Carell, *Org. Lett.* **2006**, 8, 3639–3642.
- [7] S. Nik-Zainal, P. Van Loo, D. C. Wedge, L. B. Alexandrov, C. D. Greenman, K. W. Lau, K. Raine, D. Jones, J. Marshall, M. Ramakrishna, A. Shlien, S. L. Cooke, J. Hinton, A. Menzies, L. A. Stebbings, C. Leroy, M. Jia, R. Rance, L. J. Mudie, S. J. Gamble, P. J. Stephens, S. McLaren, P. S. Tarpey, E. Papaemmanuil, H. R. Davies, I. Varela, D. J. McBride, G. R. Bignell, K. Leung, A. P. Butler, J. W. Teague, S. Martin, G. Jonsson, O. Mariani, S. Boyault, P. Miron, A. Fatima, A. Langerod, S. A. Aparicio, A. Tutt, A. M. Sieuwerts, A. Borg, G. Thomas, A. V. Salomon, A. L. Richardson, A. L. Borresen-Dale, P. A. Futreal, M. R. Stratton, P. J. Campbell, C. Breast Cancer Working Group of the International Cancer Genome, *Cell* **2012**, 149, 994–1007.
- [8] F. Zanella, J. B. Lorens, W. Link, *Trends Biotechnol.* **2010**, 28, 237–245.

Manuscript received: April 13, 2017

Accepted manuscript online: June 22, 2017

Version of record online: July 24, 2017

CHEM**BIO**CHEM

Supporting Information

Dendrimer-Based Signal Amplification of Click-Labelled DNA in Situ

Nada Raddaoui⁺, Samuele Stazzoni⁺, Leonhard Möckl, Bastien Viverge, Florian Geiger, Hanna Engelke, Christoph Bräuchle, and Thomas Carell^{*[a]}

cbic_201700209_sm_miscellaneous_information.pdf

Supporting information

Supplementary figures and text:

Supplementary figure S1	Synthesis of Tetraazide 1
Supplementary figure S2	Synthesis of Tetraalkyne 2
Supplementary figure S3	Reaction between oligonucleotides and the tetraazide dendrimer and possible products
Supplementary figure S4	Development of the double click assay (simple dendrimer)
Supplementary figure S5	Improvement of the signal to background ratio of the double click assay
Supplementary figure S6	Development of the triple click assay (double dendrimer)
Supplementary figure S7	Direct comparison between the non-dendrimer, the double and triple click dendrimer approaches

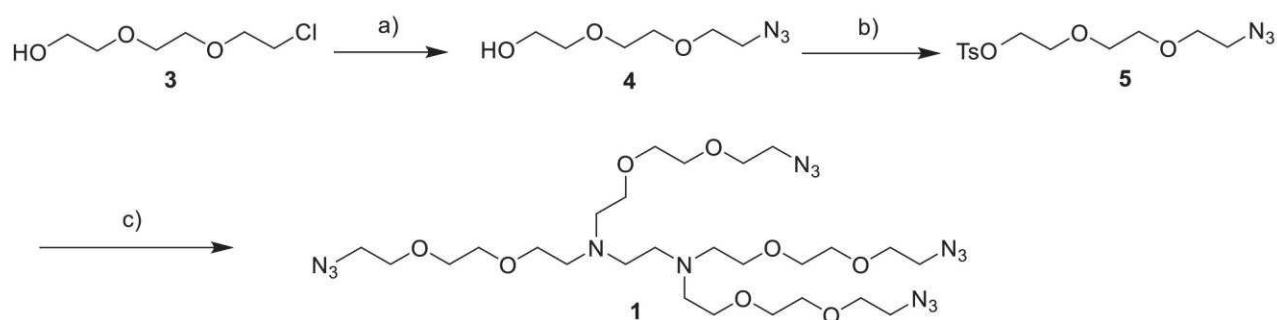
General methods

Chemicals were purchased from Sigma-Aldrich, Alfa Aesar, TCI Chemicals or Acros Organics and used without further purification. Solutions were concentrated *in vacuo* on a Heidolph rotary evaporator. The solvents were of reagent grade and purified by distillation. Dry solvents were bought from Acros Organics or Sigma-Aldrich. Water was purified by a Milli-Q Plus system from Merck Millipore. Chromatographic purification of products was accomplished using flash column chromatography on Merck Geduran Si 60 (40-63 μM) silica gel (normal phase). Thin layer chromatography (TLC) was performed on Merck 60 (silica gel F254) plates. ^1H and ^{13}C -NMR spectra were recorded in deuterated solvents on a *Bruker ARX 400* spectrometer and calibrated to the residual solvent peak. Multiplicities are abbreviated as follows: s = singlet, d = doublet, t = triplet, q = quartet, m = multiplet, brs = broad signal. For assignment of the structures, additional 2D NMR spectra (COSY, HSQC, HMBC) were measured. High resolution electrospray ionization mass spectra (HRMS-ESI) were recorded on a *Thermo Finnigan LTQ-FT* (ESI-FTICR).

DNA Oligonucleotide synthesis was performed on an Applied Biosystems Incorporated 394 automated synthesizer. Phosphoramidites and solid supports columns were purchased from Glen Research, Link Technology or Baseclick.

Analytical RP-HPLC was performed using a *Macherey-Nagel Nucleodur 100-3 C18ec* column on *Waters Alliance 2996 Photodiode Array Detector, 2695 Separation Module* using a flow of 0.5 mL/min. Conditions: Buffer A = 0.1 M TEAA (triethylammonium acetate) in water; buffer B = 0.1 M TEAA in 80% acetonitrile. When needed, the product peaks were collected, concentrated and characterized by Matrix Assisted Laser Desorption Ionization-Time of Flight (MALDI-TOF) on Bruker Daltonics Autoflex II.

Chemical synthesis



Supplementary figure S1: Synthesis of **1**. Reagents and conditions: a) NaN_3 , DMF, 90°C o/n, 96%; b) TsCl, NEt_3 , CH_2Cl_2 , o/n, 90%; c) **5**, ethylenediamine, KOH, LiBr, DMF, 60°C , o/n, 63%.

2-[2-(2-Azidoethoxy)ethoxy]ethanol (**4**)

2-[2-(2-Chloroethoxy)ethoxy]ethanol (**3**) (4.31 mL, 29.65 mmol) was dissolved in 200 mL of dry DMF under N_2 . NaN_3 (3.86 g, 59.3 mmol) was added, and the mixture was heated at 90°C overnight. After 18 h, the solvent was removed under reduced pressure and the residue was partitioned between H_2O (50 mL) and EtOAc (150 mL). The aqueous phase was extracted again with 150 mL of EtOAc and the combined organic phases were combined, washed with brine, dried over Na_2SO_4 , filtered and evaporated. The crude product was purified by column chromatography (isohexane/EtOAc 1:4 \rightarrow 1:10) to afford **4** as a colorless oil (5.0 g, 96%).

$^1\text{H NMR}$ (400 MHz, CDCl_3) δ 3.77-3.71 (m, 2H), 3.68 (s, 6H), 3.62-3.58 (m, 2H), 3.43-3.37 (m, 2H) ppm.

$^{13}\text{C NMR}$ (101 MHz, DMSO-d_6) δ 72.4, 69.88, 69.82, 69.37, 60.31, 50.09 ppm.

2-(2-(2-Azidoethoxy)ethoxy)ethyl 4-methylbenzenesulfonate (**5**)

Compound **4** (5 g, 28.54 mmol) was dissolved in 100 mL of DCM at room temperature. The solution was then cooled to 0°C and NEt_3 and TsCl were added. The mixture was then stirred overnight allowing to warm up to room temperature. After 18 hours, the reaction mixture was washed with 1 M HCl, H_2O , brine, dried over MgSO_4 and filtered. The solvent was removed under reduced pressure and the crude product was purified by column chromatography (isohexane/EtOAc 10:1) to yield **5** as a colourless oil (8.5 g, 90%).

¹H NMR (400 MHz, CDCl₃) δ 7.77 (d, *J*= 8Hz, 2H), 7.32 (d, *J*=8Hz, 2H), 4.13 (t, *J*= 6Hz, 2H), 3.70-3.55 (m, 8H), 3.34 (t, *J*= 5Hz, 2H), 2.42 (s, 3H) ppm.

**N1,N1,N2,N2-Tetrakis(2-(2-(2-azidoethoxy)ethoxy)ethyl)ethane-1,2-diamine
(tetraazide dendrimer 1)**

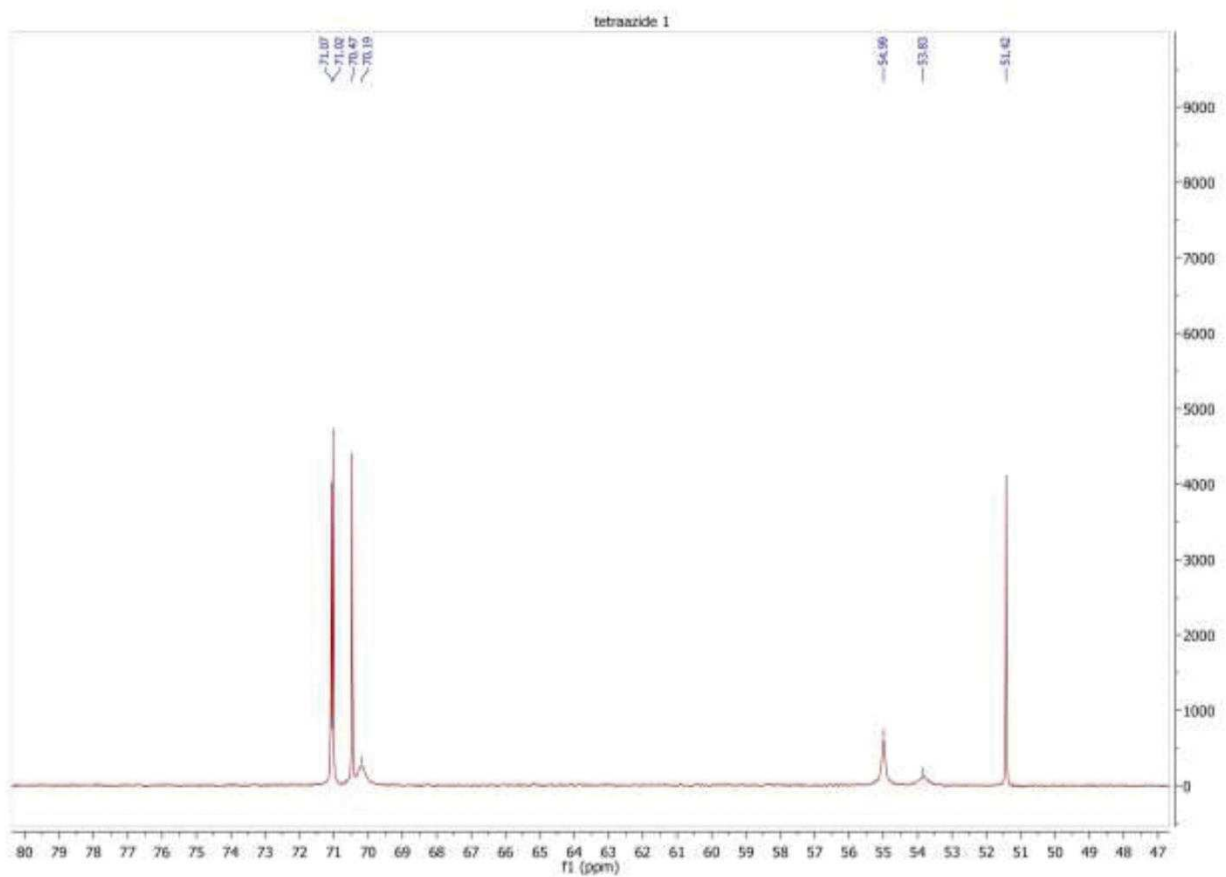
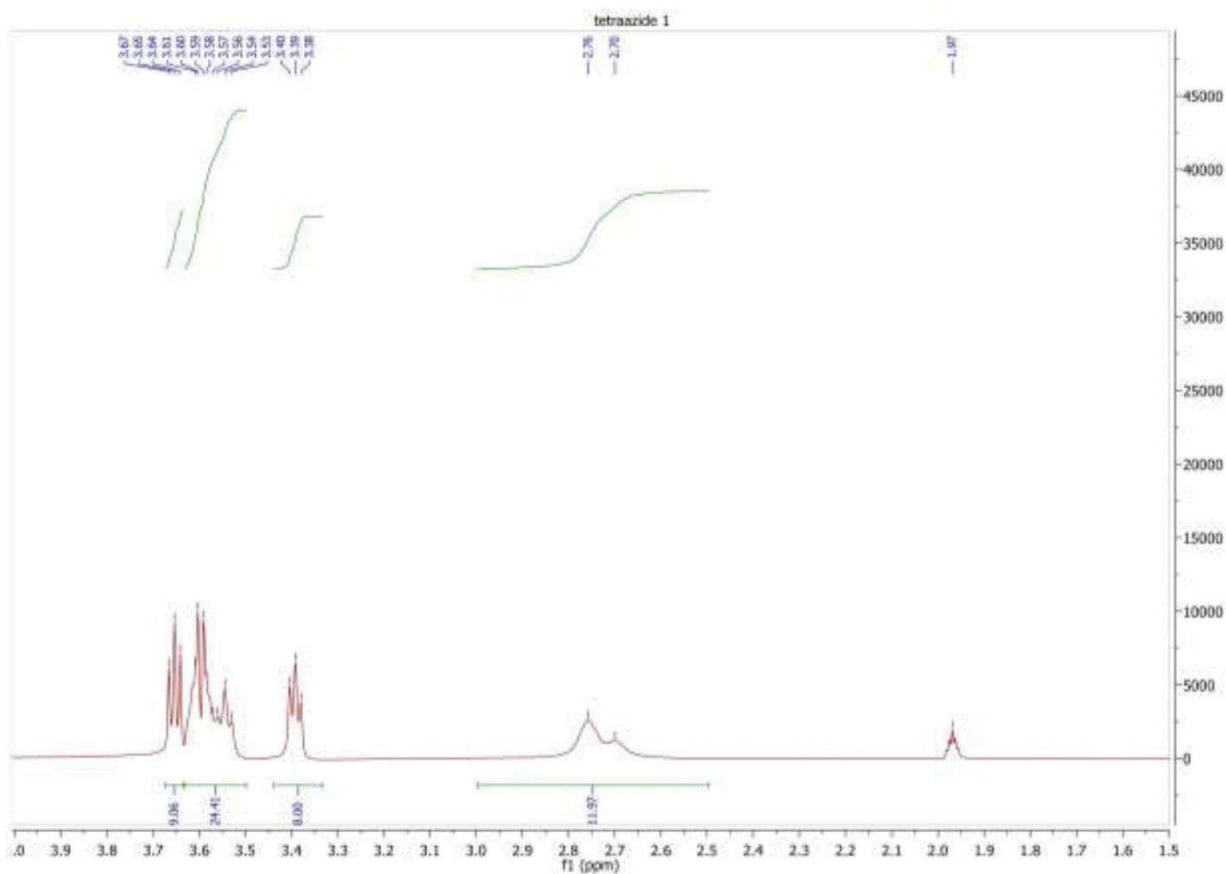
Ethylenediamine (150 mg, 167 μL, 1.66 mmol) was dissolved in 50 mL of dry DMF. KOH (613 mg, 10.8 mmol) and LiBr were added at RT. Compound **5** was then added dropwise as a solution in 20 mL of DMF, then the reaction was stirred for 2 hours at RT and heated at 60°C overnight. After 20 hours, the solvent was removed under vacuum and the residue was retaken in EtOAc, washed with sat. NaHCO₃, brine, dried over Na₂SO₄ and filtered. Evaporation of the solvent afforded a yellowish oil that was purified by column chromatography (DCM/MeOH 30:1 → 10:1). 1.1 g of product was recovered (63%).

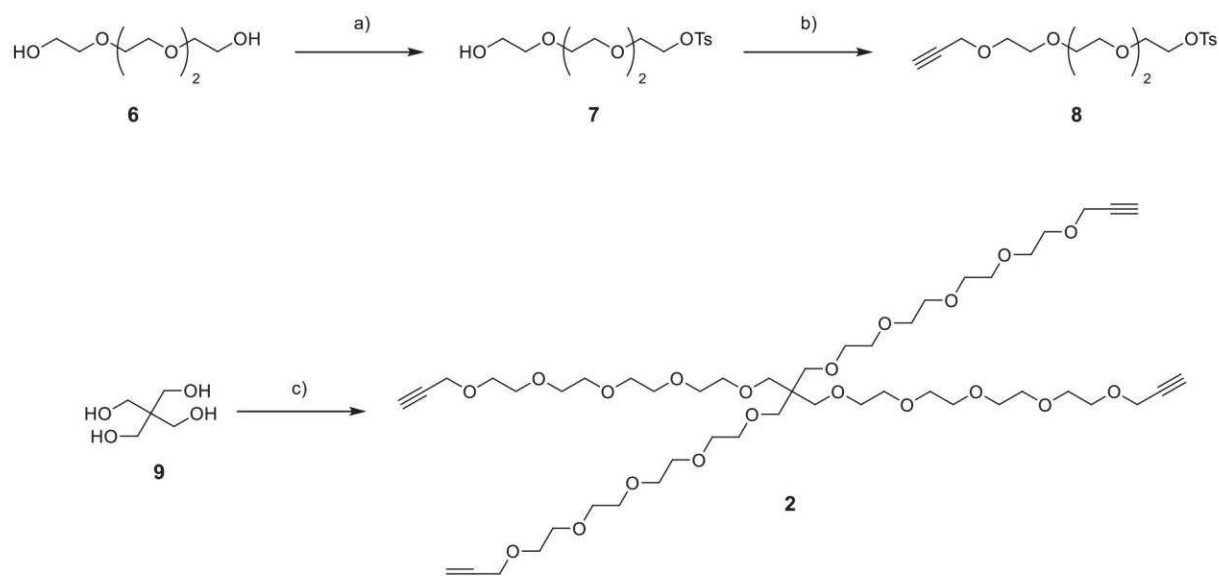
HR-MS (ESI+): calculated for C₂₆H₅₃N₁₄O₈⁺ 689.4165, found: 689.4159.

¹H NMR (400 MHz, CD₃CN) δ 3.58 (t, *J*= 6 Hz, 8H, 4 x N₃CH₂CH₂OR), 3.57-3.42 (m, 24H), 3.32 (t, *J*= 5 Hz, 8H, 4x N₃CH₂CH₂OR) 2.82-2.48 (brs, 12H, (RCH₂)₂NCH₂CH₂N(CH₂)₂) ppm.

¹³C NMR (101 MHz, CD₃CN) δ 71.07, 71.02, 70.47, 70.19, 54.99, 53.83, 51.43

NMR spectra of 1





Supplementary figure S2: Synthesis of **2**. Reagents and conditions: a) TsCl, Et₃N, THF, RT, 48 h, 92 %; b) Propargyl bromide, NaH, THF, 0°C to RT, 82 %; c) **1**, K₂CO₃, acetone, 60°C, 48 h, 30%.

2-(2-(2-(2-hydroxyethoxy)ethoxy)ethoxy)ethyl 4-methylbenzenesulfonate (**7**)

Tetraethylene glycol (29.25 g, 150.6 mmol) was dissolved in dry THF (100 mL) and triethylamine (122 g, 1.2 mol, 8.0 eq.) was added. The reaction was cooled down to 0°C and a solution of tosyl chloride (28.71 g, 150.6 mmol, 1.0 eq.) in dry THF (50 mL) was added over a period of 1 h. After 48 h stirring at room temperature the solvent was removed *in vacuo*. The mixture was taken up in HCl (2 M, 150 mL) and extracted with DCM (4 × 150 mL). The combined organic layers were dried over MgSO₄ and filtered. After removal of the solvent *in vacuo* the crude product was purified by flash chromatography (Silica, DCM → DCM/MeOH (99 :1 → 0:1)). The product was obtained as a colourless oil (48.27 g, 138.6 mmol, 92%).

¹H-NMR (400 MHz, CDCl₃): δ = 7.82-7.76 (m, 2H, CH_{arom.}), 7.37-7.30 (m, 2H, CH_{arom.}), 4.20-4.12 (m, 2H, CH₂), 3.73-3.52 (m, 14H, 7×CH₂), 2.42 (s, 3H, CH₃), 2.38-2.31 (s, 1H, OH) ppm.

¹³C-NMR (100 MHz, CDCl₃): δ = 144.9 (C_{arom.}), 133.2 (C_{arom.}), 130.0 (2×CH_{arom.}), 128.1 (2×CH_{arom.}), 72.6 (CH₂), 70.9 (CH₂), 70.8 (CH₂), 70.6 (CH₂), 70.5 (CH₂), 69.4 (CH₂), 68.9 (CH₂), 61.9 (CH₂), 21.8 (CH₃) ppm.

HR-MS (ESI): C₁₅H₂₅O₇S⁺ [M+H]⁺, calc.: 349.1315, found: 349.1316

3,6,9,12-tetraoxapentadec-14-yn-1-yl 4-methylbenzenesulfonate (8)

2-(2-(2-(2-hydroxyethoxy)ethoxy)ethoxy)ethyl 4-methylbenzenesulfonate (10 g, 28.7 mmol) was dissolved in dry THF (50 mL) and added dropwise to a solution of NaH (60%, 1.38 g, 34.44 mmol, 1.2 eq.) in dry THF (50 mL) at 0 °C. Propargylbromide (80% in toluene, 31.85 mL, 287 mmol, 10 eq.) was subsequently added to the mixture and stirred for 2 h at RT. The reaction was carefully quenched by slow addition of MeOH and the solvents were removed *in vacuo*. H₂O was added and extracted with DCM (3 × 200 mL). The combined organic layers were dried over MgSO₄, the solvent removed *in vacuo* and the crude product was purified by column chromatography (Silica, DCM → DCM/MeOH (99 :1 → 0:1)). X was obtained as a colorless oil (9.06 g, 23.4 mmol, 82 %).

¹H-NMR (400 MHz, CDCl₃): δ = 7.81-7.78 (m, 2H, CH_{arom.}), 7.35-7.33 (m, 2H, CH_{arom.}), 4.21-4.18 (m, 2H, CH₂), 4.17-4.14 (m, 2H, CH₂), 3.70-3.56 (m, 14H, 7×CH₂), 2.44 (s, 3H, CH₃), 2.42 (m, 1H, CH) ppm.

¹³C-NMR (100 MHz, CDCl₃): δ = 145.0 (C_{arom.}), 133.1 (C_{arom.}), 130.0 (2×CH_{arom.}), 128.1 (2×CH_{arom.}), 78.8 (HC≡C), 75.2 (HC≡C), 70.8 (CH₂), 70.7 (CH₂), 69.4 (CH₂), 68.8 (CH₂), 67.7 (CH₂), 56.6 (CH₂), 55.9 (CH₂), 55.4 (CH₂), 21.8 (CH₃) ppm.

HR-MS (ESI): C₁₈H₃₀O₇NS⁺ [M+NH₄]⁺, calc.: 404.1737, found: 404.1739.

18,18-di(2,5,8,11,14-pentaoxaheptadec-16-yn-1-yl)-4,7,10,13,16,20,23,26,29,32-decaoxapentatriaconta-1,34-diyne (2)

Pentaerythritole (15 mg, 110.18 μmol) was dissolved in acetone (3 mL). 3,6,9,12-tetraoxapentadec-14-yn-1-yl 4-methylbenzenesulfonate (213 mg, 550.9 μmol, 5 eq.) and K₂CO₃ (76 mg, 550.9 μmol, 5 eq.) were added. After stirring at 60°C for 48 h the solvent was removed *in vacuo*. H₂O was added and extracted with DCM (4×20 mL). The combined organic layers were dried over MgSO₄, the solvent removed *in vacuo* and the crude product was purified by column chromatography ((Silica, DCM → DCM/MeOH (99 :1 → 0:1)). The product was obtained as a colourless oil (33 mg, 33 μmol, 30%).

¹H-NMR (599 MHz, CDCl₃): δ = 4.22-4.19 (d, ³J = 2.4 Hz, 8H, CH₂), 3.85-3.40 (m, 72H, CH₂), 2.51-2.37 (t, ⁴J = 2.4 Hz, 4H, CH₂) ppm.

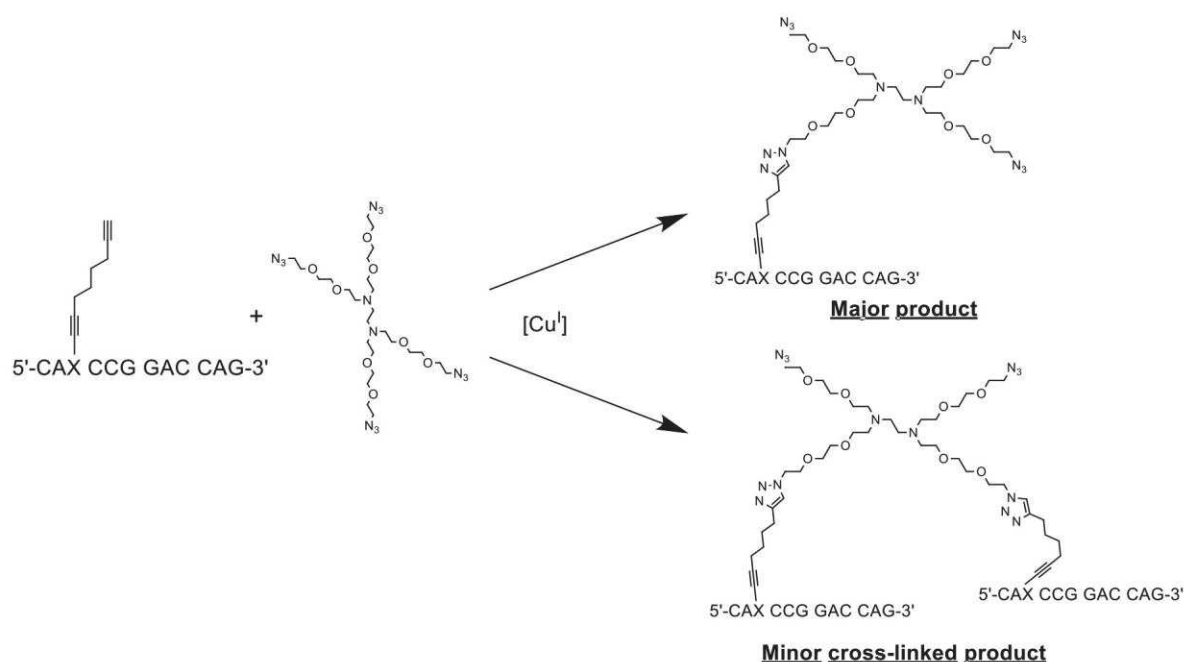
¹³C-NMR (151 MHz, CDCl₃): δ = 79.83, 74.62, 72.61, 71.52, 71.48, 70.85, 70.83, 70.81, 70.78, 70.75, 70.71, 70.68, 70.59, 70.58, 70.54, 69.29, 61.95, 58.57, 42.87 ppm.

HR-MS (ESI): C₄₉H₈₅O₂₀Na²⁺ [M+H+Na]²⁺, calc.: 508.2760, found: 508.2755.

Proof of principle of the click reactions on oligonucleotides

In order to prove that the strategy that we planned for the *in situ* detection of cell proliferation using click chemistry is applicable and yields predominantly the products shown in the main text, we performed experiments on synthetic oligonucleotides. We decided to perform the click reactions both in solution, purifying the main intermediates and products *via* HPLC and on solid phase, where we simply removed the excess of reagents with a few washing steps and then proceeded with the following click reaction. This second approach is more similar to the strategy that we ultimately applied for our cell studies and proved that it is possible to obtain the products that we wanted with good selectivity even without chromatographic purification of the intermediates.

Both pathways were successful and yielded the desired products (oligonucleotide conjugated with multiple dyes) with good selectivity as a mixture of 5/6-TAMRA isomers. As expected, especially for the solid phase reactions, we observed a limited amount of cross-linked compound, where the tetraazide binds two different oligonucleotides in the first step, and therefore can react with only two dyes in the second step (fig. S3).



Supplementary figure S3: Reaction between oligonucleotides and the tetraazide-dendrimer and possible products.

Sequence of the oligonucleotides used for the tests:

Oligonucleotide 1: 5'- CAX CCG GAC CAG-3' where X = C8-Alkynyl-dT; [M] = 3705.4

Oligonucleotide 2: 5'- TXT TTT TTT T -3' where X = EdU; [M] = 2989.9

General procedure A (click in solution): The alkyne-modified oligonucleotide was dissolved in MQ water (concentration = 1 mM) and 3 μ L of this solution (3 nmol of oligonucleotide) were transferred in a vial for the click reaction. To this solution, H₂O (15 μ L), 1 M TEAA buffer (pH 7, 6 μ L), DMSO (27 μ L) and the azide or dye-alkyne solution (20 mM in DMSO, 3 μ L) were added. A CuSO₄/TBTA solution (1 mM in H₂O /DMSO 1:1, 3 μ L) was then added, followed by a freshly prepared solution of sodium ascorbate (2.5 mM, 3 μ L). The mixture was then shaken for 1 hour on a Thermomixer at 25°C, 1200 rpm, and the solvent was then directly evaporated on a SpeedVac at 35°C. All the products were analyzed and purified using RP-HPLC and identified using MALDI-TOF-MS.

Cyanoethyl deprotection: After solid phase oligonucleotide synthesis on a 200 nmol scale, part of the resin (approximately 50 nmol of oligonucleotide), was suspended in 500 μ L of 10% DBU in dry acetonitrile to deprotect the cyanoethyl groups on the phosphates. The suspension was shaken on a Thermomixer at 30°C for 1 h. After centrifugation, the DBU solution was decanted off and the resin was washed 5 times with 1 mL of dry acetonitrile.

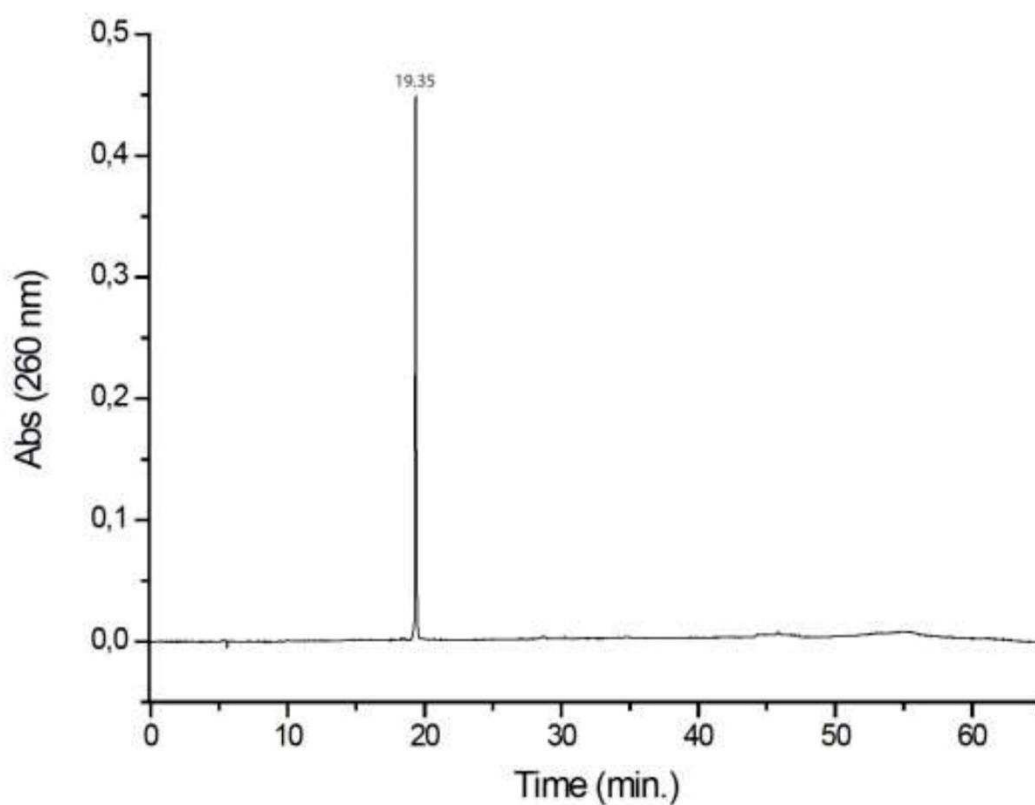
General procedure B (click on solid phase): The dried resin was suspended in 375 μ L of H₂O /DMSO 1:2. To this, 1M TEAA buffer (pH 7, 100 μ L), the azide or dye-alkyne solution (20 mM in DMSO, 50 μ L) and the CuSO₄/TBTA solution (1 mM in H₂O /DMSO 1:1, 25 μ L) were added, followed by a freshly prepared solution of sodium ascorbate (1 mM, 75 μ L). After 1.5 h shaking on a Thermomixer at 25°C, 1200 rpm, the mixture was centrifuged and the supernatant was discarded. The resin was then washed with H₂O (500 μ L), MeCN (500 μ L x 3) and dried.

Standard cleavage procedure: The resin was suspended in 400 μ L of 28-30% aqueous ammonium hydroxide and shaken at 30°C for 1h. After centrifugation, the supernatant was collected and the resin washed again with H₂O (2 x 200 μ L). The solution was then evaporated on a SpeedVac at 35°C to obtain the products that were analyzed by RP-HPLC and MALDI-TOF-MS and then purified.

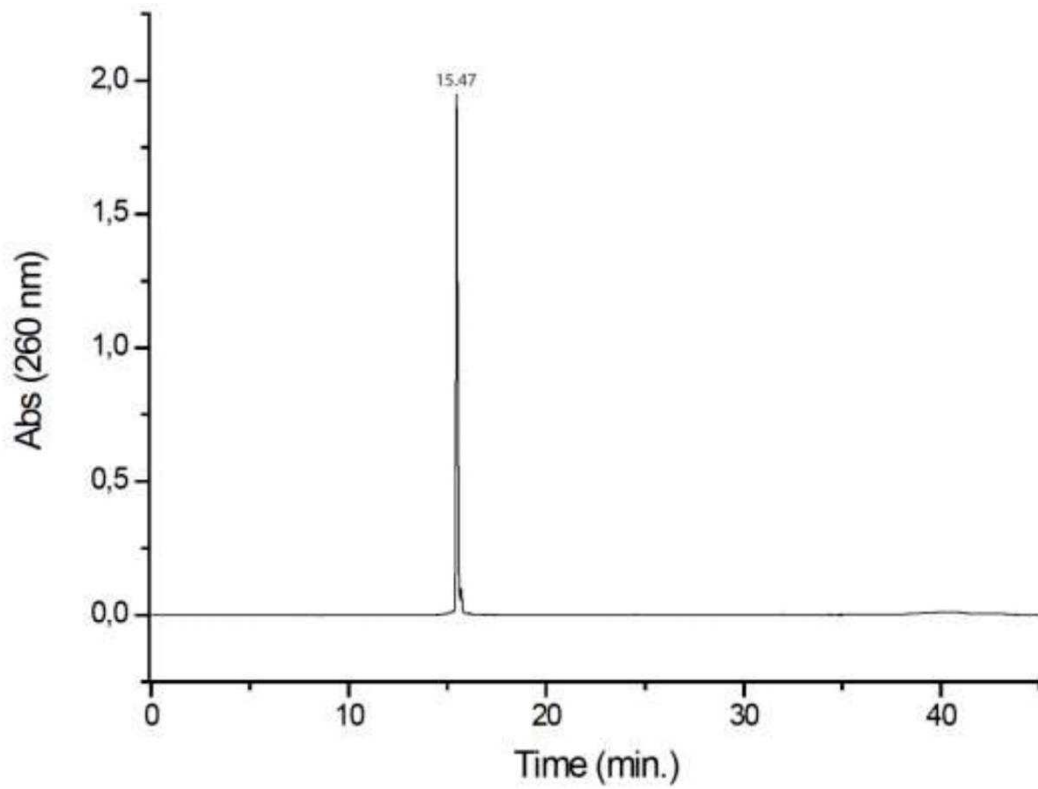
Cleavage procedure for TAMRA-containing oligonucleotides: The resin was suspended in 200 μL of a solution of $\text{tBuNH}_2/\text{MeOH}/\text{H}_2\text{O}$ 1:1:3 solution and shaken at 40 °C for 1 hour. After centrifugation, the resin was washed twice with 200 μL of H_2O and the combined solutions were evaporated on a SpeedVac at 40°C. The products were analyzed by RP-HPLC and MALDI-TOF-MS.

RP-HPLC chromatograms of the starting materials

Oligonucleotide 1 (0-70% B in 45 min)

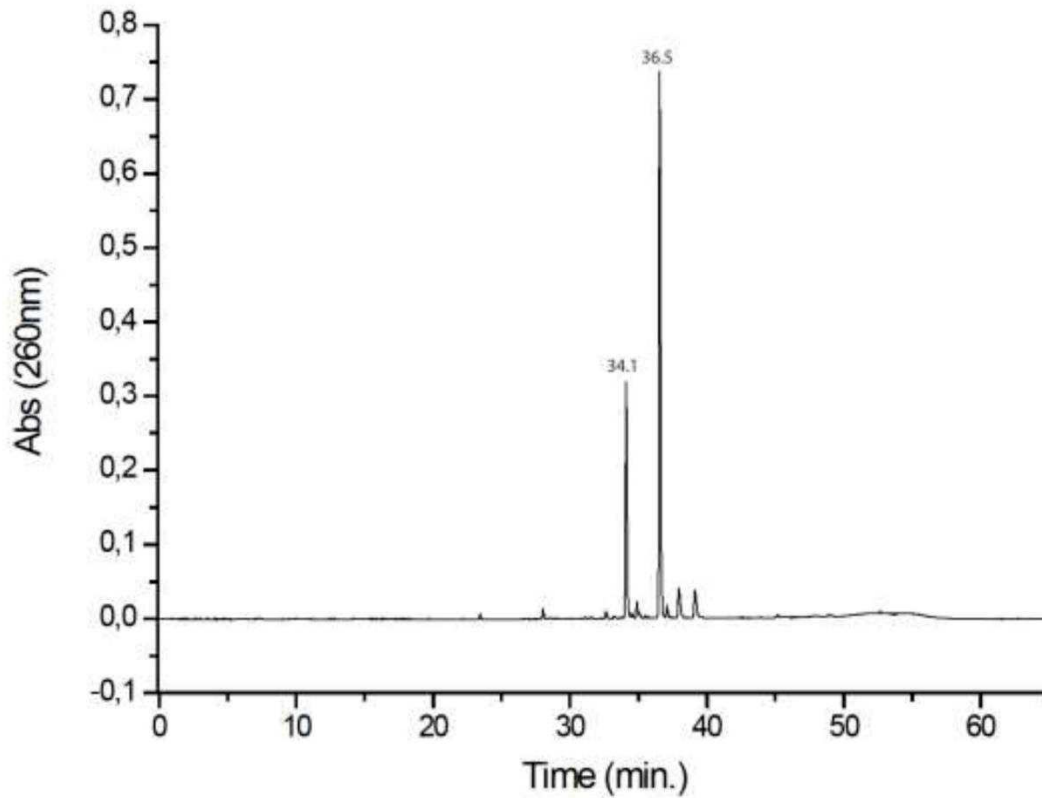


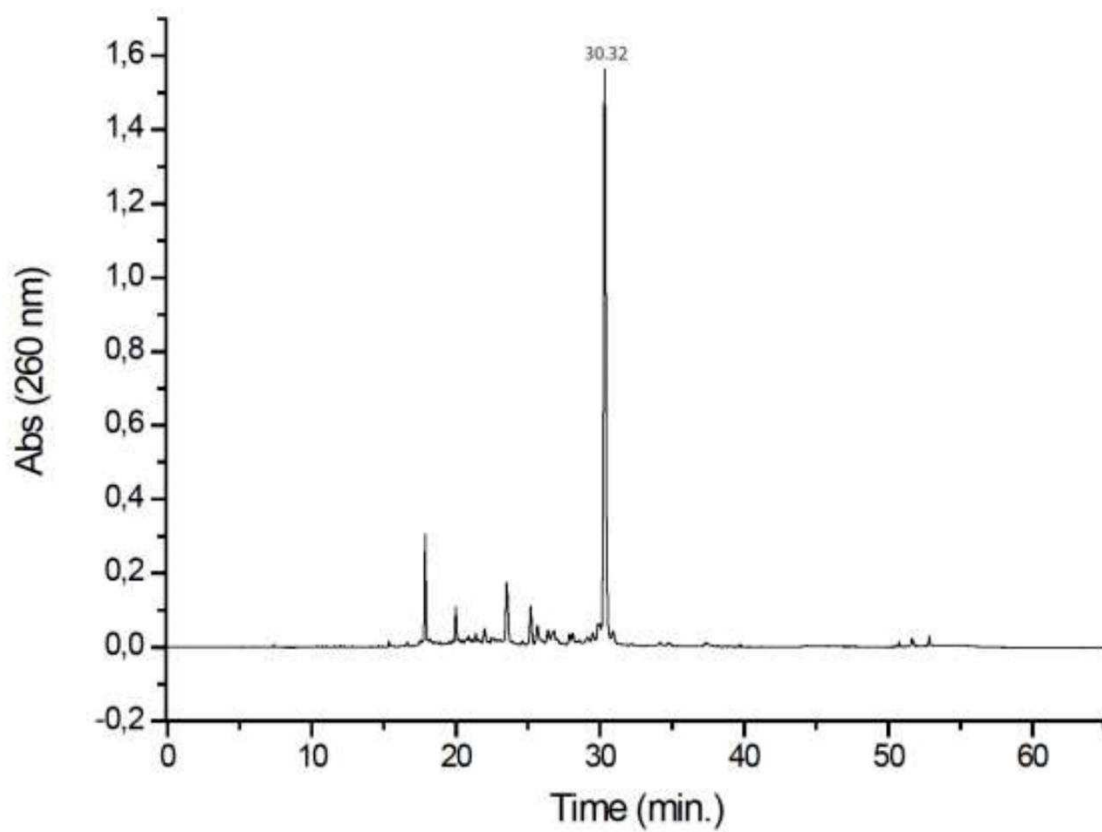
Oligonucleotide 2 (0-70% B in 33 min)



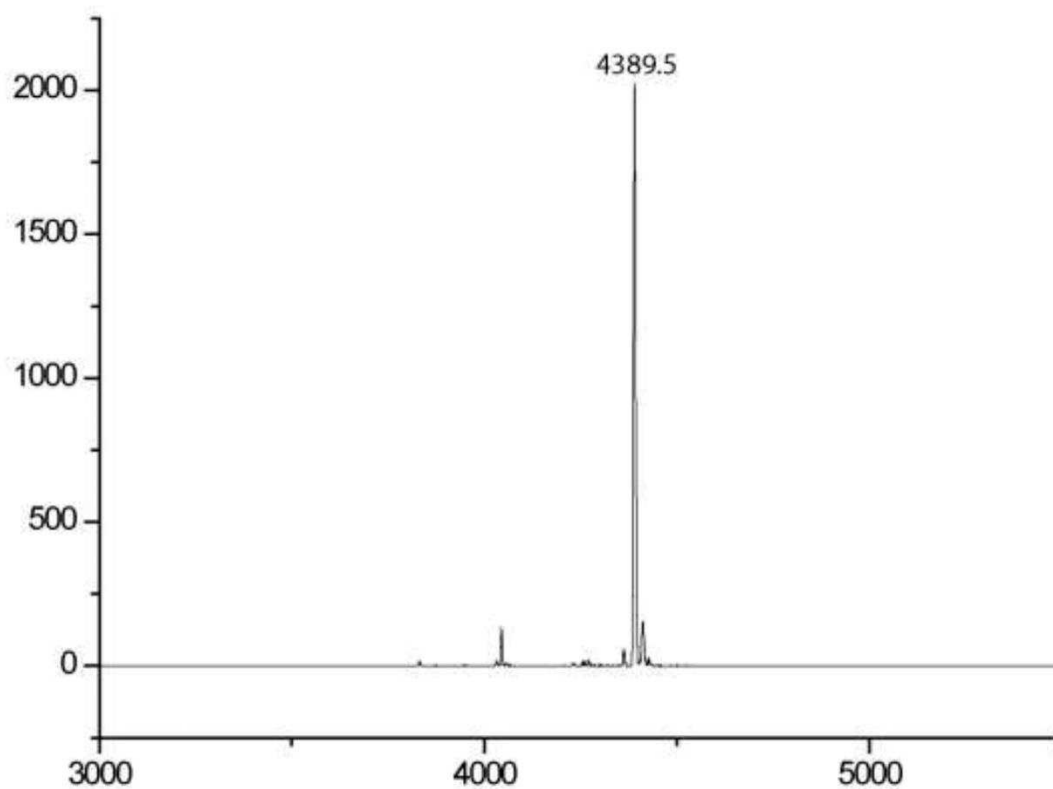
5/6-TAMRA-PEG4-alkyne

Method 0-70% B in 45 min (for click reactions in solution)

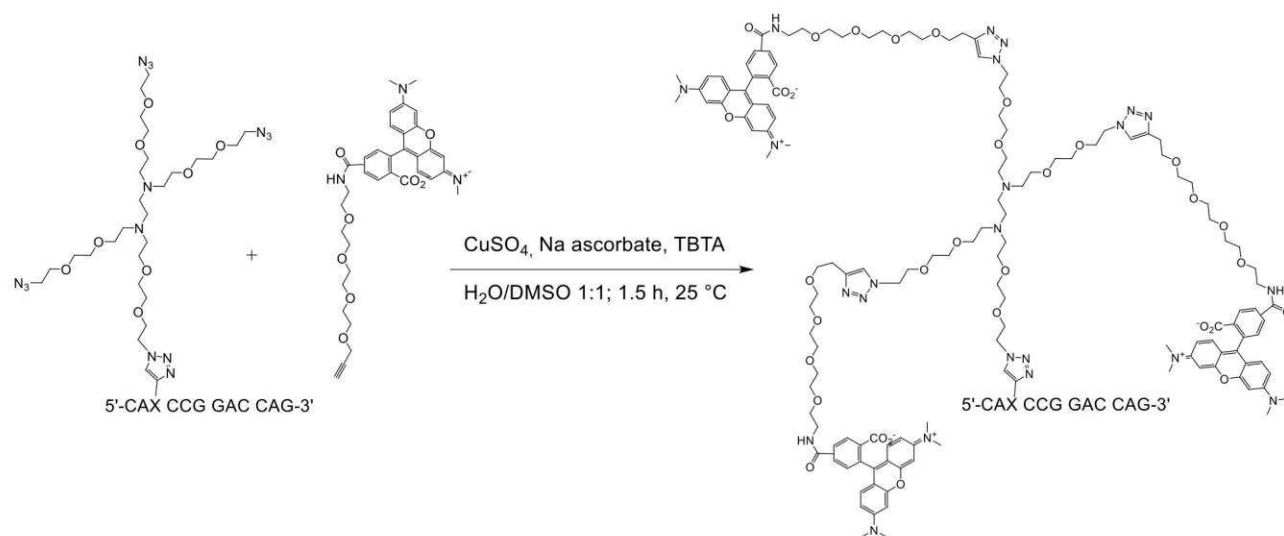




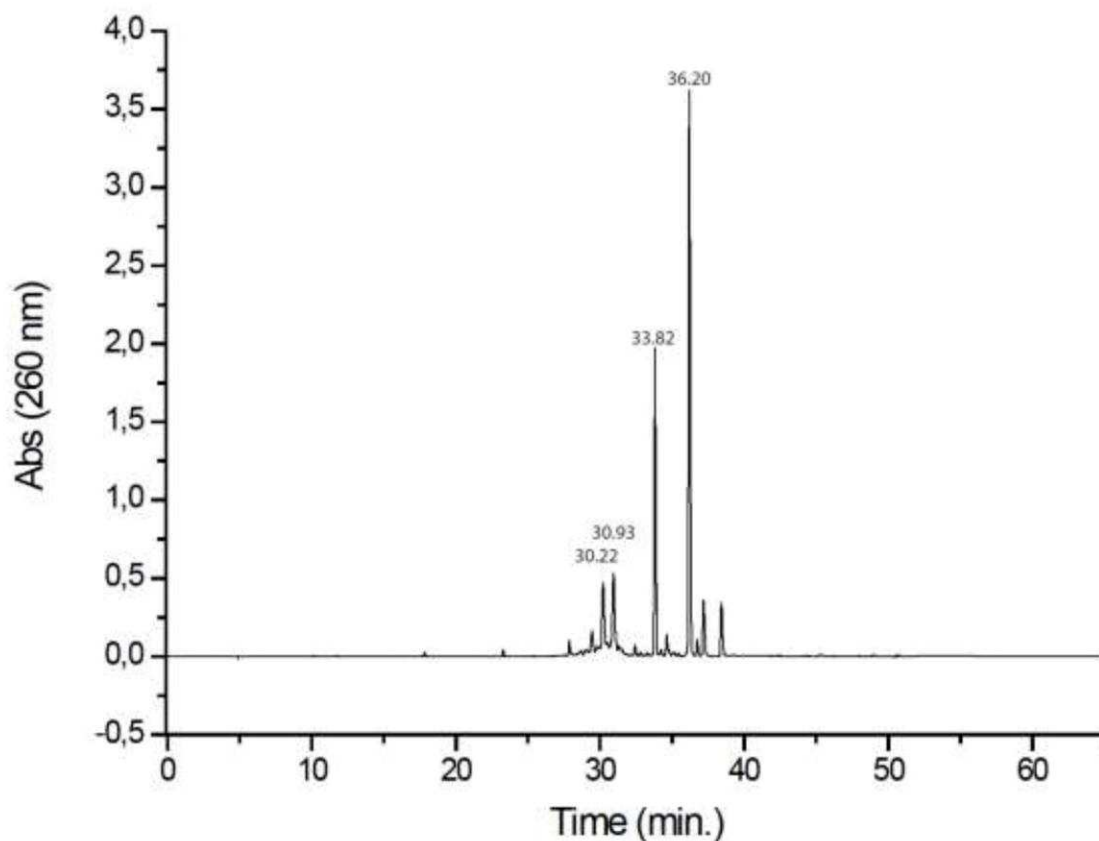
MALDI-TOF-MS: [M] calc. for oligonucleotide **1** + dendrimer = 4393.8 ; found = 4389.5.



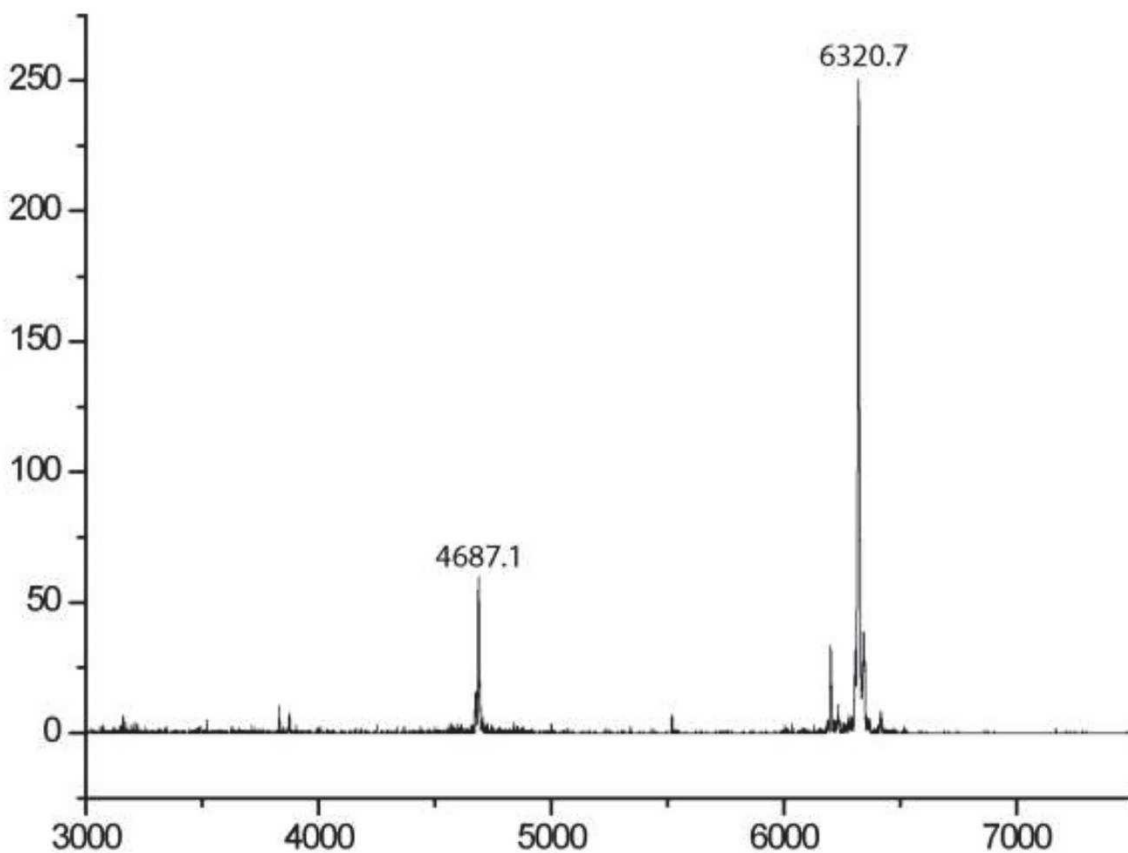
Click 2: Oligonucleotide from Click 1 + 5/6-TAMRA-PEG4-Alkyne



After the click reaction using the **general procedure A**, analysis via RP-HPLC and MALDI-TOF-MS showed a quantitative conversion of the starting material to the clicked products. For the HPLC analysis and purification, the TAMRA maximum absorption wavelength (546 nm) was also monitored to identify the clicked products. The two intense peaks at 33.8 and 36.2 min can be assigned to the unreacted dye, while the product peaks have t_R of 30.22 and 30.93 min (5/6-TAMRA isomers).

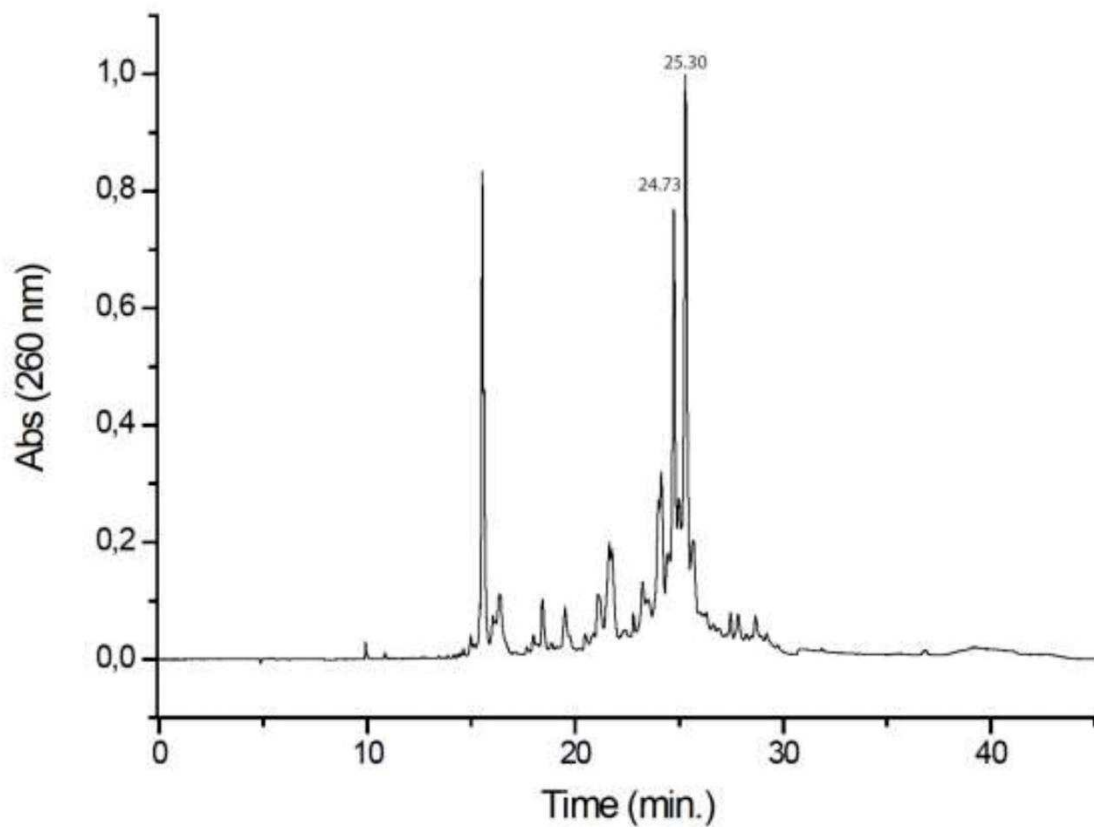
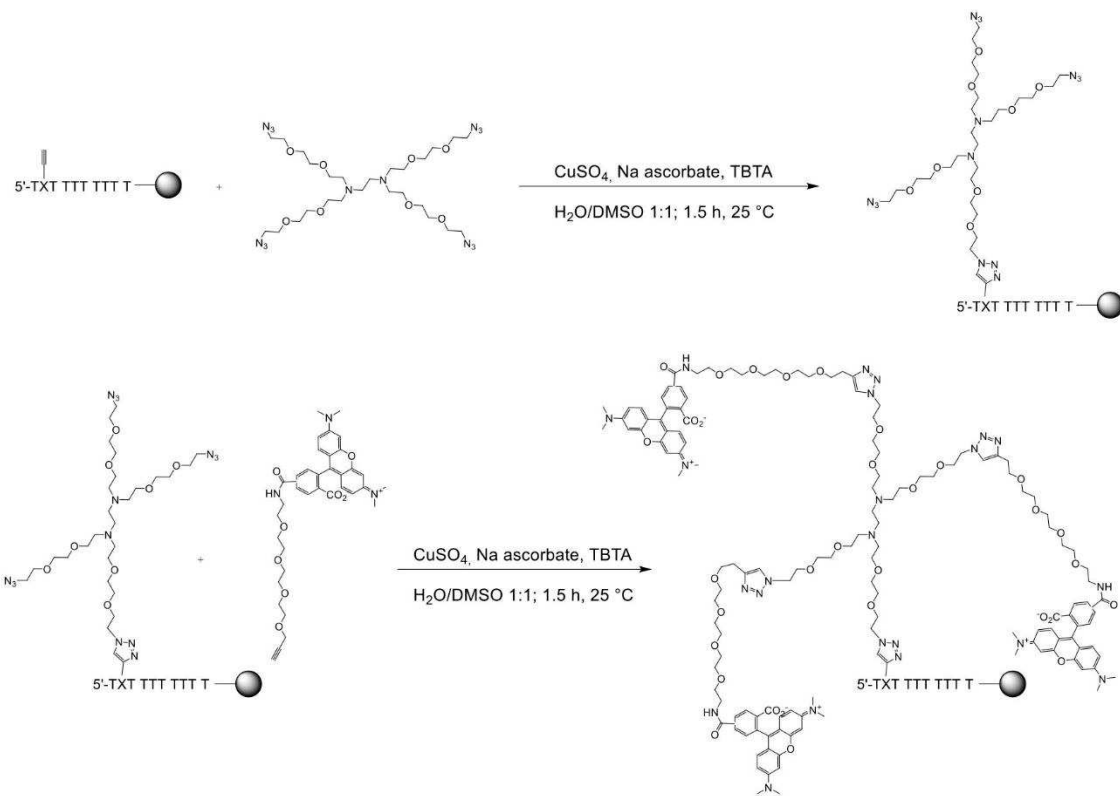


MALDI-TOF-MS: [M] calc. for oligonucleotide **1** + dendrimer + 3 dyes = 3705.4;
found = 6320.7, 4687.1 ([2 oligonucleotides **2** + dendrimer + 2 dyes]²⁻).

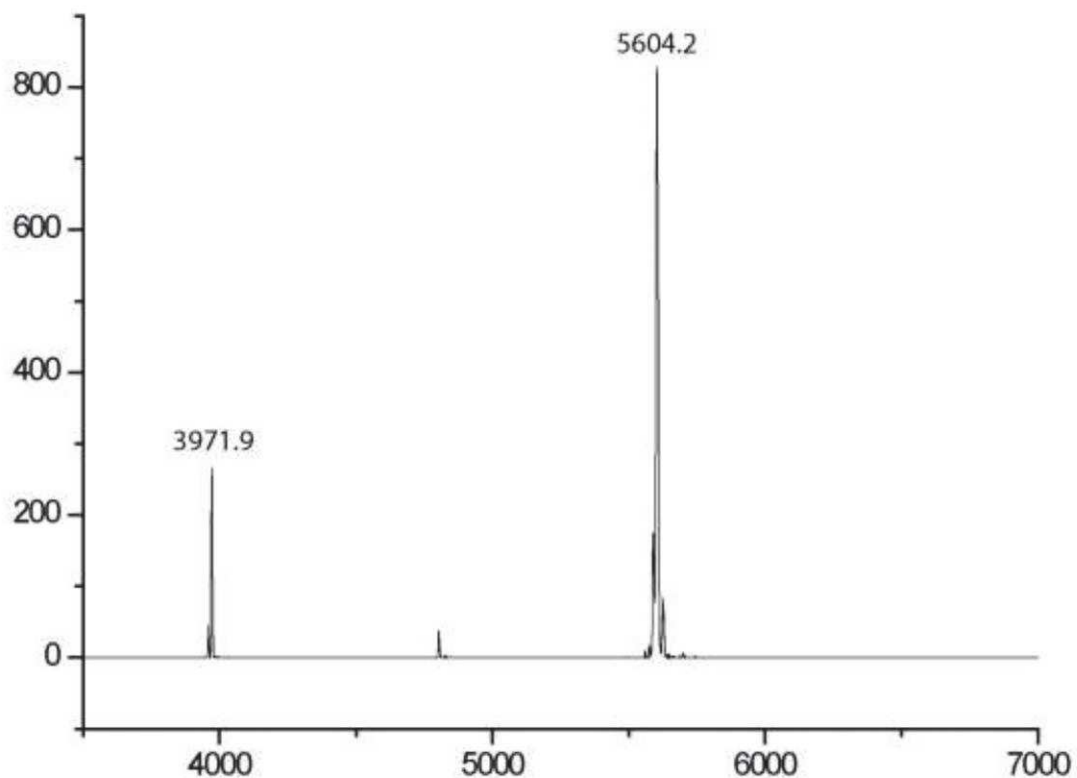


Click reactions on solid phase

After solid phase synthesis of the **oligonucleotide 2** and DBU deprotection of the cyanoethyl groups of the phosphates, 2 click reactions were performed following the **procedure B** and the final product was analyzed by RP-HPLC and MALDI-TOF-MS.



MALDI-TOF-MS: [M] calc. for oligonucleotide **2** + dendrimer + 3 dyes = 5612.4;
 found = 5604.2, 3971.2 (2 oligonucleotides **2** + dendrimer + 2 dyes)²⁻.



Cell culture cell strains and EdU labelling *in vivo*

HeLa, HEK293T and HEK293-GFP (GFP-stable cell line from Amsbio Catalog No. SC001) cells were cultivated at 37°C in water saturated, CO₂-enriched (5%) atmosphere. DMEM supplemented with 10% fetal bovine serum (FBS) (Invitrogen #10500-064), 1% penicillin and streptomycin (Sigma Aldrich # P0781), was used as growing medium. When reaching a confluence of 70% to 80%, the cells were passaged in a new culture flask. For staining experiments, 1.5×10^4 cells were seeded in each well of a μ -Slide 8 Well from ibidi (ibiTreat, #1.5 polymer coverslip, catalog No. 80826) and cultured for two days or until a density of 80% is reached.

EdU dissolved in DMSO was added to the culture medium to a final concentration of 10 μ M for 1 h (HEK-GFP) and 2 h (HEK and HeLa). The control cells without EdU feeding were exposed to the same volume of DMSO biological grade for the same period.

EdU staining *in situ* for the control experiments

All control experiments were accomplished using the EdU-Click kit from Baseclick GmbH containing the correspondent fluorescent dye and following the user manual.

EdU staining *in situ* with the double click approach

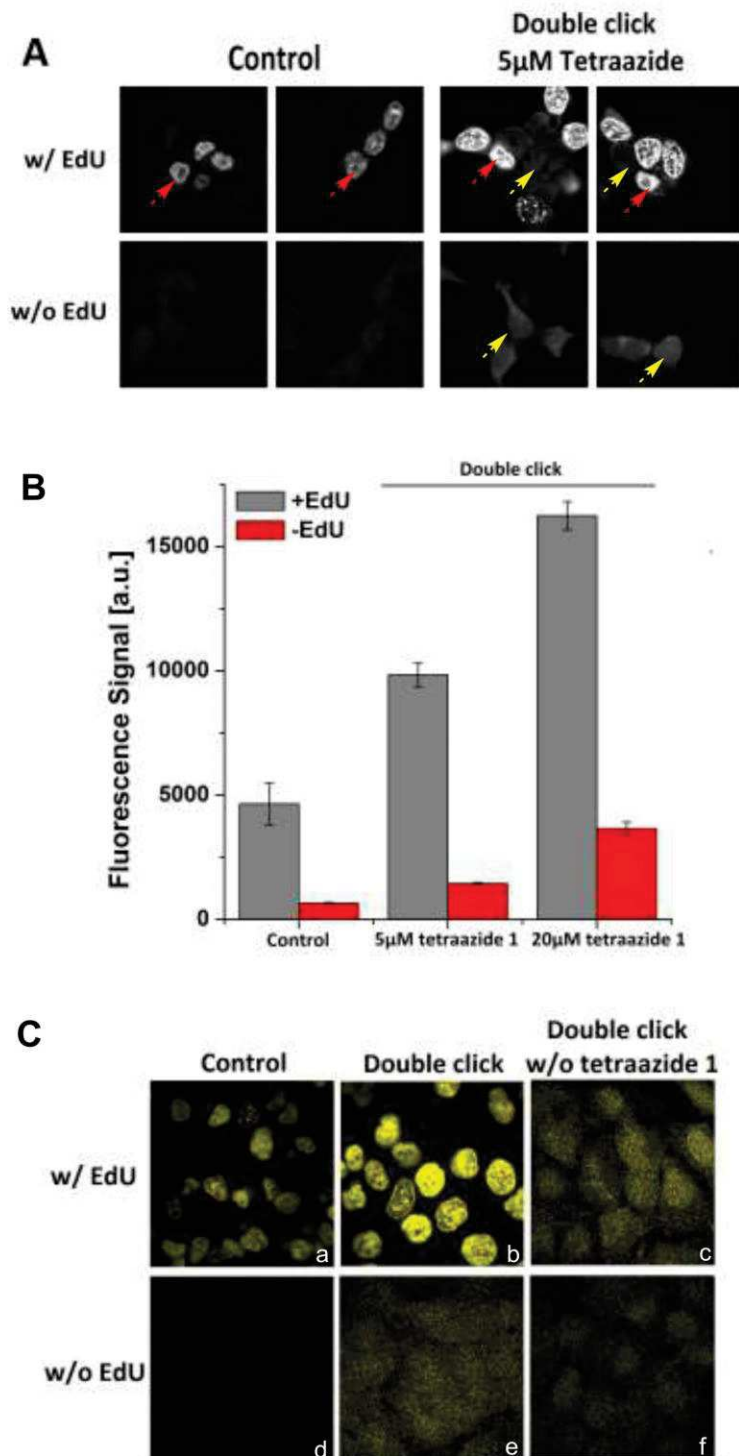
After EdU labelling, the cells were washed with phosphate buffered saline (137 mM NaCl, 10 mM Na₂HPO₄, 1.8 mM KH₂PO₄, 2.7 mM KCl), supplemented with 0,02% Tween (PBS-T) and fixed with 3,7% Formaldehyde in PBS for 15 minutes at RT. All following steps could be done outside the sterile bench. After two washing steps with PBS-T, the first click cocktail containing 20 µM tetraazide **1** was added to the cells. For this cocktail, the same buffers from the EdU-Click kit from Baseclick were used with the same final concentrations to prove, that any signal enhancement is caused by our dendrimer system. After 1 h incubation, the cells were washed twice with an acetic buffer pH 4.7 for 10 minutes each followed by two short washing steps with PBS-T.

The second click cocktail containing the dye-alkyne to a final concentration of 5 µM was then prepared and added to the cells and incubated for 30 minutes at RT. For the positive control, 20 µM of dye-azide were used. Light was avoided to prevent bleaching of the dyes. After staining, the cells were washed twice with a saturated solution of guanidinium isocyanate for 10 minutes respectively followed by two washing steps with PBS-T. When preparing the click cocktails, all buffers have to be fresh. If precipitation or changes of the colors happen, use another bench of the buffers or solutions. Cells were then stained with 200 ng/µl DAPI for 10 minutes at RT and washed twice with PBS-T.

EdU staining *in situ* with the triple click approach

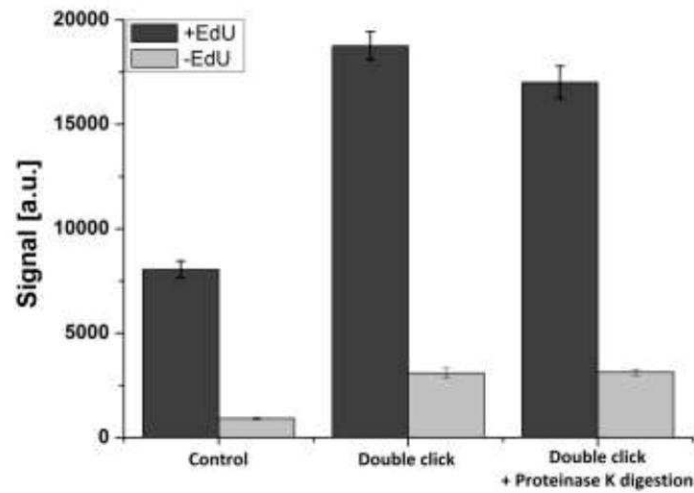
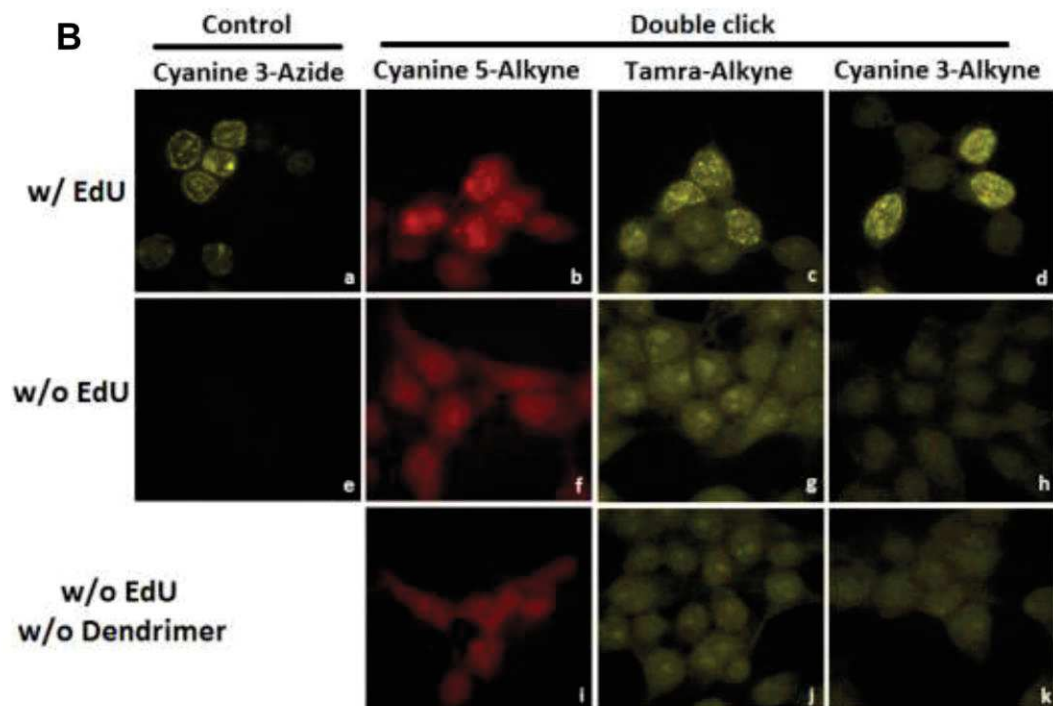
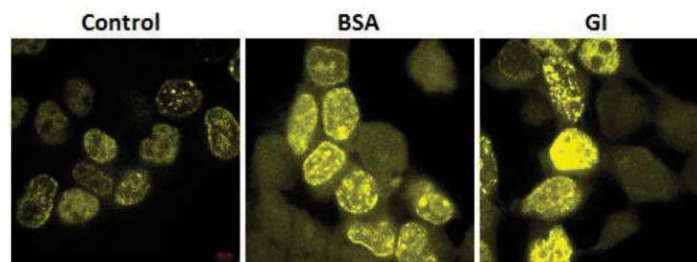
The same procedure, as described above, was used. After the first click reaction with 20 µM tetraazide **1** and the washing steps with acetic buffer and PBS-T, the second click cocktail containing 5 µM tetraalkyne **2** was added and incubated for 1 h at RT. After two washing steps with PBS-T, the click cocktail containing 20 µM dye-azide was then prepared and added to the cells and incubated for 30 minutes at RT. After staining, the cells were washed twice with a saturated solution of guanidinium isocyanate for each 10 minutes followed by two washing steps with PBS-T. Cells

were then stained with 200 ng/μl DAPI for 10 minutes at RT and washed twice with PBS-T.



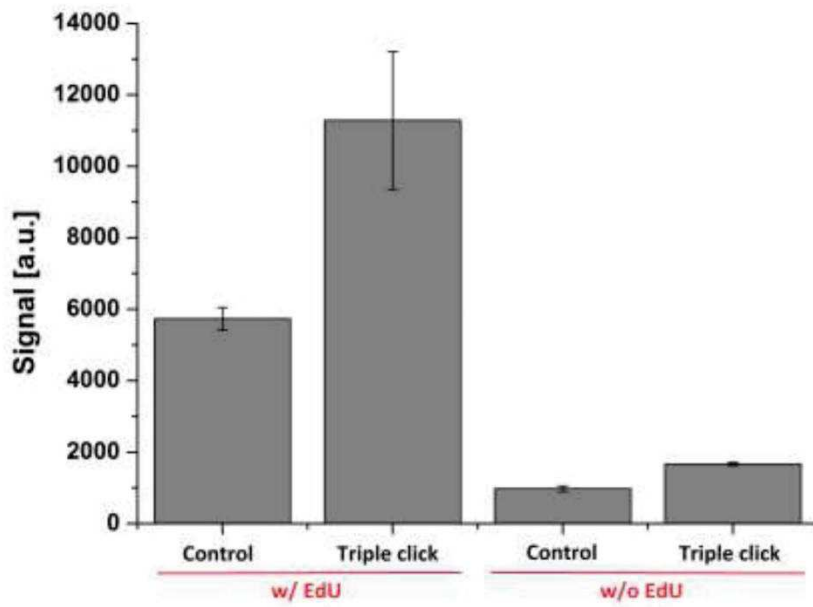
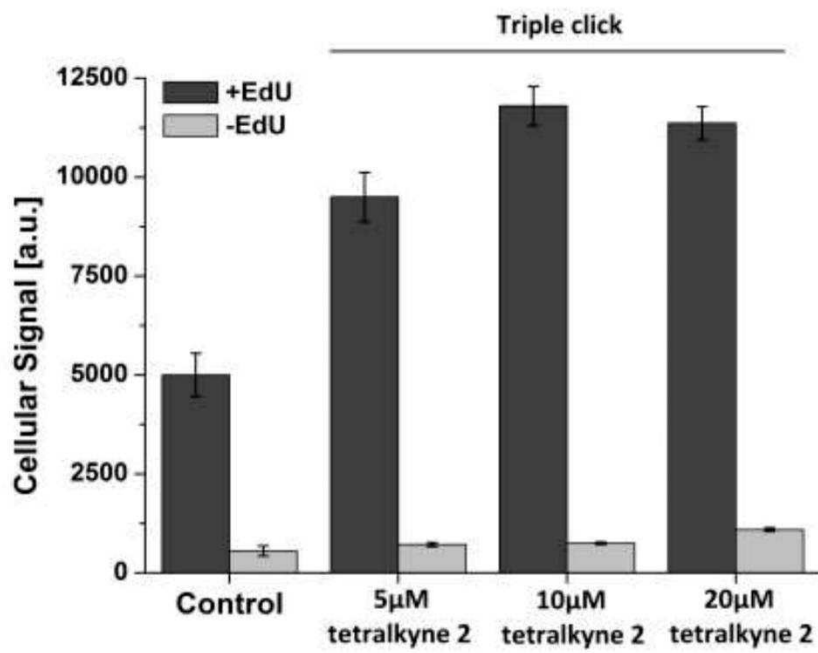
Supplementary figure S4: Development of the double click assay (simple dendrimer). **A)** A strong increase of the specific signal intensity (red arrows) was achieved with 5 μM tetraazide 1 and 5 μM Cyanine 3-alkyne. This enhancement was coupled with an increase of background fluorescence (yellow arrows), which was not seen in the control cells stained using the standard *in situ* click assay with 5 μM dye

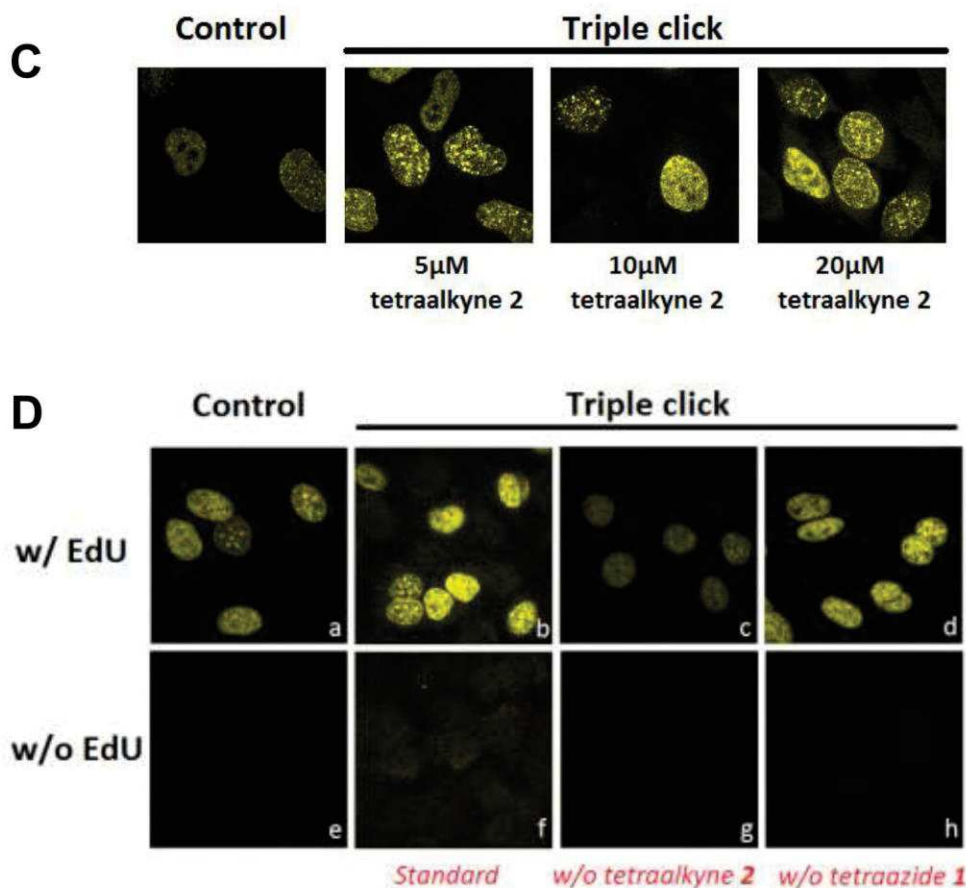
azide. **B)** Using 20 μM tetraazide **1**, an enhancement of the signal intensity and the background were measured. **C)** To prove, that the signal intensity was generated by the combination of the tetraazide and the Cyanine 3-alkyne system, control experiments were done with EdU and Cyanine 3-alkyne (5 μM) (**c**), without EdU, with tetraazide and Cyanine 3-alkyne (5 μM) (**e**) and without EdU, without tetraazide and with Cyanine 3-alkyne (5 μM) (**f**). Positive control was performed with EdU, tetraazide and Cyanine 3-alkyne (5 μM). The negative controls **c**, **e** and **f** show only background fluorescence without any kind of specific signal. Controls **a** and **d** were stained with 20 μM Cyanine 3-azide.

A**B****C**

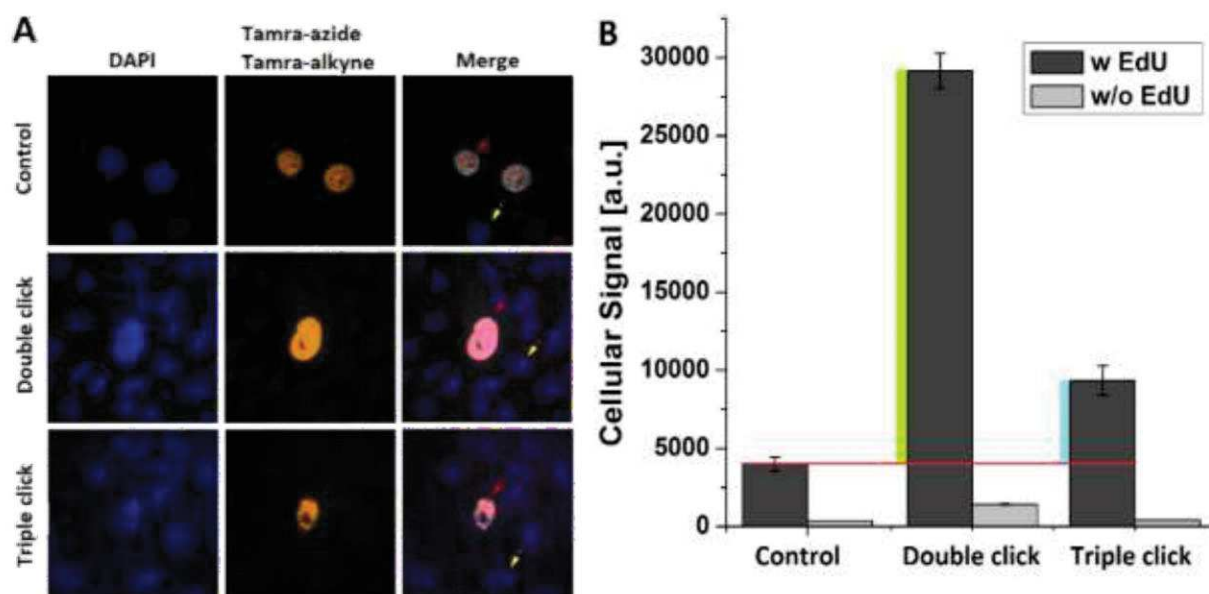
Supplementary figure S5: Improvement of the signal to background ratio of the double click assay. A) Digestion of proteins in order to reduce cross linkers, which could be binding sides for the alkyne-dye. Fixed and permeabilized cells were digested with 50 $\mu\text{g/ml}$ Proteinase K at 37°C for 1 h before performing double click assay with dendrimer 1 (20 μM) and Cyanine 3-alkyne (5 μM). Control cells were stained using the double click assay without Proteinase K digestion and with 20 μM

Cyanine 3-azide. Positive control was the standard *in situ* click assay with cyanine 3-azide (20 μM). The specific signal intensity is after digestion slightly decreased. Negative controls without EdU labelling show no decrease in background signal intensity. **B)** Screening for dye alkyne. Positive control cells (**a**) labeled with EdU were stained with Cyanine 3-azide (20 μM). For the double click assay, cells were labeled with EdU and stained using dendrimer **1** (5 μM) followed by click reactions using either Cyanine 5-alkyne (**b**), Tamra-alkyne (**c**) or Cyanine 3-alkyne (**d**) (each 5 μM). The double click assay was successful using the different dye-alkynes. For the negative controls, cells were not labeled with EdU but either stained with the dendrimer **1** (20 μM) and the corresponding dye-alkyne (5 μM) (**e-h**) or only with the dye-alkyne (5 μM) (**i-k**). **i-k** were washed additionally over night with 3% BSA in PBS. They show how the dye-alkynes stuck strongly to the cells in an unspecific way. **C)** Screening for wash buffers. To decrease the unspecific bound dye-alkyne, a screening for organic (DMSO, DMF, Acetonitril, MeOH, EtOH) and inorganic washing solvents (H_2O , Urea, guanidinium isocyanate, BSA) was performed with different incubation times and temperatures (data not shown). The best washing buffer was guanidinium isocyanate (GI), which reduces the background signal of Tamra-alkyne by about 50% in comparison to 3% BSA in PBS, when used twice after the click reaction of the dye-alkyne and before DAPI staining for 10 minutes at RT.

A**B**



Supplementary figure S6: Development of the triple click assay (double dendrimer). **A)** An increase of the signal intensity and a reduced background signal were achieved using the double dendrimer approach. **B)** and **C)** Screening for the appropriate concentration of tetraalkyne **2**. A titration for the concentration was done using 5, 10 and 20 μ M of the tetraalkyne **2**. The background intensity was dramatically reduced compared to the simple dendrimer assay. Furthermore, it was as low as the background in the control cells. The specific signal was doubled already with 5 μ M tetraalkyne **2**. **D)** In order to test, if the increase of the specific signal intensity is a result of the combination of **1**, **2** and Tamra-azide, we performed control experiments either with **1** and without **2** (**d**, **g**) or with **2** and without **1** (**d**, **h**) respectively in presence or absence of EdU. Positive controls were the non-dendrimer assay with (**a**) and without (**e**) EdU. **c)** shows that after the first click reaction, most of the genomic alkynes reacted with tetraazide **1** resulting in a very weak specific signal. **d)** shows almost the same signal intensity as the positive control (**a**), because **1** cannot react with the genomic alkynes and is washed away before the click reaction with Tamra-azide.



Supplementary figure S7: Direct comparison between the non-dendrimer, the double and triple click dendrimer approaches. A) Comparison of microscope images. The strongest signal of proliferating cells (red arrows) is achieved using the double click (20 μ M tetraazide **1** followed by 5 μ M Tamra-alkyne). The triple click (20 μ M tetraazide **1** followed by 5 μ M tetraalkyne **2** and 20 μ M Tamra-azide) showed a doubling of the specific signal intensity. Yellow arrows show non-proliferating cells **B)** Statistical quantifications. These quantifications approve the signal enhancement seen under the fluorescent microscope. The signal intensity is at least doubled using the triple click and four times higher than the control using the double click approach. All other results obtained so far were confirmed. Due to the binding of several fluorescent dyes at the dendrimer **2** using the triple click, the cellular signal intensity is reduced compared to double click approach using only dendrimer **1**. The reason for it could be the self-quenching of the fluorescent dyes.

High throughput screening: HeLa cells were seeded with different cell number (100, 500, 1000, 2000, 4000, 8000 cells) in a 96-well black microplate with a flat bottom (VWR) for 48 h. For each cell density, a duplicate was performed. Cells were fed with 10 μ M EdU for 2 h. After fixation with 3.7% PFA in PBS at RT and permeabilization with 0.5% Triton in PBS-T for 15 min at RT, cells were incubated with 20 μ M tetraazide **1** followed by incubation with 5 μ M Tamra-alkyne for the double click assay. Cells were incubated with 20 μ M tetraazide **1** followed by 5 μ M

tetraalkyne **2** than 20 μM Tamra-azide for the triple click assay. All incubations were done in presence of Cu(I). The control cells were reacted only with 20 μM Tamra-azide in presence of Cu(I). Negative control cells without EdU labeling were reacted with the same corresponding reagents. The cellular intensities were measured with a microplate reader from Tecan for the positive and negative controls. Background intensity was measured and subtracted in order to calculate the specific signal intensity.

Microscopy and image analysis: Confocal fluorescence images were acquired by the commercially available Zeiss Cell Observer SD equipped with a Yokogawa spinning disk unit. Single slices of multiple nuclei within one field of view were acquired. The laser power and exposure settings were equal for throughout the image acquisition. Using ImageJ, a rolling ball background subtraction was performed, followed by determination of the gray value of the brightest pixel (GVBP). Then, a threshold at $0.25 \times \text{GVBP}$ was applied and the mean signal of the pixels above this threshold was measured. The mean of ten fields of view was taken and defined as signal for the respective condition.

6 List of abbreviations

AIBN	2,2'-azodisobutyronitrile
APC	Antigen-presenting cell
ATP	Adenosine triphosphate
BSA	bis(trimethylsilyl)acetamide
BTT	benzylthio tetrazole
CAR-T	chimeric antigen receptor therapy
CDN	cyclic dinucleotide
c-di-AMP	cyclic di-adenosine monophosphate
CES	carboxylesterase
cGAMP	cyclic guanosine monophosphate-adenosine monophosphate
cGAS	cyclic adenosine monophosphate-adenosine monophosphate synthase
CLR	C-type lectin receptor
DAMP	damage-associated molecular pattern
DCA	dichloroacetic acid
DCM	dichloromethane
DMF	dimethylformamide
DMSO	dimethylsulfoxide
DMTr	4,4'-dimethoxytrityl
DMXAA	5,6-Dimethylxanthenone-4-acetic acid
DSF	differential scanning fluorimetry

EC₅₀	half maximal effective concentration
EdU	5-ethynyldeoxyuridine
EI	electron ionization
ENPP1	ectonucleotide pyrophosphatase/phosphodiesterase 1
ESI	electrospray ionization
EtOAc	ethyl acetate
EtOH	ethanol
GTP	guanosine triphosphate
HPLC	high pressure liquid chromatography
HTS	high throughput screening
INF	interferon
IRF	interferon regulatory factor
ITC	isothermal titration calorimetry
MeCN	acetonitrile
MeOH	methanol
MS	mass spectrometry
MSNT	1-(Mesitylene-2-sulfonyl)-3-nitro-1H-1,2,4-triazole
NF-κB	nuclear factor kappa-light-chain-enhancer of activated B-cells
NLR	NOD-like receptor
NMI	N-methylimidazol
NMR	nuclear magnetic resonance

NOD	nucleotide-binding oligomerization domain
OTf	triflate
PAMP	pathogen-associated molecular pattern
PRR	pattern recognition receptor
RIG-I	retinoic acid-inducible gene I
SATE	S-acylthioethyl
STAT1	Signal transducer and activator of transcription 1
STING	stimulator of interferon genes
TBK1	TANK-binding kinase 1
TBS	<i>t</i> -butyldimethylsilyl
<i>t</i>BuOOH	<i>t</i> -butylhydroperoxide
TEAA	triethylammonium acetate
TFA	trifluoroacetic acid
TLR	Toll-like receptor
TMS	trimethylsilyl
TPSCI	2,4,5-triisopropylbenzenesulfonyl chloride

7 Literature

1. Chaplin, D. D. Overview of the immune response. *J. Allergy Clin. Immunol.* **125**, S3-23 (2010).
2. Medzhitov, R. Recognition of microorganisms and activation of the immune response. *Nature* **449**, 819–826 (2007).
3. Marshall, J. S., Warrington, R., Watson, W. & Kim, H. L. An introduction to immunology and immunopathology. *Allergy Asthma. Clin. Immunol.* **14**, 49 (2018).
4. Buchmann, K. Evolution of Innate Immunity: Clues from Invertebrates via Fish to Mammals. *Front. Immunol.* **5**, 459 (2014).
5. Kimbrell, D. A. & Beutler, B. The evolution and genetics of innate immunity. *Nat. Rev. Genet.* **2**, 256–267 (2001).
6. Medzhitov, R. & Janeway, C. A. Innate immunity: impact on the adaptive immune response. *Curr. Opin. Immunol.* **9**, 4–9 (1997).
7. Kumar, H., Kawai, T. & Akira, S. Pathogen Recognition by the Innate Immune System. *Int. Rev. Immunol.* **30**, 16–34 (2011).
8. Akira, S., Takeda, K. & Kaisho, T. Toll-like receptors: critical proteins linking innate and acquired immunity. *Nat. Immunol.* **2**, 675–680 (2001).
9. Pancer, Z. & Cooper, M. D. The Evolution of Adaptive Immunity. *Annu. Rev. Immunol.* **24**, 497–518 (2006).
10. Medzhitov, R. & Janeway, C. Innate immune recognition: mechanisms and pathways. *Immunol. Rev.* **173**, 89–97 (2000).
11. Davies, L. C., Jenkins, S. J., Allen, J. E. & Taylor, P. R. Tissue-resident macrophages. *Nat. Immunol.* **14**, 986–995 (2013).
12. Kumar, V. & Sharma, A. Mast cells: Emerging sentinel innate immune cells with diverse role in immunity. *Mol. Immunol.* **48**, 14–25 (2010).
13. Mahla, R. S., Reddy, C. M., Prasad, D. & Kumar, H. Sweeten PAMPs: role of sugar complexed PAMPs in innate immunity and vaccine biology. *Front. Immunol.* **4**, 248 (2013).
14. Schroder, K. & Tschopp, J. The inflammasomes. *Cell* **140**, 821–32 (2010).
15. Newton, K. & Dixit, V. M. Signaling in innate immunity and inflammation. *Cold Spring Harb. Perspect. Biol.* **4**, (2012).
16. Abdulkhaleq, L. A. *et al.* The crucial roles of inflammatory mediators in inflammation: A review. *Vet. world* **11**, 627–635 (2018).
17. Kawai, T. & Akira, S. Toll-like Receptors and Their Crosstalk with Other Innate

- Receptors in Infection and Immunity. *Immunity* **34**, 637–650 (2011).
18. Hoving, J. C., Wilson, G. J. & Brown, G. D. Signalling C-type lectin receptors, microbial recognition and immunity. *Cell. Microbiol.* **16**, 185–94 (2014).
 19. Zelensky, A. N. & Gready, J. E. The C-type lectin-like domain superfamily. *FEBS J.* **272**, 6179–6217 (2005).
 20. Geijtenbeek, T. B. H. & Gringhuis, S. I. Signalling through C-type lectin receptors: shaping immune responses. *Nat. Rev. Immunol.* **9**, 465–479 (2009).
 21. Kim, Y.-G. *et al.* The cytosolic sensors Nod1 and Nod2 are critical for bacterial recognition and host defense after exposure to Toll-like receptor ligands. *Immunity* **28**, 246–57 (2008).
 22. Inohara, N., Chamailard, M., McDonald, C. & Nuñez, G. NOD-LRR PROTEINS: Role in Host-Microbial Interactions and Inflammatory Disease. *Annu. Rev. Biochem.* **74**, 355–383 (2005).
 23. Strober, W., Murray, P. J., Kitani, A. & Watanabe, T. Signalling pathways and molecular interactions of NOD1 and NOD2. *Nat. Rev. Immunol.* **6**, 9–20 (2006).
 24. Chow, K. T., Gale, M. & Loo, Y.-M. RIG-I and Other RNA Sensors in Antiviral Immunity. *Annu. Rev. Immunol.* **36**, 667–694 (2018).
 25. Loo, Y.-M. & Gale, M. Immune signaling by RIG-I-like receptors. *Immunity* **34**, 680–92 (2011).
 26. Luo, D., Kohlway, A., Vela, A. & Pyle, A. M. Visualizing the Determinants of Viral RNA Recognition by Innate Immune Sensor RIG-I. *Structure* **20**, 1983–1988 (2012).
 27. Stetson, D. B. & Medzhitov, R. Recognition of cytosolic DNA activates an IRF3-dependent innate immune response. *Immunity* **24**, 93–103 (2006).
 28. Sun, L., Wu, J., Du, F., Chen, X. & Chen, Z. J. Cyclic GMP-AMP Synthase Is a Cytosolic DNA Sensor That Activates the Type I Interferon Pathway. *Science (80-.)*. **339**, 786–791 (2013).
 29. Ablasser, A. *et al.* cGAS produces a 2' -5' -linked cyclic dinucleotide second messenger that activates STING. *Nature* **498**, 380 (2013).
 30. Civril, F. *et al.* Structural mechanism of cytosolic DNA sensing by cGAS. *Nature* **498**, 332–337 (2013).
 31. Gao, P. *et al.* Cyclic [G(2' ,5')pA(3' ,5')p] Is the Metazoan Second Messenger Produced by DNA-Activated Cyclic GMP-AMP Synthase. *Cell* **153**, 1094–1107 (2013).
 32. Kato, K. *et al.* Structural and Functional Analyses of DNA-Sensing and Immune Activation by Human cGAS. *PLoS One* **8**, e76983 (2013).
 33. Ablasser, A. *et al.* Cell intrinsic immunity spreads to bystander cells via the intercellular transfer of cGAMP. *Nature* **503**, 530 (2013).

34. Bridgeman, A. *et al.* Viruses transfer the antiviral second messenger cGAMP between cells. *Science* **349**, 1228–32 (2015).
35. Ishikawa, H. & Barber, G. N. STING is an endoplasmic reticulum adaptor that facilitates innate immune signalling. *Nature* **455**, 674–678 (2008).
36. Ishikawa, H., Ma, Z. & Barber, G. N. STING regulates intracellular DNA-mediated, type I interferon-dependent innate immunity. *Nature* **461**, 788–792 (2009).
37. Sun, W. *et al.* ERIS, an endoplasmic reticulum IFN stimulator, activates innate immune signaling through dimerization. *Proc. Natl. Acad. Sci.* **106**, 8653–8658 (2009).
38. Zhong, B. *et al.* The Adaptor Protein MITA Links Virus-Sensing Receptors to IRF3 Transcription Factor Activation. *Immunity* **29**, 538–550 (2008).
39. Liu, S. *et al.* Phosphorylation of innate immune adaptor proteins MAVS, STING, and TRIF induces IRF3 activation. *Science (80-.)*. **347**, aaa2630-aaa2630 (2015).
40. Saitoh, T. *et al.* Atg9a controls dsDNA-driven dynamic translocation of STING and the innate immune response. *Proc. Natl. Acad. Sci.* **106**, 20842–20846 (2009).
41. Tanaka, Y. & Chen, Z. J. STING specifies IRF3 phosphorylation by TBK1 in the cytosolic DNA signaling pathway. *Sci. Signal.* **5**, ra20-ra20 (2012).
42. Zhao, B. *et al.* Structural basis for concerted recruitment and activation of IRF-3 by innate immune adaptor proteins. *Proc. Natl. Acad. Sci.* **113**, E3403–E3412 (2016).
43. Shu, C. *et al.* Structural Insights into the Functions of TBK1 in Innate Antimicrobial Immunity. *Structure* **21**, 1137–1148 (2013).
44. Abe, T. & Barber, G. N. Cytosolic-DNA-Mediated, STING-Dependent Proinflammatory Gene Induction Necessitates Canonical NF- κ B Activation through TBK1. *J. Virol.* **88**, 5328–5341 (2014).
45. Dunphy, G. *et al.* Non-canonical Activation of the DNA Sensing Adaptor STING by ATM and IFI16 Mediates NF- κ B Signaling after Nuclear DNA Damage. *Mol. Cell* **71**, 745–760.e5 (2018).
46. Corrales, L. *et al.* Direct Activation of STING in the Tumor Microenvironment Leads to Potent and Systemic Tumor Regression and Immunity. *Cell Rep.* **11**, 1018–30 (2015).
47. Ergun, S. L., Fernandez, D., Weiss, T. M. & Li, L. STING Polymer Structure Reveals Mechanisms for Activation, Hyperactivation, and Inhibition. *Cell* **178**, 290–301.e10 (2019).
48. Volckmar, J. *et al.* The STING activator c-di-AMP exerts superior adjuvant properties than the formulation poly(I:C)/CpG after subcutaneous vaccination with soluble protein antigen or DEC-205-mediated antigen targeting to dendritic cells. *Vaccine* **37**, 4963–4974 (2019).
49. Marinho, F. V, Benmerzoug, S., Oliveira, S. C., Ryffel, B. & Quesniaux, V. F. J. The Emerging Roles of STING in Bacterial Infections. *Trends Microbiol.* **25**, 906–918

- (2017).
50. Chen, Z., Sun, L., Jiayi, S. & Heping, C. Pharmaceutical Targeting of a Mammalian Cyclic di-Nucleotide signaling Pathway. (2015).
 51. Zhang, X. *et al.* Cyclic GMP-AMP Containing Mixed Phosphodiester Linkages Is An Endogenous High-Affinity Ligand for STING. *Mol. Cell* **51**, 226–235 (2013).
 52. Gao, P. *et al.* Structure-Function Analysis of STING Activation by c[G(2' ,5')pA(3' ,5')p] and Targeting by Antiviral DMXAA. *Cell* **154**, 748–762 (2013).
 53. Zhang, C. *et al.* Structural basis of STING binding with and phosphorylation by TBK1. *Nature* **567**, 394–398 (2019).
 54. Shang, G., Zhang, C., Chen, Z. J., Bai, X. & Zhang, X. Cryo-EM structures of STING reveal its mechanism of activation by cyclic GMP–AMP. *Nature* **567**, 389–393 (2019).
 55. Gui, X. *et al.* Autophagy induction via STING trafficking is a primordial function of the cGAS pathway. *Nature* **567**, 262–266 (2019).
 56. Murray, R. Z. & Stow, J. L. Cytokine Secretion in Macrophages: SNAREs, Rabs, and Membrane Trafficking. *Front. Immunol.* **5**, 538 (2014).
 57. Turner, M. D., Nedjai, B., Hurst, T. & Pennington, D. J. Cytokines and chemokines: At the crossroads of cell signalling and inflammatory disease. *Biochim. Biophys. Acta - Mol. Cell Res.* **1843**, 2563–2582 (2014).
 58. Ritchie, C., Cordova, A. F., Hess, G. T., Bassik, M. C. & Li, L. SLC19A1 Is an Importer of the Immunotransmitter cGAMP. *Mol. Cell* **75**, 372–381.e5 (2019).
 59. Luteijn, R. D. *et al.* SLC19A1 transports immunoreactive cyclic dinucleotides. *Nature* **573**, 434–438 (2019).
 60. Bender, A. T. & Beavo, J. A. Cyclic nucleotide phosphodiesterases: molecular regulation to clinical use. *Pharmacol. Rev.* **58**, 488–520 (2006).
 61. Maurice, D. H. *et al.* Advances in targeting cyclic nucleotide phosphodiesterases. *Nat. Rev. Drug Discov.* **13**, 290–314 (2014).
 62. Deng, M. *et al.* Novel Mechanism for Cyclic Dinucleotide Degradation Revealed by Structural Studies of Vibrio Phosphodiesterase V-cGAP3. *J. Mol. Biol.* **430**, 5080–5093 (2018).
 63. Gao, J. *et al.* Identification and characterization of phosphodiesterases that specifically degrade 3' 3' -cyclic GMP-AMP. *Cell Res.* **25**, 539–550 (2015).
 64. Bai, Y. *et al.* Two DHH subfamily 1 proteins in *Streptococcus pneumoniae* possess cyclic di-AMP phosphodiesterase activity and affect bacterial growth and virulence. *J. Bacteriol.* **195**, 5123–32 (2013).
 65. Rao, F. *et al.* YybT Is a Signaling Protein That Contains a Cyclic Dinucleotide

- Phosphodiesterase Domain and a GGDEF Domain with ATPase Activity. *J. Biol. Chem.* **285**, 473–482 (2010).
66. Huynh, T. N. *et al.* An HD-domain phosphodiesterase mediates cooperative hydrolysis of c-di-AMP to affect bacterial growth and virulence. *Proc. Natl. Acad. Sci.* **112**, E747–E756 (2015).
 67. Kubota, K. *et al.* Identification of 2'-phosphodiesterase, which plays a role in the 2-5A system regulated by interferon. *J. Biol. Chem.* **279**, 37832–41 (2004).
 68. Poulsen, J. B. *et al.* Human 2' -phosphodiesterase localizes to the mitochondrial matrix with a putative function in mitochondrial RNA turnover. *Nucleic Acids Res.* **39**, 3754–3770 (2011).
 69. Li, L. *et al.* Hydrolysis of 2'3'-cGAMP by ENPP1 and design of nonhydrolyzable analogs. *Nat. Chem. Biol.* **10**, 1043–1048 (2014).
 70. Kato, K. *et al.* Structural insights into cGAMP degradation by Ecto-nucleotide pyrophosphatase phosphodiesterase 1. *Nat. Commun.* **9**, 4424 (2018).
 71. Eaglesham, J. B., Pan, Y., Kupper, T. S. & Kranzusch, P. J. Viral and metazoan poxins are cGAMP-specific nucleases that restrict cGAS–STING signalling. *Nature* **566**, 259–263 (2019).
 72. Trinchieri, G. Innate inflammation and cancer: Is it time for cancer prevention? *F1000 Med. Rep.* **3**, 11 (2011).
 73. O'Byrne, K. J. & Dalglish, A. G. Chronic immune activation and inflammation as the cause of malignancy. *Br. J. Cancer* **85**, 473–483 (2001).
 74. Colotta, F., Allavena, P., Sica, A., Garlanda, C. & Mantovani, A. Cancer-related inflammation, the seventh hallmark of cancer: links to genetic instability. *Carcinogenesis* **30**, 1073–1081 (2009).
 75. Borrello, M. G., Degl'Innocenti, D. & Pierotti, M. A. Inflammation and cancer: The oncogene-driven connection. *Cancer Lett.* **267**, 262–270 (2008).
 76. Korniluk, A., Koper, O., Kemon, H. & Dymicka-Piekarska, V. From inflammation to cancer. *Ir. J. Med. Sci.* **186**, 57–62 (2017).
 77. Schumacher, T. N., Scheper, W. & Kvistborg, P. Cancer Neoantigens. *Annu. Rev. Immunol.* **37**, 173–200 (2019).
 78. Schumacher, T. N. & Schreiber, R. D. Neoantigens in cancer immunotherapy. *Science* **348**, 69–74 (2015).
 79. Yarchoan, M., Johnson, B. A., Lutz, E. R., Laheru, D. A. & Jaffee, E. M. Targeting neoantigens to augment antitumour immunity. *Nat. Rev. Cancer* **17**, 209–222 (2017).
 80. Adams, J. L., Smothers, J., Srinivasan, R. & Hoos, A. Big opportunities for small molecules in immuno-oncology. *Nat. Rev. Drug Discov.* **14**, 603–622 (2015).

81. Grivennikov, S. I., Greten, F. R. & Karin, M. Immunity, Inflammation, and Cancer. *Cell* **140**, 883–899 (2010).
82. Adeegbe, D. O. & Nishikawa, H. Natural and Induced T Regulatory Cells in Cancer. *Front. Immunol.* **4**, 190 (2013).
83. Wang, H. Y. & Wang, R.-F. Regulatory T cells and cancer. *Curr. Opin. Immunol.* **19**, 217–223 (2007).
84. Madar, S., Goldstein, I. & Rotter, V. ‘Cancer associated fibroblasts’ – more than meets the eye. *Trends Mol. Med.* **19**, 447–453 (2013).
85. Farkona, S., Diamandis, E. P. & Blasutig, I. M. Cancer immunotherapy: the beginning of the end of cancer? *BMC Med.* **14**, 73 (2016).
86. Weiner, L. M., Surana, R. & Wang, S. Monoclonal antibodies: versatile platforms for cancer immunotherapy. *Nat. Rev. Immunol.* **10**, 317–27 (2010).
87. Kimiz-Gebologlu, I., Gulce-Iz, S. & Biray-Avci, C. Monoclonal antibodies in cancer immunotherapy. *Mol. Biol. Rep.* **45**, 2935–2940 (2018).
88. Leavy, O. Therapeutic antibodies: past, present and future. *Nat. Rev. Immunol.* **10**, 297 (2010).
89. Weiner, L. M., Murray, J. C. & Shuptrine, C. W. Antibody-based immunotherapy of cancer. *Cell* **148**, 1081–4 (2012).
90. Scotti, C., Iamele, L. & Vecchia, L. Antibody–drug conjugates: targeted weapons against cancer. *Antib. Technol. J.* **5**, 1 (2015).
91. Birrer, M. J., Moore, K. N., Betella, I. & Bates, R. C. Antibody-Drug Conjugate-Based Therapeutics: State of the Science. *JNCI J. Natl. Cancer Inst.* **111**, 538–549 (2019).
92. Egen, J. G., Kuhns, M. S. & Allison, J. P. CTLA-4: new insights into its biological function and use in tumor immunotherapy. *Nat. Immunol.* **3**, 611–618 (2002).
93. Barber, D. L. *et al.* Restoring function in exhausted CD8 T cells during chronic viral infection. *Nature* **439**, 682–687 (2006).
94. Probst, H. C., McCoy, K., Okazaki, T., Honjo, T. & van den Broek, M. Resting dendritic cells induce peripheral CD8⁺ T cell tolerance through PD-1 and CTLA-4. *Nat. Immunol.* **6**, 280–286 (2005).
95. Okazaki, T., Chikuma, S., Iwai, Y., Fagarasan, S. & Honjo, T. A rheostat for immune responses: the unique properties of PD-1 and their advantages for clinical application. *Nat. Immunol.* **14**, 1212–1218 (2013).
96. Soularue, E. *et al.* Enterocolitis due to immune checkpoint inhibitors: a systematic review. *Gut* **67**, 2056–2067 (2018).
97. Iwai, Y., Hamanishi, J., Chamoto, K. & Honjo, T. Cancer immunotherapies targeting the PD-1 signaling pathway. *J. Biomed. Sci.* **24**, 26 (2017).

98. Mohanty, R. *et al.* CAR T cell therapy: A new era for cancer treatment. *Oncol. Rep.* **42**, 2183–2195 (2019).
99. Miliotou, A. N. & Papadopoulou, L. C. CAR T-cell Therapy: A New Era in Cancer Immunotherapy. *Curr. Pharm. Biotechnol.* **19**, 5–18 (2018).
100. Klebanoff, C. A., Yamamoto, T. N. & Restifo, N. P. Treatment of aggressive lymphomas with anti-CD19 CAR T cells. *Nat. Rev. Clin. Oncol.* **11**, 685 (2014).
101. Neelapu, S. S. *et al.* Axicabtagene Ciloleucel CAR T-Cell Therapy in Refractory Large B-Cell Lymphoma. *N. Engl. J. Med.* **377**, 2531–2544 (2017).
102. Ledford, H. Engineered cell therapy for cancer gets thumbs up from FDA advisers. *Nature* **547**, 270–270 (2017).
103. Mohty, M. *et al.* CD19 chimeric antigen receptor-T cells in B-cell leukemia and lymphoma: current status and perspectives. *Leukemia* **33**, 2767–2778 (2019).
104. Zavras, P., Wang, Y., Gandhi, A., Lontos, K. & Delgoffe, G. Evaluating tisagenlecleucel and its potential in the treatment of relapsed or refractory diffuse large B cell lymphoma: evidence to date. *Onco. Targets. Ther.* **Volume 12**, 4543–4554 (2019).
105. Hay, A. E. & Cheung, M. C. CAR T-cells: costs, comparisons, and commentary. *J. Med. Econ.* **22**, 613–615 (2019).
106. Silbert, S., Yanik, G. A. & Shuman, A. G. How Should We Determine the Value of CAR T-Cell Therapy? *AMA J. Ethics* **21**, E844-851 (2019).
107. Chen, S., Song, Z. & Zhang, A. Small-Molecule Immuno-Oncology Therapy: Advances, Challenges and New Directions. *Curr. Top. Med. Chem.* **19**, 180–185 (2019).
108. Weinmann, H. Cancer Immunotherapy: Selected Targets and Small-Molecule Modulators. *ChemMedChem* **11**, 450–466 (2016).
109. Kerr, W. G. & Chisholm, J. D. The Next Generation of Immunotherapy for Cancer: Small Molecules Could Make Big Waves. *J. Immunol.* **202**, 11–19 (2019).
110. Dockrell, D. H. & Kinghorn, G. R. Imiquimod and resiquimod as novel immunomodulators. *J. Antimicrob. Chemother.* **48**, 751–755 (2001).
111. Chi, H. *et al.* Anti-tumor Activity of Toll-Like Receptor 7 Agonists. *Front. Pharmacol.* **8**, 304 (2017).
112. Furman, R. R. *et al.* Idelalisib and rituximab in relapsed chronic lymphocytic leukemia. *N. Engl. J. Med.* **370**, 997–1007 (2014).
113. Wu, M., Akinleye, A. & Zhu, X. Novel agents for chronic lymphocytic leukemia. *J. Hematol. Oncol.* **6**, 36 (2013).
114. Ahn, J., Ruiz, P. & Barber, G. N. Intrinsic self-DNA triggers inflammatory disease dependent on STING. *J. Immunol.* **193**, 4634–42 (2014).

115. Liu, X. & Wang, C. The emerging roles of the STING adaptor protein in immunity and diseases. *Immunology* **147**, 285–91 (2016).
116. Yan, N. Immune Diseases Associated with TREX1 and STING Dysfunction. *J. Interf. Cytokine Res.* **37**, 198–206 (2017).
117. Zhou, R. *et al.* The triggers of the cGAS-STING pathway and the connection with inflammatory and autoimmune diseases. *Infect. Genet. Evol.* **77**, 104094 (2020).
118. Li, Y., Wilson, H. L. & Kiss-Toth, E. Regulating STING in health and disease. *J. Inflamm.* **14**, 11 (2017).
119. Ahn, J., Gutman, D., Saijo, S. & Barber, G. N. STING manifests self DNA-dependent inflammatory disease. *Proc. Natl. Acad. Sci.* **109**, 19386–19391 (2012).
120. Fu, J. *et al.* STING agonist formulated cancer vaccines can cure established tumors resistant to PD-1 blockade. *Sci. Transl. Med.* **7**, 283ra52-283ra52 (2015).
121. Zhang, H., You, Q. D. & Xu, X. L. Targeting Stimulator of Interferon Genes (STING): A Medicinal Chemistry Perspective. *J. Med. Chem.* **63**, 3785–3816 (2020).
122. Feng, X., Liu, D., Li, Z. & Bian, J. Bioactive modulators targeting STING adaptor in cGAS-STING pathway. *Drug Discov. Today* **25**, 230–237 (2020).
123. Daei Farshchi Adli, A., Jahanban-Esfahlan, R., Seidi, K., Samandari-Rad, S. & Zarghami, N. An overview on Vadimezan (DMXAA): The vascular disrupting agent. *Chem. Biol. Drug Des.* **91**, 996–1006 (2018).
124. Shih, A. Y., Damm-Ganamet, K. L. & Mirzadegan, T. Dynamic Structural Differences between Human and Mouse STING Lead to Differing Sensitivity to DMXAA. *Biophys. J.* **114**, 32–39 (2018).
125. Conlon, J. *et al.* Mouse, but not Human STING, Binds and Signals in Response to the Vascular Disrupting Agent 5,6-Dimethylxanthenone-4-Acetic Acid. *J. Immunol.* **190**, 5216–5225 (2013).
126. Gao, P. *et al.* Binding-Pocket and Lid-Region Substitutions Render Human STING Sensitive to the Species-Specific Drug DMXAA. *Cell Rep.* **8**, 1668–1676 (2014).
127. Zhang, H. *et al.* Rat and human STINGs profile similarly towards anticancer/antiviral compounds. *Sci. Rep.* **5**, 18035 (2015).
128. Zhang, Y. *et al.* Identification of α -Mangostin as an Agonist of Human STING. *ChemMedChem* **13**, 2057–2064 (2018).
129. Ramanjulu, J. M. *et al.* Design of amidobenzimidazole STING receptor agonists with systemic activity. *Nature* **564**, 439–443 (2018).
130. Xi, Q. *et al.* Design, Synthesis, and Biological Evaluation of Amidobenzimidazole Derivatives as Stimulator of Interferon Genes (STING) Receptor Agonists. *J. Med. Chem.* **63**, 260–282 (2020).

131. Zhang, X. *et al.* Discovery and Mechanistic Study of a Novel Human-Stimulator-of-Interferon-Genes Agonist. *ACS Infect. Dis.* **5**, 1139–1149 (2019).
132. Johannes, L. & Lucchino, M. Current Challenges in Delivery and Cytosolic Translocation of Therapeutic RNAs. *Nucleic Acid Ther.* **28**, 178–193 (2018).
133. Iannitti, T., Morales-Medina, J. & Palmieri, B. Phosphorothioate Oligonucleotides: Effectiveness and Toxicity. *Curr. Drug Targets* **15**, 663–673 (2014).
134. Fu, J. *et al.* STING agonist formulated cancer vaccines can cure established tumors resistant to PD-1 blockade. *Sci. Transl. Med.* **7**, 283ra52-283ra52 (2015).
135. Katibah, G. E. *et al.* Compositions and Methods for Activating “Stimulator of Interferon Gene” -Dependent Signalling. WO2017075477A1. (2017).
136. Dubensky, T. W. J. *et al.* Compositions and Methods for Activating “Stimulator of Interferon Gene”-dependent Signalling WO2014189805A1. (2014).
137. Li, L. *et al.* Hydrolysis of 2' 3' -cGAMP by ENPP1 and design of nonhydrolyzable analogs. *Nat. Chem. Biol.* **10**, 1043 (2014).
138. Shaw, B. R. *et al.* Boranophosphate backbone: a mimic of phosphodiester, phosphorothioate, and methyl phosphonate. *Methods Enzymol.* **313**, 226–257 (2000).
139. Hall, A. H. S., Wan, J., Shaughnessy, E. E., Ramsay Shaw, B. & Alexander, K. A. RNA interference using boranophosphate siRNAs: structure-activity relationships. *Nucleic Acids Res.* **32**, 5991–6000 (2004).
140. Zhong, B. *et al.* Cyclic Di-nucleotide Compounds and Methods of Use. WO2017161349A1. (2017).
141. Glick, G., Ghosh, S., Roush, W. R., Olhava, E. J. & Jones, R. Cyclic Dinucleotide Analogs for Treating Conditions Associated with STING (Stimulator of Interferon Genes) Activity WO2018045204A1. (2018).
142. Dialer, C. R. *et al.* A Click-Chemistry Linked 2' 3' -cGAMP Analogue. *Chem. Eur. J.* **25**, 2089–2095 (2019).
143. Lioux, T. *et al.* Design, Synthesis, and Biological Evaluation of Novel Cyclic Adenosine-Inosine Monophosphate (cAIMP) Analogs That Activate Stimulator of Interferon Genes (STING). *J. Med. Chem.* **59**, 10253–10267 (2016).
144. M. Huttunen, K. & Rautio, J. Prodrugs - An Efficient Way to Breach Delivery and Targeting Barriers. *Curr. Top. Med. Chem.* **11**, 2265–2287 (2011).
145. Ariza, M. Current Prodrug Strategies for the Delivery of Nucleotides into Cells. *Drug Des. Rev. - Online* **2**, 373–387 (2005).
146. Wiemer, A. J. & Wiemer, D. F. Prodrugs of phosphonates and phosphates: crossing the membrane barrier. *Phosphorus Chem. I Asymmetric Synth. Bioact. Compd.* **360**, 115–160 (2015).

147. Sofia, M. J. *et al.* Discovery of a β -d-2'-Deoxy-2'- α -fluoro-2'- β -C-methyluridine Nucleotide Prodrug (PSI-7977) for the Treatment of Hepatitis C Virus. *J. Med. Chem.* **53**, 7202–7218 (2010).
148. Sofia, M. J., Chang, W., Furman, P. A., Mosley, R. T. & Ross, B. S. Nucleoside, Nucleotide, and Non-Nucleoside Inhibitors of Hepatitis C Virus NS5B RNA-Dependent RNA-Polymerase. *J. Med. Chem.* **55**, 2481–2531 (2012).
149. Bobeck, D. R., Schinazi, R. F. & Coats, S. J. Advances in nucleoside monophosphate prodrugs as anti-HCV agents. *Antivir. Ther.* **15**, 935–950 (2010).
150. Ray, A. S. & Hostetler, K. Y. Application of kinase bypass strategies to nucleoside antivirals. *Antiviral Res.* **92**, 277–291 (2011).
151. Pradere, U., Garnier-Amblard, E. C., Coats, S. J., Amblard, F. & Schinazi, R. F. Synthesis of Nucleoside Phosphate and Phosphonate Prodrugs. *Chem. Rev.* **114**, 9154–9218 (2014).
152. Erion, M. D. *et al.* Liver-Targeted Drug Delivery Using HepDirect Prodrugs. *J. Pharmacol. Exp. Ther.* **312**, 554–560 (2005).
153. Erion, M. D. *et al.* Design, Synthesis, and Characterization of a Series of Cytochrome P 450 3A-Activated Prodrugs (HepDirect Prodrugs) Useful for Targeting Phosph(on)ate-Based Drugs to the Liver. *J. Am. Chem. Soc.* **126**, 5154–5163 (2004).
154. Erion, M. D., Bullough, D. A., Lin, C.-C. & Hong, Z. HepDirect prodrugs for targeting nucleotide-based antiviral drugs to the liver. *Curr. Opin. Investig. Drugs* **7**, 109–117 (2006).
155. Kalia, D. *et al.* Nucleotide, c-di-GMP, c-di-AMP, cGMP, cAMP, (p)ppGpp signaling in bacteria and implications in pathogenesis. *Chem. Soc. Rev.* **42**, 305–41 (2013).
156. Clivio, P., Coantic-Castex, S. & Guillaume, D. (3' -5')-Cyclic Dinucleotides: Synthetic Strategies and Biological Potential. *Chem. Rev.* **113**, 7354–7401 (2013).
157. Roy, B., Depaix, A., Périgaud, C. & Peyrottes, S. Recent Trends in Nucleotide Synthesis. *Chem. Rev.* **116**, 7854–7897 (2016).
158. Schwede, F., Genieser, H.-G. & Rentsch, A. The Chemistry of the Noncanonical Cyclic Dinucleotide 2'3'-cGAMP and Its Analogs. *Handb. Exp. Pharmacol.* **238**, 251–263 (2015).
159. Gaffney, B. L. & Jones, R. A. One-Flask Synthesis of Cyclic Diguanosine Monophosphate (c-di-GMP). *Curr. Protoc. Nucleic Acid Chem.* **48**, 14.8.1-14.8.7 (2012).
160. Gaffney, B. L., Veliath, E., Zhao, J. & Jones, R. A. One-Flask Syntheses of c-di-GMP and the [Rp,Rp] and [Rp,Sp] Thiophosphate Analogues. *Org. Lett.* **12**, 3269–3271 (2010).
161. Zhang, X. *et al.* Cyclic GMP-AMP Containing Mixed Phosphodiester Linkages Is An Endogenous High-Affinity Ligand for STING. *Mol. Cell* **51**, 226–235 (2013).

162. Novotná, B. *et al.* Enzymatic Preparation of 2'–5', 3'–5' -Cyclic Dinucleotides, Their Binding Properties to Stimulator of Interferon Genes Adaptor Protein, and Structure/Activity Correlations. *J. Med. Chem.* **62**, 10676–10690 (2019).
163. Corrales, L., McWhirter, S. M., Dubensky Jr., T. W. & Gajewski, T. F. The host STING pathway at the interface of cancer and immunity. *J. Clin. Invest.* **126**, 2404–2411 (2016).
164. Wang, D. *et al.* Human carboxylesterases: a comprehensive review. *Acta Pharm. Sin. B* **8**, 699–712 (2018).
165. Brunner, K. *et al.* Cell- Penetrating and Neurotargeting Dendritic siRNA Nanostructures. *Angew. Chem.* **54**, 1946–1949 (2015).
166. Willibald, J., Harder, J., Sparrer, K., Conzelmann, K.-K. K. & Carell, T. Click-Modified Anandamide siRNA Enables Delivery and Gene Silencing in Neuronal and Immune Cells. *J. Am. Chem. Soc.* **134**, 12330–12333 (2012).
167. Zlatev, I., Vasseur, J.-J. & Morvan, F. Deoxygenation of 5-O-benzoyl-1,2-isopropylidene-3-O-imidazolylthiocarbonyl- α -D-xylofuranose using dimethyl phosphite: an efficient alternate method towards a 3' -deoxynucleoside glycosyl donor. *Tetrahedron Lett.* **49**, 3288–3290 (2008).
168. Kumar, A., Khan, S. I., Manglani, A., Khan, Z. K. & Katti, S. B. Synthesis and Antifungal Activity of 3' -Deoxyribonucleosides. *Nucleosides and Nucleotides* **13**, 1049–1058 (1994).
169. Meier, C., Neumann, J. M., Andre, F., Henin, Y. & Huynh Dinh Tam, H. D. O-Alkyl-5',5'-dinucleoside phosphates as prodrugs of 3'-azidothymidine and cordycepin. *J. Org. Chem.* **57**, 7300–7308 (1992).
170. Ding, H. *et al.* Total Synthesis of Mycalisine B. *Mar. Drugs* **17**, 226 (2019).
171. Heikkilä, J., Bjoerkman, S., Oeberg, B. & Chattopadhyaya, J. 5'-O-Trityl Group Promoted Directive Effect in the Preparation of 2'-O-Methylribonucleosides. *Acta Chem. Scand. B* **36**, 715–718 (1982).
172. Stacey, D. W. & Hitomi, M. Cell cycle studies based upon quantitative image analysis. *Cytom. Part A* **73A**, 270–278 (2008).
173. Romar, G. A., Kupper, T. S. & Divito, S. J. Research Techniques Made Simple: Techniques to Assess Cell Proliferation. *J. Invest. Dermatol.* **136**, e1–e7 (2016).
174. Fakan, S. High-resolution autoradiography as a tool for the localization of nucleic acid synthesis and distribution in the mammalian cell nucleus. *J. Microsc.* **106**, 159–171 (1976).
175. Hu, V. W., Black, G. E., Torres-Duarte, A. & Abramson, F. P. 3H-thymidine is a defective tool with which to measure rates of DNA synthesis. *FASEB J.* **16**, 1456–1457 (2002).
176. Taupin, P. BrdU immunohistochemistry for studying adult neurogenesis: Paradigms,

- pitfalls, limitations, and validation. *Brain Res. Rev.* **53**, 198–214 (2007).
177. Quiñones-Hinojosa, A., Sanai, N., Smith, J. S. & McDermott, M. W. Techniques to assess the proliferative potential of brain tumors. *J. Neurooncol.* **74**, 19–30 (2005).
 178. Gratzner, H. Monoclonal antibody to 5-bromo- and 5-iododeoxyuridine: A new reagent for detection of DNA replication. *Science (80-.)*. **218**, 474–475 (1982).
 179. H. Georg Kuhn & Christiana M. Cooper-Kuhn. Bromodeoxyuridine and the Detection of Neurogenesis. *Curr. Pharm. Biotechnol.* **8**, 127–131 (2007).
 180. Salic, A. & Mitchison, T. J. A chemical method for fast and sensitive detection of DNA synthesis in vivo. *Proc. Natl. Acad. Sci.* **105**, 2415–2420 (2008).
 181. Gierlich, J., Burley, G. A., Gramlich, P. M. E., Hammond, D. M. & Carell, T. Click chemistry as a reliable method for the high-density postsynthetic functionalization of alkyne-modified DNA. *Org. Lett.* **8**, 3639–3642 (2006).
 182. Gierlich, J. *et al.* Synthesis of Highly Modified DNA by a Combination of PCR with Alkyne-Bearing Triphosphates and Click Chemistry. *Chem. Eur. J.* **13**, 9486–9494 (2007).